

Minna Siekkinen

**The Impact of Dissolution
Products and Solution
pH on *In Vitro* Behaviour
of the Bioactive Glasses
45S5 and S53P4**





Minna Siekkinen

Born 1991

Previous studies and degrees

Master of Science, Åbo Akademi University, 2018



The Impact of Dissolution Products
and Solution pH on *In Vitro*
Behaviour of the Bioactive Glasses
45S5 and S53P4

Minna Siekkinen

Inorganic Chemistry
Faculty of Science and Engineering
Åbo Akademi University
Turku, Finland, 2024

Supervisor

Professor Leena Hupa
Åbo Akademi University

Co-supervisors

Docent Markus Engblom
Åbo Akademi University

and

Associate Professor Oskar Karlström
University of Turku

Opponent and reviewer

Associate Professor Dana Rohanová
University of Chemistry and Technology
Prague, Czechia

Reviewer

Professor Jukka Matinlinna
The University of Manchester
Manchester, United Kingdom

ISBN 978-952-12-4341-7 (printed)

ISBN 978-952-12-4342-4 (digital)

Painosalama, Turku, Finland 2024

*“Nothing in life is to be feared, it is only to be understood.
Now is the time to understand more, so that we may fear less.”*

Marie Skłodowska-Curie

Preface

The work presented in this thesis was carried out at the Faculty of Science and Engineering at Åbo Akademi University, as part of the research activities at the High-Temperature Processes and Materials laboratory. The work was part of the Business Finland project Bio-based Smart Materials at Biomaterial Interface in collaboration with Bonalive Biomaterials Ltd, StickTech Ltd, Mirka Ltd, CH-Bioforce Ltd, University of Turku and Aalto University. The Maud Kuistila Memorial Foundation, Swedish Cultural Foundation, and Victoriastiftelsen are greatly acknowledged for their financial support. Finnland-Institut in Deutschland TelepART Mobility Support and Åbo Akademi University travel grants are acknowledged for their financial support towards conferences and international meetings.

Firstly, my biggest gratitude goes to Professor Leena Hupa who has functioned as my main supervisor and introduced me to bioactive glasses when I first started my bachelor thesis work. With many meetings and discussions, Professor Hupa has increased my interest and knowledge of the material. It has been a great privilege to learn from someone that distinguished and respected in the field.

The help received from Docent Markus Engblom and Associate Professor Oskar Karlström (presently at the University of Turku) does not go unnoticed. Their valuable comments on manuscripts and meaningful questions during meetings have guided my research forward. Their commitment to supervising me in a field completely different from their own is highly appreciated.

Thank you to everybody who has helped with the analyses and around in the laboratory. Jaana Paananen introduced me to the laboratory and helped me become confident with the experimental part of this thesis. Luis Bezerra has made countless ion analyses with ICP-OES. Linus Silvander has analysed the surfaces with SEM-EDX. Frej Bjondahl helped me with the particle size distribution measurements. Without your expertise, the thesis would only be halfway completed. Additional thanks to Tor Laurén who has kept the working environment safe and has quickly solved the practical questions.

To the bioactive glass group, Polina Sinitsyna and Adrian Stiller, thank you for the hours in the laboratory, time in the office, and overall discussions about our research and everything else. It would have been a lot more challenging and lonelier to do this by myself. The rest of the inorganic chemistry group has also made the past years much easier. It has always been easy to ask questions or discuss various topics in the office, laboratory, coffee room, or during our free time.

To my friends back in my hometown Nykarleby and surroundings. Thank you for showing interest and keeping me grounded by having me focused on other things than my research. Jessica Häger, thank you for always opening your door when I was in that part of the country and letting me feel like a piece of your family. Emma Kengo and Diana Westerholm, thank you for all the adventure, near and far, and for a friendship that has lasted over 25 years. Ida Björkman and Melina Saari, thank you for continuously visiting me in Turku, for important and less important discussions over the years, and thank you for quick guidance when I needed any help.

To my brothers, Sami, Mika, and Jimi, and their families. My brothers were my role models when growing up. They have shown me what is important in life and how to focus on things that interest you. To my nieces and nephew, follow your dreams and set them free.

Finally, to my parents, Britt-Marie and Pekka. Thank you for the unconditional support over the years, for being a safety net in an ever-changing world, and for a home away from home where I was always welcomed with warmth and food. Thank you for showing me stability, recognition, and love.

Tack! Kiitos! Thank you!

Turku, October 2023

A handwritten signature in cursive script that reads "Minna Siekkinen". The signature is written in black ink and has a long, horizontal flourish extending to the right.

Minna Siekkinen

Abstract

Glass is a versatile material used in our everyday life. The chemical durability of glass depends on its composition. Some applications benefit from lower chemical durability. Glasses in a narrow compositional range are reactive in aqueous solutions and form hydroxyapatite on the surface. Such glasses are defined as bioactive glasses. Bioactive glasses are clinically used as a filler material due to diseases causing bone cavities. The formed hydroxyapatite bonds to bone apatite and new bone regenerates as the implanted bioactive glass dissolves. The dissolution occurs from the surface of the bioactive glass and is highly dependent on the environment. The environment inside and outside of a porous implant can differ (e.g., due to dissolution products) and the local environment can change depending on the implant site (e.g., fluid flow rate) or due to diseases (e.g., decrease of pH).

In vitro dissolution experiments are commonly conducted by immersing the bioactive glass in physiological-like solutions. Mimicking the circulating solutions in the human body *in vitro* contributes to an increased knowledge of the behaviour of bioactive glasses. Such experiments lead to better estimations of *in vivo* reactions, ultimately decreasing the number of *in vivo* tests needed before clinical applications.

This thesis investigated how dissolution products, fluid flow rate, and solution pH influence the *in vitro* behaviour of the bioactive glasses 45S5 and S53P4 in a dynamic environment. Also, the impact of solution pH and ion concentrations on the bioactive glass S53P4 in a static environment was studied. Dissolution experiments were performed in simulated body fluid, Tris buffer solution of different initial pH values, acetic acid-sodium hydroxide solution, and lactic acid. The impact of solution composition was studied using a cascade reactor, i.e., multiple reactors in series, to a continuous flow-through setup. The glass dissolution reactions were expressed as changes in the outflow solutions from each reactor and the glass samples in the reactors. Static tests were conducted by immersing the bioactive glass samples in extracts containing dissolution products from previous dissolutions. Also, two different flow rates were studied.

The reaction products, fluid flow rate, and pH influenced the *in vitro* reaction behaviour of the bioactive glasses. In the physiological pH range (7.4), the increasing ion concentrations hindered the bioactive glass dissolution, but typical reaction layers on the particle surfaces developed regardless. The results from the cascade reactors suggested that particles react differently depending on their location in a particle bed. Particles inside a bed or the interior of a porous implant would dissolve slower than the

material on the outer surfaces. In contrast, particles in the bed dissolved similarly in lactic acid (pH 2), i.e., the dissolution products did not influence the release of alkali and alkaline earth ions.

Although the pH and ion concentrations increased with decreasing flow rate in the physiological pH range, the release rate normalised to the solution volume suggested slower release for the lower flow rate. In contrast, the fluid flow rate change did not similarly impact the release rate in the acidic solutions (pH 2). Thus, to avoid undesired cellular effects, the local fluid flow rates must be considered when tailoring bioactive glasses to clinical applications.

The key features of bioactive glasses are the silica-rich and hydroxyapatite layers that form on the surfaces *in vitro* and *in vivo*. The formation and nature of these reaction layers depended on the pH of the test solutions. Solutions with an alkaline pH (9) dissolved glass without typical reaction layers. Silica-rich and calcium phosphate layers formed in dynamic and static solutions with a physiological-like pH (7.4). However, increased ion concentrations in the solutions resulted in mixed layers of silica and calcium phosphate. Static acidic pH (5) solutions resulted in a thick silica-rich layer with some calcium phosphate. In contrast, only a thick silica-rich layer formed in solutions with a lower pH (2).

The results of the thesis increased the knowledge of bioactive glass reactions and can be used to develop new compositions for new clinical applications. This thesis suggests that developing new experimental methods that better imitate the complex human body would further minimise the gap between *in vitro* and *in vivo*, ultimately decreasing the animal tests needed before clinical use.

Svensk sammanfattning

Glas är ett versatilt material vi använder i vårt vardagliga liv. Den kemiska hållbarheten av glas beror på dess sammansättning. En del glastillämpningar gynnas av en lägre kemisk hållbarhet. Glas i ett begränsat sammansättningsområde är reaktiva i vätskor och bildar hydroxiapatit på ytan. Sådana glas definieras som bioaktiva glas. Bioaktiva glas används kliniskt som utfyllnadsmaterial i benhåligheter orsakade av till exempel sjukdomar. Hydroxiapatit som bildats på glasets yta binder till benapatit och nytt ben regenereras samtidigt som det implanterade bioaktiva glaset löses upp. Upplösningen av glaset sker från materialets yta och är i hög grad beroende på miljön. Bland annat är miljön utanpå och inuti ett poröst implantat olika (på grund av upplösningssprodukter) och miljön kan variera beroende på implantatläget (varierande flödes hastighet) eller sjukdomar (lägre pH).

Upplösningsexperiment av bioaktivt glas *in vitro* är vanligtvis utförda genom att placera materialet i vätskor som simulerar kroppens. Genom att utförligare imitera den cirkulerande vätskan i människokroppen *in vitro* kan ökad förståelse om bioaktiva glasets reaktionsbeteende erhållas. Detta leder till en bättre uppskattning om beteendet *in vivo*, således behövs färre *in vivo*-test före den kliniska tillämpningen.

Denna avhandling studerade hur reaktionsprodukterna, flödes hastigheten, och lösningens pH påverkade bioaktiva glaserna 45S5 och S53P4 *in vitro*-reaktioner i en dynamisk miljö. Effekten av pH och reaktionsprodukter studerades också på det bioaktiva glaset S53P4 i en statisk miljö. Upplösningsexperiment utfördes i simulerad kroppsvätska, Tris-buffertlösningar med varierande pH-värden, ättiksyra-buffertlösning och mjölksyralösning. Effekten av lösningens sammansättning studerades i en kaskadreaktor, det vill säga reaktorer kopplade i serie, i den dynamiska genomströmningssuppsättningen. Glasets reaktioner studerades som förändringar i utflödet från reaktorerna samt förändringar i materialstrukturen. Statiska experiment utfördes genom att placera glasprovet i vätskor med reaktionsprodukter från tidigare upplösning. Två olika flödes hastigheter studerades.

Reaktionsprodukterna, flödes hastigheten och pH påverkade de bioaktiva glasens *in vitro*-reaktioner. En ökad jonkoncentration hindrade upplösningen av bioaktivt glas i det fysiologiska pH-området (7.4), däremot hindrades inte den typiska lagerbildningen. Resultaten från kaskadreaktorn antyder att partiklar reagerar olika beroende på deras placering i en partikelbädd. Partiklar inuti en bädd eller inuti ett poröst implantat skulle reagera långsammare än partiklar på ytan. Däremot upplöstes partikel-

bädden likformigt i mjölksyra (pH 2), det vill säga, upplösningarna påverkade inte upplösningen av alkalimetaller och alkaliska jordartsmetaller.

Även om pH och jonkoncentrationerna ökade med en lägre flödes hastighet i det fysiologiska pH-området, indikerade en normalisering av genomströmmad volym en lägre upplösning för den lägre flödes hastigheten. Däremot påverkade inte upplösningen i mjölksyran på ett liknande sätt vid förändrad flödes hastighet. Alltså, för att undvika oönskade celleffekter behövs den lokala flödes hastigheten beaktas när bioaktivt glas skraddarsys för klinisk användning.

En av huvudfunktionerna av bioaktivt glas är det kiselrika lagret och hydroxiapatit som bildas på ytan *in vitro* och *in vivo*. Bildningen och typen av dessa lager var beroende på testvätskans pH. Alkaliska vätskor (pH 9) löste glaset utan att bilda de typiska lagren. I både dynamiska och statiska lösningar med ett fysiologiskt pH (7.4) bildades typiska kiselrika och kalciumfosfatlager. Däremot bildades ett blandat lager av kisel och kalciumfosfat när reaktionsprodukter fanns med i lösningen. En statisk syrlig lösning (pH 5) resulterade i ett tjockare kiselrikt lager med kalciumfosfat på ytan. Däremot bildades enbart ett kiselrikt lager i vätskor med ett lägre pH (2).

Resultaten från denna avhandling ökade förståelsen av bioaktiva glasreaktioner *in vitro*. Denna förståelse kan användas i framtiden för en utveckling av nya glassammansättningar för nya kliniska tillämpningar. Avhandlingen föreslår att nya experimentella metoder behövs för att bättre simulera den komplexa människokroppen och således minimera gapet mellan *in vitro* och *in vivo*, följaktligen minska användningen av djur innan den kliniska användningen.

Abbreviations and Terms

3R	Replace, Reduce, Refine
45S5	Bioactive glass, Bioglass® (wt-%) $45\text{SiO}_2\text{-}24.5\text{CaO-}24.5\text{Na}_2\text{O-}6\text{P}_2\text{O}_5$
Allograft	Graft harvested from one patient/cadaver and implanted in another patient
ATP	Adenosine triphosphate
Autograft	Graft harvested and implanted in the same patient
BCE	Before common era
BES	N,N-Bis(2-hydroxyethyl)-2-aminoethanesulfonic acid
Bone matrix	Intercellular substance of bone
Ca/P	Calcium phosphate
Cancellous bone	Spongy bone found in the centre of the bone
CE mark	Product following EU legislation
Cortical bone	Compact bone found at the surface of the bone
Differentiation	Cell division to change function
DNA	Deoxyribonucleic acid
EDX/A	Energy-dispersive X-ray/analysis
FDA	U.S. Food and Drug Administration
FTIR	Fourier-transform infrared spectroscopy
HA	Hydroxyapatite
HEPES	4-(2-hydroxyethyl)-1-piperazineethanesulfonic acid
ICP-OES	Inductively coupled plasma-optical emission spectroscopy
<i>In vitro</i>	Latin "within the glass", laboratory tests
<i>In vivo</i>	Latin "within the living", animal/clinical tests
ISG	International Simple Glass (wt-%) $56.2\text{SiO}_2\text{-}5\text{CaO-}12.2\text{Na}_2\text{O-}17.3\text{B}_2\text{O}_3\text{-}6.1\text{Al}_2\text{O}_3\text{-}3.3\text{ZrO}_2$
ISO	International Organization for Standardization
ISO 23317	Implants for surgery - <i>In vitro</i> evaluation for apatite-forming ability of implant materials
LA	Lactic acid
LOQ	Limit of quantification
Macrophage	Type of white blood cell that digests pathogens
MGP	Matrix Gla protein
MOPS	3-(N-morpholino)propanesulfonic acid
Osteoblast	Bone cell
Osteoinduction	Induces stem cells to bone cells
Osteomyelitis	Bone infection

Osteostimulation	Promote proliferation and differentiation of bone cells by inducing growth factors
PLA	Poly(lactic acid)
PMMA	Poly(methyl methacrylate)
ppm	Parts per million (mg/l)
Proliferation	Cell division to produce daughter cells
Prosthesis	Artificial replacement of body part
RNA	Ribonucleic acid
rpm	Revolutions per minute (rotation frequency)
S53P4	Bioactive glass (wt-%) $53\text{SiO}_2\text{-}20\text{CaO-}23\text{Na}_2\text{O-}4\text{P}_2\text{O}_5$
SBF	Simulated body fluid
SEM	Scanning electron microscope
Stem cell	The earliest type of cell
T_g	Glass transition temperature
Tris	Tris(hydroxymethyl)aminomethane
Xenograft	Graft harvested from a non-human animal
XRD	X-ray diffraction analysis

Table of contents

Preface	I
Abstract	III
Svensk sammanfattning	V
Abbreviations and Terms	VII
Table of contents	IX
1. Introduction	1
1.1 Glass	1
1.1.1 Bioactive glass	2
1.2 Motivation of the work	3
1.3 Objective of the work	4
1.4 List of Publications	6
1.5 Contribution of the author	7
1.6 Introduction to the Publications	7
1.7 List of supporting Publications	8
2. Literature review	9
2.1 Biomaterials	9
2.2 Bioactive glass	10
2.2.1 Bioactive glass - aqueous solution reactions	12
2.2.2 <i>In vitro</i> studies	16
2.2.3 <i>In vivo</i> studies	19
2.2.4 Clinical use of the bioactive glasses 45S5 and S53P4	20
2.3 Elements in bioactive glass	21
2.3.1 Dissolution products from bioactive glass	22
3. Experimental	23
3.1 Bioactive glass	23
3.2 Dissolution media	24
3.3 Dynamic environment	26
3.3.1 Cascade reactor setup	26

3.4 Static environment.....	27
3.5 Analyses	27
3.5.1 Solution pH	28
3.5.2 Ion concentrations	28
3.5.3 Particle analyses.....	29
4. Results and discussion	30
4.1 Particle and scaffold characterisation	30
4.2 Dynamic dissolution	31
4.2.1 Comparison of 45S5 and S53P4 dissolution	31
4.2.2 Effect of fluid flow rate on S53P4 dissolution	36
4.2.3 Effect of initial pH on S53P4 dissolution.....	39
4.2.4 Impact of prolonged dissolution on S53P4 scaffolds	41
4.3 Static dissolution.....	43
4.4 Dissolution of elements from glasses.....	47
5. Conclusions and future work.....	49
6. References	52
Original publications.....	63

1. Introduction

The human skeletal system changes throughout its lifecycle. These changes can result from external forces, such as traumas or disuse, or internal ones, for example, diseases or hormonal/nutritional imbalance [1–3]. Ageing also naturally weakens the bone tissue after age 30 [4]. Critical-sized bone defects caused by disruption to the natural bone healing mechanism may need materials to correct the defect [5]. Such materials are commonly defined as biomaterials. Biomaterials are used to increase the quality of life by replacing, restoring, or regenerating bodily functions [6]. Implanted biomaterials for treating a disease or injury are in close contact with the living tissue. Because these materials are considered foreign to the human body, it is necessary to understand their behaviour in the physiological environment before implantation [7]. The early implantable biomaterials were desired to be as inert as possible, e.g., metals, to not react with the surrounding tissue [8]. Today, prostheses for total joint replacements are still metals, mainly titanium-based alloys [9]. However, even inert materials stimulate a tissue response causing an inflammation known as a *foreign body reaction* [10]. Due to the foreign body reaction, “inert” materials cause fibrous scar tissue to form and encapsulate the material inside the body [11]. The body environment is also corrosive, easily causing corrosion even on “inert” metals [12]. As an alternative, degradable materials, such as biodegradable polymers and reactive materials that actively form a bond with the living tissue and activate bone regeneration have been used as implant materials [13,14]. Synthetic materials have been suggested as biomaterials due to their higher availability and producibility [15]. However, extensive research is needed to go from innovation to a marketable product [16]. For example, glass is a multifunctional synthetic material used early as ocular prostheses [17] and has been studied as a further biomaterial [18].

1.1 Glass

Glass has been produced intentionally and unintentionally throughout the years, where a few found glass samples date to 8000 BCE, with more prevalence to 2500 BCE [19]. Currently, commercial glasses are mainly soda-lime-silica glasses [20]. Glass has been considered one of the most important materials for human civilisation, where people use common glass in everyday life [21]. Windows, electronics, drinking vessels, medicinal technology, and interior design use glass in different forms.

Glass is commonly seen as a solid material, but is sometimes defined as a liquid [22]. However, melting is not mandatory for producing glasses [23].

Therefore, the current definition of glass is a non-crystalline solid exhibiting a glass transformation behaviour [24]. In molten glasses, crystallinity is avoided by supercooling the molten phase to the transition temperature (T_g), which determines at what temperature the glass solidifies or softens [25]. Solidifying the glass too slowly risks crystallisation, and solidifying the glass too fast can cause shattering due to internal stresses. At the same time, sintering occurs above T_g , indicating that crystals can easily appear in sintered scaffolds [26].

Commercially used soda-lime-silica glasses are synthetic inorganic mixtures in the oxide system $\text{Na}_2\text{O}-\text{CaO}-\text{SiO}_2$. Other elements can be added to the composition to tailor the glass toward specific properties [27,28]. The main component, silica, is essentially quartz sand and functions as the network former when melted from a crystalline to an amorphous structure at a high temperature (1700°C) [29]. To decrease the melting temperature, network modifiers (Na_2O and CaO) are added to the composition to disrupt the highly connected SiO_2 network by replacing bridging oxygen with non-bridging oxygen [30].

Two of the most important properties of glass are mechanical and chemical durability. High mechanical durability is desired in almost every glass application, while chemical durability can differ depending on the application. High chemical durability is desired for float glasses (windows) [31] and nuclear waste glasses [32]. However, all glasses in contact with solutions will react, and usually develop a surface layer structurally different to the bulk glass [33]. The durability is highly dependent on the composition of the glass [34] and controlled degradation is desired for specific purposes [35]. Understanding the dissolution of glasses increases the possible utilisation of glass in, for example, the medical field.

1.1.1 Bioactive glass

Bioactive glass is a synthetic speciality glass intended for use inside or in close contact with the human body [36]. The unique properties of bioactive glasses cause the material to react, dissolve, and form reaction layers on the surface when in contact with aqueous solutions [37]. Compared to common soda-lime-silica glasses, bioactive glasses contain less silica and more other oxides. Additionally, phosphorus pentoxide (P_2O_5) is added to the glass to enhance bioactivity [38]. The history of bioactive glasses began during a discussion between an army veteran and a glass scientist, Professor Larry L. Hench, travelling to a conference on a bus:

“The human body rejects metallic and synthetic polymeric materials by forming scar tissue because living tissues are not composed of such materials.

Bone contains a hydrated calcium phosphate component, hydroxyapatite [HA] and therefore if a material is able to form a HA layer in vivo it may not be rejected by the body.” [39]

This hypothesis behind a new material to be used as implants resulted in the invention of bioactive glasses in the late 1960s [39]. Professor Hench and colleagues developed the first bioactive glass, 45S5, with the composition (in weight percentage, wt-%) $45\text{SiO}_2\text{-}24.5\text{CaO}\text{-}24.5\text{Na}_2\text{O}\text{-}6\text{P}_2\text{O}_5$ [40]. This composition was easy to melt and had a high Ca/P ratio inducing bioactivity. Upon implantation, bioactive glass bonds to bones through a chemical fixation between a developed hydroxyapatite layer on the glass surface and the apatite in the bone [41]. *In vitro* experiments confirmed that the layer formed on the bioactive glass was structurally the same as the hydroxyapatite crystals in bone [39]. Today, bioactive glass 45S5 is trademarked as Bioglass®. From this invention forward, over 9000 publications can be found on Web of Science™ using the words “bioactive glass” or “bioglass”. The publication and citation trends are shown in Figure 1 [42].

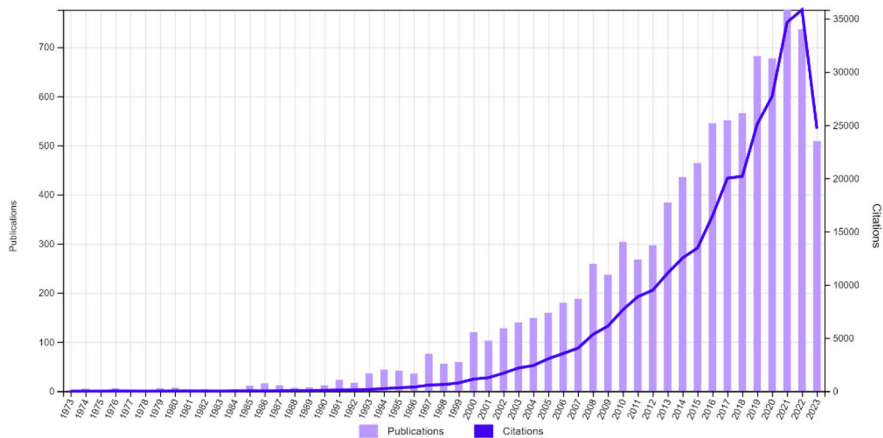


Figure 1. Publication and citation trends of "bioactive glass" or "bioglass" since its discovery to today. Acquired from Web of Science™ on 6.10.2023.

1.2 Motivation of the work

Most *in vitro* experiments use a static, physiological-like environment to investigate the bioactive glass/solution reactions upon contact. However, the human body is not a static system due to the dynamic fluid flows with different rates in different body parts. Understanding the fundamental *in vitro* reactions in different environments paves the road for better

estimations of the bioactive glass' reactions *in vivo*. Simultaneously, the number of *in vivo* experiments needed before clinical use decreases.

Late Professor Hench, the inventor of bioactive glass wrote in one of the last papers:

"Authors should strive for unique and innovative approaches at a fundamental molecular biology level to create new bioactive conditions that mimic their use clinically." [43]

This work strives to enhance the knowledge of bioactive glasses by studying *in vitro* reactions in settings better mimicking the *in vivo* conditions and focusing on earlier dismissed variables, such as solution composition changes and fluid flow rate. Bioactive glasses react with the body fluids while releasing ions. In literature, the research on ions, i.e., dissolution products from bioactive glasses, has focused on the biological and cellular responses. However, in this work, dissolved ions are hypothesised to change the bioactive glass' dissolution behaviour and reaction layers, which likely influences biological reactions. Researching the continuous dissolution of bioactive glasses in solutions already containing ions released from the material has not been systematically done.

Today, most clinical applications of bioactive glass are based on implanted particles. Whether the particles react similarly independent of their location in the implant is unknown. Further, classic static *in vitro* studies are not ideal for estimating the reactions in dynamic conditions. For example, the static experiments are not suitable for tracing back how the dissolving particles interact with each other. This thesis aimed to develop a novel method to study the average dissolution behaviour of bioactive glass particles depending on increasing dissolution products in the surrounding solution.

1.3 Objective of the work

This thesis aimed to clarify the impact of dissolution products, fluid flow rate, and pH on the reaction behaviour of well-known bioactive glasses. The setup used was developed during the work of the thesis and is based on the Åbo Akademi University dynamic *in vitro* flow-through setup [44], to mimic the dynamic human body environment better than static *in vitro* tests. Thus, the implant's *in vivo* environment can be estimated more accurately using *in vitro* experiments. The novel setup introduced a cascade reactor of three reactors coupled in series to the flow-through setup. Connecting reactors in the dynamic setup allowed a practical investigation of bioactive glass particles regarding their placement in a particle bed and increasing dissolution products in the surrounding solution. The reactor series was interpreted in

the following way: particles in the first reactor represent the outermost part of a particle implant with the first solution contact, while the subsequent reactors represent the internal parts of a particle implant with a solution containing dissolved ions from the outermost part. The thesis aimed to:

1. Investigate the glass *in vitro* behaviour in environments mimicking the *in vivo* environment using dynamic flow-through tests.
2. Investigate various parameters that likely influence the reaction behaviour *in vivo*. These parameters included different fluid flow rates and changes in the solution composition as the solution flows through an implanted particle bed.
3. Clarify the influence of pH on dissolution and reaction layers. Understanding the pH effects is crucial, as an infection or composite implant degradation may decrease the pH of the surrounding solution.

1.4 List of Publications

The thesis is compiled around the following peer-reviewed original publications:

- I. Siekkinen M., Karlström O., Hupa L. ***“Effect of local ion concentrations on the in vitro reactions of bioactive glass 45S5 particles”*** International Journal of Applied Glass Science, Vol 13 (2022) 4, pp. 695-707, DOI: 10.1111/ijag.16579
- II. Siekkinen M., Karlström O., Hupa L. ***“Dissolution of bioactive glass S53P4 in a three-reactor cascade in continuous flow conditions”*** Open Ceramics, Vol 13 (2023), DOI: 10.1016/j.oceram.2022.100327
- III. Siekkinen M., Engblom M., Hupa L. ***“Impact of solution pH (5-9) and dissolution products on in vitro behaviour of the bioactive glass S53P4”*** Journal of Non-Crystalline Solids: X, Vol 20 (2023) DOI: 10.1016/j.nocx.2023.100199
- IV. Siekkinen M., Engblom M., Karlström O., Hupa L. ***“Dissolution of bioactive glass S53P4 in continuous flows of Tris buffer and lactic acid”*** Biomedical Materials & Devices, (2023), DOI: 10.1007/s44174-023-00140-6
- V. Aalto-Setälä L., Siekkinen M., Lindfors N., Hupa L. ***“Dissolution of Glass-Ceramic Scaffolds of Bioactive Glasses 45S5 and S53P4”*** Biomedical Materials & Devices, (2023), DOI: 10.1007/s44174-022-00059-4

Throughout the thesis, the corresponding Roman numerals I-V will refer to the original publications. The original publications are printed at the end of the thesis with permission from the original copyright holders.

1.5 Contribution of the author

Publications I-IV: The author collaborated with the co-authors to construct the experimental design. The experimental work was conducted by the author. Specialists conducted particle size analyses and SEM-EDXA while the author was present. ICP-OES was measured and analysed by a specialist. The author evaluated the results and wrote the first drafts of the manuscripts. The drafts were later finalised with the co-authors.

Publication V: The author helped with the samples and conducted a part of the dissolution study. The author participated in writing the manuscript.

1.6 Introduction to the Publications

This work is based on five peer-reviewed articles that are presented in their original form at the end of the thesis. All articles investigate the dissolution of bioactive glasses *in vitro*.

- I. The article introduces the concept of using a cascade reactor system as a practical method to study the impact of ion concentration changes on bioactive glass dissolution using the well-known bioactive glass 45S5.
- II. The article discusses the use of bioactive glass S53P4 in the cascade reactor, and the results are compared to the findings in Publication I.
- III. The article investigates the changes to the solution pH due to material/solution reactions or infections at the implant site. The changes are studied *in vitro* in static solutions while discussing the impact of increasing dissolution products in the immersion solutions.
- IV. The article studies the dissolution behaviour of bioactive glass S53P4 particles depending on the solution flow rate, ion concentration changes, and solution pH in the cascade reactor.
- V. The article presents the long-term dissolution of bioactive glass 45S5 and S53P4 particles and sintered scaffolds in a dynamic environment.

1.7 List of supporting Publications

The author has contributed to the following peer-reviewed publications that are not included in the thesis:

- VI. Hoikkala N., Siekkinen M., Hupa L., Vallittu PK. ***"Behaviour of different bioactive glasses incorporated in polydimethylsiloxane endodontic sealer"*** Dental Materials, Vol 37 (2021) 2, pp. 321-327, DOI: 10.1016/j.dental.2020.11.013
- VII. Sirkiä SV., Nakamura M., Qudisia S., Siekkinen M., Smått JH., Peltonen J., Heino TJ., Hupa L., Vallittu PK. ***"Structural and elemental characterization of glass and ceramic particles for bone surgery"*** Dental Materials, Vol 37 (2021) 9, pp. 1350-1357, DOI: 10.1016/j.dental.2021.06.004
- VIII. Sirkiä SV., Siekkinen M., Qudisia S., Smått JH., Peltonen J., Hupa L., Heino TJ., Vallittu PK. ***"Physicochemical and biological characterization of silica-coated alumina particles"*** Dental Materials Vol 38 (2022) 2, pp. 1878-1885, DOI: 10.1016/j.dental.2022.09.012
- IX. Sirkiä SV., Qudisia S., Siekkinen M., Hoepfl W., Budde T., Smått JH., Peltonen J., Hupa L., Heino TJ., Vallittu PK. ***"Physicochemical and biological characterization of functionalized calcium carbonate"*** Materialia, Vol 28 (2023) DOI: 10.1016/j.mtla.2023.101742

International scientific conferences and meetings:

- X. ***"Influence of reaction products on the dissolution of bioactive glass particles"*** 26th International Congress on Glass (July 2022) Berlin, Germany – oral presentation.
- XI. ***"A dynamic solution for the dynamic body"*** Bioglass networking event (September 2022) Jena, Germany – oral presentation.
- XII. ***"Impact of common ions on in vitro dissolution of bioactive glass S53P4"*** 18th Conference of the European Ceramic Society (July 2023) Lyon, France – oral presentation.
- XIII. ***"Effect of ion concentrations and flow rate on bioactive glass dissolution in vitro"*** 33rd Annual Conference of the European Society for Biomaterials (September 2023) Davos, Switzerland – poster presentation.

2. Literature review

2.1 Biomaterials

A biomaterial is any implant or device of a biological or synthetic nature used to interact with the human body [45]. The properties needed for biomaterials are thoroughly determined, and the four following categories are characterised before implantation [46]:

1. **Biocompatibility:** An implant with living tissue contact cannot cause any harm to the surrounding tissue, i.e., the implant must be non-toxic, non-allergenic, and non-carcinogenic.
2. **Mechanical and physical properties:** Adequate mechanical and physical properties are needed to replace and restore tissue. Important properties are strength, hardness, wear resistance, and fatigue. For bone implants, sufficient porosity is also needed to match the porous structure of both cortical and cancellous bone.
3. **Chemical properties:** Chemical degradation of the material may influence the biocompatibility negatively.
4. **Manufacturing:** The manufacturing of the biomaterial should be of high quality and at a reasonable economical cost. Also, the finished products must be sterilisable.

For ideal implantable scaffolds used for bone regeneration, the following nine criteria must be fulfilled [47]:

1. Biocompatibility.
2. Chemical bond to host bone.
3. Sufficient porosity to allow vascularisation and bone ingrowth.
4. Same degradation rate as the regeneration rate of bone.
5. Proper surface for osteogenic cell attachment.
6. Ability to promote bone regeneration.
7. Similar mechanical properties as host bone.
8. Possible to be shaped to fill the implant site.
9. Potential to be commercially produced and be sterilisable.

Human bones are complicated biological systems, with vascularisation and increased porosity towards the centre [14]. Therefore, autologous bone grafts (autografts) are the most common procedure when filling bone cavities [48]. Autografts are bone tissue harvested and implanted in the same patient [49]. However, the supply is limited and using autografts for cavities

increases the risks by adding a surgical site and extending the surgical time [50]. Allografts, bone tissue harvested from one patient/cadaver and implanted in another patient, are also widely used as filler materials [51]. However, the risks associated with allografts include infections, rejections, and disease transmission, which are more common than risks with autografts [52]. Xenografts, i.e., grafts harvested from non-human species, are a third option for bone grafting [53]. However, xenografts carry the risk of zoonotic diseases [54], and no clinical standard is currently in use [55]. Synthetic materials are, therefore, also used for replacing hard tissues and restoring bodily functions [56].

Synthetic biomaterials can be divided into four groups: metals, ceramics, polymers, and composites [57]. Each synthetic biomaterial has advantages and disadvantages. The goal is to mimic the bone as closely as possible while fulfilling the previously mentioned properties and criteria. The desirable properties of synthetic biomaterials are their tuneable physicochemical properties and adjustable degradability [58]. For example, composites of polylactic acid (PLA) and hydroxyapatite (HA) degraded slower *in vivo* than pure PLA implants [59]. With its unique properties, bioactive glass is a relatively new synthetic material used as a grafting material [60].

2.2 Bioactive glass

Bioactive glass is a non-crystalline material able to bond to the bone while simultaneously dissolving over time and stimulating tissue growth [61]. As of 2023, a proposed updated definition of bioactive glass is “*a non-crystalline material at non-equilibrium that is intended to promote biological activity*” [62]. Bioactive glasses can be produced by either melting or using a sol-gel technique [63]. This thesis discusses only bioactive glasses produced by melting.

From the first bioactive glass developed in the 1960s, many different compositions have been studied to analyse their possible bioactivity. However, it has been found that glasses are only bioactive in a narrow compositional range. For example, the bone-bonding diagram for soda-lime-silica glasses with a fixed 6 wt-% P_2O_5 (as in 45S5) is given in Figure 2 [39]. The composition of the bioactive glass 45S5 is marked as B. The glasses in the other areas provide the following interactions: A = bone bonding, C = non-bonding due to too low reactivity, D = non-bonding due to the reactivity being too high, E = non-bonding due to a non-glass forming composition, and S = soft tissue bonding compositions. Only compositions in the A area are considered when developing new bioactive glasses based on the given oxides. Even though the P_2O_5 content varies from 6 wt-% for several new

compositions, the ternary diagram in Figure 2 can be used to illustrate composition differences. For example, bioactive glass S53P4 would be slightly above the B-point in the diagram [64]. S53P4 was developed at ÅAU in the 1980s and showed similar properties and bioactivity as 45S5 in initial *in vitro* and *in vivo* tests [65].

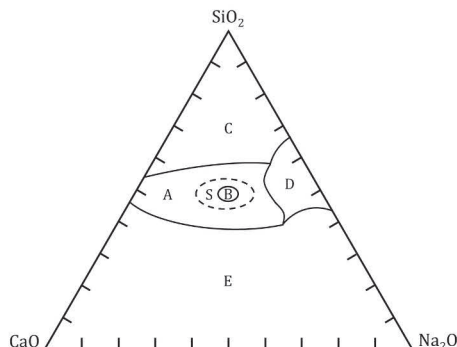


Figure 2. Bioactive glass phase diagram with a fixed 6 wt-% P_2O_5 . Bioactive glass 45S5 is found at B. Area A indicates bone bonding compositions, C = non-bonding due to too low reactivity, D = non-bonding due to too high reactivity, E = non-glass forming compositions, and S = soft tissue bonding [39].

Table 1 presents the oxide compositions of four silicate-based bioactive glasses. Of these compositions, 45S5 is the most studied and cited glass. However, the research at ÅAU has focused on S53P4. Today, 45S5 and S53P4 are clinically used, but comparisons between the glasses in the same indications are unavailable. 13-93 was also developed at ÅAU and showed good hot-working properties with similar bioactivity as S53P4 [66]. These properties imply that 13-93 could be applicable as scaffolds or fibres as the crystallisation risk would be decreased. Similarly, the ÅAU bioactive glass 1-98 also demonstrated high processing temperatures without crystallisation [67]. Only 45S5 and S53P4 will be discussed further in this thesis.

Table 1. The oxide composition (wt-%) of four silicate-based bioactive glasses

Bioactive glass	SiO ₂	CaO	Na ₂ O	P ₂ O ₅	K ₂ O	MgO	B ₂ O ₃
45S5	45	24.5	24.5	6	-	-	-
S53P4	53	20	23	4	-	-	-
13-93	53	20	6	4	12	5	-
1-98	53	22	6	2	11	5	1

Bioactive glass fulfils eight out of nine criteria discussed in 2.1 (Biomaterials) for implantable scaffolds and only misses out on similar mechanical

properties as host bone. Even though it has a compressive modulus of 60 GPa (45S5), compared to 7-30 GPa of cortical bone [68], bioactive glass is, like common glass, brittle and fails without warning. Additionally, sintering bioactive glass particles into porous scaffolds easily leads to crystallisation into a glass-ceramic, causing a loss of bioactivity [69]. For example, the T_g of 45S5 is 532°C, the onset of crystallisation temperature 655°C, and the crystallisation peak temperature 708°C [67]. These temperatures indicate a narrow range of sintering without crystallisation. Therefore, bioactive glass is currently not used in load-bearing applications due to the loss of bioactivity of sintered scaffolds and natural brittleness, and clinical utilisation is limited to particles.

2.2.1 Bioactive glass – aqueous solution reactions

Bioactive glasses start to react immediately upon contact with aqueous solutions. The reaction behaviour can be simplified into leaching, nucleation, and precipitation. The reactions can be highly impacted by changes in the environment or the material, as follows:

Physiological pH (7.40)

In physiological solutions *in vivo* or in *in vitro* solutions mimicking the body solutions, rapid reactions occur initially at the surface/solution interface. The reactions change the solution's pH and composition, and the material structure. Figure 3 shows the typical reaction behaviour of bioactive glasses in contact with physiological-like solutions. The following reactions take place [70]:

1. Ion exchange of the hydrogen ions in the solution and the network modifier ions (sodium and calcium) in the glass structure. During this stage, phosphate ions are also released. The decrease of hydrogen ions in the solution leads to a pH increase, and the increase of H^+ ions in the glass structure increases silanol groups (Si-OH) on the material surface.
2. The increase of the local pH and, consequently, a relative increase of hydroxide ions breaks the Si-O-Si bonds in the glass network and dissolves silicon species ($Si(OH)_4$) into the solution. After these reactions, more silanol groups are present on the glass surface.
3. Silanol groups condense on the glass surface, followed by a repolymerisation of a silica-rich surface layer. The gelatinous silica-rich layer functions as a nucleation site for apatite formation.

4. Calcium and phosphate ions left in the glass structure migrate through the silica-rich layer to the surface simultaneously as calcium and phosphate ions in the solution precipitate on the surface. An amorphous $\text{CaO-P}_2\text{O}_5$ -film forms on the surface.
5. The amorphous $\text{CaO-P}_2\text{O}_5$ -film crystallises to hydroxyapatite by incorporating hydroxyls and carbonates from the solution.

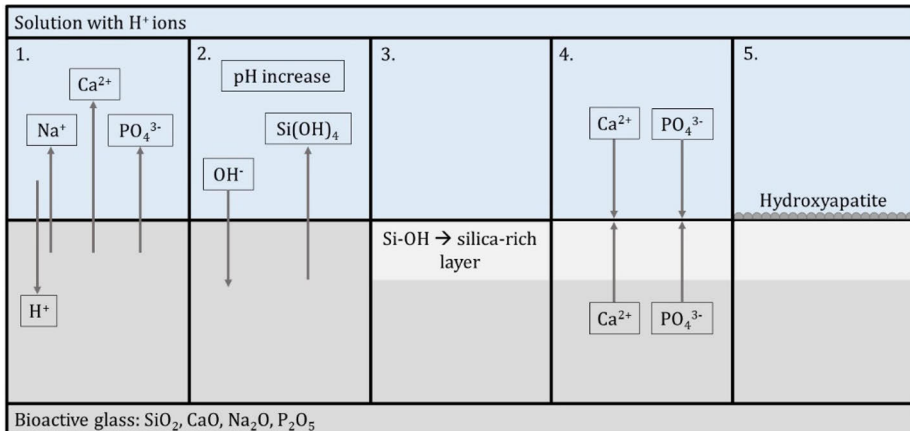


Figure 3. The five initial steps between the bioactive glass surface and the surrounding solution. (1) a rapid ion exchange between solution and material, (2) the increase of solution pH breaks the silicon bonds in the glass, leaving silanol groups on the surface, (3) the silanol groups condensate and repolymerise to a silica-rich layer, (4) calcium and phosphate ions from the bulk glass and solution precipitate on the surface and form an amorphous Ca/P layer, (5) the amorphous Ca/P layer crystallises to hydroxyapatite.

The five steps have been thoroughly investigated under common *in vitro* environments. Due to structural likeness, the crystallised HA layer can later bond to biological apatite *in vivo*. The biological reactions are not as studied but are proposed to be the following [71]:

6. Protein adsorption in the hydroxyapatite layer.
7. Stimulation of macrophages.
8. Osteoblast stem cell attachment to the surface.
9. Osteoblasts differentiate and proliferate.
10. The bone matrix generates.
11. The bone matrix crystallises.
12. New bone proliferates and regenerates.

Alkaline solutions

Increased pH, and consequently, an increase of OH⁻ concentration in solutions, favours the solubility of silicon from binary alkali-silicate glasses [72,73]. Similarly, silicon dissolves more rapidly when bioactive glasses react with solutions with increased pH [74]. Above pH 9, an excessive dissolution of silicon from the bioactive glass can be expected [75]. Simultaneously, calcium and phosphorus dissolve slower due to the decrease of available hydrogen ions for ion exchange, leading to a delayed apatite formation [76]. A physiological solution pH above 9 is unlikely. However, in some cases *in vitro*, the local pH inside a particle bed can increase to above 11 due to the rapid ion exchange [77]. Below pH 9, reactions are equivalent to the physiological pH reactions explained above. However, above pH 8, the polymerised silica-rich layer is more soluble than at a physiological pH, indicating thinner reaction layers on bioactive glass [78].

Acidic solutions

A decrease in the solution pH impacts the reaction behaviour of bioactive glasses. For example, hydroxyapatite developed on bioactive glass plates in solutions with a pH above 4. In contrast, the plates gradually became silica-rich when the solution stayed below pH 4 [79]. Thus, the release of alkali and alkaline earth ions from the bulk glass increased with decreasing pH. Even though the silica-rich layer functions as nucleation sites for calcium phosphate [80], the decrease in pH leads to increased solubility of calcium compounds, i.e., calcium phosphates [81]. In the human body, the pH around infected bone tissue can be as low as 5 to 6 [82]. Also, biodegradable polymer reactions can decrease pH [79]. An *in vitro* study with immersion solutions at pH 5 showed similar apatite formation, analysed with XRD, on bioactive glass 45S5 as in physiological pH [76]. However, FTIR analyses showed an increased peak of vibrations correlating to a crystalline apatite layer at pH 5 compared to the physiological pH indicating faster precipitation of Ca/P at the lower pH.

Glass composition

Commercial soda-lime glasses are inert in physiological solutions, while bioactive glasses dissolve due to their lower content of network formers. Melt-derived silicate-based bioactive glasses show varying degrees of bioactivity depending on their silica content. Table 2 shows the ion concentration changes after immersion of bioactive glass particles 45S5 and S53P4 in Tris buffer solution (Tris) and simulated body fluid (SBF) [83]. At 24 h, the degree of dissolution was higher for 45S5 as compared to S53P4.

However, at increased immersion time, a more consistent dissolution of S53P4 was reported [84].

Solution composition

Depending on the solution composition, the reaction behaviour changes. Calcium dissolves slower in SBF as compared to Tris (Table 2). Therefore, the weight loss of bioactive glass was slightly lower in SBF as compared to a Tris buffer solution [85]. Saturating a solution with silicon resulted in the formation of an amorphous alteration layer on immersed *International Simple Glass* (ISG), inhibiting silicon dissolution [86]. In addition, dissolution studies in unbuffered solutions, such as water, increased the pH quickly to above 10, and silicon was released more rapidly than in the Tris-buffered solutions [74].

Table 2. Ion concentration changes (mg/l) in Tris and SBF for bioactive glasses 45S5 and S53P4 as a function of time (100 mg glass/ml solution) [83]

Tris						
	Si		Ca		Na	
h	45S5	S53P4	45S5	S53P4	45S5	S53P4
1	17.5	9	41	18	69	34
4	23.1	13	53	22	91	50
24	37	27	93	65	176	124

SBF						
	Si		Ca		Na	
h	45S5	S53P4	45S5	S53P4	45S5	S53P4
1	19	11	35	4.9	66	30
4	22	17	43	16	173	37
24	34	26	72	43	124	127

Solution flow rate

Most *in vitro* studies on bioactive glass dissolution have been conducted in a static environment. As a result, the effect of flow rate on the dissolution has not been extensively investigated. However, introducing a dynamic *in vitro* environment also allows the investigation of increased or decreased solution flow rates. The flow rate inside the human body depends on location, health, and age [87]. Measuring the exact flow rate inside the bones is challenging, and non-invasive methods for precise measurements are still needed [88]. Ultrasound measurements can be used to estimate the blood flow inside the bones by measuring vessels outside of them. For 100 g of bone, a blood flow

rate of 5-20 ml/min has been given as an estimation [89]. On the other hand, ultrasound measurements of the common femoral artery gave a flow of around 280 ml/min and in the mandibular lingual vascular canal 9 ml/min [90,91]. Initial dynamic tests show that the reaction behaviour of bioactive glasses also depends on the flow rate. For example, slower flow rates increased ion concentrations and pH in the dynamic solution outflows from bioactive glass particle beds [44,92].

Other parameters that may influence the dissolution but are not discussed in this thesis include solution temperature, surface area to solution ratio, and particle bed dimension.

2.2.2 *In vitro* studies

One of the most important properties of bioactive glass is its bioactivity. In bone grafting, a bioactive material influences bone formation [93]. Assessing the bioactivity of bioactive glasses *in vitro* combines analyses of the pH changes in the fluid around the glass sample, the changes in ion concentrations in the solution, and layers formed on the glass surface [94]. Researching the bioactivity *in vitro* of potential bioactive glasses is generally done in static physiological-like solutions [95]. Also, implants with the ability to form apatite are evaluated *in vitro* according to ISO 23317 [96]. SBF was introduced as a solution for testing the bioactivity of bioactive glasses [97]. As shown in Table 3, SBF is a solution with ion concentrations close to human blood plasma. Additionally, SBF is Tris-buffered in the interval 7-9 [98], meaning that SBF can be pH adjusted to 7.40, similar to buffered blood [99].

Table 3. Ion concentrations (mM) in human blood plasma and simulated body fluid (SBF) as prepared by Kokubo and Takadama [97]

	Ion concentrations (mM)							
	Na ⁺	K ⁺	Mg ²⁺	Ca ²⁺	Cl ⁻	HCO ₃ ⁻	HPO ₄ ²⁻	SO ₄ ²⁻
Human blood plasma	142.0	5.0	1.5	2.5	103.0	27.0	1.0	0.5
SBF	142.0	5.0	1.5	2.5	147.8	4.2	1.0	0.5

Noticeably, Cl⁻ and HCO₃⁻ in SBF differ from the ion concentrations in the blood plasma. Other SBF compositions have been tested, but solutions with increased HCO₃⁻ are unstable, and calcium carbonates precipitate more easily in such solutions [100]. Due to the complexity and complicated preparation, the use of SBF has been questioned [101]. Tris as the buffer in SBF has also

been discussed and questioned, as it increased the dissolution and influenced the apatite formation of glass-ceramics [102]. However, no replacement of Tris has been found, as buffers such as HEPES [103], MOPS [104], and BES [105] also influenced the dissolution and apatite formation of glass-ceramics. Therefore, it was suggested that the reaction layers of biomaterials should not only be considered when investigating the reactivity [106]. The dissolution behaviour of bioactive glasses has been studied in simplified solutions, which do not contain initial common ions affecting or exhausting the reactions [107]. Tris-HCl buffer is free of the inorganic ions possibly interfering in the supersaturated SBF but is buffered similarly [108].

As explained above, the reaction behaviour differs depending on the solution's pH. Even though biomaterials are mainly implanted in locations experiencing a physiological pH, a local decrease of pH could occur at an infection [82] or due to acidic degradation of an implant [109], as well as in the oral cavity with the intake of acidic foods and drinks [110]. Additionally, an increase in local pH occurs at the solution/material interface due to the ion exchange between bioactive glasses and the surrounding solution [111]

Static environment

Previous studies on bioactive glass dissolution have primarily been conducted in static environments by immersing the material in a solution mimicking the body solution. ISO 23317 was developed for bioactive coatings on metal discs with a specific surface area (S_a) to volume (V_s) ratio calculated for dense samples ($V_s = 100 \cdot S_a$) [96]. The clinical use of bioactive glasses is still in particle form, and particles exhibit a larger relative surface area than dense plates. In 2015, the International Commission on Glass Technical Committee TC04 (Glasses for Medicine and Biotechnology) carried out a round-robin test for a unified method to test bioactive glasses *in vitro* [95]. The method uses various characterisations for evaluating the apatite formation on bioactive glasses by immersing 75 mg of 45-90 μm bioactive glass particles in 50 ml SBF for up to 4 weeks. The suggested method proved to be most suitable for studying bioactive glasses with a high surface area. However, the size range of bioactive glasses for clinical use varies, and the reaction behaviour of bioactive glasses is dependent on the surface area to volume ratio. Therefore, the total surface area of the particles to be tested must also be taken into consideration.

The immersion of a sample into a static solution gives an initial understanding of the reaction behaviour of the studied bioactive glass. A static environment can be considered well-controlled, and changes to different parameters can easily be done. However, immersion of bioactive

glass samples might lead to a quick saturation of the static solution. Consequently, the reaction behaviour of the immersed sample is impacted. Simultaneously, it is well known that the human body is a dynamic system where bone grafts are in contact with a flowing solution and not immersed in a static body solution.

Dynamic environment

Dynamic *in vitro* studies have been proposed to mimic the dynamic flow conditions in the human body [112]. Still, investigating bioactive glass reactions in a dynamic environment has been done to a limited extent. Initial tests have been done by replenishing a static solution [113], circulating the solution above a particle bed [114], or continuously feeding an as-prepared solution through the material [44]. Results of studies in these dynamic environments showed uniform reaction layers due to a more homogeneous environment than a static one. The continuous flow-through setup developed by Fagerlund et al [44] at ÅAU is presented in Figure 4. In this setup, bioactive glass particles are placed in a reactor, where a pump feeds a fresh solution continuously through the material bed.

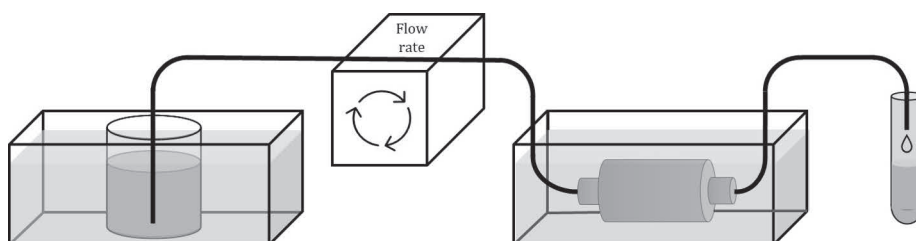


Figure 4. A continuous flow-through setup for experiments with bioactive glasses in a dynamic environment as developed by Fagerlund et al [44]. The figure is acquired from Publication I. ©Wiley

Studies utilising the continuous flow-through setup to study bioactive glasses are limited. Early tests developing the flow-through setup showed that changes to different parameters also changed the bioactive glass reactions in aqueous solutions. The tests continuously measured pH and ion concentrations for the initial 30 minutes to evaluate the method for studying the bioactivity through continuous dissolution [44]. For example, the solution pH increased rapidly as compared to the gradual pH increase in static solutions. An online ICP method concluded that the flow-through setup could be used to follow the ions released from bioactive glass, especially to compare different glass compositions [115]. Recent research at ÅAU has implemented the flow-through setup by focusing on specific parameters that

may influence the dissolution behaviour. Microspheres have been of interest due to their well-defined surface area. However, fine commercial S53P4 microspheres (45-90 μm) were almost inert, possibly due to compositional change during production [116]. It was possible to produce bioactive S53P4 and 13-93 microspheres with flame-spraying that showed similar surface changes as irregular-shaped particles [117]. Sintered bioactive glass scaffolds have also been studied, where the 50% porous scaffolds dissolved gradually in SBF while the necks were strengthened by Ca/P precipitation [118]. Changes to the fluid flow rate have been discussed, and it was concluded that the ion release was incongruent at a slow flow rate [92].

In addition, static-dynamic tests have been developed to combine the well-controlled static environment with the dynamic environment, mimicking the human body [102–105]. These studies were mainly conducted by placing a glass-ceramic scaffold in a solution volume corresponding to the volume flowing through the dynamic reactor for one day. In these studies, the solution was replenished each day. Further, *in vitro* test also indicates different cell tests, e.g., testing the cytotoxicity of newly developed bioactive glasses [119].

2.2.3 *In vivo* studies

The results from *in vitro* experiments can be used to estimate reactions *in vivo*. However, poor correlation between *in vitro* tests and *in vivo* results still causes the need for *in vivo* studies to fully understand the reaction behaviour of bioactive glass in contact with living tissues [120]. Compared to complex body solutions, *in vitro* tests are still made in simplified environments. For example, solutions may include ions comparable to the blood plasma (such as SBF) but incorporate no cells or proteins found in the blood. Therefore, it is still necessary to use *in vivo* models to evaluate the reactions of materials in a complex physiological environment [121]. Today, many research facilities are working with the 3R principle. The EU Directive 86/609 3R implies *replacing* animal tests with alternative methods, *reducing* the use of animals, and *refining* test procedures to minimise pain and discomfort [122]. In Finland, the Project Authorisation Board must authorise all projects that include *in vivo* tests [123].

Necessary *in vivo* models are chosen to resemble the human as closely as possible and include changes to time, tissue quality, and age [124]. Early *in vivo* studies concluded that bioactive glass formed a bond to the cortical bone after 6 weeks that was equal to or stronger than the host bone strength [125]. In contrast, SiO_2 control implants did not bond to the bone. The “*Oonishi model*” introduced a method to drill holes with a diameter of 6 mm in the

animal bones and fill them with bioactive glass particles after the bleeding was momentarily halted [126]. This method used an animal with several defects, where each defect was filled with particles of different sizes and shapes. It can be debated that multiple critical-sized defects could influence each other. Therefore, one implant per femur was used in a recent study to research possible new bioactive glasses showing promising results *in vitro* [127]. This thesis will not further discuss *in vivo* studies as the experimental part is only *in vitro*.

2.2.4 Clinical use of the bioactive glasses 45S5 and S53P4

Bioactive glass has been clinically used since 1985 when 45S5 was FDA-approved as an implantable monolith in the ear canal to restore hearing loss [128]. Due to the material degradation, the implant was found to experience fragmentation in the ear canal and was removed from the US market at the beginning of the 2000s [129]. In the late 1980s, a 45S5-based implant functioning as a strong base for dental implants was introduced and is still used today [130]. At the beginning of the 1990s, 45S5 particles were FDA-approved as a filler material for jaw and dental defects [131], and in 1995 they were awarded the CE mark for the European market [47]. 45S5 is also used to remodel maxillofacial defects and other non-load-bearing hard tissue corrections [132]. The bioactive glass S53P4 got the CE mark for orthopaedic corrections in 2006 and further FDA approval in 2008 [133]. Today, S53P4 is marketed as Bonalive® as particles or a premade putty and is used in, for example, trauma surgery, benign bone tumour surgery, and mastoid surgery [134].

Surgical treatment of osteomyelitis, i.e., infected bone tissue, leaves a cavity in the bone that is commonly filled with biomaterials presenting antibacterial properties [135]. A desired property of bioactive glasses is their antibacterial effects [136]. For example, bioactive glass S53P4 powder showed antibacterial properties against 17 anaerobic and 29 aerobic bacteria [137,138]. Therefore, bioactive glasses have been used as a treatment option for chronic osteomyelitis [139,140]. Bioactive glass S53P4 has shown a similar level of bone healing in cases with chronic osteomyelitis as autografts [141]. Furthermore, a 50-people study showed that treating chronic osteomyelitis with bioactive glass S53P4 decreased the overall medical costs by an average of 6573 €/patient compared to treatment with PMMA [142].

Apart from a filler material, bioactive glass 45S5 is also used as the active ingredient in certain toothpastes to treat dentin hypersensitivity [143]. In this case, the bioactive glass remineralises the tooth structure and blocks the

opened tubules in the enamel [144]. Recently, bioactive glass toothpaste with either fluoride or chloride ions to increase apatite precipitation entered the market with FDA approval in 2020 [143].

2.3 Elements in bioactive glass

In this thesis, the elements discussed are those in the bioactive glasses 45S5 and S53P4. The elements further discussed, silicon, calcium, sodium, and phosphorus, are all naturally abundant and found in the earth's crust [145] as well as in the human body [146,147].

Silicon

Silicon is naturally present in bones, ligaments, and other tissues in the human body [148]. Silicon plays an important role in new bone formation [149] and is involved in collagen synthesis and bone matrix mineralisation [147]. The dissolution of silicon from bioactive glasses refers to soluble silicon species (Si(OH)_4) released into the surrounding solution due to the increased local pH [70]. In cell tests mimicking the human body, Si(OH)_4 increased the collagen type 1 synthesis and enhanced differentiation of the osteoblasts [150]. Also, aqueous silicon was found to induce the precipitation of hydroxyapatite *in vitro* [151].

Calcium

99% of the calcium in the human body is found in either bones or teeth as hydroxyapatite [152]. Calcium deficiency highly affects bone structures and decreases bone mineral density [153]. Initial reactions between a bioactive glass and the surrounding solution cause a release of calcium ions (Ca^{2+}) into the solution. Ca^{2+} increases the mineralisation of the extracellular matrix *in vitro* by increasing the proliferation and differentiation of osteoblasts [154].

Sodium

Sodium ions maintain the internal homeostasis of the human body [155]. Consequently, most sodium is found in blood, particularly in plasma [156]. The solution, either physiological or simulated body fluid, already contains high levels of sodium ions (142 mM). Sodium is also present in bones, indicating that bone would work as a sodium reservoir [157]. In the initial reactions between bioactive glass and the surrounding solution, abundant sodium ions (Na^+) are released into the solution.

Phosphorus

Over 80% of the phosphorus in the body is found as hydroxyapatite in the bones and teeth [158]. Additionally, phosphorus is found on a cellular level in the human body in DNA, RNA, and ATP [159]. Inorganic phosphate stimulated the MGP for bone formation *in vitro* [160]. During bioactive glass dissolution, phosphorus is released into the solution as phosphate (PO_4^{3-}). Together with the released calcium, phosphorus will precipitate on the bioactive glass surface and later crystallise to hydroxyapatite, as explained in 2.2.1.

2.3.1 Dissolution products from bioactive glass

Early on, the dissolution of silicon and calcium ions from bioactive glasses was considered to play a key role in apatite formation [161]. Also, dissolved silicon and calcium from bioactive glass 45S5 were found *osteostimulative* in the range of 15-30 ppm Si and 60-90 ppm Ca [162]. However, it might be difficult to identify which reaction step impacts the dissolution due to a rapid initial release.

The change in solution pH and the following impact on the bioactive glass dissolution have been studied in detail. However, studies on the effect of the dissolution products from bioactive glass are limited and mainly focused on the biological and cellular responses in static environments. Biologically, the dissolution products from bioactive glasses are proposed to alter cell metabolic activity, spreading, and proliferation [163]. Dissolved ions from bioactive glass 45S5 improved bone regeneration by shortening the osteoblast growth cycle [164]. Ions dissolved from an experimental bioactive glass have also been found to mineralise human adipose stem cells in a hydrogel [165]. In addition, dissolution products from bioactive glass S53P4 have been shown to promote calcium phosphate mineralisation in an osteogenic medium [166]. However, one study concluded that dissolved ions from bioactive glass only stimulated bone formation if chemical supplements known to induce osteogenesis were present in the cell culture tests [167].

3. Experimental

This chapter presents the bioactive glasses and solutions, and the experimental methods used in the thesis. The thesis focused on understanding the impact of dissolution products on the reaction behaviour of bioactive glasses. Hence, the studied compositions were the two most common and most researched bioactive glasses, 45S5 (Publications I and V) and S53P4 (Publications II, III, IV, and V).

3.1 Bioactive glass

Table 4 presents the nominal compositions, in wt-% (mol-%), of the two bioactive glasses studied, the mass fraction of each element, and the reagents used for melting the glasses. The glasses were melted in-house for Publications I, III, IV, and V. The Belgian quartz sand (SiO_2) and analytical grade reagents (CaO , Na_2CO_3 , and $\text{CaHPO}_4 \cdot 2(\text{H}_2\text{O})$) were mixed in a container, added to a platinum crucible in an electric oven, and kept at 1360°C for 3 hours to fully melt. The melt was then cast to a bar in a graphite mould and annealed for 1 h at 520°C . Afterwards, the annealing oven was turned off, and the solidified glass bar was cooled overnight. The melting and annealing procedure was repeated once more to obtain homogeneity. For Publication II, Bonalive Biomaterials Ltd provided a wide particle size range of bioactive glass S53P4.

Table 4. The nominal glass compositions of 45S5 and S53P4 in wt-% (mol-%), the mass fractions, and the reagents used for glass preparation

	wt-% (mol-%)			
	SiO_2	CaO	Na_2O	P_2O_5
45S5	45 (46.1)	24.5 (26.9)	24.5 (24.3)	6 (2.6)
S53P4	53 (53.9)	20 (21.8)	23 (22.7)	4 (1.7)
	mass fraction			
	Si	Ca	Na	P
45S5	0.210	0.175	0.182	0.026
S53P4	0.248	0.143	0.171	0.017
<i>Manufacturer</i>	reagents			
	SiO_2	CaCO_3	Na_2CO_3	$\text{CaHPO}_4 \cdot 2(\text{H}_2\text{O})$
	<i>origin Belgium</i>	<i>Fluka</i>	<i>Sigma</i>	<i>Thermo Scientific</i>

Bioactive glass particles with a size range of 300-500 μm were chosen for all studies. The particles were produced by crushing the bioactive glass bar to particles with a puck and ring mill. Glass particles passing through a 500 μm sieve and staying on a 300 μm sieve were used. Similarly, the wide size range particles for Publication II were sieved to a 300-500 μm size range. Before analyses and dissolution studies, the particles were cleaned in acetone in an ultrasound bath to remove fine dust and powder attached to the surfaces that might disrupt the accuracy of the dissolution studies.

Scaffolds for Publication V were prepared by filling cylindrical graphite moulds of a diameter of 5 mm and height of 10 mm with crushed and cleaned bioactive glass particles (300-500 μm). The porous scaffolds were sintered for 90 minutes in nitrogen at 1030°C for 45S5, and at 720°C for S53P4. The temperatures were chosen according to previous studies to produce partially crystallised scaffolds with sufficient handling strength [168,169].

Melted bioactive glass, cleaned particles, and sintered scaffolds were stored in plastic bags in a desiccator until use.

3.2 Dissolution media

Table 5 presents the solutions used in the publications. Each solution was prepared in-house. Before preparation, beakers, flasks, and other glassware and tools were thoroughly cleaned with HCl, ethanol, and purified water to minimise contamination. Particular caution was taken with SBF preparations. Purified water (ELGA Veolia) was used as the solvent for all solutions. Solutions buffered with tris(hydroxymethyl)aminomethane (Tris) were prepared as a 50 mM base. The solutions were stored in a refrigerator until the experiments. The final solution pH was checked before each experimental run.

Table 5. Solutions used for the studies reported in the attached publications

	SBF	Tris (7.4)	Tris (9)	Tris (5)	HAc (5)	LA
Publication	I, II, V	I, II, III, IV, V	III	III	III	IV

Simulated body fluid (Publications I, II, and V)

Table 6 presents the reagents added to 800 ml of purified water to prepare 1 L of SBF. When not used, the reagents were stored in a desiccator to minimise exposure to air. The reagents were added separately and carefully to the solvent. The solution was continuously stirred throughout the preparation. Each reagent was completely dissolved before adding the following one. The HCl was added cautiously to minimise precipitation due to a rapid pH change.

Finally, separately dissolved Tris was slowly added to the solution. The solution was brought to 37°C in a water bath and kept for 4 hours at the temperature to thoroughly dissolve the reagents. Later, the pH of the solution was adjusted to 7.40 at 37°C.

Table 6. Reagents for 1L of SBF to give the solution composition according to Kokubo and Takadama [97] and the reagent for Tris buffer solutions

Reagent	SBF	Tris	Manufacturer
NaCl	7.996	-	VWR Chemicals
NaHCO ₃	0.350	-	J.T. Baker
KCl	0.220	-	Sigma Aldrich
K ₂ HPO ₄ ·3H ₂ O	0.228	-	Sigma Aldrich
MgCl ₂ ·6H ₂ O	0.305	-	Sigma Aldrich
1M HCl (aq)	35 ml	-	Sigma Aldrich
CaCl ₂ ·2H ₂ O	0.368	-	VWR Chemicals
Na ₂ SO ₄	0.071	-	Sigma Aldrich
Tris	6.057	6.057 ^{1L} 3.029 ^{0.5L}	Sigma Aldrich/Fluka

Tris (*Publications I, II, III, IV, and V*)

For Tris buffer, the Tris reagent in Table 6 was added to purified water, and the temperature was increased to 37°C in a water bath. After a couple of hours, the pH was adjusted to 9 or 7.40 with 1M HCl. Tris (5) was pH adjusted to 5 with 1M acetic acid (HAc) instead of HCl to avoid excessive chloride precipitation on the immersed glass samples.

Acetic acid sodium hydroxide (*Publication III*)

0.5 L of 0.1M HAc was prepared by adding 3 ml of HAc (J.T. Baker) to 450 ml of purified water. The solution was later pH adjusted to 5 with 1M NaOH at 37°C.

Lactic acid (*Publication IV*)

35 ml of 85% DL-Lactic acid (Sigma) was added to 965 ml of purified water to prepare 1 L of 0.4M LA (pH 2).

3.3 Dynamic environment

Publications I, II, IV, and V were conducted in a dynamic environment. For a single-pass continuous flow-through setup, the reactor was connected through a thin thermoplastic tube (Tygon®) to a peristaltic pump (Ismatec IPC High Precision Multichannel Pump) feeding the solution. Figure 5 shows the reactor parts and explanations. The bioactive glass particles were placed in the inner compartment. For Publication V, sintered scaffolds, crushed sintered scaffolds, or crushed particles were used. Filter papers prevented the particles from flowing with the solutions to the thin tubes and from causing blockages.

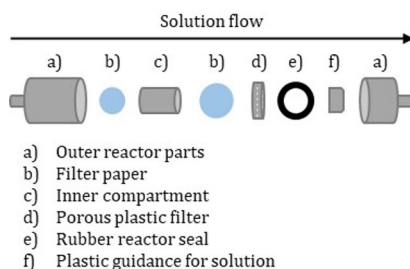


Figure 5. Reactor parts of a single-pass flow-through reactor for experiments in a dynamic environment.

3.3.1 Cascade reactor setup

In the dynamic continuous flow-through setup, a three-step cascade reactor was utilised. The cascade was inspired by a standard cascade reactor used to analyse the steady-state growth kinetics of microorganisms [170]. In this work, up to three reactors were coupled in series, as seen in Figure 6. This experimental setup allowed the investigation of the solution outflows from each reactor, i.e., the solution inflows to the next reactors. The cascade enabled the examination of differences in the reactions of the particles in the three reactors.



Figure 6. A cascade reactor setup with three reactors coupled in series. The solution flows from left to right.

The particles in the first reactor were assumed to mimic the outer part of an implanted particle bed with the first solution contact. In contrast, the particles in the second and third reactors were supposed to simulate

particles inside a porous particle bed where the solution flows after reacting with the outer particles. The reactions, such as the increase of pH and ion concentrations, occurring in the first reactor were assumed to influence the reactions in the consecutive reactors.

For Publications I, II, and IV, 210 ± 10 mg of bioactive glass particles were placed in each reactor. The peristaltic pump continuously fed the solutions to the cascades with either 0.2 ml/min (Publications I, II, IV, and V) or 0.04 ml/min (Publication IV). These rates led to a total solution of 288 ml or 57.6 ml passing through the reactors each day. The solution outflow was collected continuously throughout the experimental time. The dynamic experiments were conducted for up to 3 weeks (Publication V), 1 week (Publication I), 120 h (Publication II), and 24 h (Publication IV).

3.4 Static environment

Immersion in Publication III were conducted in a static environment, while a static environment was used as a reference for Publication IV. In all static *in vitro* experiments, the theoretical surface area of glass particles to solution volume ratio was around 0.4 cm^{-1} . This ratio was calculated by assuming spherical particles with an average diameter of 400 μm . However, the actual surface area to solution volume ratio was lower, as suggested by the irregular particles and the measured particle size distribution, giving an average ratio of 0.33 cm^{-1} (see 4.1). In the conventional static experiments, 30 ml of the solution was poured into polypropylene centrifuge tubes and the temperature was increased to 37°C before adding 210 ± 5 mg of bioactive glass particles. The static immersions were done in a shaking incubator (Stuart Orbital Incubator SI500) set at 37°C and rotated at 100 rpm.

In Publication III, the supernatants were extracted at 24 and 72 h for reuse as immersion solutions with unreacted particles. As small samples of the solutions were extracted for ion analysis, the mass of unreacted glass particles was 202 ± 3 mg in 28.5 ml of the extracted solutions to keep the surface area to solution volume ratio constant. The bioactive glass particles were immersed for 120 h in Publication III and 24 h in Publication IV.

3.5 Analyses

Changes to the solutions and bioactive glass particles were analysed as functions of time. Bioactive glass/solution reactions occur rapidly upon contact. Therefore, solution collections and measurements were conducted more frequently at the beginning of the experiments.

3.5.1 Solution pH

The pH (Mettler Toledo SevenEasy or VWR pHenomenal pH 1100 L) of the collected outflows from the dynamic experiments and the supernatant solutions in the static experiments were measured at either room temperature (Publications I, II, and V) or 37°C in a water bath (Publications III and IV). Before each run, the pH-electrode was calibrated with buffer solutions (4.01, 7.00, and 9.21, VWR/Fluka/Merck). The solution pH was measured directly in the collected outflow. The supernatant pH was measured close to the particle bed without the electrode touching the particles. The pH of a supernatant solution increases the closer to the particle bed it is measured [114]. The reference solution pH was also measured before and after each experimental run.

The solution pH varies with the temperature. An increase in temperature decreases the pH. Therefore, the pH values measured at room temperature were calculated into pH at 37°C according to Equation 1. Equation 1 is based on the Tris buffer solution [171]. The pH of SBF was also converted with the same equation. The equation was verified by measuring the pH of Tris and SBF solutions in a water bath in the 20-45°C temperature range.

$$pH_{37} = pH_{measured} - (0.027 * (37 - T_{measured})) \quad (1)$$

3.5.2 Ion concentrations

Ion concentrations were analysed with an inductively coupled plasma-optical emission spectrometer (ICP-OES, Optima 5300 DV; PerkinElmer, Waltham, MA). For dynamic tests, 1 ml of the collected outflows was diluted with 9 ml of ultrapure water before analysis. An aliquot (1 ml) from the supernatant solution was similarly diluted before analysing the solutions from the static tests. The extracted aliquot was not replaced with a new solution, but the decrease in total immersion volume was considered for further calculations.

The ICP-OES was calibrated with commercial standard solutions (Spectrascan) of 1, 5, and 20 ppm silicon, calcium, sodium, and phosphorus. The calibration was verified by measuring the 1 ppm standard before each run and after every 60 samples. The background was measured simultaneously. The presented results are background corrected. Each reported measurement point represents three parallel samples analysed 3-5 times with the ICP-OES.

Aliquots were extracted multiple times during the static immersions, changing the surface area to solution volume ratio. The reported values for Publication III are, therefore, normalised according to Equation 2 [172]:

$$C_{i,j}^* = C_{i,j} + \frac{V^a}{V^s} \sum_j^N C_{i,j-1} \quad (2)$$

where $C_{i,j}^*$ is the normalised ion concentration of element i at time point j (mg/l), $C_{i,j}$ is the measured ion concentration with ICP-OES of element i at time point j (mg/l), V^a is the volume of the aliquot (ml), V^s is the volume of the immersion solution (ml), and $C_{i,j-1}$ is the measured ion concentration of element i at time point $j-1$.

3.5.3 Particle analyses

Particle size distribution

The particle size distribution was measured with a laser diffraction system coupled with a wet dispersion unit (Malvern Panalytical Mastersized 3000) for each new crushed, sieved, and cleaned batch of 300-500 μm bioactive glass particles. Bioactive glass particles were added to distilled water until the measuring device sensed particles in the flowing solution. Five parallel measurements were done. The irregular-sized particles were measured according to their volume and compiled to their corresponding spherical diameter with the software.

Surface characterisation

Surfaces and cross-sections of particles were investigated with a scanning electron microscope (SEM, Leo Gemini, Carl Zeiss), and the reaction layers were analysed with energy-dispersive X-rays (EDX, Thermo Scientific UltraDry, Thermo Scientific) coupled with the SEM. After the dissolution, the bioactive glass particles were washed with ethanol to stop the reactions and dried in a 40°C oven overnight. For surface images, the particles were directly analysed with the SEM. For particle cross-sections, the particles were embedded in epoxy resin (polyester resin with organic peroxide catalyst) until hardened and later ground and polished with abrasive paper and ethanol to reveal the cross-sections. SEM images were taken with different magnifications over the particles, but EDX analyses were focused on randomly selected particles with visible changes to the surface or cross-section. The elements silicon, calcium, sodium, phosphorus, and oxygen in the bioactive glasses were analysed using SEM-EDXA.

4. Results and discussion

4.1 Particle and scaffold characterisation

Figure 7 a) shows particle size distributions for the samples studied in Publications I-IV. The SEM image in Figure 7 b) shows unreacted particles used in Publication IV. Figures 7 c) and d) give the surface of a sintered 45S5 scaffold in two magnifications (Publication V). Even though the glass particles were sieved to 300-500 μm , the measured particle size range was larger. This is partly because the measurements give the average diameter based on measuring the particle volumes and estimating spherical particles and partly due to elongated irregular particles passing through the 500 μm sieve and contributing to an overall increased particle size range. The share of particles in the sieved size range was 59% in Publication I, 52% in Publication II, and 69% in Publications III and IV. The specific surface area of the particles was 4.686 m^2/kg (Publications III and IV). The surface of the sintered 45S5 scaffold (Figure 7 c) shows somewhat rounded particles, compared to the sharp edges of crushed particles (Figure 7 b). Figure 7 d) shows part of the surfaces of two sintered particles with a surface roughness suggesting partial crystallisation.

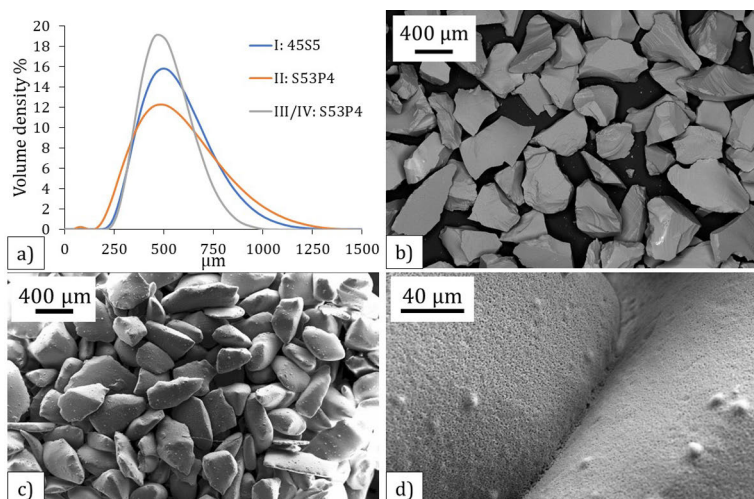


Figure 7. a) Particle size distribution of 45S5 and S53P4 particles, b) surface of unreacted S53P4 particles, c) and d) surface of a sintered 45S5 scaffold. Figures reproduced from Publications I, II, III, IV, and V ©Wiley, Elsevier, Springer.

SEM images of the scaffold cross-sections (Figure 8) show the extent of surface crystallisation caused by the sintering of the S53P4 scaffolds. Figure 8 b) shows the grey crystalline structure and the black amorphous structure.

The extent of surface crystallisation caused by the sintering was estimated to be 58 vol-%. In contrast, the sintered 45S5 scaffolds consisted of fine-grained crystals throughout a residual amorphous phase.

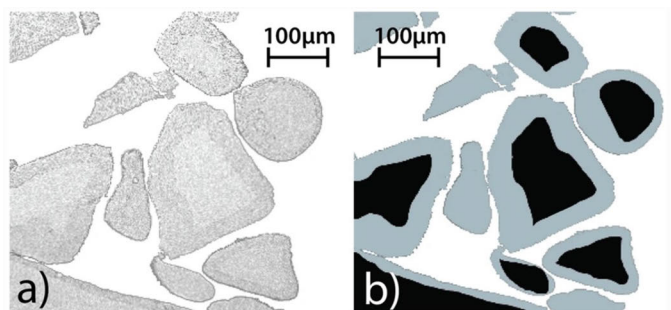


Figure 8. Cross-section of an as-prepared sintered S53P4 scaffold. Manipulated figure (b) shows the amorphous structure in black and the crystallisation in grey. Publication V ©Springer

4.2 Dynamic dissolution

Figure 9 compares the silica-rich layers formed on particles after 24 h in the dynamic (0.04 ml/min, 1st reactor) and static LA with an initial pH of 2 (Publication IV). Compared to the static environment, more homogenous and thicker layers formed in the dynamic environment. Even though the static solution was agitated throughout immersion, the solution environment was not homogeneous in the particle bed. Thus, the static *in vitro* experiments likely did not give a comparable environment to the dynamic human body.

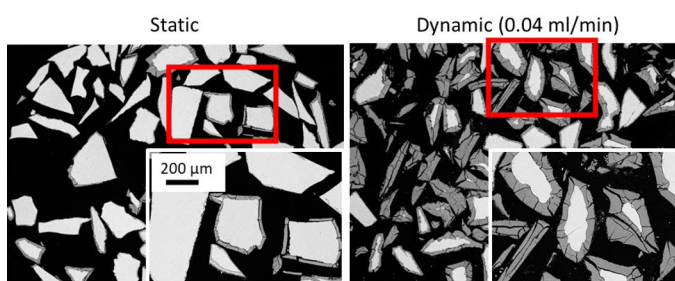


Figure 9. SEM images of S53P4 particle cross-sections after 24 h in static (left) and dynamic (right) 0.4M LA environments. Publication IV ©Springer

4.2.1 Comparison of 45S5 and S53P4 dissolution

In the dynamic environment, silica-rich layers were visible after 4 hours of flow-through of Tris and SBF (7.4) on 45S5 particles in most reactor combinations (see Publication I). In SBF, the third reactor particles showed

uneven sporadic reaction layers typical for the initial release of calcium, sodium, and phosphorus from the glass. Similar progress at 4 h of the reaction layer forming trend was not seen on bioactive glass S53P4 particles (see Publication II), indicating an overall slower reaction behaviour compared to 45S5. Also, the 45S5 particles in SBF had around 10% less silica analysed in the silica-rich layer than in Tris. The apatite formation has been suggested to be slower in SBF than Tris [173].

Figure 10 shows SEM-EDXA of selected bioactive glass S53P4 particles after 24 h of continuous (0.04 ml/min) flow-through of Tris (7.4) for the reactor series (Publication IV). The SEM images do not show apparent differences between the layer structures on particles in the three reactors. In all reactors, the particles had formed a silica-rich surface layer with some Ca/P, given by the EDX analyses.

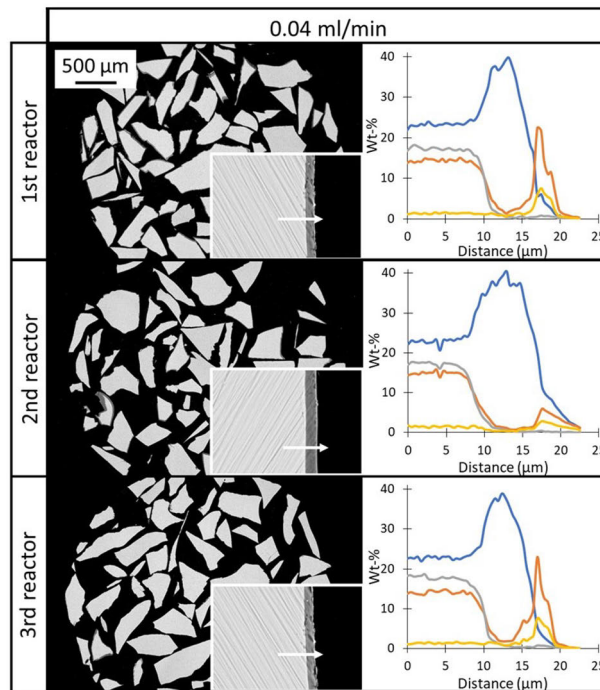


Figure 10. SEM-EDXA of reacted S53P4 particles after 24 h of dissolution with 0.04 ml/min Tris for the three reactors. Publication IV ©Springer

Figure 11 shows the pH changes in the outflows for the first 48 h of cascade reactor experiments conducted in Tris (left) and SBF (right) with 45S5 and S53P4 bioactive glass particles (Publication II). The pH decreased and stabilised slightly above the solutions' reference values at prolonged experiments. Importantly, the pH stayed consistently between the buffering

capacity of Tris (7-9). This indicates that the pH remained below the levels of increased silicon dissolution [75].

In all cases, the pH increased initially to 7.6-8, where the highest increase was always noted in the outflow of the third reactor. The pH change was initially slightly higher for 45S5 than S53P4. The pH increased to a lower extent in SBF than in Tris. Interestingly, a second increase in SBF pH was seen with multiple reactors in the setup. The second increase was measured around 8 h with 45S5 and 24 h with S53P4. This was assumed to correlate with the known lower bioactivity of S53P4 compared to 45S5 [84]. These results imply that the ion exchange will proceed in the second and third reactors when the reactions have started to slow down in the first reactor as the solution is continuously fed through the system.

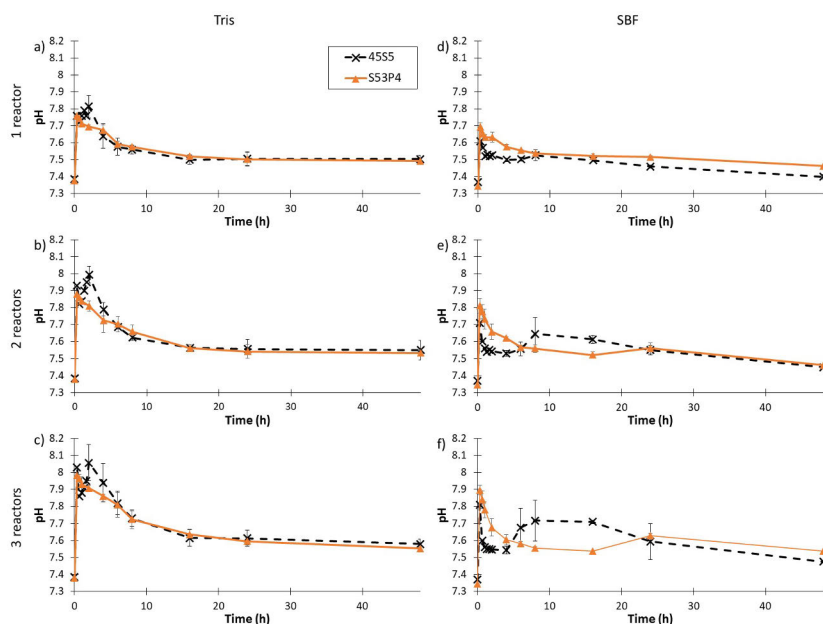


Figure 11. The pH changes as a function of time for dynamic experiments conducted in Tris (left) and SBF (right) with 45S5 and S53P4. Publication II ©Elsevier

The ion concentration changes in Tris (7.4) for each reactor with 45S5 and S53P4 for 120 h are seen in Figure 12 (reworked from Publications I and II). The changes were calculated from the measured values in the outflows subtracted with the measured values of the inflows to the reactors, i.e., the outflows from the previous reactors. The figure shows that most of the dissolution into Tris occurred from the first reactor. Also, the dissolution from the second and third reactors was equal. It can be assumed that the

dissolved ions in the first reactor decreased the ion release in the second reactor. Consequently, as the dissolution did not increase dramatically in the second reactor, the dissolution from the third reactor was still mainly influenced by the dissolved ions from the first reactor. As seen in Figure 10, decreased dissolution did not inhibit the formation of reaction layers on the particles. Thus, it is proposed that the layers formed on the second and third reactor particles were not limited to the dissolution from the particles in respective reactors. On the other hand, the dissolved ions from the previous reactors contributed to the layer growth.

These results also show that the release of silicon differed between 45S5 and S53P4 in the first reactor. Silicon released quickly from 45S5 and stabilised around 20 mg/l after 24 h of dissolution. In contrast, silicon was released at a higher rate from S53P4 for the first couple of days and stabilised around 20 mg/l after 72 h of dissolution. Static dissolution has shown that S53P4 initially dissolved slower than 45S5 but dissolved more consistently over two weeks [83,84]. This can be explained by S53P4 containing 53 wt-% SiO₂ compared to 45 wt-% in 45S5, i.e., 8 wt-% more network formers which consequently increases the chemical durability of the glass. However, these bioactive glasses are still highly reactive materials and gradually dissolve over time.

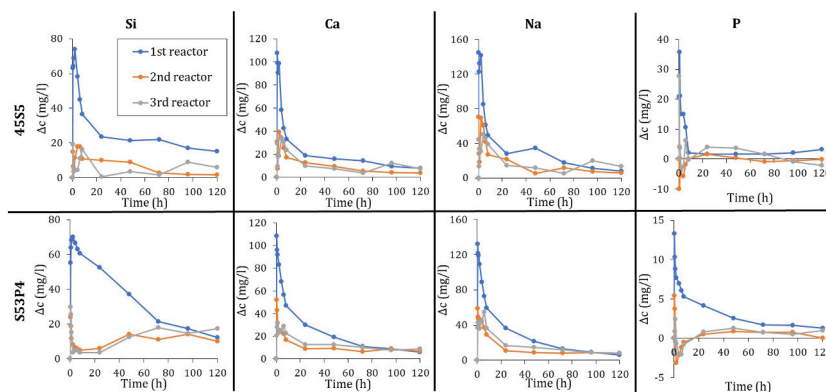


Figure 12. Change of ion concentrations in the solution (outflow-inflow) after each reactor in the cascade for dynamic (0.2 ml/min) experiments conducted in Tris with 45S5 and S53P4. Reworked from Publications I and II.

SBF contains calcium and phosphorus. Thus, Ca/P precipitation is not limited to the released calcium and phosphorus from the bioactive glass into the solution, as in Tris. Figure 13 shows the calcium and phosphorus concentrations in the SBF solution outflows of cascade reactor experiments

with 45S5 and S53P4 for 120 h of dissolution (reworked from Publications I and II).

The figure shows an initial increase of calcium and phosphorus in the outflows for the first hour of flow-through. Noticeably, the calcium concentrations from 45S5 have a similar second increase as seen in the pH (Figure 11), correlating with the ion exchange between hydrogen and calcium ions. For S53P4, the calcium concentrations decreased towards the reference solution without a similar second increase as for 45S5. This suggests a more consistent ion exchange between S53P4 and the SBF throughout the experiments; the second pH increase for S53P4 was also not as pronounced as for 45S5. In contrast, the phosphorus concentration decreased quickly below the reference solutions' values after an initial ion release peak, indicating phosphorus precipitation in the reactors. The lowest phosphorus concentrations were measured in the outflow after three reactors. This implies that most phosphorus would have precipitated in the last reactor. Thus, the dissolved phosphorus in the first reactor promoted precipitation in the second and third reactors. Overall, these results suggest that the phosphorus concentration is the limiting factor of Ca/P precipitation.

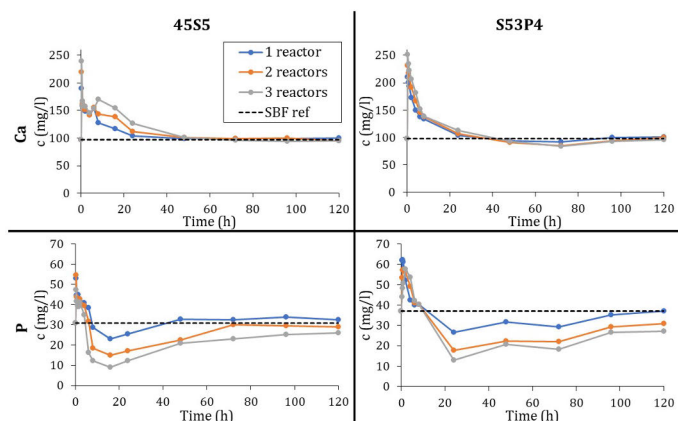


Figure 13. The concentration of calcium and phosphorus in the SBF solution outflows for dynamic (0.2 ml/min) cascade reactor experiments with 45S5 and S53P4. The dotted line indicates Ca and P concentrations in the reference SBF. Reworked from Publications I and II.

The thickness of silica-rich layers and precipitation of Ca/P increased in both Tris and SBF with the flow-through time. Figure 14 shows SEM-EDXA over selected bioactive glass 45S5 and S53P4 particles in experiments after 72 h with Tris and SBF for each reactor in the series (reworked from Publications I and II). The faster formation of the silica-rich layer providing nucleation

sites for apatite likely explains the difference in the apatite growth in the two solutions (see Publications I and II). The figure shows that a pure Ca/P outer layer developed only in SBF. In Tris, the precipitation from the solution was minor. Thus, the released Ca and P species were assumed to form a mixed layer of silica and Ca/P. Such a mixed layer was typically analysed on 45S5 particles. In contrast, a similar mixed layer structure was not seen on particles exposed to SBF. This suggests that the bulk glass dissolution decreased in SBF as a function of time, but precipitation occurred due to calcium and phosphorus ions in the surrounding solution. The Ca/P-layer has earlier been proposed to slow down the dissolution [174].

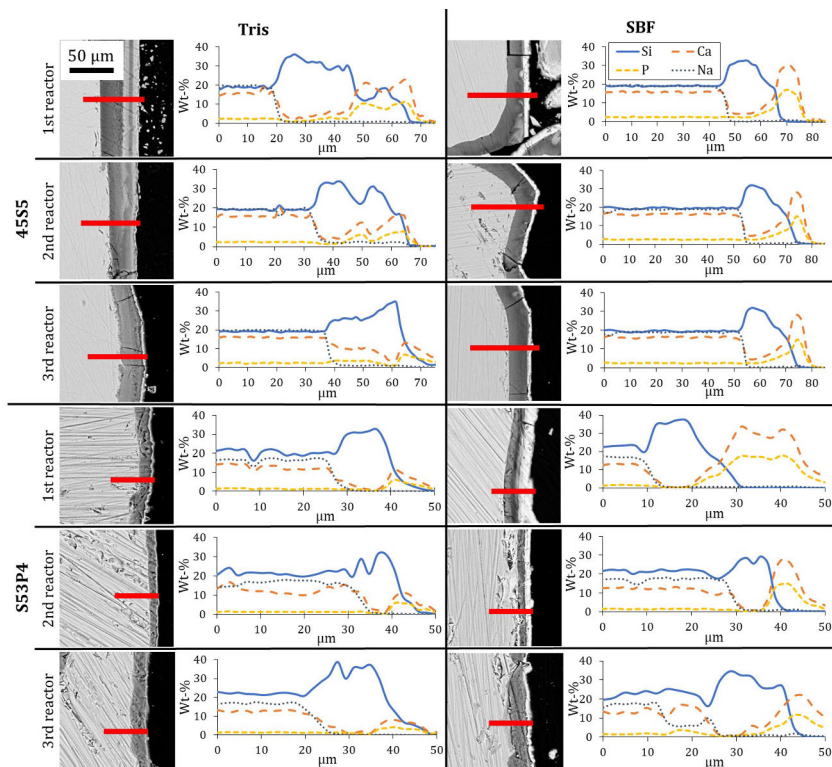


Figure 14. SEM-EDXA of reacted 45S5 and S53P4 particles after 72 h of continuous flow-through (0.2 ml/min) of Tris and SBF in each reactor in the series. Reworked from Publications I and II.

4.2.2 Effect of fluid flow rate on S53P4 dissolution

Table 7 presents the ion concentrations (mg/l) released from S53P4 in the LA outflows for 0.2 and 0.04 ml/min flow rates after each reactor combination (Publication IV). Also, the ion concentrations at 24 h of immersion in static LA are indicated. Calcium, sodium, and phosphorus

dissolved from S53P4 to LA at elevated levels. The high release of these ions was due to the low pH (2) and, consequently, a high concentration of hydrogen ions available for ion exchange. This suggests a higher alkali and alkaline earth ion dissolution at implant sites experiencing a local pH decrease due to an infection or in composites with an acidic degradation.

The silicon release was much lower compared to the buffered Tris and SBF. Comparing the concentration differences between the outflows and inflows from each consecutive reactor shows similar dissolution levels from each reactor. Accordingly, the dissolution of silicon from the second and third reactors was consistently equal to that from the first reactor. Decreasing the flow from 0.2 to 0.04 ml/min increased the other ion concentrations 4- to 7-fold, which is proportional to the flow rate and suggests similar dissolution in both flow rates.

Table 7. Ion concentrations in the outflows from each reactor for dissolution of S53P4 in 0.4 M LA using the flow rates of 0.2 and 0.04 ml/min. 24S gives the ion concentrations after static immersion after 24 h. Publication IV

		Si						Ca					
		0.2 ml/min			0.04 ml/min			0.2 ml/min			0.04 ml/min		
h		(1)	(2)	(3)	(1)	(2)	(3)	(1)	(2)	(3)	(1)	(2)	(3)
1		2.2	4.4	6.4	16	32	49	211	409	582	1489	2640	3627
2		2.1	4.3	5.8	10	20	31	138	283	399	863	1659	2475
4		2.2	4.3	6.2	10	18	27	103	206	296	585	1131	1673
6		2.5	4.6	6.5	10	19	26	86	169	248	469	909	1314
8		2.8	4.8	6.9	11	20	27	71	143	209	402	809	1142
24		3.8	6.8	9.8	16	25	34	32	64	91	171	330	512
24S		3.2						154					
		Na						P					
		0.2 ml/min			0.04 ml/min			0.2 ml/min			0.04 ml/min		
h		(1)	(2)	(3)	(1)	(2)	(3)	(1)	(2)	(3)	(1)	(2)	(3)
1		233	456	654	1625	2869	3963	25	49	71	187	319	449
2		152	316	446	932	1760	2614	16	35	48	109	226	338
4		112	231	334	630	1201	1771	12	25	37	74	142	210
6		94	190	278	504	981	1439	10	21	31	59	114	168
8		79	162	234	434	857	1226	9	18	26	51	102	144
24		35	70	104	202	363	552	4	8	12	22	42	65
24S		269						11					

The ion concentrations dissolved in Tris (7.4) were also higher for the slower flow rate. However, the concentration differences between Tris fed with two flow rates were smaller than for LA (see Publication IV). For the flow rates 0.2 and 0.04 ml/min, the volume of solution flowing through the system varied significantly, from 2.4 ml for the slower flow to 12 ml for the faster flow for one hour. The significant difference in the solution volume makes a

direct comparison between the glass dissolution at the two flow rates difficult. For an easier comparison of the impact of dissolved ions from each reactor on the dissolution mechanism, the normalised surface-specific mass loss rate (NR_i) was calculated according to Equation (3) [44]

$$NR_i = \frac{C_i}{f_i \left(\frac{SA}{F}\right)} \quad (3)$$

where C_i is the ion concentration of element i (mg/l), f_i is the mass fraction of element i in the unreacted glass (unitless), SA is the total initial surface area (m^2), and F is the flow rate of the dynamic solution (m^3/s). The total initial surface area was calculated using the specific surface area analysed during particle size distribution ($4.686 m^2/kg$) and the mass of S53P4 particles in each reactor (210 mg). This gave a total unreacted surface area of $0.00098 m^2/reactor$.

Figure 15 shows the calculated reactor-specific NR_i for dissolution of S53P4 into Tris (7.4) for 0.2 and 0.04 ml/min. The elements initially dissolved incongruently from the first reactor with the 0.2 ml/min flow rate. Calcium, sodium, and phosphorus were released similarly from the glass particles, while silicon dissolved at a slower rate. At around 24 h, the mass loss rate from the surfaces was equal, and the elements released more congruently.

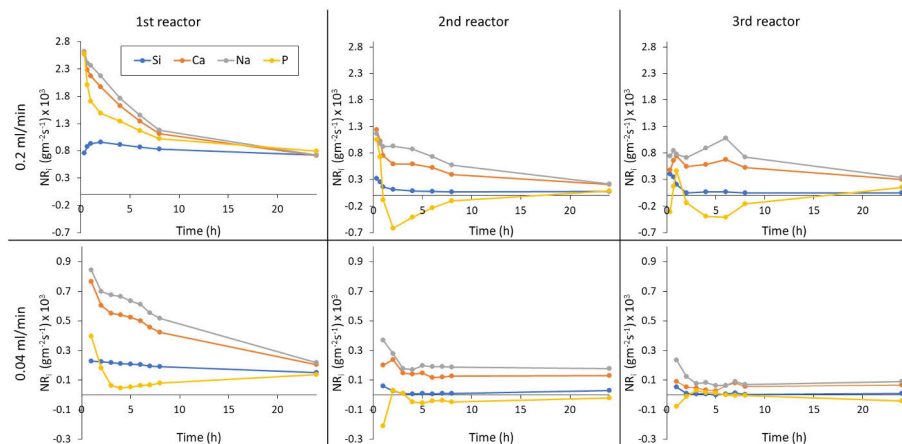


Figure 15. Normalised surface-specific mass loss rate of elements from S53P4 to Tris (7.4) for the three reactors. Publication IV ©Springer

The mass loss rate from S53P4 decreased with the flow rate. For 0.2 ml/min, the release of sodium was around 120 mg/l from the first reactor at 1 h. For the slower flow rate (0.04 ml/min), an equal mass loss rate would mean around 600 mg/l from the first reactor. However, the measured

concentration was about 210 mg/l. This difference indicates that the flow rate highly influenced the dissolution of bioactive glasses in solutions with a pH of around 7. Similarly, the dissolution products in the solution also decreased the mass loss rate, as seen for the second and third reactors in Figure 15. This implies that particles inside a particle bed react slower than the exterior particles. Whether the location of individual particles in a particle bed would partly explain remnants reported in long-term clinical studies is unclear [175,176].

Similar calculations for surface-specific mass loss rate conducted with LA (see Publication IV) suggested similar dissolution rates of calcium, sodium, and phosphorus from S53P4 particles regardless of reactor or flow rate but a slower silicon dissolution rate. Thus, a lower pH did not impact the dissolution behaviour of bioactive glasses as much as a physiological-like pH.

4.2.3 Effect of initial pH on S53P4 dissolution

Figure 16 shows the pH change in the solution outflows for the two flow rates of Tris (above) and LA (below) with an increasing number of reactors loaded with S53P4 particles (Publication IV). The figure also includes results from the dissolution of S53P4 particles in static Tris (Publication III) and static LA as a comparison. The graphs do not include deviations, as most were below ± 0.05 pH units (highest ± 0.12 pH units). In all dynamic cases, pH initially increased rapidly and slowly decreased towards the reference solutions' values.

The pH was consistently highest in the outflows with the slower flow rates and third reactor. However, the measured pH of Tris was always within the buffering capacity range of 7-9, as in the dynamic 0.2 ml/min flows of Tris and SBF through 45S5 and S53P4 particles in Publications I and II. The solution fed through the S53P4 using the slower flow rate led to higher concentrations of released calcium and sodium ions, thus explaining its higher pH (Publication IV). After 24 h, the pH of static Tris in contact with S53P4 particles approached the same value as the dynamic Tris solutions fed through the particles using both flow rates. On the other hand, the pH of static LA in contact with S53P4 particles increased rapidly close to the outflow pH from the third reactor for the flow rate of 0.04 ml/min at 24 h. This increase correlated with the higher ion exchange at the glass surface at a lower pH.

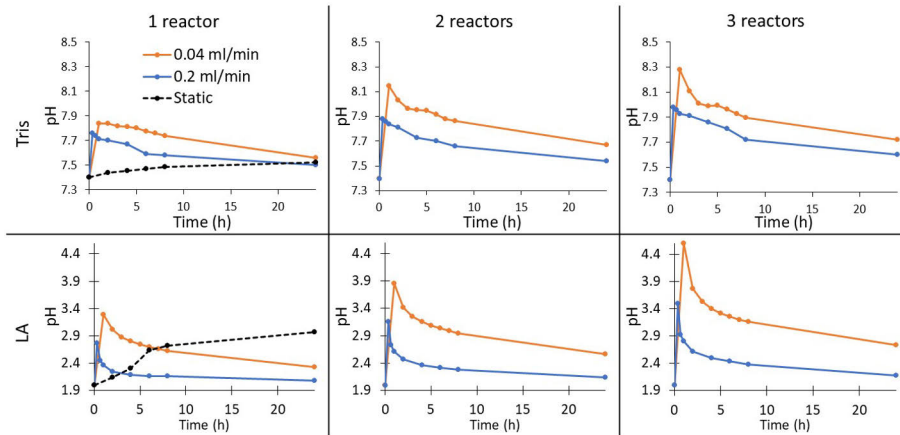


Figure 16. pH of Tris and LA (0.2 and 0.04 ml/min) outflows from an increasing number of reactors loaded with S53P4 particles for 24 h. pH of the static solutions are shown in the 1st reactor graphs. Publication IV ©Springer

Figure 17 shows the SEM-EDXA of bioactive glass S53P4 particles after 24 h of dynamic LA for the two flow rates of 0.2 and 0.04 ml/min (Publication IV). All particles had developed a silica-rich layer due to the extensive ion exchange. The layers were similar, and no significant differences in the layer compositions, regardless of fluid flow rate or reactor in which the particles had been exposed, were analysed. The silica-rich layer provided nucleation sites for calcium and phosphorus precipitation in the physiological pH range. However, the local pH stayed acidic throughout the experiment when LA was continuously fed through the reactor system. Ca/P did not precipitate as the solubility of calcium compounds increases with decreasing pH [81]. In contrast, LA chelates with the released calcium and phosphorus, further hindering Ca/P precipitation [177]. Whether the chelates would influence or interfere with hydroxyapatite formation in composites of PLA-based polymers and bioactive glasses is unclear.

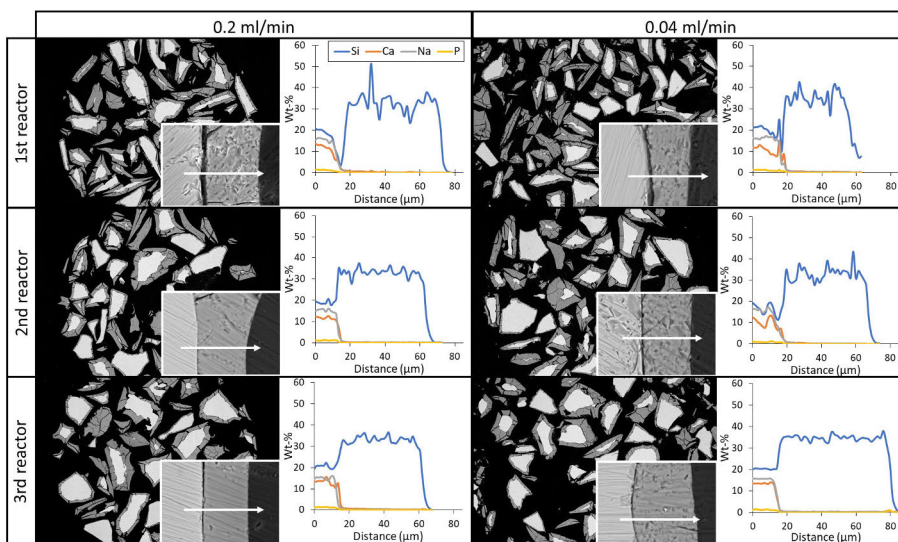


Figure 17. SEM-EDXA of S53P4 particles after 24 h of continuous flow-through with 0.2 or 0.04 ml/min 0.4M LA for the three reactors in the series. ©Springer

Bioactive glass plates immersed in static acidic solutions (LA and HCl) suggested Ca/P precipitation when the pH increased above 4 [79]. However, thicker Ca/P formed in a solution based on HCl than LA. In another study, a high level of chloride ions led to the precipitation of calcium chloride on bioactive glasses [178]. Even though the highest measured pH in the collected LA outflows in this work was 4.59 after three reactors and the local pH inside the particle bed was likely higher, the pH was not high enough to promote Ca/P precipitation. The chelation of calcium ions would explain this observation.

4.2.4 Impact of prolonged dissolution on S53P4 scaffolds

Figure 18 shows SEM images of sintered S53P4 scaffold cross-sections after 21 days of continuous flow-through with Tris (7.4) (Publication V). The EDXA corresponding to the points 1A-B, 2A-C, 3A-B, and 4A-C is presented as oxides in Table 8. The figure shows a particle in the scaffold with a partly dissolved outer crystallised layer and a completely dissolved amorphous core (a) and a particle in the scaffold with a partly dissolved inner amorphous core and a less dissolved outer crystallised surface layer (b). The scaffolds continued to dissolve over time in Tris. After 21 days, the scaffolds had lost their structure due to dissolution, and some particles in the scaffolds were mainly shells (a) comprised of silica and low levels of calcium oxide and sodium oxide (Table 8).

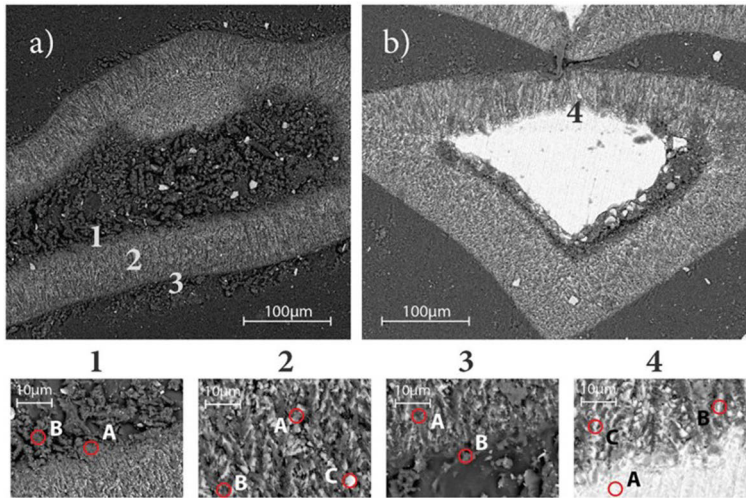


Figure 18. SEM images of S53P4 scaffolds after 21 days of continuous flow-through of Tris. a) particle in scaffold with a partly dissolved outer crystalline structure and almost completely dissolved amorphous core. b) particle in scaffold with partly dissolved amorphous core and outer unreacted crystalline structure. EDX analyses of points 1-4 are seen in Table 8. Publication V ©Springer

Some Ca/P was analysed on particles after 72 h in Tris (Figure 14), but after 21 days of continuous Tris flow, S53P4 particles were almost completely dissolved. Table 8 presents the EDX analyses of the oxides, in wt-%, from the points in Figure 18. Low compositions of CaO and P₂O₅ were analysed on some of the reacted scaffolds (2A and B). The unreacted amorphous core (4A) had a composition close to that of the bulk glass. In contrast, the crystalline structure (4B and C) was mainly silica with lower levels of the other oxides.

Table 8. EDXA (in wt-%) of points in Figure 18 and theoretical wt-% of S53P4. Publication V

	S53P4	1		2			3		4		
		A	B	A	B	C	A	B	A	B	C
SiO ₂	53.0	93.4	73.6	91.1	92.4	99	94.2	45.2	56.1	87.9	87.2
CaO	20.0	1.8	12.9	6.8	5.8	1.0	4.8	26.7	19.2	7.8	8.1
Na ₂ O	23.0	1.0	13.5	0.3	0	0	0	28.1	20.4	2.6	2.5
P ₂ O ₅	4.0	0	0	1.0	0.7	0	0	0	4.2	1.0	1.7

4.3 Static dissolution

Table 9 presents the measured average pH of the four immersion solutions before immersion and during immersion (Publication III). The deviations are omitted for clarity but varied between ± 0.01 and 0.08 pH units. The as-prepared solutions are marked as (0), and the 24 and 72 h extracts as (24) and (72), respectively. The decrease of reference pH in the extracts compared to the measured pH of the corresponding supernatant before extraction, for example, 9.31 to 9.10 in Tris (9), is likely due to the time lag for pH equalisation throughout the solutions. Upon immersion, the pH increased gradually throughout the immersion time for all solutions. The highest pH was measured at 120 h in all solutions. This indicates gradual dissolution throughout the experiments regardless of dissolution products present or the solution's initial pH.

Table 9. The pH of the supernatant solutions as functions of time before (0 h) and during immersion of S53P4 particles. The as-prepared solutions are noted as (0). The bold values indicate the pH measured above the glass particles before extraction, while the underlined values indicate the pH values in the extracted and mixed solutions before adding new particles. Publication III

h	Tris (9)			Tris (7.4)			Tris (5)			HAc (5)		
	(0)	(24)	(72)	(0)	(24)	(72)	(0)	(24)	(72)	(0)	(24)	(72)
0	8.97	<u>9.12</u>	<u>9.10</u>	7.35	<u>7.46</u>	<u>7.58</u>	4.96	<u>5.09</u>	<u>5.15</u>	4.93	<u>5.05</u>	<u>5.08</u>
2	9.10	9.15	9.11	7.44	7.57	7.59	5.06	5.11	5.19	5.01	5.05	5.11
4	9.11	9.15	9.12	7.46	7.53	7.61	5.07	5.12	5.22	5.05	5.07	5.14
6	9.12	9.15	9.14	7.47	7.52	7.62	5.08	5.13	5.24	5.03	5.09	5.16
8	9.13	9.17	9.15	7.49	7.53	7.59	5.10	5.15	5.26	5.04	5.08	5.17
24	9.15	9.20	9.17	7.52	7.57	7.69	5.15	5.23	5.32	5.11	5.14	5.17
48	9.23	9.25	9.28	7.59	7.60	7.69	5.26	5.26	5.48	5.16	5.15	5.24
72	9.31	9.29	9.33	7.62	7.64	7.71	5.26	5.36	5.55	5.16	5.20	5.29
96	9.31	9.34	9.37	7.62	7.65	7.73	5.27	5.35	5.60	5.23	5.25	5.35
120	9.38	9.37	9.41	7.66	7.68	7.75	5.38	5.42	5.68	5.27	5.30	5.40

Figure 19 shows the normalised ion concentrations of silicon, calcium, and sodium in the aliquots extracted from the static supernatant solutions as calculated with Equation 2 (Publication III). Phosphorus concentrations are omitted from the figure. All measured phosphorus values were below the limit of quantification (LOQ) in Tris (9) and between LOQ and 2.8 mg/l in other solutions (see Publication III). In most of the solutions, the ion concentrations of all ions increased with immersion time. The dissolution products in the extracts did not inhibit further ion release from S53P4

particles. However, in Tris (9) and Tris (7.4), dissolved ions in the extracts decreased the dissolution. The decrease was linear in Tris (9) and highest for the 24 h extract of Tris (7.4).

Interestingly, the silicon concentrations at 120 h were on an equal level for Tris (9) and Tris (7.4), even though the final pH (9.38) of the as-prepared Tris (9) could have led to higher dissolution [75]. HAc (5) contains a high sodium concentration in the as-prepared solution (1570 mg/l). The sodium analysis suffered from a much higher concentration than the calibration standard for sodium (20 mg/l). Nevertheless, the concentration trends were assumed to correlate with the sodium release. Sodium release trends in HAc (5) were similar to Tris (5) for the first 72 h. Calcium and sodium releases were higher in the initial pH 5 solutions, as in the dynamic LA (pH 2) experiments.

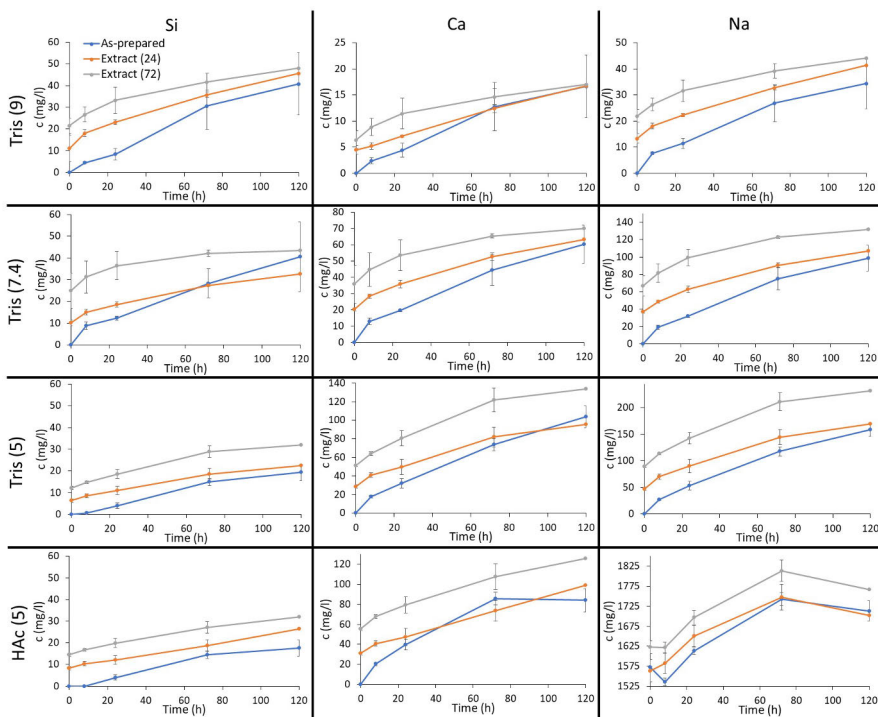


Figure 19. Normalised ion concentrations in the as-prepared and extract solutions after the static dissolution of S53P4 particles. Publication III ©Elsevier

The normalised silicon, calcium, sodium, and phosphorus mass loss rates in static solutions (Figure 20) were calculated according to Equation 4 [179].

$$NL_i = \frac{C_i^* - C_0}{\left(\frac{SA}{V}\right)f_i} \quad (4)$$

NL_i gives the normalised mass loss of element i (g/m^2), C_i^* is the normalised ion concentration of element i calculated with Equation (2) (mg/l), C_0 is the ion concentration in the reference solution (mg/l), SA is the total surface area of unreacted bioactive glass particles (m^2), V is the volume of the immersion solution (L), and f_i is the mass fraction of element i (unitless). The mass losses of silicon, calcium, and sodium in Tris (9) were at similar levels and increased linearly with time. The mass loss slightly decreased in the extracts. Figure 20 suggests a congruent silicon, calcium, and sodium dissolution in Tris (9) and its extracts. In contrast, the elements dissolved incongruently in Tris (7.4), Tris (5), HAc (5), and their extracts.

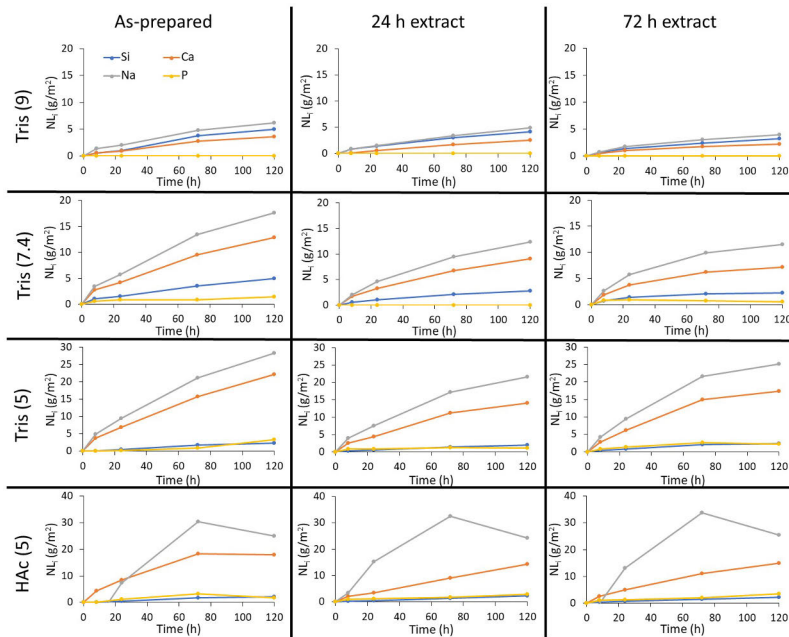


Figure 20. Normalised surface-specific mass loss of elements from S53P4 during immersion in the as-prepared Tris (9), Tris (7.4), Tris (5), HAc (5) and their extract solutions after 24 and 72 h of dissolution. Publication III ©Elsevier

Figure 21 shows SEM micrographs of bioactive glass S53P4 particle surfaces before (reference) and after 120 h in the four as-prepared static solutions (Publication III). Particles immersed in Tris (7.4) show a typical silica-rich layer (as a cracked surface) and Ca/P accumulations on the surface. Similar structures had formed on particles immersed in Tris (5) and HAc (5). In contrast, no Ca/P precipitation was identified on particles in static LA (Figure

9). Particles immersed in Tris (9) did not show specific layers but signs of glass corrosion due to congruent dissolution.

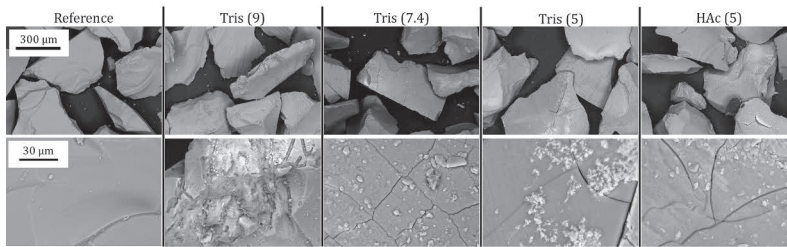


Figure 21. SEM images of S53P4 particles before immersion (reference) and after 120 h in the four as-prepared solutions. Publication III ©Elsevier

Figure 22 shows the SEM-EDX analyses of S53P4 particles immersed for 120 h in Tris (7.4), Tris (5), and HAc (5) and their 24 and 72 h extracts. Immersion in Tris (9) did not lead to any reaction layers on the surfaces (Figure 21) or on the cross-sections (Publication III). Even after 120 h, pure Ca/P was not identified on any of the analysed particles. The presence of dissolved ions in the 24 and 72 h extracts of Tris (5) and HAc (5) did not impact the reaction layer compositions. In contrast, after immersion in Tris (7.4) 72 h extract, the particles had a mixed Si/Ca/P layer, suggesting that the increased concentration of dissolution products in the solution led to precipitates and formation of the mixed layer on the particles, as also analysed in dynamic Tris (7.4) (Figure 14).

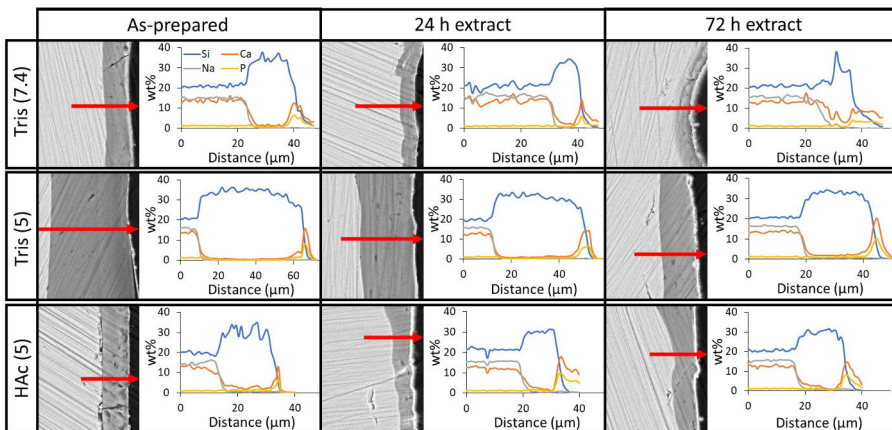


Figure 22. SEM-EDXA of S53P4 particles after 120 h in three as-prepared solutions and their 24 and 72 h extracts. Publication III ©Elsevier

4.4 Dissolution of elements from glasses

The cumulative dissolution was calculated from the ion analysis data (ICP-OES), the volume of the solution, and the mass of elements in the unreacted glass sample. SBF already containing ions present in the bioactive glass challenged the accuracy of the dissolution calculations. However, as SBF is initially free of silicon, the calculated cumulative silicon dissolution was used to compare the overall dissolution of 45S5 and S53P4 into Tris and SBF in the cascade reactor (Figure 23, Publication II).

Silicon dissolved in Tris throughout the experiment. Even though the silicon release in the second and third reactors was significantly less than in the first reactor, it increased slowly over time. In contrast, the silicon release into SBF ceased at around 48 h for both 45S5 and S53P4 in all reactors. It was assumed that the precipitated Ca/P, as seen in Figure 14 on the particle surfaces, hindered further dissolution.

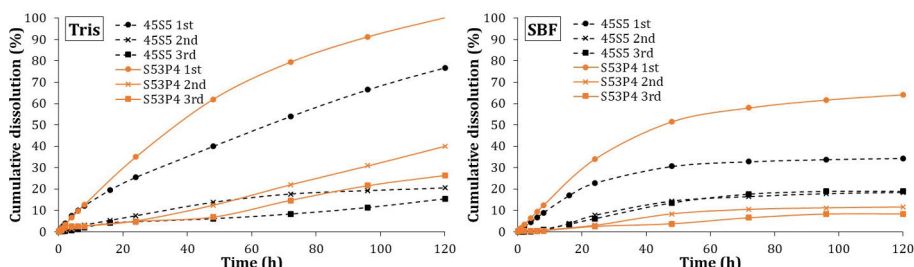


Figure 23. Calculated cumulative dissolution of silicon from 45S5 and S53P4 in dynamic (0.2 ml/min) Tris and SBF in the cascade reactor. Publication II ©Elsevier

The ion concentration of the inflow highly influenced the silicon dissolution. Even in Tris, which is initially free of interfering ions, the silicon dissolution from 45S5 decreased from 77% in the first reactor to 20 and 15% in the following reactors at 120 h. In SBF, the dissolution decreased from 34% in the first reactor to 18-19% in the second and third reactors. Simultaneously, as shown by the SEM images (Figure 14), the reaction layers grew in thickness. As discussed in 4.3.2, the dissolved ions from the first reactor likely contributed to the growth of the reaction layers on the particles in the second and third reactors, thereby partly hindering the dissolution.

Figure 24 shows the calculated share of silicon, calcium, and sodium dissolved from S53P4 in the static as-prepared Tris (9), Tris (7.4), Tris (5), HAc (5), and their 24 and 72 h extracts at 120 h (Publication III). The final pH of the Tris (9) solutions varied between 9.37 and 9.41 in the supernatants. However, the local solution pH next to the dissolving particles was likely

higher than the measured pH. Thus, the pH was high enough to provide congruent dissolution, as suggested by the minor differences in dissolved silicon, calcium, and sodium. The slight decrease of dissolved species in the extracts was assumed to depend on the ions present. Thus, the impact of the ions in the extracts was higher than the impact of pH on the dissolution. However, the decrease in the percentages of dissolved species is slight and close to the range of the experimental error.

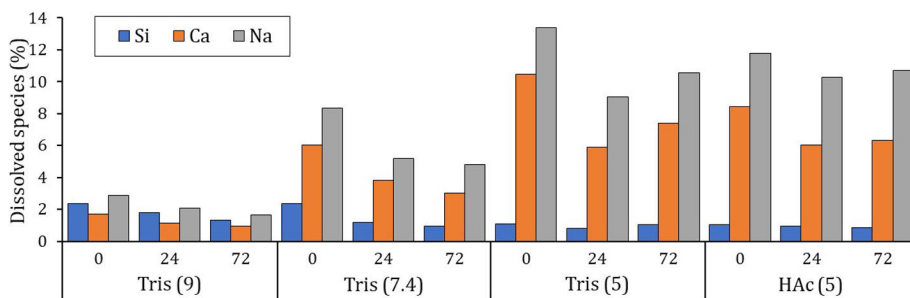


Figure 24. Dissolution of silicon, calcium, and sodium from S53P4 particles after 120 h of static immersion in the as-prepared solutions (0) and their 24 and 72 h extracts (24 and 72). Publication III ©Elsevier

In the other static solutions, the increased dissolution of calcium and sodium indicates an incongruent dissolution typical for bioactive glasses, as seen in Figure 20. For Tris (7.4), the dissolution products in the extracts decreased the dissolution of all ions. Thus, a local ion concentration increase might decrease the dissolution of implanted bioactive glasses. The silicon dissolution was almost constant in the as-prepared pH 5 solutions and their extracts, implying that the silica network dissolution was not influenced by the dissolved ions in the immersion solutions but depended on the immersion time. Similar to the dynamic environment, the dissolved ions in the static extracts hindered the dissolution but not the reaction layers.

Interestingly, the silicon dissolution was similar in Tris (9) and Tris (7.4). The pH of Tris (7.4) stayed within the buffering capacity (7-9), while the pH of Tris (9) only slightly exceeded the nominal buffering range. Thus, it was assumed that the pH did not considerably influence the silicon dissolution within or close to the buffering capacity. However, prolonged immersion would likely lead to higher silicon dissolution into Tris (9) than Tris (7.4).

5. Conclusions and future work

A cascade reactor with three reactors coupled in a series was used to explore the impact of solution composition changes, solution flow rate, and solution pH on reactions of bioactive glasses 45S5 and S53P4 in a particle bed. The three reactors separated a larger particle bed into three parts to compare local conditions in various fluid flow environments. The first reactor can be considered to mimic the outer part of an implant with the first fluid contact. The fluid with dissolution products from the first reactor was then fed into the second reactor, which simulated an inner part of a larger particle bed, and so on. A static setup was also utilised to investigate the influence of solution pH and dissolved ions on the further reactions of bioactive glass particles. The results indicated that a more homogenous environment was achieved in the dynamic setup. The results showed that:

1. Dissolution products from the bioactive glasses 45S5 and S53P4 decreased the dissolution rate in physiological-like pH environments. Still, they did not impact the glasses' ability to form surface layers responsible for bone tissue bonding.

The slightly increased pH of Tris and SBF in the dynamic fluid flow conditions did not considerably impact the glasses' dissolution behaviour, as the fluids were consistently within their buffering capacity. In contrast, differences in the glass dissolution were mainly associated with the dissolution products in the fluids and not the pH increase.

The relative dissolution decreased in the cascade downstream reactors. The dissolution decrease did not hinder the formation of the silica-rich layer and Ca/P precipitation on the bioactive glass particle surfaces in the physiological-like pH environments. Thus, the ions dissolved from the first reactor particles likely contributed to the reaction layers that formed on the second and third reactor particles. Therefore, the dissolution of ions from the particles in the second and third reactors had less impact on the surface layers. Also, rather than contributing to an outer layer of pure precipitated Ca/P, the ions released into Tris (7.4) precipitated within the silica-rich layer on the second and third reactor particles, leading to mixed layers. In the static experiments, particles immersed in fluid extracts formed similar mixed layers as in flow-through conditions.

In lactic acid (pH 2.00), the mechanism and dissolution rate of S53P4 particles were similar in the different reactors, i.e., independent of their

location in the cascade. A thick silica-rich layer developed on particles in all reactors, indicating a highly incongruent dissolution in lactic acid.

2. The dissolution rate of S53P4 was highly influenced by the flow rate.

The pH and ion concentrations were locally higher at a slower fluid flow rate. This indicates that implanted bioactive glass particles may locally experience an environment of higher pH or elevated ion concentrations. These factors might influence the biological response around the dissolving bioactive glasses. In the physiological range of about pH 7.40, the bioactive glass released ions at a much lower rate when normalised to the surrounding volume in slower fluid flow than in higher flow. In contrast, the flow rate in lactic acid did not affect the ion release. This suggests that the ion diffusion through the silica-rich layer on the glass surface was the rate-limiting dissolution mechanism in lactic acid.

3. The fluid pH influenced the dissolution rate and reaction layer morphology.

The incongruent dissolution in lactic acid led to a silica-rich layer. High solubility of calcium compounds in acidic solutions and chelation of calcium ions with lactate prevented calcium phosphate (hydroxyapatite) precipitation. Ca/P precipitated on the silica-rich surface in less acidic environments (pH 5). In physiological-like solutions (pH 7.4), the bioactive glasses formed a thinner silica-rich layer, compared to acidic solutions, with a Ca/P precipitate. In the slightly alkaline solution (pH 9), only surface corrosion occurred without any typical surface layers for bioactive glasses.

This work increased the understanding of bioactive glass reactions in environments not systemically studied previously. The knowledge gained can be used to design new compositions for new clinical applications. The results indicated that the reaction behaviour of bioactive glass particles in near-neutral solutions depended on the previous reactions of the neighbouring particles. Thus, the reactions proceeded differently over a particle bed. In contrast, bioactive glass particles in acidic solutions would react more similarly in the implant.

Future work includes developing new experimental setups that better simulate the complex human body and, thus, decrease the gap between *in vitro* and *in vivo* tests. For example, designing reactors with multiple inflows to mimic the extensive vascularisation in bones would provide a novel approach to exploring the fate of bioactive glasses and decrease the number

of animal tests needed to assess their performance. Also, utilising artificial intelligence to interpret the results from experiments could aid in developing individual solutions for patient-specific requirements.

Bioactive glasses doped with various trace elements in the body are intensively explored for their impacts on specific cellular effects in tissue engineering. Understanding their release from the bioactive glass matrix is crucial for achieving the desired effect and avoiding toxicity due to uncontrolled, high local concentrations. Therefore, dynamic fluid flow studies with accurate ion analyses are also needed for future bioactive glass development.

6. References

- [1] Bigham-Sadegh, A. and Oryan, A. (2015) Basic concepts regarding fracture healing and the current options and future directions in managing bone fractures. *International Wound Journal*. 12 (3), 238–247.
- [2] Buettmann, E.G., Goldscheitter, G.M., Hoppock, G.A., Friedman, M.A., Suva, L.J., and Donahue, H.J. (2022) Similarities Between Disuse and Age-Induced Bone Loss. *Journal of Bone and Mineral Research*. 37 (8), 1417–1434.
- [3] Sale, C. and Elliott-Sale, K.J. (2019) Nutrition and Athlete Bone Health. *Sports Medicine*. 49 (2), 139–151.
- [4] Ilich, J.Z., Kelly, O.J., Inglis, J.E., Panton, L.B., Duque, G., and Ormsbee, M.J. (2014) Interrelationship among muscle, fat, and bone: Connecting the dots on cellular, hormonal, and whole body levels. *Ageing Research Reviews*. 15 51–60.
- [5] Qu, H., Fu, H., Han, Z., and Sun, Y. (2019) Biomaterials for bone tissue engineering scaffolds: a review. *RSC Advances*. 9 (45), 26252–26262.
- [6] Kulinets, I. (2015) Biomaterials and their applications in medicine. in: *Regulatory Affairs for Biomaterials and Medical Devices*, Woodhead Publishing, pp. 1–10.
- [7] Klopffleisch, R. and Jung, F. (2017) The pathology of the foreign body reaction against biomaterials. *Journal of Biomedical Materials Research Part A*. 105 (3), 927–940.
- [8] Yu, X., Tang, X., Gohil, S.V., and Laurencin, C.T. (2015) Biomaterials for Bone Regenerative Engineering. *Advanced Healthcare Materials*. 4 (9), 1268–1285.
- [9] Geetha, M., Singh, A.K., Asokamani, R., and Gogia, A.K. (2009) Ti based biomaterials, the ultimate choice for orthopaedic implants – A review. *Progress in Materials Science*. 54 (3), 397–425.
- [10] Carnicer-Lombarte, A., Chen, S.-T., Malliaras, G.G., and Barone, D.G. (2021) Foreign Body Reaction to Implanted Biomaterials and Its Impact in Nerve Neuroprosthetics. *Frontiers in Bioengineering and Biotechnology*. 9.
- [11] Morais, J.M., Papadimitrakopoulos, F., and Burgess, D.J. (2010) Biomaterials/Tissue Interactions: Possible Solutions to Overcome Foreign Body Response. *The AAPS Journal*. 12 (2), 188–196.
- [12] Hedberg, Y.S. (2018) Role of proteins in the degradation of relatively inert alloys in the human body. *Npj Materials Degradation*. 2 (1), 1–5.
- [13] Ulery, B.D., Nair, L.S., and Laurencin, C.T. (2011) Biomedical applications of biodegradable polymers. *Journal of Polymer Science. Part B, Polymer Physics*. 49 (12), 832–864.
- [14] Armiento, A.R., Hatt, L.P., Sanchez Rosenberg, G., Thompson, K., and Stoddart, M.J. (2020) Functional Biomaterials for Bone Regeneration: A Lesson in Complex Biology. *Advanced Functional Materials*. 30 (44), 1909874.
- [15] Kumawat, V.S., Bandyopadhyay-Ghosh, S., and Ghosh, S.B. (2023) An overview of translational research in bone graft biomaterials. *Journal of Biomaterials Science, Polymer Edition*. 34 (4), 497–540.
- [16] Serban, M.A. (2016) Translational biomaterials—the journey from the bench to the market—think ‘product.’ *Current Opinion in Biotechnology*. 40 31–34.
- [17] Marin, E., Boschetto, F., and Pezzotti, G. (2020) Biomaterials and biocompatibility: An historical overview. *Journal of Biomedical Materials Research Part A*. 108 (8), 1617.
- [18] Stroganova, E.E., Mikhailenko, N.Yu., and Moroz, O.A. (2003) Glass-Based Biomaterials: Present and Future (A Review). *Glass and Ceramics*. 60 (9), 315–319.

- [19] Macfarlane, A. and Martin, G. (2004) A World of Glass. *Science*. 305 (5689), 1407–1408.
- [20] Kurkjian, C.R. and Prindle, W.R. (1998) Perspectives on the History of Glass Composition. *Journal of the American Ceramic Society*. 81 (4), 795–813.
- [21] Mauro, J.C. and Zanutto, E.D. (2014) Two Centuries of Glass Research: Historical Trends, Current Status, and Grand Challenges for the Future. *International Journal of Applied Glass Science*. 5 (3), 313–327.
- [22] Kasapis, S. (2006) Definition and applications of the network glass transition temperature. *Food Hydrocolloids*. 20 (2), 218–228.
- [23] Pirayesh, H. and Nychka, J.A. (2013) Sol–Gel Synthesis of Bioactive Glass-Ceramic 45S5 and its in vitro Dissolution and Mineralization Behavior. *Journal of the American Ceramic Society*. 96 (5), 1643–1650.
- [24] Shelby, J.E. (2020) Introduction. in: Introduction to Glass Science and Technology, 3rd Edition, Royal Society of Chemistry, pp. 1–6.
- [25] Cassar, D.R., de Carvalho, A.C.P.L.F., and Zanutto, E.D. (2018) Predicting glass transition temperatures using neural networks. *Acta Materialia*. 159 249–256.
- [26] Prado, M.O., Nascimento, M.L.F., and Zanutto, E.D. (2008) On the sinterability of crystallizing glass powders. *Journal of Non-Crystalline Solids*. 354 (40), 4589–4597.
- [27] Hand, R.J. and Tadjiev, D.R. (2010) Mechanical properties of silicate glasses as a function of composition. *Journal of Non-Crystalline Solids*. 356 (44), 2417–2423.
- [28] Guldiren, D. and Aydın, S. (2017) Antimicrobial property of silver, silver-zinc and silver-copper incorporated soda lime glass prepared by ion exchange. *Materials Science and Engineering: C*. 78 826–832.
- [29] Ngo, D., Liu, H., Kaya, H., Chen, Z., and Kim, S.H. (2019) Dissolution of silica component of glass network at early stage of corrosion in initially silica-saturated solution. *Journal of the American Ceramic Society*. 102 (11), 6649–6657.
- [30] Cormier, L., Calas, G., and Beuneu, B. (2011) Structural changes between soda-lime silicate glass and melt. *Journal of Non-Crystalline Solids*. 357 (3), 926–931.
- [31] Sinton, C.W. and LaCourse, W.C. (2001) Experimental survey of the chemical durability of commercial soda-lime-silicate glasses. *Materials Research Bulletin*. 36 (13), 2471–2479.
- [32] Vernaz, É.Y. (2002) Estimating the lifetime of R7T7 glass in various media. *Comptes Rendus Physique*. 3 (7), 813–825.
- [33] Conradt, R. (2008) Chemical Durability of Oxide Glasses in Aqueous Solutions: A Review. *Journal of the American Ceramic Society*. 91 (3), 728–735.
- [34] Hench, L.L. and Clark, D.E. (1978) Physical chemistry of glass surfaces. *Journal of Non-Crystalline Solids*. 28 (1), 83–105.
- [35] Rahaman, M.N., Day, D.E., Bal, B.S., Fu, Q., Jung, S.B., Bonewald, L.F., et al. (2011) Bioactive glass in tissue engineering. *Acta Biomaterialia*. 7 (6), 2355–2373.
- [36] Jones, J.R., Brauer, D.S., Hupa, L., and Greenspan, D.C. (2016) Bioglass and Bioactive Glasses and Their Impact on Healthcare. *International Journal of Applied Glass Science*. 7 (4), 423–434.
- [37] Hench, L.L., Xynos, I.D., and Polak, J.M. (2004) Bioactive glasses for in situ tissue regeneration. *Journal of Biomaterials Science, Polymer Edition*. 15 (4), 543–562.
- [38] O'Donnell, M.D., Watts, S.J., Law, R.V., and Hill, R.G. (2008) Effect of P2O5 content in two series of soda lime phosphosilicate glasses on structure and

- properties – Part I: NMR. *Journal of Non-Crystalline Solids*. 354 (30), 3554–3560.
- [39] Hench, L. (2006) The story of Bioglass. *Journal of Materials Science. Materials in Medicine*. 17 (11), 967–978.
- [40] Hench, L.L. (1991) Bioceramics: From Concept to Clinic. *Journal of the American Ceramic Society*. 74 (7), 1487–1510.
- [41] Hench, L.L. (1998) Biomaterials: a forecast for the future. *Biomaterials*. 19 (16), 1419–1423.
- [42] Web of Science (2022) Document search. [Accessed 6.10.2023].
- [43] Hench, L.L. (2015) Opening paper 2015- Some comments on Bioglass: Four Eras of Discovery and Development. *Biomedical Glasses*. 1 (1), 1–11.
- [44] Fagerlund, S., Ek, P., Hupa, L., and Hupa, M. (2012) Dissolution Kinetics of a Bioactive Glass by Continuous Measurement. *Journal of the American Ceramic Society*. 95 (10), 3130–3137.
- [45] Hudecki, A., Kiryczyński, G., and Łos, M.J. (2019) Biomaterials, Definition, Overview. in: *Stem Cells and Biomaterials for Regenerative Medicine*, Academic Press, pp. 85–98.
- [46] Park, J.B. and Lakes, R.S., Eds. (2007) Introduction. in: *Biomaterials An Introduction*, Springer, pp. 1–16.
- [47] Jones, J.R., Lin, S., Yue, S., Lee, P.D., Hanna, J.V., Smith, M.E., et al. (2010) Bioactive glass scaffolds for bone regeneration and their hierarchical characterisation. *Proceedings of the Institution of Mechanical Engineers, Part H: Journal of Engineering in Medicine*. 224 (12), 1373–1387.
- [48] Azi, M.L., Aprato, A., Santi, I., Kfuri, M., Masse, A., and Joeris, A. (2016) Autologous bone graft in the treatment of post-traumatic bone defects: a systematic review and meta-analysis. *BMC Musculoskeletal Disorders*. 17 (1), 465.
- [49] Barone, D.T.-J., Raquez, J.-M., and Dubois, Ph. (2011) Bone-guided regeneration: from inert biomaterials to bioactive polymer (nano)composites. *Polymers for Advanced Technologies*. 22 (5), 463–475.
- [50] Schmidt, A.H. (2021) Autologous bone graft: Is it still the gold standard? *Injury*. 52 S18–S22.
- [51] Wang, W. and Yeung, K.W.K. (2017) Bone grafts and biomaterials substitutes for bone defect repair: A review. *Bioactive Materials*. 2 (4), 224–247.
- [52] Delloye, C., Cornu, O., Druez, V., and Barbier, O. (2007) Bone allografts: What they can offer and what they cannot. *The Journal of Bone & Joint Surgery British Volume*. 89-B (5), 574–580.
- [53] de Azambuja Carvalho, P.H., dos Santos Trento, G., Moura, L.B., Cunha, G., Gabrielli, M.A.C., and Pereira-Filho, V.A. (2019) Horizontal ridge augmentation using xenogenous bone graft—systematic review. *Oral and Maxillofacial Surgery*. 23 (3), 271–279.
- [54] Oryan, A., Alidadi, S., Moshiri, A., and Maffulli, N. (2014) Bone regenerative medicine: classic options, novel strategies, and future directions. *Journal of Orthopaedic Surgery and Research*. 9 (1), 18.
- [55] Campana, V., Milano, G., Pagano, E., Barba, M., Cicione, C., Salonna, G., et al. (2014) Bone substitutes in orthopaedic surgery: from basic science to clinical practice. *Journal of Materials Science: Materials in Medicine*. 25 (10), 2445–2461.
- [56] Bhat, S.V. (2002) Overview of Biomaterials. in: *Biomaterials*, Springer Netherlands, pp. 1–11.

- [57] Habibovic, P. and de Groot, K. (2007) Osteoinductive biomaterials—properties and relevance in bone repair. *Journal of Tissue Engineering and Regenerative Medicine*. 1 (1), 25–32.
- [58] Haugen, H.J., Lyngstadaas, S.P., Rossi, F., and Perale, G. (2019) Bone grafts: which is the ideal biomaterial? *Journal of Clinical Periodontology*. 46 (S21), 92–102.
- [59] Danoux, C.B., Barbieri, D., Yuan, H., de Bruijn, J.D., van Blitterswijk, C.A., and Habibovic, P. (2014) In vitro and in vivo bioactivity assessment of a polylactic acid/hydroxyapatite composite for bone regeneration. *Biomatter*. 4 (1), e27664.
- [60] Samavedi, S., Poindexter, L.K., Van Dyke, M., and Goldstein, A.S. (2014) Synthetic Biomaterials for Regenerative Medicine Applications. in: *Regenerative Medicine Applications in Organ Transplantation*, Academic Press, pp. 81–99.
- [61] Baino, F., Novajra, G., Miguez-Pacheco, V., Boccaccini, A.R., and Vitale-Brovarone, C. (2016) Bioactive glasses: Special applications outside the skeletal system. *Journal of Non-Crystalline Solids*. 432 15–30.
- [62] Shearer, A., Montazerian, M., and Mauro, J.C. (2023) Modern definition of bioactive glasses and glass-ceramics. *Journal of Non-Crystalline Solids*. 608 122228.
- [63] Sepulveda, P., Jones, J.R., and Hench, L.L. (2001) Characterization of melt-derived 45S5 and sol-gel-derived 58S bioactive glasses. *Journal of Biomedical Materials Research*. 58 (6), 734–740.
- [64] Bonalive (2022) S53P4 bioactive glass in healthcare - International Year of Glass. [Accessed 15.8.2023].
- [65] Andersson, Ö.H., Liu, G., Karlsson, K.H., Niemi, L., Miettinen, J., and Juhanoja, J. (1990) In vivo behaviour of glasses in the SiO₂-Na₂O-CaO-P₂O₅-Al₂O₃-B₂O₃ system. *Journal of Materials Science: Materials in Medicine*. 1 (4), 219–227.
- [66] Brink, M. (1997) The influence of alkali and alkaline earths on the working range for bioactive glasses. *Journal of Biomedical Materials Research*. 36 (1), 109–117.
- [67] Arstila, H., Vedel, E., Hupa, L., and Hupa, M. (2007) Factors affecting crystallization of bioactive glasses. *Journal of the European Ceramic Society*. 27 (2), 1543–1546.
- [68] Kaur, G., Kumar, V., Baino, F., Mauro, J.C., Pickrell, G., Evans, I., et al. (2019) Mechanical properties of bioactive glasses, ceramics, glass-ceramics and composites: State-of-the-art review and future challenges. *Materials Science and Engineering: C*. 104 109895.
- [69] Kaur, G., Pandey, O. p., Singh, K., Homa, D., Scott, B., and Pickrell, G. (2014) A review of bioactive glasses: Their structure, properties, fabrication and apatite formation. *Journal of Biomedical Materials Research Part A*. 102 (1), 254–274.
- [70] Jones, J.R. (2013) Review of bioactive glass: From Hench to hybrids. *Acta Biomaterialia*. 9 (1), 4457–4486.
- [71] Hench, L.L., Roki, N., and Fenn, M.B. (2014) Bioactive glasses: Importance of structure and properties in bone regeneration. *Journal of Molecular Structure*. 1073 24–30.
- [72] Douglas, R.W. and El-Shamy, T.M.M. (1967) Reactions of Glasses with Aqueous Solutions. *Journal of the American Ceramic Society*. 50 (1), 1–8.
- [73] Paul, A. (1982) Chemical Durability of Glass. in: *Chemistry of Glasses*, Springer Netherlands, Dordrechtpp. 108–147.

- [74] Cerruti, M., Greenspan, D., and Powers, K. (2005) Effect of pH and ionic strength on the reactivity of Bioglass® 45S5. *Biomaterials*. 26 (14), 1665–1674.
- [75] Iler, R.K. (1979) The solubility of silica. in: *The Chemistry of Silica*, John Wiley & Sons, pp. 30–49.
- [76] Bingel, L., Groh, D., Karpukhina, N., and Brauer, D.S. (2015) Influence of dissolution medium pH on ion release and apatite formation of Bioglass 45S5. *Materials Letters*. 143 279–282.
- [77] Zhang, D., Hupa, M., and Hupa, L. (2008) In situ pH within particle beds of bioactive glasses. *Acta Biomaterialia*. 4 (5), 1498–1505.
- [78] Nommeots-Nomm, A., Hupa, L., Rohanová, D., and Brauer, D.S. (2020) A review of acellular immersion tests on bioactive glasses--influence of medium on ion release and apatite formation. *International Journal of Applied Glass Science*. 11 (3), 537–551.
- [79] Björkvik, L., Wang, X., and Hupa, L. (2016) Dissolution of Bioactive Glasses in Acidic Solutions with the Focus on Lactic Acid. *International Journal of Applied Glass Science*. 7 (2), 154–163.
- [80] Pereira, M.M. and Hench, L.L. (1996) Mechanisms of hydroxyapatite formation on porous gel-silica substrates. *Journal of Sol-Gel Science and Technology*. 7 (1), 59–68.
- [81] Fernández, E., Gil, F.J., Ginebra, M.P., Driessens, F.C.M., Planell, J.A., and Best, S.M. (1999) Calcium phosphate bone cements for clinical applications. Part I: Solution chemistry. *Journal of Materials Science: Materials in Medicine*. 10 (3), 169–176.
- [82] Cicuéndez, M., Doadrio, J.C., Hernández, A., Portolés, M.T., Izquierdo-Barba, I., and Vallet-Regí, M. (2018) Multifunctional pH sensitive 3D scaffolds for treatment and prevention of bone infection. *Acta Biomaterialia*. 65 450–461.
- [83] Fagerlund, S., Hupa, L., and Hupa, M. (2010) Comparison of reactions of bioactive glasses in different aqueous solutions. in: *Advances in Bioceramics and Biotechnologies*, John Wiley & Sons, Ltd, pp. 101–113.
- [84] Varila, L., Fagerlund, S., Lehtonen, T., Tuominen, J., and Hupa, L. (2012) Surface reactions of bioactive glasses in buffered solutions. *Journal of the European Ceramic Society*. 32 (11), 2757–2763.
- [85] Andersson, Ö.H. and Karlsson, K.H. (1990) Corrosion of bioactive glass under various in vitro conditions. *Clinical Implant Materials, Advances in Biomaterials*. 259–264.
- [86] Gin, S., Jollivet, P., Fournier, M., Berthon, C., Wang, Z., Mitroshkov, A., et al. (2015) The fate of silicon during glass corrosion under alkaline conditions: A mechanistic and kinetic study with the International Simple Glass. *Geochimica et Cosmochimica Acta*. 151 68–85.
- [87] Marenzana, M. and Arnett, T.R. (2013) The Key Role of the Blood Supply to Bone. *Bone Research*. 1 (1), 203–215.
- [88] Salles, S., Shepherd, J., Vos, H.J., and Renaud, G. (2021) Revealing Intraosseous Blood Flow in the Human Tibia With Ultrasound. *JBMR Plus*. 5 (11),.
- [89] Laroche, M. (2002) Intraosseous circulation from physiology to disease. *Joint Bone Spine*. 69 (3), 262–269.
- [90] Holland, C.K., Brown, J.M., Scutt, L.M., and Taylor, K.J.W. (1998) Lower extremity volumetric arterial blood flow in normal subjects. *Ultrasound in Medicine & Biology*. 24 (8), 1079–1086.
- [91] Lakha, T., Kheur, M., Mühlemann, S., Kheur, S., and Le, B. (2021) Ultrasound and CBCT analysis of blood flow and dimensions of the lingual vascular canal:

- A case control study. *Journal of Oral Biology and Craniofacial Research*. 11 (1), 40–46.
- [92] Stiller, A., Engblom, M., Karlström, O., Lindén, M., and Hupa, L. (2023) Impact of fluid flow rate on the dissolution behavior of bioactive glass S53P4. *Journal of Non-Crystalline Solids*. 607 122219.
- [93] Blokhuis, T.J. and Arts, J.J.C. (2011) Bioactive and osteoinductive bone graft substitutes: Definitions, facts and myths. *Injury*. 42 S26–S29.
- [94] Fagerlund, S. and Hupa, L. (2016) Melt-derived Bioactive Silicate Glasses. in: Smart Materials Series, Royal Society of Chemistry, pp. 1–26.
- [95] Maçon, A., Kim, T., Valliant, E., Goetschius, K., Brow, R., Day, D., et al. (2015) A unified in vitro evaluation for apatite-forming ability of bioactive glasses and their variants. *Journal of Materials Science: Materials in Medicine*. 26 (2), 1–10.
- [96] International Organization for Standardization (2014) ISO - ISO 23317:2014 - Implants for surgery — In vitro evaluation for apatite-forming ability of implant materials.
- [97] Kokubo, T. and Takadama, H. (2006) How useful is SBF in predicting in vivo bone bioactivity? *Biomaterials*. 27 (15), 2907–2915.
- [98] Stone-Weiss, N., Smith, N.J., Youngman, R.E., Pierce, E.M., and Goel, A. (2021) Dissolution kinetics of a sodium borosilicate glass in Tris buffer solutions: impact of Tris concentration and acid (HCl/HNO₃) identity. *Physical Chemistry Chemical Physics*. 23 (30), 16165–16179.
- [99] Constable, P. (2009) Clinical Acid-Base Chemistry. in: Critical Care Nephrology, Elsevier, pp. 581–586.
- [100] Oyane, A., Kim, H.-M., Furuya, T., Kokubo, T., Miyazaki, T., and Nakamura, T. (2003) Preparation and assessment of revised simulated body fluids. *Journal of Biomedical Materials Research Part A*. 65A (2), 188–195.
- [101] Bohner, M. and Lemaître, J. (2009) Can bioactivity be tested in vitro with SBF solution? *Biomaterials*. 30 (12), 2175–2179.
- [102] Rohanová, D., Boccaccini, A.R., Yunos, D.M., Horkavcová, D., Březovská, I., and Helebrant, A. (2011) TRIS buffer in simulated body fluid distorts the assessment of glass–ceramic scaffold bioactivity. *Acta Biomaterialia*. 7 (6), 2623–2630.
- [103] Rohanová, D., Horkavcová, D., Paidere, L., Boccaccini, A.R., Bozděchová, P., and Bezdička, P. (2018) Interaction of HEPES buffer with glass-ceramic scaffold: Can HEPES replace TRIS in SBF? *Journal of Biomedical Materials Research Part B: Applied Biomaterials*. 106 (1), 143–152.
- [104] Horkavcová, D., Rohanová, D., Stříbny, A., Schuhladden, K., Boccaccini, A.R., and Bezdička, P. (2020) Interaction of MOPS buffer with glass–ceramic scaffold: Effect of (PO₄)³⁻ ions in SBF on kinetics and morphology of formatted hydroxyapatite. *Journal of Biomedical Materials Research Part B: Applied Biomaterials*. 108 (5), 1888–1896.
- [105] Horkavcová, D., Stříbny, A., Schuhladden, K., Bezdička, P., Boccaccini, A.R., and Rohanová, D. (2021) Effect of buffer in simulated body fluid on morphology and crystallinity of hydroxyapatite precipitated on 45S5 bioactive glass-derived glass–ceramic scaffolds: comparison of Good’s buffer systems and TRIS. *Materials Today Chemistry*. 21 100527.
- [106] Rohanová, D., Horkavcová, D., Helebrant, A., and Boccaccini, A.R. (2016) Assessment of in vitro testing approaches for bioactive inorganic materials. *Journal of Non-Crystalline Solids*. 432 53–59.

- [107] Fagerlund, S., Hupa, L., and Hupa, M. (2013) Dissolution patterns of biocompatible glasses in 2-amino-2-hydroxymethyl-propane-1,3-diol (Tris) buffer. *Acta Biomaterialia*. 9 (2), 5400–5410.
- [108] Cerruti, M.G., Greenspan, D., and Powers, K. (2005) An analytical model for the dissolution of different particle size samples of Bioglass® in TRIS-buffered solution. *Biomaterials*. 26 (24), 4903–4911.
- [109] Singh, D., Babbar, A., Jain, V., Gupta, D., Saxena, S., and Dwibedi, V. (2019) Synthesis, characterization, and bioactivity investigation of biomimetic biodegradable PLA scaffold fabricated by fused filament fabrication process. *Journal of the Brazilian Society of Mechanical Sciences and Engineering*. 41 (3), 121.
- [110] Loke, C., Lee, J., Sander, S., Mei, L., and Farella, M. (2016) Factors affecting intra-oral pH - a review. *Journal of Oral Rehabilitation*. 43 (10), 778–785.
- [111] Brauer, D.S. (2015) Bioactive Glasses-Structure and Properties. *Angewandte Chemie International Edition*. 54 (14), 4160–4181.
- [112] Yue, S., Lee, P.D., Poologasundarampillai, G., and Jones, J.R. (2011) Evaluation of 3-D bioactive glass scaffolds dissolution in a perfusion flow system with X-ray microtomography. *Acta Biomaterialia*. 7 (6), 2637–2643.
- [113] Theodorou, G., Goudouri, O.M., Kontonasaki, E., Chatzistavrou, X., Papadopoulou, L., Kantiranis, N., et al. (2011) Comparative Bioactivity Study of 45S5 and 58S Bioglasses in Organic and Inorganic Environment. *Bioceramics Development and Applications*. 1 1–4.
- [114] Zhang, D., Hupa, M., Aro, H.T., and Hupa, L. (2008) Influence of fluid circulation on in vitro reactivity of bioactive glass particles. *Materials Chemistry and Physics*. 111 (2), 497–502.
- [115] Galusková, D., Kaňková, H., Švančárková, A., and Galusek, D. (2021) Early-Stage Dissolution Kinetics of Silicate-Based Bioactive Glass under Dynamic Conditions: Critical Evaluation. *Materials*. 14 (12), 3384.
- [116] Sinitsyna, P., Karlström, O., and Hupa, L. (2022) *In vitro* dissolution of bioactive glass S53P4 microspheres. *Journal of the American Ceramic Society*. 105 (3), 1658–1670.
- [117] Sinitsyna, P., Karlström, O., Sevonius, C., and Hupa, L. (2022) In vitro dissolution and characterisation of flame-sprayed bioactive glass microspheres S53P4 and 13–93. *Journal of Non-Crystalline Solids*. 591 121736.
- [118] Aalto-Setälä, L., Uppstu, P., Sinitsyna, P., Lindfors, N.C., Hupa, L., and Baino, F. (2021) Dissolution of Amorphous S53P4 Glass Scaffolds in Dynamic In Vitro Conditions. *Materials*. 14 (17),.
- [119] Atkinson, I., Anghel, E.M., Petrescu, S., Seciu, A.M., Stefan, L.M., Mocioiu, O.C., et al. (2019) Cerium-containing mesoporous bioactive glasses: Material characterization, in vitro bioactivity, biocompatibility and cytotoxicity evaluation. *Microporous and Mesoporous Materials*. 276 76–88.
- [120] Hulsart-Billström, G., Dawson, J.I., Hofmann, S., Müller, R., Stoddart, M.J., Alini, M., et al. (2016) A surprisingly poor correlation between in vitro and in vivo testing of biomaterials for bone regeneration: results of a multicentre analysis. *European Cells and Materials*. 31 312–322.
- [121] Huang, C., Yu, M., Li, H., Wan, X., Ding, Z., Zeng, W., et al. (2021) Research Progress of Bioactive Glass and Its Application in Orthopedics. *Advanced Materials Interfaces*. 8 (22), 2100606.
- [122] Liebsch, M., Grune, B., Seiler, A., Butzke, D., Oelgeschläger, M., Pirow, R., et al. (2011) Alternatives to animal testing: current status and future perspectives. *Archives of Toxicology*. 85 (8), 841–858.

- [123] Regional State Administrative Agency (2023) Laboratory animals - Animals - Our services - About us. [Accessed 15.8.2023].
- [124] El-Rashidy, A.A., Roether, J.A., Harhaus, L., Kneser, U., and Boccaccini, A.R. (2017) Regenerating bone with bioactive glass scaffolds: A review of in vivo studies in bone defect models. *Acta Biomaterialia*. 62 1–28.
- [125] Hench, L.L., Splinter, R.J., Allen, W.C., and Greenlee, T.K. (1971) Bonding mechanisms at the interface of ceramic prosthetic materials. *Journal of Biomedical Materials Research*. 5 (6), 117–141.
- [126] Oonishi, H., Hench, L.L., Wilson, J., Sugihara, F., Tsuji, E., Kushitani, S., et al. (1999) Comparative bone growth behavior in granules of bioceramic materials of various sizes. *Journal of Biomedical Materials Research*. 44 (1), 31–43.
- [127] Anesi, A., Ferretti, M., Salvatori, R., Bellucci, D., Cavani, F., Di Bartolomeo, M., et al. (2023) In-vivo evaluations of bone regenerative potential of two novel bioactive glasses. *Journal of Biomedical Materials Research Part A*. 111 (8), 1264–1278.
- [128] Merwin, G.E. (1986) Bioglass Middle Ear Prosthesis: Preliminary Report. *Annals of Otolaryngology & Laryngology*. 95 (1), 78–82.
- [129] Bahmad, F. and Merchant, S.N. (2007) Histopathology of ossicular grafts and implants in chronic otitis media. *The Annals of Otolaryngology, Rhinology, and Laryngology*. 116 (3), 181–191.
- [130] Stanley, H.R., Hall, M.B., Clark, A.E., King III, C.J., Hench, L.L., and Berte, J.J. (1997) Using 45S5 Bioglass Cones as Endosseous Ridge Maintenance Implants to Prevent Alveolar Ridge Resorption: A 5-Year Evaluation. *International Journal of Oral & Maxillofacial Implants*. 12 (1), 1–19.
- [131] Fiume, E., Barberi, J., Verné, E., and Baino, F. (2018) Bioactive Glasses: From Parent 45S5 Composition to Scaffold-Assisted Tissue-Healing Therapies. *Journal of Functional Biomaterials*. 9 (1), 24.
- [132] Baino, F., Hamzehlou, S., and Kargozar, S. (2018) Bioactive Glasses: Where Are We and Where Are We Going? *Journal of Functional Biomaterials*. 9 (1),
- [133] Hupa, L. and Lindfors, N.C. (2022) Bioactive Glass S53P4 – From a Statistically Suggested Composition to Clinical Success. in: *Bioactive Glasses and Glass-Ceramics*, John Wiley & Sons, Ltd, pp. 33–59.
- [134] Bonalive (2021) Bonalive Products. [Accessed 14.8.2023].
- [135] van Vugt, T.A., Geurts, J.A.P., Arts, J.J., and Lindfors, N.C. (2017) Biomaterials in treatment of orthopedic infections. in: *Management of Periprosthetic Joint Infections (PJIs)*, Woodhead Publishing, pp. 41–68.
- [136] Cunha, M.T., Murça, M.A., Nigro, S., Klautau, G.B., and Salles, M.J.C. (2018) In vitro antibacterial activity of bioactive glass S53P4 on multiresistant pathogens causing osteomyelitis and prosthetic joint infection. *BMC Infectious Diseases*. 18 (1), 157.
- [137] Leppäranta, O., Vaahtio, M., Peltola, T., Zhang, D., Hupa, L., Hupa, M., et al. (2007) Antibacterial effect of bioactive glasses on clinically important anaerobic bacteria in vitro. *Journal of Materials Science: Materials in Medicine*. 19 (2), 547–551.
- [138] Munukka, E., Leppäranta, O., Korkeamäki, M., Vaahtio, M., Peltola, T., Zhang, D., et al. (2008) Bactericidal effects of bioactive glasses on clinically important aerobic bacteria. *Journal of Materials Science: Materials in Medicine*. 19 (1), 27–32.
- [139] Lindfors, N., Geurts, J., Drago, L., Arts, J.J., Juutilainen, V., Hyvönen, P., et al. (2017) Antibacterial Bioactive Glass, S53P4, for Chronic Bone Infections – A Multinational Study. in: *A Modern Approach to Biofilm-Related Orthopaedic*

Implant Infections: Advances in Microbiology, Infectious Diseases and Public Health Volume 5, Springer International Publishing, pp. 81–92.

- [140] Drago, L., Romanò, D., De Vecchi, E., Vassena, C., Logoluso, N., Mattina, R., et al. (2013) Bioactive glass BAG-S53P4 for the adjunctive treatment of chronic osteomyelitis of the long bones: an in vitro and prospective clinical study. *BMC Infectious Diseases*. 13 (1), 584.
- [141] Steinhausen, E., Lefering, R., Glombitza, M., Brinkmann, N., Vogel, C., Mester, B., et al. (2021) Bioactive glass S53P4 vs. autologous bone graft for filling defects in patients with chronic osteomyelitis and infected non-unions – a single center experience. *Journal of Bone and Joint Infection*. 6 (4), 73–83.
- [142] Geurts, J., van Vugt, T., Thijssen, E., and Arts, J.J. (2019) Cost-Effectiveness Study of One-Stage Treatment of Chronic Osteomyelitis with Bioactive Glass S53P4. *Materials*. 12 (19), 3209.
- [143] Shearer, A., Montazerian, M., Sly, J.J., Hill, R.G., and Mauro, J.C. (2023) Trends and perspectives on the commercialization of bioactive glasses. *Acta Biomaterialia*. 160 14–31.
- [144] Vahid Golpayegani, M., Sohrabi, A., Biria, M., and Ansari, G. (2012) Remineralization Effect of Topical NovaMin Versus Sodium Fluoride (1.1%) on Caries-Like Lesions in Permanent Teeth. *Journal of Dentistry (Tehran, Iran)*. 9 (1), 68–75.
- [145] Yaroshevsky, A.A. (2006) Abundances of chemical elements in the Earth's crust. *Geochemistry International*. 44 (1), 48–55.
- [146] B. Heymsfield, S., Wang, Z., Baumgartner, R.N., and Ross, R. (1997) Human Body Composition: Advances in Models and Methods. *Annual Review of Nutrition*. 17 (1), 527–558.
- [147] Jugdaohsingh, R. (2007) Silicon and Bone Health. *The Journal of Nutrition, Health & Aging*. 11 (2), 99–110.
- [148] Ksenofontova, O.I., Vasin, A.V., Egorov, V.V., Bobyl', A.V., Soldatenkov, F.Yu., Terukov, E.I., et al. (2014) Porous silicon and its applications in biology and medicine. *Technical Physics*. 59 (1), 66–77.
- [149] Carlisle, E.M. (1970) Silicon: A Possible Factor in Bone Calcification. *Science*. 167 (3916), 279–280.
- [150] Reffitt, D.M., Ogston, N., Jugdaohsingh, R., Cheung, H.F.J., Evans, B.A.J., Thompson, R.P.H., et al. (2003) Orthosilicic acid stimulates collagen type 1 synthesis and osteoblastic differentiation in human osteoblast-like cells in vitro. *Bone*. 32 (2), 127–135.
- [151] Damen, J.J.M. and Ten Cate, J.M. (1992) Silica-induced Precipitation of Calcium Phosphate in the Presence of Inhibitors of Hydroxyapatite Formation. *Journal of Dental Research*. 71 (3), 453–457.
- [152] Dermience, M., Lognay, G., Mathieu, F., and Goyens, P. (2015) Effects of thirty elements on bone metabolism. *Journal of Trace Elements in Medicine and Biology*. 32 86–106.
- [153] Fujita, T. (2000) Calcium paradox: Consequences of calcium deficiency manifested by a wide variety of diseases. *Journal of Bone and Mineral Metabolism*. 18 (4), 234–236.
- [154] Maeno, S., Niki, Y., Matsumoto, H., Morioka, H., Yatabe, T., Funayama, A., et al. (2005) The effect of calcium ion concentration on osteoblast viability, proliferation and differentiation in monolayer and 3D culture. *Biomaterials*. 26 (23), 4847–4855.

- [155] Minegishi, S., Luft, F.C., Titze, J., and Kitada, K. (2020) Sodium Handling and Interaction in Numerous Organs. *American Journal of Hypertension*. 33 (8), 687–694.
- [156] Lewis, J.L. (2022) Overview of Sodium’s Role in the Body - Hormonal and Metabolic Disorders. [Accessed 15.8.2023].
- [157] DiNicolantonio, J.J., Mehta, V., Zaman, S.B., and O’Keefe, J.H. (2018) Not Salt But Sugar As Aetiological In Osteoporosis: A Review. *Missouri Medicine*. 115 (3), 247–252.
- [158] Takeda, E., Yamamoto, H., Yamanaka-Okumura, H., and Taketani, Y. (2012) Dietary phosphorus in bone health and quality of life. *Nutrition Reviews*. 70 (6), 311–321.
- [159] Walsh, C.T. (2020) Introduction to Phosphorus Chemical Biology. in: *The Chemical Biology of Phosphorus*, 1st ed., The Royal Society of Chemistry, pp. 3–26.
- [160] Julien, M., Khoshniat, S., Lacreusette, A., Gatius, M., Bozec, A., Wagner, E.F., et al. (2009) Phosphate-Dependent Regulation of MGP in Osteoblasts: Role of ERK1/2 and Fra-1. *Journal of Bone and Mineral Research*. 24 (11), 1856–1868.
- [161] Kokubo, T. (1991) Bioactive glass ceramics: properties and applications. *Biomaterials*. 12 (2), 155–163.
- [162] Hench, L.L. (2009) Genetic design of bioactive glass. *Journal of the European Ceramic Society*. 29 (7), 1257–1265.
- [163] Qazi, T.H., Hafeez, S., Schmidt, J., Duda, G.N., Boccaccini, A.R., and Lippens, E. (2017) Comparison of the effects of 45S5 and 1393 bioactive glass microparticles on hMSC behavior. *Journal of Biomedical Materials Research Part A*. 105 (10), 2772–2782.
- [164] Xynos, I.D., Edgar, A.J., Buttery, L.D.K., Hench, L.L., and Polak, J.M. (2000) Ionic Products of Bioactive Glass Dissolution Increase Proliferation of Human Osteoblasts and Induce Insulin-like Growth Factor II mRNA Expression and Protein Synthesis. *Biochemical and Biophysical Research Communications*. 276 (2), 461–465.
- [165] Vuornos, K., Ojansivu, M., Koivisto, J.T., Häkkänen, H., Belay, B., Montonen, T., et al. (2019) Bioactive glass ions induce efficient osteogenic differentiation of human adipose stem cells encapsulated in gellan gum and collagen type I hydrogels. *Materials Science and Engineering: C*. 99 905–918.
- [166] Ojansivu, M., Vanhatupa, S., Björkvik, L., Häkkänen, H., Kellomäki, M., Autio, R., et al. (2015) Bioactive glass ions as strong enhancers of osteogenic differentiation in human adipose stem cells. *Acta Biomaterialia*. 21 190–203.
- [167] Ojansivu, M., Wang, X., Hyväri, L., Kellomäki, M., Hupa, L., Vanhatupa, S., et al. (2018) Bioactive glass induced osteogenic differentiation of human adipose stem cells is dependent on cell attachment mechanism and mitogen-activated protein kinases. *European Cells and Materials*. 35 54–72.
- [168] Fagerlund, S., Massera, J., Moritz, N., Hupa, L., and Hupa, M. (2012) Phase composition and in vitro bioactivity of porous implants made of bioactive glass S53P4. *Acta Biomaterialia*. 8 (6), 2331–2339.
- [169] Lefebvre, L., Gremillard, L., Chevalier, J., Zenati, R., and Bernache-Assolant, D. (2008) Sintering behaviour of 45S5 bioactive glass. *Acta Biomaterialia*. 4 (6), 1894–1903.
- [170] Sidhu, H.S., Nelson, M.I., and Balakrishnan, E. (2015) An Analysis of a Standard Reactor Cascade and a Step-Feed Reactor Cascade for Biological Processes Described by Monod Kinetics. *Chemical Product and Process Modeling*. 10 (1), 27–37.

- [171] New England Biolabs Inc. (2020) pH vs Temperature for Tris Buffer. [Accessed 7.2.2022].
- [172] Trivelpiece, C.L., Rice, J.A., Clark, N.L., Kabius, B., Jantzen, C.M., and Pantano, C.G. (2017) Corrosion of ISG fibers in alkaline solutions. *Journal of the American Ceramic Society*. 100 (10), 4533–4547.
- [173] Wetzel, R. and Brauer, D.S. (2019) Apatite formation of substituted Bioglass 45S5: SBF vs. Tris. *Materials Letters*. 257 126760.
- [174] Haimi, S., Moimas, L., Pirhonen, E., Lindroos, B., Huhtala, H., Rätty, S., et al. (2009) Calcium phosphate surface treatment of bioactive glass causes a delay in early osteogenic differentiation of adipose stem cells. *Journal of Biomedical Materials Research. Part A*. 91A (2), 540–547.
- [175] Lindfors, N.C., Koski, I., Heikkilä, J.T., Mattila, K., and Aho, A.J. (2010) A prospective randomized 14-year follow-up study of bioactive glass and autogenous bone as bone graft substitutes in benign bone tumors. *Journal of Biomedical Materials Research Part B: Applied Biomaterials*. 94B (1), 157–164.
- [176] Aro, H.T., Välimäki, V.-V., Strandberg, N., Lankinen, P., Löyttyniemi, E., Saunavaara, V., et al. (2022) Bioactive glass granules versus standard autologous and allogeneic bone grafts: a randomized trial of 49 adult bone tumor patients with a 10-year follow-up. *Acta Orthopaedica*. 93 519–527.
- [177] Neves, J.G., Navarro da Rocha, D., Lopes, C.C., Prado da Silva, M.H., Sinhoreti, M. a. C., Correr-Sobrinho, L., et al. (2021) Effect of pH level and calcination on the production of calcium phosphates by acidic route of wet precipitation. *Cerâmica*. 67 236–243.
- [178] Kirste, G., Brandt-Slowik, J., Bocker, C., Steinert, M., Geiss, R., and Brauer, D.S. (2017) Effect of chloride ions in Tris buffer solution on bioactive glass apatite mineralization. *International Journal of Applied Glass Science*. 8 (4), 438–449.
- [179] Qin, Q., Stone-Weiss, N., Zhao, T., Mukherjee, P., Ren, J., Mauro, J.C., et al. (2023) Insights into the mechanism and kinetics of dissolution of aluminoborosilicate glasses in acidic media: Impact of high ionic field strength cations. *Acta Materialia*. 242 118468.

Original publications

Siekkinen M., Karlström O., Hupa L. ***“Effect of local ion concentrations on the in vitro reactions of bioactive glass 45S5 particles”***
International Journal of Applied Glass Science, Vol 13 (2022) 4, pp. 695-707, DOI: 10.1111/ijag.16579

RESEARCH ARTICLE

Effect of local ion concentrations on the in vitro reactions of bioactive glass 45S5 particles

Minna Siekkinen  | Oskar Karlström | Leena HupaJohan Gadolin Process Chemistry Centre,
Åbo Akademi University, Turku, Finland**Correspondence**Leena Hupa, Johan Gadolin Process
Chemistry Centre, Åbo Akademi
University, Turku, 20500, Finland.
Email: leena.hupa@abo.fi**Abstract**

Bioglass 45S5 is the most widely used bioactive glass composition in orthopedics to regenerate bone tissue. Although its reactions in vitro and in vivo are well established, the impact of the local environment on the dissolution behavior in the dynamic environment is not fully understood. Here, we show that the ion concentrations released from 45S5 into Tris-buffer solution and simulated body fluid (SBF) in a cascade system of three reactors in a series significantly differed depending on the ion concentrations in the inflow solutions to each reactor. The ion concentrations and pH of the solutions were measured after each reactor for up to 7 days. Also, the reaction layers at the glass particles were analyzed. The release of Si species into Tris decreased in the consecutive reactors from 92% to 26% and 24% at 168 h. Correspondingly, the release of Si species into SBF decreased from 35% to 20% and 19%. The share of elements in the remaining glass particles markedly varied between the reactors throughout the dissolution. The results imply that gradients of local ion concentrations have an essential effect on the dissolution of 45S5. The results provide guidelines for utilizing Bioglass 45S5 in different bone and soft tissue applications.

KEYWORDS

bioactive glass, durability, in vitro, leaching

1 | INTRODUCTION

When implanted into the human body, a bioactive glass develops a hydroxyapatite (HA) surface layer, which binds the material chemically with living tissues.¹ The bone-like HA layer formation occurs in the body and in vitro in SBF through three simplified reaction steps: leaching, nucleation, and precipitation.² The initial reaction rates depend on the glass composition, surface to volume ratio, sample dosage, solution composition, and flow

rate.³ After implantation, the bioactive glass also stimulates tissue growth⁴ while dissolving over time.⁵ Thus, the concentrations of the ions released into the extracellular solution control the biocompatibility and osteoconductivity of bioactive glasses.⁶ The local increases in the ion concentrations and pH have been shown to induce antibacterial effects around the dissolving glass.^{7,8} For example, bioactive glass particulates and nanoparticles of 45S5, the most widely utilized bioactive glass composition used in orthopedics to regenerate bone tissue,

This is an open access article under the terms of the [Creative Commons Attribution-NonCommercial](https://creativecommons.org/licenses/by-nc/4.0/) License, which permits use, distribution and reproduction in any medium, provided the original work is properly cited and is not used for commercial purposes.

© 2022 The Authors. *International Journal of Applied Glass Science* published by American Ceramics Society and Wiley Periodicals LLC.

showed antibacterial properties against several microorganisms associated with caries and periodontal disease.⁹ In two extensive studies, the antibacterial effects of several bioactive glasses were tested in broth cultures of 29 aerobic and 17 anaerobic microorganisms.^{10–12} Of the tested bioactive glass compositions, S53P4 showed the best ability to inhibit the growth of pathogens usually connected with enamel caries, root caries, and periodontitis *in vitro*.¹³

As the bioactive glass reacts, the composition of the surrounding solution changes.¹⁴ Various *in vitro* techniques have been applied, as a result, to investigate the ion release behavior of bioactive glasses. In conventional static studies, the bioactive glass is immersed into a buffered solution for various time periods.^{15–17} Such static environments provide well-controlled conditions and the possibility to adjust a range of parameters. Maçon et al.¹⁸ recommended a procedure for analyzing time dependent *in vitro* dissolution and reactions of bioactive glasses. In that procedure, bioactive glass particles or powders are immersed in SBF in a shaking incubator at 37°C. Sepulveda et al.¹⁹ suggested utilizing various particle sizes, glass types (porous sol-gel derived particles and solid particles), and volume fractions for achieving well-controlled dissolution rates and bioactivity of 45S5. In general, experiments in static solutions provide valuable information regarding the overall reaction behavior of bioactive glasses. However, the immersion in static conditions results in gradual pH changes and ion concentration changes of the solution.²⁰ The saturation of SBF in static solutions, especially for Si species,¹⁸ will eventually inhibit the dissolution. Such critical solution composition changes occur in a lower degree in dynamic body conditions and also in systems with a controlled and adjustable feed of fresh solution, mimicking the dissolution of bioactive glass *in vivo*.^{21,22}

In static conditions, the reactions start with the release of alkali ions from the bioactive glass through ion exchange with the H⁺ ions in the solution leading eventually to a pH increase. Breaking of Si-O-Si bonds in the glass leads to partial dissolution of silicon species and formation of silanols.²³

The formed silanols then condensate on the glass surface to a porous silica-rich gel.^{23,24} In the following steps, Ca²⁺ and PO₄³⁻ groups migrate from the glass and solution to form an amorphous CaO-P₂O₅-rich surface film.²³ The CaO-P₂O₅-rich film incorporates carbonates and hydroxyls from the solution. Finally, the film crystallizes into HA.²⁵

Zhang et al.²⁶ studied the pH of the solution in a bioactive glass particle bed to better understand the local environment's importance on the dissolution. The particles were placed in a bottom cavity of a small container, thus separated from the static bulk fluid. The pH varied signif-

icantly in the bed of particles. Also, the thickness of the reaction layers at the particle surfaces varied. On the other hand, when the solution was circulated above the glass particle bed, more even reaction layers were formed at the particles.²⁷ Local solution saturation was a plausible explanation for the observed differences in pH and reaction layer thicknesses. There has also been reports of differences in the *in vitro* and *in vivo* reactivity of bioactive glass particles. Radin et al.²⁸ reported cases where only the outermost calcium phosphate (Ca/P) shell was present after long-term *in vitro* studies of bioactive glasses. In a clinical follow-up study using bioactive glass to fill bone defects, Lindfors et al.²⁹ reported glass residues embedded in bone still after 14 years. The reason for the residual amorphous phase left in the clinical study is unclear. One plausible explanation could be that the glass dissolution had ceased due to local saturation of, for example, Si-species and extensive HA precipitation.

To better understand the variable dissolution behavior of bioactive glass, Fagerlund et al.³ developed a dynamic *in vitro* method to mimic the body's fluid flow conditions. In these experiments, a fresh solution was continuously fed through a reactor filled with bioactive glass particles. The pH and ion concentrations were measured on-line for the first 20 min of the dissolution. These results suggest that such a dynamic environment better mimics an *in vivo* fluid environment than a static test.²⁰

Sidhu et al.³⁰ compared standard and step-feed cascade reactors to analyze the steady-state growth kinetics of microorganisms. In the standard cascade reactor, the reactors were coupled in series. The solution was fed into the first reactor, and the flow from this reactor was entered into the second reactor, and so on. In the step-feed cascade reactor, an equal proportion of the feed stream entered into each reactor. From the first reactor, the solution was then fed into the second one, and so on. Interestingly, they found no differences in the final effluent concentrations of the two reactor arrangements.

This work aimed to explore the impact of local ion concentrations on the dissolution of bioactive glass 45S5 in continuous fluid flow conditions. Three identical reactors filled with the glass particles were coupled to a standard cascade reactor system for mimicking the conditions in glass particle beds implanted in the dynamic body environment. With this reactor arrangement, the ion concentrations of the outflow in tris(hydroxymethyl)aminomethane (Tris) and simulated body fluid (SBF) solutions were assumed to increase after each consecutive reactor. Consequently, this should lead to variations in the reactor layer development on the glass particles. Accordingly, the differences in the reaction layers on the glass particles in the consecutive reactors can be used to achieve a novel

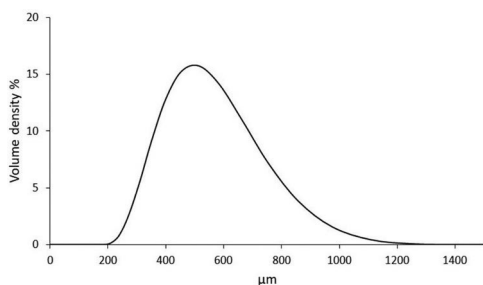


FIGURE 1 Particle size distribution

understanding of the impact of local ion concentrations on bioactive glass 45S5 dissolution reactions.

2 | MATERIALS AND METHODS

2.1 | Glass sample preparation

Bioactive glass 45S5 particles with the nominal composition (in wt%) 45 SiO₂, 24.5 CaO, 24.5 Na₂O, and 6 P₂O₅ were prepared in-house.³¹ The batch consisting of quartz sand for SiO₂ and analytical grade reagents Na₂CO₃, CaHPO₄·2H₂O, and CaCO₃ for the other oxides were melted together in a platinum crucible in an electric furnace at 1360°C for 3 h. A graphite mold was used for casting molten glass. The glass block was annealed at 520°C for 1 h and then cooled to room temperature. The glass bar was then crushed and re-melted to obtain a homogenous glass bar. The glass bar was ground with a ring and puck mill and sieved into different fractions. For the dissolution experiments, particles that passed a 500 μm sieve and collected on a 300 μm sieve were used. The glass particles were cleaned in acetone with ultrasound to remove any fine powder attached to the particles. The cleaned glass particles were stored in a desiccator until further usage. The particle size fraction 300–500 μm for the dissolution studies was selected for two reasons. Firstly, smaller particles with a larger surface react more rapidly and might lead to supersaturation of the solution in the cascade reactor, thus causing blockage of the tubes. Secondly, the size fraction is close to commercial products used in bone cavity filling. The particle size distribution of the 300–500-μm fraction was measured with a laser diffraction system (Malvern Panalytical Mastersized 3000). As shown in Figure 1, the median size of the particles was 520 μm and included particles from 200 to around 1200 μm. The 300–500-μm fraction outliers are likely due to the irregular, often elongated particle shapes, as seen in the scanning electron microscope (SEM) micrographs (Figure 4).

2.2 | Buffer solution preparation

Tris(hydroxymethyl)aminomethane (Tris) and SBF solutions were prepared using standardized methods for buffer solution making.³² Chemicals for each solution were added into purified water while stirring continuously. Before adjusting the pH of the solution to 7.4 (37°C) by adding 1 M HCl, the solutions were kept in a 37°C water bath for 4 h (SBF) and 2 h (Tris). SBF is a Tris-buffered solution that contains inorganic ions in similar conditions as human blood plasma. Accordingly, SBF is considered to better mimic in vivo reactions than the sole Tris. The ion concentrations in SBF are given in Table 1. The high initial concentrations of especially Na ions in SBF influence accurate measurements of Na release from glass 45S5. In contrast, Tris enables more accurate measurements of the fundamental glass dissolution steps.

2.3 | Cascade reactor system

The experimental set-up for a single reactor is illustrated in Figure 2A. The ion release from bioactive glass 45S5 was studied after each reactor in a cascade reactor system of three identical reactors coupled in a series (Figure 2B). In Figure 2C, the three reactors are fused to a larger reactor, corresponding to the assumed ion change along a single reactor. Hypothesized increases in ion concentrations of the solution along the system are shown as a gradually darker color throughout the reactors. Glass particles in the first reactor (Figure 2B) and the first section of the fused reactor (Figure 2C) can be assumed to represent implanted particles at the outer surface of a particle-filled cavity. These particles have the first contact with the solution with ion concentrations close to the nominal fluid composition, that is, extracellular fluid. The second reactor (Figure 2B) and the middle part of the reactor (Figure 2C) were assumed to represent the bulk phase of the implanted articles. Finally, the third reactor (Figure 2B) and the section just before the outflow from the large reactor (Figure 2C) were assumed to describe the environment of the innermost parts of a particle bed.

2.4 | Continuous flow-through reactor set-up

Before each experiment, the three reactors were cleaned (1 M HCl with ultrasound) and then filled with 210 ± 10 mg 45S5 glass particles. This amount of particles was assumed to be suitable for revealing the reactions typical for particles in different locations of a bioactive glass-filled cavity. The reactors were connected from the buffer solution

TABLE 1 Measured ion concentrations in mg/l for experiments conducted with Tris and simulated body fluid (SBF) up to 168 h

t (h)	c (mg/l)												
	1 reactor				2 reactors				3 reactors				
	Si	Ca	Na	P	Si	Ca	Na	P	Si	Ca	Na	P	
Tris	.33	63	108	144	21	78	138	215	11	97	168	259	39
	1.33	75	100	145	16	80	120	175	12	87	139	209	10
	8	38	34	49	2	49	54	80	2	65	70	111	2
	24	24	18	26	2	36	32	51	3	44	43	65	7
	168	7	3	2	1	16	7	9	1	23	13	17	2
SBF	.33	40	191	3540	53	47	219	3559	55	50	240	3443	47
	1.33	43	154	3498	45	45	154	3398	42	43	159	3293	39
	8	35	110	3277	28	49	128	3354	21	62	167	3277	14
	24	19	98	3364	28	22	105	3407	16	53	124	3225	11
	168	3	82	3494	17	1	80	3439	23	9	65	3601	11
SBF	ref	.0	97	3195	31								
Accuracy	Tris	1	1	3	4								
	SBF	1	6	97	2								

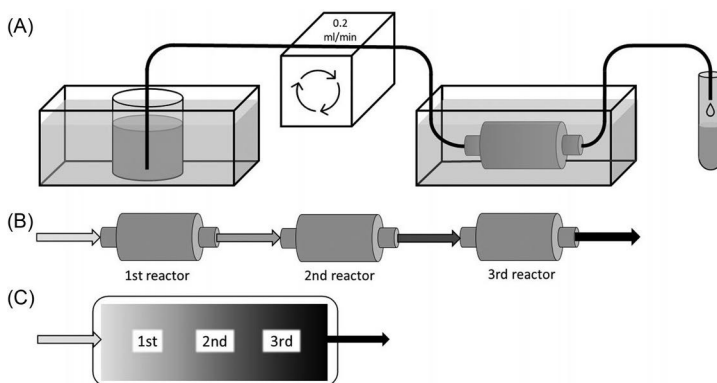


FIGURE 2 (A) Conventional continuous dissolution set-up with a single reactor. (B) The cascade reactor system with three identical reactors coupled in series; (C) the cascade reactor system applied onto a singular reactor. The solution flows first through the first section, continuing to the second section with dissolution products from the first section and finishes through the third section with ions released in both the first and second sections of glass particles

flasks via a peristaltic pump to each other to a container for the outflow. Fagerlund et al.³ give a detailed description of the reactor system for continuous-flow dissolution in a single reactor. The flow rate was set to .2 ml/min, and the temperature in the reactor was set to 37°C. Before starting an experiment, a reference solution from the buffer solution was taken in a test vial. At different time points, 4 ml of the outflow was collected for temperature and pH-measurements, and ion analysis. The experiments were stopped at several selected times, and the glass particles were collected for analysis. The reactions were expected to occur more rapidly during the first hours. Accordingly, the ion release measurements were conducted more frequently during the beginning of the experiments.

During the first 2 h, solutions were collected every 20 min. After that, solutions were collected at hours 4, 6, 8, 16, and 24. From 24 h and onward, solutions were collected every 24 h up to 7 days.

2.5 | Temperature and pH

The temperature and pH were measured for all the collected outflow solutions. The solution temperature in the thin tubes decreased during solution tapping into vials after the reactors. The pH meter was calibrated using

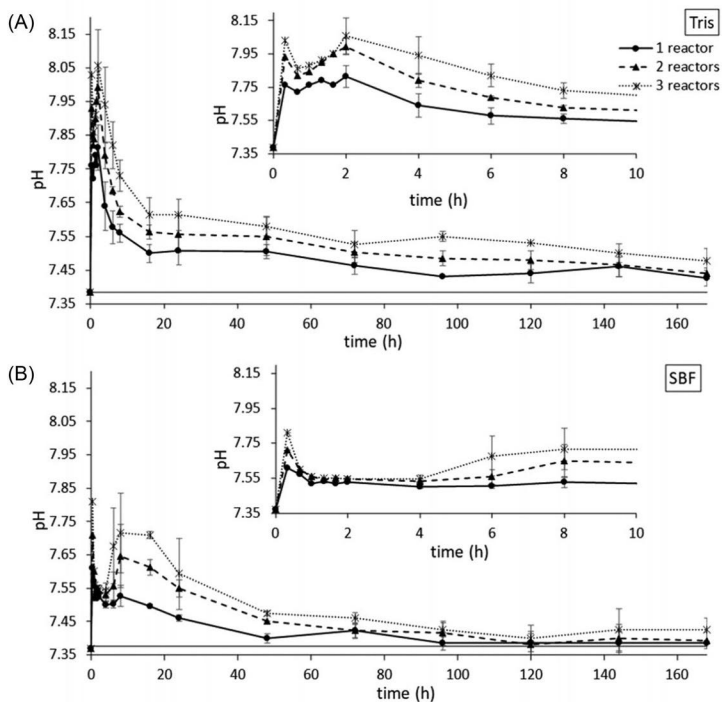


FIGURE 3 The pH of the solution as a function of time (h) for 45S5 dissolution in Tris (A) and simulated body fluid (SBF) (B), in one, two, or three reactors coupled in a series

standardized buffer solutions with pH 4.01, 7.00, and 9.21. The pH measurements were conducted at room temperature, but the results were converted to pH at 37°C by using Equation (1).³³ The equation was verified by measuring the pH of three sets of the buffer solutions at five different temperatures in the interval of 20–45°C in a water bath.

$$\text{pH}_{37} = \text{pH}_{\text{measured}} - (0.02664(37 - T_{\text{measured}})) \quad (1)$$

2.6 | Ion analysis

Inductively coupled plasma optical emission spectroscopy (ICP-OES, Optima 5300 DV; Perkin Elmer, Waltham, MA) was used to determine concentrations of elements in the solutions collected in the vials. The solutions for the ICP analysis were prepared by diluting 1 ml of the collected solution with 9 ml of ultrapure water and acidifying it with concentrated HNO₃. The elements analyzed in Tris and SBF with ICP-OES were silicon ($\lambda = 251.611$ nm, limit of quantification (LOQ) $\approx .004$ mg l⁻¹), calcium ($\lambda = 317.933$ nm, LOQ $\approx .03$ mg l⁻¹), sodium ($\lambda = 589.592$ nm, LOQ \approx

.2 mg l⁻¹), and phosphorous ($\lambda = 213.617$ nm, LOQ $\approx .03$ mg l⁻¹).

2.7 | Reaction layer formation

An SEM (Leo Gemini; Carl Zeiss, Oberkochen, Germany) with energy-dispersive X-ray analysis (EDX, Leo Gemini; Carl Zeiss, Oberkochen, Germany) was used to study the changes in the cross-sectional area of the partly dissolved particles. The EDX analysis focused on separate particles of each sample with distinct layers. Before the SEM-EDX analysis, the particles were cast in epoxy resin, ground, and polished to show the cross-sectional area.

3 | RESULTS

3.1 | Influence of glass dissolution rates on pH

Figure 3 shows the pH change for Tris and SBF as functions of time after each reactor, including an inset plot for

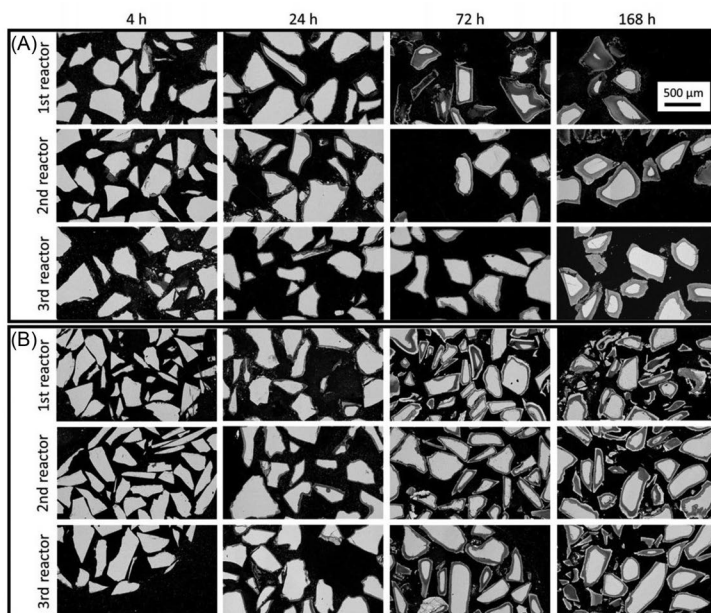


FIGURE 4 Scanning electron microscope (SEM) images of the cross-sectional surfaces of 45S5 glass after 4, 24, 72, and 168 h in Tris (A) and simulated body fluid (SBF) (B)

the pH change for the initial 10 h. All presented pH values are averages of 2–5 parallel pH measurements. The pH was consistently higher after the third reactor than the first reactor. Also, the pH of the second reactor was higher than after the first reactor for 144 h in Tris and 120 h in SBF. The pH differences were minor at prolonged dissolution. The pH of Tris showed a narrow and high initial peak at 2 h (Figure 3A). After around 18 h, the pH was almost constant, but slightly higher than the reference solution's pH.

The initial pH change in SBF showed a similar rapid increase as in Tris (Figure 3B). However, the peak pH value was at 20 min (.33 h) as compared to 2 h for Tris. After the initial pH peak, the pH increased again, followed by a gradual decrease in the second and third reactors. During the 3 last days, that is, after 72 h, the pH of SBF remained at a low but stable level for all three reactor configurations. Also, the pH of the solutions was higher than the reference solution's pH at each time point.

3.2 | Effects of cascade reactor system on ion concentrations

Table 1 shows ion concentrations in Tris and SBF after the three different reactor set-ups at selected time points. Each value is an average of 2–3 separate ICP-OES measurements

of the collected solutions. All values are given as mg/l. The analyzed ion concentrations in the initial SBF and ion analysis accuracy in both Tris and SBF are also given in Table 1. A low initial P content of the unreacted bioactive glass and thus relatively low P concentration changes in the solutions explain the low accuracy of P.

The highest element concentrations (shown in bold in Table 1) in Tris were measured at the two first time points, 20 min (.33 h) or 80 min (1.33 h), after which concentrations gradually decreased. The highest ion concentrations in SBF were measured in the second and third reactors at around 8 h. The highest Na release in SBF, corresponding to an increase of about 400 mg/l, was measured after the third reactor at 168h. At each time point, the Si release was lower in SBF than in Tris.

3.3 | Formation of surface reaction layers

SEM images of the overall layer developments on the cross-sectional areas of 45S5 particles in both solutions after 4, 24, 72, and 168 h are presented in Figure 4. Some particles in the SEM images can perceive finer than the average diameter of 300–500 μm. This is due to the cross-section for some particles being closer to the particle surfaces than the middle parts. In both solutions, Si-rich layers were observed

TABLE 2 Elemental analysis in wt-% of the Si-rich layer at selected 45S5 glass particles in the three reactors after 4 h of continuous dissolution in Tris and simulated body fluid (SBF)

		%							
		SiO ₂		CaO		Na ₂ O		P ₂ O ₅	
		Tris	SBF	Tris	SBF	Tris	SBF	Tris	SBF
Si-rich	1st	93.8	82.4	3.0	9.2	1.7	3.7	1.3	3.3
	2nd	92.8	84.3	4.0	7.3	1.0	2.4	1.3	4.8
	3rd	91.9	-	2.7	-	1.3	-	.9	-

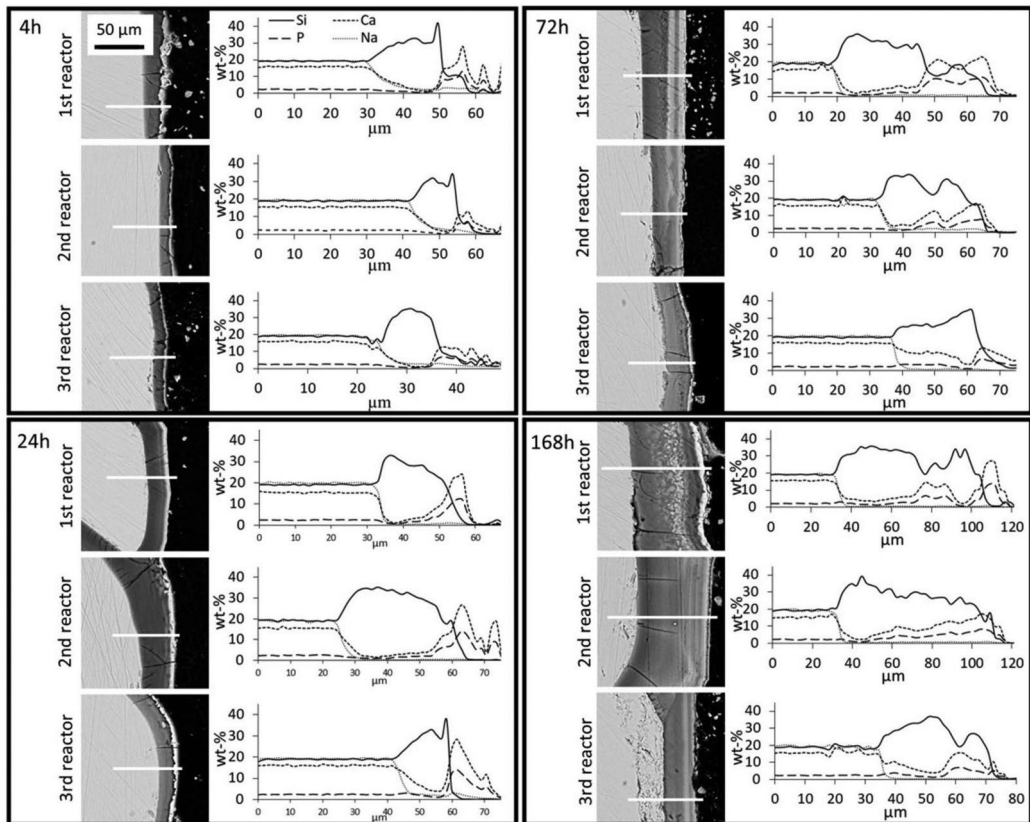


FIGURE 5 Scanning electron microscope (SEM) images and energy-dispersive X-ray (EDX) analyses of the cross-sections of 45S5 particles in each reactor after the continuous flow of Tris after 4, 24, 72, and 168 h

(thin gray surface layers in the SEM images). SEM images of the particles in the first reactor showed signs of a silica-rich layer after the exposure to both solutions already after 2 h. However, the layer development could not be verified on the particles in the third reactor.

After 4 h in SBF, the glass particles did not show any apparent progress in the layer development as compared to the 2-h dissolutions. The elemental analyses of the oxides

in the Si-rich surfaces at 4 h are seen in Table 2. In general, the results suggest that the Si-rich layer had proceeded to a larger extent in Tris than SBF.

Figure 5 (Tris) and Figure 6 (SBF) show SEM images and EDX analyses over the cross-section of the partially reacted 45S5 particles after continuous dissolution for 4, 24, 72, and 168 h. With increasing time, there are apparent differences between particles after the dissolution in the two

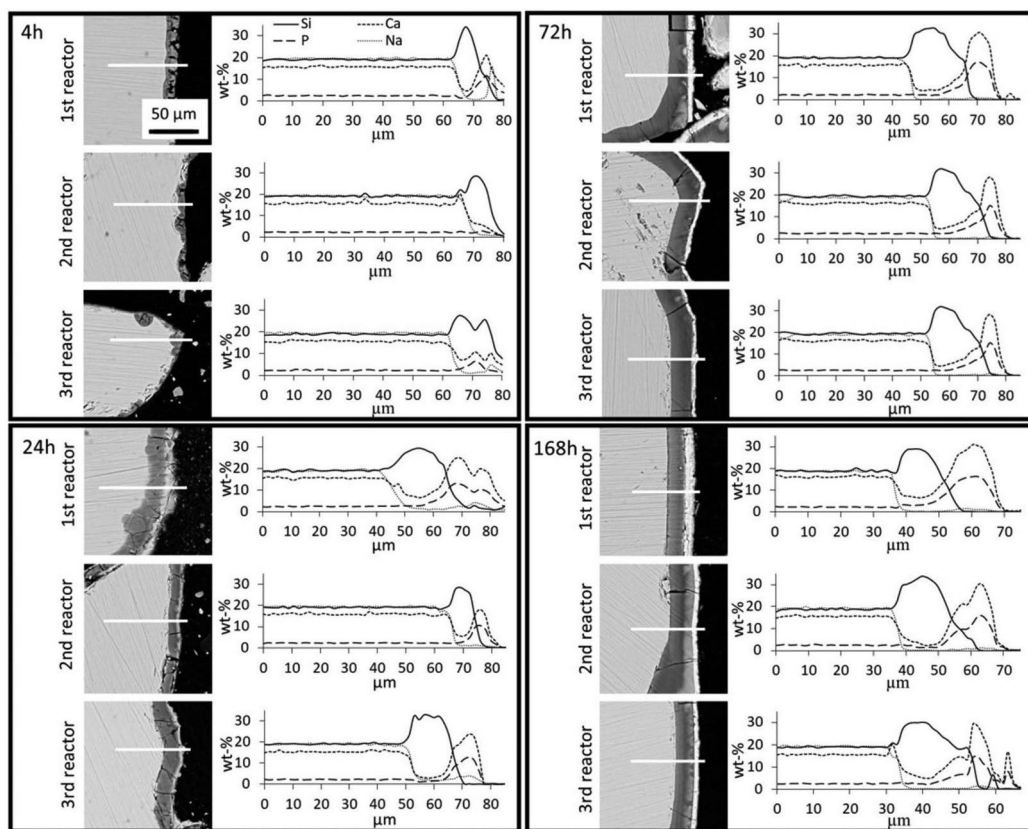


FIGURE 6 Scanning electron microscope (SEM) images and energy-dispersive X-ray (EDX) analyses of the cross-sections of 45S5 particles in each reactor after the continuous flow of simulated body fluid (SBF) after 4, 24, 72, and 168 h

solutions. The EDX line analyses show the content (wt-%) of elements from the particle bulk to the surface.

After prolonged dissolution in Tris, Ca/P embedded in the outer part of the silica-rich surface layer was identified. At the longest time points, also thin Ca/P layers with molar ratios close to HA were analyzed. In contrast, particles in experiments conducted with SBF (Figure 6) do not show significant differences in the mixed silica-rich and Ca/P layers between 72 and 168 h. The EDX analyses show that the weight percentages of Ca and P are related to each other after the initial decrease of the elements in the Si-rich layer. As of the observed mixed layers, the trends of Ca and P follow each other.

At 168 h, most of the bulk glass had dissolved in the first reactor in Tris, and the residual particles consisted mainly of mixed silica-Ca/P shells. The reactions had progressed to a lesser degree in the two following reactors. On the other hand, the substantial Ca/P formation had fused the

particles in SBF. The sample shattered into pieces when removed from the reactor. In SBF, the individual particles showed distinct silica-rich and Ca/P rich layers with a mixed layer in between. In the second and third reactors, the reaction layers showed similar trends to the layers at particles in the first reactors for both solutions. However, the reactions had progressed to a lower degree in the successive reactors.

3.4 | Dissolution of silicon

The cumulative dissolution of Si from the bioactive glass during the Tris and SBF experiments is given in Figure 7. The dissolution was calculated from the ion concentrations (Table 1), the volume of solution flown through the system, and the mass of Si in the unreacted glass, assuming linear dissolution between two consecutive time points.

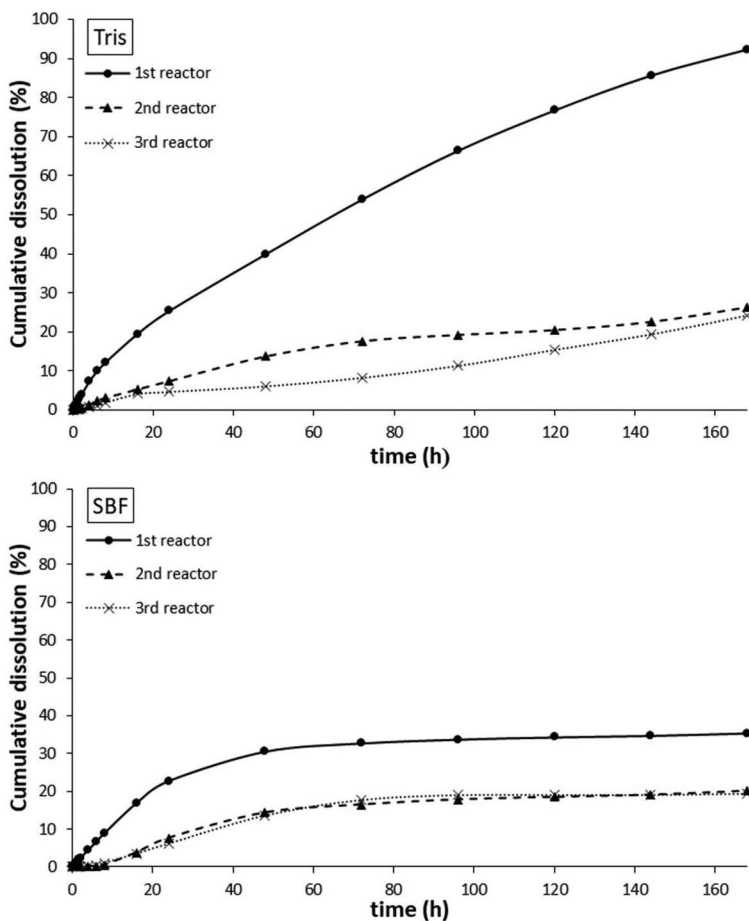


FIGURE 7 Cumulative dissolution of Si (mass-%) from 45S5 in Tris (above) and simulated body fluid (SBF) (below) as functions of time (h) in each reactor

The Si released from particles in the first reactor shows apparent differences between the dissolution in Tris and SBF. The cumulative dissolution profiles suggest an almost complete dissolution of Si in the first reactor during the 168 h experiment. On the other hand, only 40% of the Si dissolved in the experiment with SBF. The dissolution of Si steadily increased in Tris, whereas the dissolution in SBF leveled out within 3 days.

3.5 | Mass share of elements in particles

Figure 8 shows the average Si, Ca, Na, and P shares in the 45S5 particles in the three reactors as functions of dissolution time in Tris. The complexity and high initial ion con-

centrations did not provide a reliable basis for similar calculations in SBF. The mass shares of elements were calculated from their initial theoretical mass in the sample subtracted with the measured cumulative dissolution. Then, this value was compared to the overall calculated mass of the elements in the remaining particles.

The share of Si in the particles in the first reactor increased initially but then steadily decreased. Si left in particles in the second and third reactors continued to increase with time, as also indicated by the Si-rich layers in Figure 5. The Ca share neither increased nor decreased in the second and third reactors. In contrast, the share of Ca in particles increased in the first reactor during the experiment. At 168 h, there was almost no Na left in the first reactor particle. The Na share in the second reactor particles

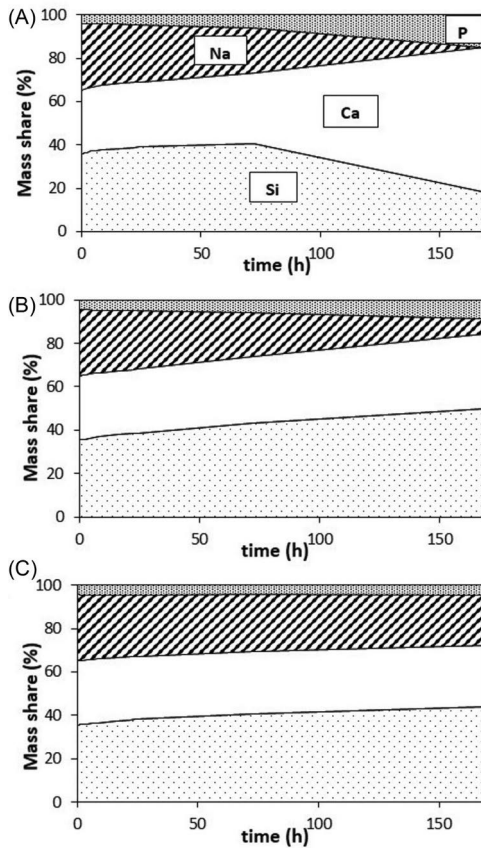


FIGURE 8 Shares of silicon, calcium, sodium, and phosphorous (wt-%) in the remaining particles in (A) the first, (B) second, and (C) third reactors as functions of dissolution time in Tris

decreased slowly, while its share in the third reactor particles decreased slightly throughout the dissolution. The only noticeable change in the P shares throughout the dissolution can be seen as an increase in the first reactor and a minor increase in the second reactor. Overall, the share of elements in the third reactor particles did not significantly change during the dissolution. In contrast, notable changes in the share of elements were noticed in the first reactor particles.

4 | DISCUSSION

To the authors' knowledge, no similar dissolution studies of bioactive glasses in a continuous fluid flow using multiple reactors connected in a series have been reported. The

three reactors can be assumed to represent a single particle bed, where each reactor represents different sections of the bed (Figure 2). Thus, the first reactor would describe the outermost particles, the second reactor the particles in the next layer, while the third reactor shows reactions of the innermost particles in the single bed. The results imply the differences when such a bioactive glass implant reacts in a cavity: the outermost particles react more rapidly than the innermost particles.

The lower release of Si in the second and third reactors (Figure 7) is interesting. The ion dissolution from the particles in the first reactor with fresh solution feed affects the ion release from the particles in the next two reactors with changed ion concentrations in the inflow (Table 1). The decrease in Si concentration with prolonged dissolution also correlates to the decreasing Si content of the unreacted bioactive glass left in the reactors.

The solubility of silica glasses is affected by the glass composition, the solution pH, and the alkali ions in the solution.³⁴ The rapid ion exchange between the glass and solution increases the pH of the solution and subsequently decreases the H^+ ion concentration. Decreased H^+ in the solution reduces the ion exchange between the glass and solution, ultimately leading to an inhibited dissolution of alkali ions from the bulk glass. On the other hand, increased pH and thus increased OH^- concentration favor the solubility of Si from the bulk glass³⁵ by attacking the silica network in the bulk glass. Extreme dissolution of silica is usually noticed when the pH of the solution is above 9.³⁶ However, the solubility of silica has also been reported at pH 7–8.³⁶ On the other hand, the pH of buffered solutions is controlled. In this work, the highest measured bulk solution pH was 8.06, that is, close to pH = 8.0, at which the buffering capacity of Tris is highest. After the maximum bulk values, the pH started to decrease gradually. This decrease is most likely due to the less unreacted material left in the reactors. However, the relative Si dissolution differences in the three reactors were assumed to depend on the local conditions around the dissolving particles. The fresh solution fed into the first reactor supported rapid ion exchange and increased the pH of the outflow. The dissolution decreased in the second and third reactors due to the lower hydrogen ion concentration available.³⁴ Although the pH was likely to increase inside the particle bed locally,²⁷ the solution's buffering capacity was assumed to prevent any further pH increase beyond the maximum capacity, thus suppressing the relative Si-dissolution from the samples. The formation of the Ca/P rich layer on the particles in the two first reactors also likely affected the dissolution as high concentrations of Ca and P species promote Ca/P precipitation.³⁷ In SBF, the solubility of silica is strongly hindered by the less soluble Ca/P layer.³⁸

The stabilization of the release of Si species in SBF at around 72 h (Figure 7) implies that an inhibiting layer had formed on the glass particle surface (Figure 6), thus retarding the dissolution. Aqueous Si species have been reported to induce HA precipitation on the surface of bioactive glasses.^{39,40} Several studies in static environments have shown that HA can be noticed after 2 days of immersion of bioactive glasses.^{41,42} After 72 h in Tris and SBF, the Ca/P molar ratio in the outermost layer particles in all reactors is close to the molar ratio of 1.67⁴³ of HA. After 168 h in SBF, Ca/P had glued the glass particles in the first reactor, and the sample shattered in pieces when removed from the reactor. In the subsequent reactors, the Ca/P formation was less pronounced (Figure 6). This suggests that the silica-rich layer providing the nucleation site for Ca/P had formed later in the second and third reactors. After the first reactor, the Ca and P ion concentrations in the solution after the first reactor were lower than in the original SBF, suggesting that these concentrations were not high enough to provide thick Ca/P layers on the particles in the second and third reactors (Table 1, Figure 6).

In Tris, the low P species concentration seems to contribute mainly to the precipitation of a mixed Si-rich and Ca/P layer at the particles in all three reactors (Figure 5). Bingel et al.²² reported that the ion exchange between the glass and the solution, and the apatite formation on the surface, are slower at a higher pH. As the pH increased after each subsequent reactor, less ion exchange occurred between the glass and the solutions in the second and third reactors. Similarly, Wetzel and Brauer⁴⁴ showed that SBF had a slower apatite formation ability than Tris on immersed bioactive glass, as seen when comparing the SEM images at 4 h for both solutions (Table 2, Figure 4).

The first reactions between the solution and the bioactive glass particles increased the pH of the solution, followed by the initial release of soluble Si species and precipitation and condensation of the silica-rich surface layer.⁴⁵ The results of this study agree with previous studies according to which common ions in the solution retard the ion release into the solution.^{19,22,46} In the present study, the solution was fresh when fed into the first reactor. However, the higher ion concentrations slowed down the ion release in the second and third reactors.

Some studies^{4,47} have investigated the dissolution of bioactive glass 45S5 in cell culture media. Solutions containing ionic products from bioactive glass stimulated the gene transcription in osteoblasts and, consequently, shortened the human osteoblast growth cycle. Biologically, this is considered as a beneficial property of the material. The present study has shown differences in the dissolution of bioactive glass 45S5 particles in conditions where the solution's ion concentrations gradually change. The differences in pH, ion concentrations and reaction layer for-

mation imply that small variations in the solution's local ion concentrations influence the ion release rates and subsequent layer formation. The concentration differences between the in- and outflow solutions were much smaller after the second and third reactors, thus verifying that the glass particles react slower when the ion concentrations in the solution increase. The slower reactions were especially noticeable for experiments with SBF. The initial pH increase and the significant increase in all ion concentrations resulted in rapid reactions between the surface area and SBF. However, the higher pH of the inflow to the second and third reactors did not provide a higher ion release.

The cross-sectional images (Figure 5) after 168h of continuous dissolution in Tris showed that the particles dissolved faster in the first reactor than the second and third reactors. The low P concentrations in the outflow solutions suggest that some of the released P forms Ca/P in each reactor (Table 1). However, as the P content was low in the original glass, only thin Ca/P layers formed. The SEM images of the 45S5 particles in the first reactor suggest a rapid dissolution in Tris (Figure 5), where the lack of phosphate in the solution restricts the formation of Ca/P. In contrast, the continuous phosphate feed with SBF led to an extensive formation of an almost pure Ca/P at the particle surfaces (Figure 6). However, for the layer formation to occur, the glass dissolution must first proceed to such an extent that the silica-rich layer supports Ca/P-nucleation. In SBF, thick mixed silica-rich and Ca/P layers had formed at the particle surfaces in all reactors after 168 h. The Ca/P precipitation was most extensive in the first reactor. The SEM-EDX analyses of the samples in all three reactors suggest that thick Ca/P slows down the dissolution of the glass, as expected.³⁸

In general, the differences in the reaction layers at the particles in the three reactors imply that the formation of the silica-rich layer providing suitable nucleation sites controls the Ca/P precipitation. When the common ion concentrations in the solution increase, the dissolution of the glass and layer forming ability decreases. Thus, the local environment strongly affects the in vitro reactivity of the bioactive glass. These results also indicate that in packed beds of implanted bioactive glass particles, the outermost particles react more rapidly while the particles well inside the sample react slower, provided that there are similar ion concentration differences as described above. Although the pH trends (Figure 3) show the overall values, the pH differences between the successive reactors suggest local variations and thus partly explain the differences in ion release and layer formation (Table 1 and Figures 5 and 6). Differences in the local ion concentrations would explain the remnants of implanted bioactive glass particles reported in some clinical trials.^{29,48}

5 | CONCLUSIONS

The ion release from bioactive glass 45S5 into Tris-buffer and SBF was studied in a continuous cascade reactor system consisting of three reactors coupled in series. This approach provided a more detailed insight into local effects at glass-to-solution interfaces. The release of ions from the reactors differed significantly, strongly implying that gradients of local ion concentrations have an essential effect on the dissolution and reaction layer formation. The share of elements in the remaining glass particles varied between the three reactors throughout the experiments.

The ion dissolution and surface layer development typical for bioactive glasses occurred more rapidly in the first than the second and third reactor. The pH increase after each consecutive reactor did not increase the overall dissolution, most likely due to fewer hydrogen ions available for alkali ion exchange reactions after the first reactor. Thus, the slower reactions in the second and third reactors imply that changes in the local ion concentrations lead to lower overall dissolution rates. The results imply that individual bioactive glass particles in an implanted particle bed might react nonuniformly in conditions where the ion concentrations locally increase due to fluid flow path differences.

ACKNOWLEDGMENTS

This work is part of the Business Finland project Biobased smart materials at biomaterials interface. Financial support by The Maud Kuistila Memorial Foundation (Minna Siekkinen) and Academy of Finland (project number: 321598) (Oskar Karlström) is acknowledged. Linus Silvaner and Luis Bezerra are acknowledged for their technical assistance with SEM and ICP-OES.


CONFLICT OF INTEREST

The authors declare that there is no conflict of interest that could be perceived as prejudicing the impartiality of the research reported.

FUNDING INFORMATION

The Maud Kuistila Memorial Foundation; Academy of Finland, Grant Number: 321598

ORCID

Minna Siekkinen  <https://orcid.org/0000-0002-5393-7636>

REFERENCES

- Baino F, Novajra G, Míguez-Pacheco V, Boccaccini AR, Vitale-Brovvarone C. Bioactive glasses: special applications outside the skeletal system. *J Non-Cryst Solids*. 2016;432:15–30. <https://doi.org/10.1016/j.jnoncrsol.2015.02.015>
- Varila L, Fagerlund S, Lehtonen T, Tuominen J, Hupa L. Surface reactions of bioactive glasses in buffered solutions. *J Eur Ceram Soc*. 2012;32(11):2757–63. <https://doi.org/10.1016/j.jeurceramsoc.2012.01.025>
- Fagerlund S, Ek P, Hupa L, Hupa M, Jantzen C. Dissolution kinetics of a bioactive glass by continuous measurement. *J Am Ceram Soc*. 2012;95(10):3130–7. <https://doi.org/10.1111/j.1551-2916.2012.05374.x>
- Xynos ID, Edgar AJ, Buttery LDK, Hench LL, Polak JM. Gene-expression profiling of human osteoblasts following treatment with the ionic products of Bioglass® 45S5 dissolution. *J Biomed Mater Res*. 2001;55(2):151–7. [https://doi.org/10.1002/1097-4636\(200105\)55:23.0.CO;2-D](https://doi.org/10.1002/1097-4636(200105)55:23.0.CO;2-D)
- Ducheyne P, Qiu Q. Bioactive ceramics: the effect of surface reactivity on bone formation and bone cell function. *Biomaterials* 1999;20(23):2287–303. [https://doi.org/10.1016/S0142-9612\(99\)00181-7](https://doi.org/10.1016/S0142-9612(99)00181-7)
- Cao W, Hench LL. Bioactive materials. *Ceram Int*. 1996;22(6):493–507. [https://doi.org/10.1016/0272-8842\(95\)00126-3](https://doi.org/10.1016/0272-8842(95)00126-3)
- Stoor P, Söderling E, Salonen JI. Antibacterial effects of a bioactive glass paste on oral microorganisms. *Acta Odontol Scand*. 1998;56(3):161–5. <https://doi.org/10.1080/000163598422901>
- Jones JR. Review of bioactive glass: from Hench to hybrids. *Acta Biomater*. 2013;9(1):4457–86. <https://doi.org/10.1016/j.actbio.2012.08.023>
- Allan I, Newman H, Wilson M. Antibacterial activity of particulate Bioglass® against supra- and subgingival bacteria. *Biomaterials* 2001;22(12):1683–7. [https://doi.org/10.1016/S0142-9612\(00\)00330-6](https://doi.org/10.1016/S0142-9612(00)00330-6)
- Leppäranta O, Vaahtio M, Peltola T, Zhang D, Hupa L, Hupa M, et al. Antibacterial effect of bioactive glasses on clinically important anaerobic bacteria in vitro. *J Mater Sci: Mater Med*. 2007;19(2):547–51. <https://doi.org/10.1007/s10856-007-3018-5>
- Zhang D, Leppäranta O, Munukka E, Ylänen H, Viljanen MK, Eerola E, et al. Antibacterial effects and dissolution behavior of six bioactive glasses. *J Biomed Mater Res Part A*. 2010;93(2):475–83. <https://doi.org/10.1002/jbm.a.32564>
- Munukka E, Leppäranta O, Korkeamäki M, Vaahtio M, Peltola T, Zhang D, et al. Bactericidal effects of bioactive glasses on clinically important aerobic bacteria. *J Mater Sci: Mater Med*. 2008;19(1):27–32. <https://doi.org/10.1007/s10856-007-3143-1>
- Jones JR, Brauer DS, Hupa L, Greenspan DC. Bioglass and bioactive glasses and their impact on healthcare. *Int J Appl Glass Sci*. 2016;7(4):423–34. <https://doi.org/10.1111/ijag.12252>
- Taipale S, Ek P, Hupa M, Hupa L. Continuous measurement of the dissolution rate of ions from glasses. *Adv Mater Res*. 2008;39–40:341–6. <https://doi.org/10.4028/www.scientific.net/AMR.39-40.341>
- Andersson ÖH, Vähätalo K, Yli-Urpo A, Happonen R, Karlsson KH. Short-term reaction kinetics of bioactive glass in simulated body fluid and in subcutaneous tissue. *Bioceramics* 1994;67–72. <https://doi.org/10.1016/B978-0-08-042144-5.50014-5>
- Brauer DS, Brückner R, Tylkowski M, Hupa L. Sodium-free mixed alkali bioactive glasses. *Biomed Glasses*. 2016;2(1):99–110. <https://doi.org/10.1515/bglass-2016-0012>
- Rámila A, Vallet-Regí M. Static and dynamic in vitro study of a sol-gel glass bioactivity. *Biomaterials* 2001;22(16):2301–6. [https://doi.org/10.1016/S0142-9612\(00\)00419-1](https://doi.org/10.1016/S0142-9612(00)00419-1)
- Maçon A, Kim T, Valliant E, Goetschius K, Brow R, Day D, et al. A unified in vitro evaluation for apatite-forming ability

- of bioactive glasses and their variants. *J Mater Sci: Mater Med*. 2015;26(2):1–10. <https://doi.org/10.1007/s10856-015-5403-9>
19. Sepulveda P, Jones JR, Hench LL. In vitro dissolution of melt-derived 45S5 and sol-gel derived 58S bioactive glasses. *J Biomed Mater Res*. 2002;61(2):301–11. <https://doi.org/10.1002/jbm.10207>
 20. Fagerlund S, Hupa L, Hupa M. Dissolution patterns of bio-compatible glasses in 2-amino-2-hydroxymethyl-propane-1,3-diol (Tris) buffer. *Acta Biomater*. 2013;9(2):5400–10. <https://doi.org/10.1016/j.actbio.2012.08.051>
 21. Fagerlund S, Hupa L, Hupa M. Comparison of reactions of bioactive glasses in different aqueous solutions. *Adv Bioceram Biotechnol*. 2010;218:101–13.
 22. Bingel L, Groh D, Karpukhina N, Brauer DS. Influence of dissolution medium pH on ion release and apatite formation of Bioglass 45S5. *Mater Lett*. 2015;143:279–82.
 23. Hench LL. Bioceramics: from concept to clinic. *J Am Ceram Soc*. 1991;74(7):1487–510. <https://doi.org/10.1111/j.1151-2916.1991.tb07132.x>
 24. Fernandes H, Gaddam A, Rebelo A, Brazete D, Stan G, Ferreira J. Bioactive glasses and glass-ceramics for healthcare applications in bone regeneration and tissue engineering. *Materials* 2018;11:2530. <https://doi.org/10.3390/ma1122530>
 25. Hench LL. Bioceramics. *J Am Ceram Soc*. 1998;81(7):1705–28.
 26. Zhang D, Hupa M, Aro HT, Hupa L. Influence of fluid circulation on in vitro reactivity of bioactive glass particles. *Mater Chem Phys*. 2008;111:497–502. <https://doi.org/10.1016/j.matchemphys.2008.04.055>
 27. Zhang D, Hupa M, Hupa L. In situ pH within particle beds of bioactive glasses. *Acta Biomater*. 2008;4(5):1498–505. <https://doi.org/10.1016/j.actbio.2008.04.007>
 28. Radin S, Ducheyne P, Falaize S, Hammond A. In vitro transformation of bioactive glass granules into Ca-P shells. *J Biomed Mater Res*. 2000;49(2):264–72. [https://doi.org/10.1002/\(SICI\)1097-4636\(200002\)49:2<264::CO;2-2](https://doi.org/10.1002/(SICI)1097-4636(200002)49:2<264::CO;2-2)
 29. Lindfors NC, Koski I, Heikkilä JT, Mattila K, Aho AJ. A prospective randomized 14-year follow-up study of bioactive glass and autogenous bone as bone graft substitutes in benign bone tumors. *J Biomed Mater Res B Appl Biomater*. 2010;94(1):157–64. <https://doi.org/10.1002/jbm.b.31636>
 30. Sidhu HS, Nelson MI, Balakrishnan E. An analysis of a standard reactor cascade and a step-feed reactor cascade for biological processes described by Monod kinetics. *Chem Prod Process Model*. 2015;10(1):27–37. <https://doi.org/10.1515/cppm-2014-0022>
 31. Hench L. The story of Bioglass. *J Mater Sci: Mater Med*. 2006;17(11):967–78. <https://doi.org/10.1007/s10856-006-0432-z>
 32. Kokubo T, Takadama H. How useful is SBF in predicting in vivo bone bioactivity? *Biomaterials* 2006;27(15):2907–15. <https://doi.org/10.1016/j.biomaterials.2006.01.017>
 33. New England Biolabs Inc. pH vs temperature for tris buffer. Available from: <https://international.neb.com/tools-and-resources/usage-guidelines/ph-vs-temperature-for-tris-buffer>. Accessed 17 Nov 2020.
 34. Conradt R. Chemical durability of oxide glasses in aqueous solutions: a review. *J Am Ceram Soc*. 2008;91(3):728–35. <https://doi.org/10.1111/j.1551-2916.2007.02101.x>
 35. Paul A. Chemical durability of glass. *Chemistry of glasses*. London, United Kingdom: Chapman and Hall Ltd; 1982. p. 108–47.
 36. Iler RK. The solubility of silica. *The chemistry of silica*. Hoboken, NJ: John Wiley & Sons; 1979. p. 30–49.
 37. Cannillo V, Pierli F, Ronchetti I, Siligardi C, Zaffe D. Chemical durability and microstructural analysis of glasses soaked in water and in biological fluids. *Ceram Int*. 2009;35(7):2853–69. <https://doi.org/10.1016/j.ceramint.2009.03.029>
 38. Häimi S, Moimas L, Pirhonen E, Lindroos B, Huhtala H, Rätty S, et al. Calcium phosphate surface treatment of bioactive glass causes a delay in early osteogenic differentiation of adipose stem cells. *J Biomed Mater Res A*. 2009;91(2):540–7. <https://doi.org/10.1002/jbm.a.32233>
 39. Hoppe A, Güldal NS, Boccaccini AR. A review of the biological response to ionic dissolution products from bioactive glasses and glass-ceramics. *Biomaterials* 2011;32(11):2757–74. <https://doi.org/10.1016/j.biomaterials.2011.01.004>
 40. Damen JJM, Ten Cate JM. Silica-induced precipitation of calcium phosphate in the presence of inhibitors of hydroxyapatite formation. *J Dent Res*. 1992;71(3):453–7. <https://doi.org/10.1177/00220345920710030601>
 41. Stanciu G, Sandulescu I, Savu B, Stanciu S, Paraskevopoulos K, Chatzistavrou X, et al. Investigation of the hydroxyapatite growth on bioactive glass surface. *J Biomed Pharm Eng*. 2007;1(1):34–9.
 42. Oonishi H, Hench LL, Wilson J, Sugihara F, Tsuji E, Matsuura M, et al. Quantitative comparison of bone growth behavior in granules of Bioglass®, A-W glass-ceramic, and hydroxyapatite. *J Biomed Mater Res*. 2000;51(1):37–46. [https://doi.org/10.1002/\(SICI\)1097-4636\(200007\)51:1<37::CO;2-T](https://doi.org/10.1002/(SICI)1097-4636(200007)51:1<37::CO;2-T)
 43. Barrère F, van Blitterswijk CA, de Groot K. Bone regeneration: molecular and cellular interactions with calcium phosphate ceramics. *Int J Nanomed*. 2006;1(3):317–32.
 44. Wetzel R, Brauer DS. Apatite formation of substituted Bioglass 45S5: SBF vs. Tris. *Mater Lett*. 2019;257:126760. <https://doi.org/10.1016/j.matlet.2019.126760>
 45. Shirdiff V, Hench L. Bioactive materials for tissue engineering, regeneration and repair. *J Mater Sci*. 2003;38(23):4697–707. <https://doi.org/10.1023/A:1027414700111>
 46. Cerruti MG, Greenspan D, Powers K. An analytical model for the dissolution of different particle size samples of Bioglass® in TRIS-buffered solution. *Biomaterials* 2005;26(24):4903–11. <https://doi.org/10.1016/j.biomaterials.2005.01.013>
 47. Sun J, Yang Y, Zhong J, Greenspan DC. The effect of the ionic products of Bioglass dissolution on human osteoblasts growth cycle in vitro. *J Tissue Eng Regen Med*. 2007;1(4):281–6.
 48. Drago L, Romanò D, De Vecchi E, Vassena C, Logoluso N, Mattina R, et al. Bioactive glass BAG-S53P4 for the adjunctive treatment of chronic osteomyelitis of the long bones: an in vitro and prospective clinical study. *BMC Infect Dis*. 2013;13(1):584. <https://doi.org/10.1186/1471-2334-13-584>

How to cite this article: Siekkinen M, Karlström O, Hupa L. Effect of local ion concentrations on the in vitro reactions of bioactive glass 45S5 particles. *Int J Appl Glass Sci*. 2022;13:695–707. <https://doi.org/10.1111/ijag.16579>

Siekkinen M., Karlström O., Hupa L. "***Dissolution of bioactive glass S53P4 in a three-reactor cascade in continuous flow conditions***"
Open Ceramics, Vol 13 (2023), DOI: 10.1016/j.oceram.2022.100327



Contents lists available at ScienceDirect

Open Ceramics

journal homepage: www.sciencedirect.com/journal/open-ceramics

Dissolution of bioactive glass S53P4 in a three-reactor cascade in continuous flow conditions

Minna Siekkinen, Oskar Karlström, Leena Hupa^{*}

Johan Gadolin Process Chemistry Centre, Åbo Akademi University, Henrikinkatu 2, 20500, Turku, Finland

ARTICLE INFO

Handling Editor: P Colombo

Keywords:
Bioactive glass
In vitro dissolution
Ion-release
Reaction layer

ABSTRACT

This study expands the knowledge of bioactive glass S53P4 dissolution by implementing a cascade reactor to a continuous dissolution setup. Three reactors were coupled in a series to study the effects of released ions on S53P4 reactions in each reactor. The pH and ion concentrations were measured in Tris-buffer and simulated body fluid flowing through the cascade reactor for five days. The reaction layer formed on the particles in each reactor were also analysed. In Tris, the dissolved Si decreased from 100% to 40% and 26% in the consecutive reactors after five days. In SBF, Si decreased from 64% to 11% and 8%. Thus, the ions released and decrease of available hydrogen ions for ion exchange influenced the dissolution behaviour of S53P4. The results partly explain the differences in the reaction degree between individual bioactive glass particles used as a bone graft in the same defect site.

1. Introduction

Biocompatible materials for repairing or replacing tissue include inert materials, such as metals, and active, such as bioactive, and regenerative materials [1]. A particular category of bioactive implant materials is bioactive glass, used to repair injured or diseased bones since 1985 [2]. Professor Hench and colleagues discovered and developed the first bioactive glass 45S5 in 1969 [2]. Since then, several glass compositions have been proven to gradually dissolve while forming a characteristic hydroxyapatite surface layer in aqueous solutions. This surface layer binds the material with hard and soft tissues [3]. The dissolution of bioactive glasses has been investigated *in vitro* and *in vivo* to verify the bioactivity of different compositions [4–7]. 45S5, also known as Bioglass®, consists of (in wt-%) 45 SiO₂, 24.5 CaO, 24.5 Na₂O, and 6 P₂O₅ [8]. Another clinically used bioactive glass, S53P4, was developed in the 1990s [9]. S53P4 has been reported to show antibacterial properties and have a similar dissolution behaviour as 45S5 [7, 10]. The oxide composition of S53P4 is (in wt-%) 53 SiO₂, 20 CaO, 23 Na₂O, and 4 P₂O₅.

In vitro comparison of bioactive glass 45S5 and S53P4 plates showed that S53P4 immersed in static buffered solutions increased the solution pH to a smaller extent than 45S5 [11]. On the other hand, the released Si concentration from the plates after one week was of a similar level for both glasses. S53P4 powder has antibacterial properties against 17

anaerobic and 29 aerobic bacteria [12,13]. The antibacterial properties of S53P4 have been clinically verified, e.g., in treating chronic osteomyelitis of long bones [14]. Further, using S53P4 provided antibacterial properties without the need for additional antibiotic therapies [15]. S53P4 has also been reported as well-tolerated in patients and supports faster healing of chronic osteomyelitis than conventional bone grafts when removing benign bone tumours [16,17]. Both the antibacterial effects and the bone regeneration depend on the ion dissolution rate from the glass. Long-term clinical results also reported residual glass within the well-regenerated bone [17]. The composition of these S53P4 remnants, however, is not known.

The reactions occurring at the bioactive glass surface upon exposure to physiological solutions in the human body or simulated body fluid (SBF) *in vitro* are usually described with the five following steps [18]: (i) exchange of alkali and alkaline ions from the glass with hydrogen ions from the solution and creating silanol bonds on the glass surface, (ii) local increase of solution pH leading to breaking of the glass structure (Si–O–Si bonds) and leaching of soluble silicon species to the solution, (iii) formation of a Si-rich layer on the surface as Si–OH groups condensate, (iv) migration of Ca²⁺ and PO₄³⁻ groups from bulk glass and solution to form an amorphous film of CaO–P₂O₅ on the surface, and (v) incorporation of hydroxyls and carbonates from the solution into the film followed by crystallization of the CaO–P₂O₅-film to a hydroxyapatite layer similar to bone apatite. After the hydroxyapatite layer has

^{*} Corresponding author.

E-mail address: leena.hupa@abo.fi (L. Hupa).

<https://doi.org/10.1016/j.oceram.2022.100327>

Received 4 September 2022; Received in revised form 13 December 2022; Accepted 22 December 2022

Available online 31 December 2022

2666-5395/© 2023 The Authors. Published by Elsevier Ltd on behalf of European Ceramic Society. This is an open access article under the CC BY-NC-ND license (<http://creativecommons.org/licenses/by-nc-nd/4.0/>).

formed, a series of biological mechanisms result in the bonding to the bone.

In vitro experiments are often performed by immersing either small blocks or particles of the bioactive glass in a static, buffered solution [4, 19,20]. As such static tests are conducted in a well-controlled environment, they allow changing parameters to investigate the effect of glass composition, solution, or time on the dissolution behaviour. However, it has been suggested that static studies do not reflect the dynamic environment of the body [21,22] and, as a result, dynamic *in vitro* experiments have been introduced [23]. Since bioactive glasses are highly soluble materials, tests with a circulating solution have been evaluated to avoid solution supersaturation [24]. Some studies replaced the immersion solution SBF with fresh SBF after 6, 24, and 48 h [25] or every day for 28 days [26]. Also circulating the SBF with a flow of 1 ml/min through the sample has been studied [27]. These studies concluded that experiments in replenished or circulating solutions mimic the dynamic body environment better than experiments in static solutions. Furthermore, thinner but more uniform layers formed on particles in tests where the solution was circulated above the particle bed [28,29]. Continuous flow-through reactor with the possibility to adjust the fluid flow rate was developed to study the initial ion release from bioactive glasses into a fresh solution fed through the glass particles [10,30]. In these studies, the glass surface area, particle bed dimensions, flow rate, temperature, and composition of the solution affected the initial ion release from the bioactive glass 1–98 (in wt-% 53 SiO₂, 22 CaO, 6 Na₂O, 2 P₂O₅, 11 K₂O, 5 MgO, and 1 B₂O₃).

The role of surface area on bioactive glass dissolution has been studied using different particle size fractions [31,32]. Smaller particles, i.e., a larger specific surface area, release ions quicker than larger particles, i.e., smaller specific surface area. As the released ions change the local ion concentrations of the surrounding solution, the ions are likely to affect the overall dissolution behaviour of the glass. So far, research focusing on the effect of local ion concentrations on glass dissolution is scarce. Although the solution pH inside a particle bed undergoing dissolution can be measured [28,29], analysing the reaction layers after the experiment is challenging as the particles' location in the bed during the experiment is difficult to trace.

In our recent study, a cascade reactor was used to separate 4555 particles section-wise into three batches, and the solution was fed through the reactors connected in series [33]. Faster reactions and increased dissolution of particles were identified for particles in the first reactor compared to the second and third reactors. Also, the dissolution of silicon decreased from 92% in the first reactor to 26% and 24% in the second and third reactors after seven days of continuous Tris flow. For dissolution in SBF, the Si release was 35%, 20%, and 19% of the Si in the samples in the three consecutive reactors. Although the experiments with 4555 in the cascade reactor system with a continuous fluid flow introduced a novel experimental procedure to consider for researching new implantable materials, the understanding of the impact of the local ion concentration on the overall dissolution is still poorly understood.

The present study investigates the impact of dissolved reaction products from the bulk glass, i.e., how the ion concentrations and pH changes in the surrounding solution influence the dissolution behaviour of S53P4 *in vitro*. The experiments were conducted in the cascade reactor system with a continuous flow of Tris and SBF. The ultimate goal was to shed light on the long-term dissolution behaviour of bioactive glasses used as bone grafts.

2. Materials and methods

2.1. Glass particles

S53P4 particles were provided by Bonalive Biomaterials Ltd (Turku, Finland). The wide size range of particles was sieved to a 300–500 µm size fraction. The particles were cleaned with acetone in an ultrasound bath until the acetone stayed transparent after the cleaning, to remove

powder adhered to the particle surfaces. Fig. 1 presents (a) the particle size distribution (Malvern Analytical Mastersized 3000) and (b) an SEM image of the unreacted glass particles. The average diameter was 500 µm, and 57% of the particles had a diameter between 272 and 515 µm. Due to the irregular shapes of the crushed glass particles, some elongated particles could pass through the 500 µm sieve, influencing the size distribution. It should be noted that the SEM image in Fig. 1 represents particle cross-sections taken in a random location of a particle bed.

2.2. Buffer solution preparation

The *in vitro* studies were conducted in simulated body fluid (SBF) [34] and tris(hydroxymethyl)aminomethane (Tris) and were prepared in-house. SBF is considered to mimic the reactions occurring *in vivo* more effectively than sole Tris, due to its similar content of inorganic ions as human blood plasma. However, as SBF already contains high concentrations of some inorganic ions, supersaturation during the ion release from the glass may be an issue [35]. The Tris-buffered SBF was prepared according to ISO 23317:2014 [36] by adding each chemical (Table 1) into 850 ml of purified water in a beaker with a magnet continuously stirring throughout the dissolution. The Tris-buffer for SBF was separately dissolved in a small amount of purified water before slowly being added to the solution with the inorganic ions. Before adjusting the pH, the solutions were kept at 37 °C in a water bath for 4 h (SBF) and 2 h (Tris). The pH was adjusted by adding 1 M HCl into the buffered solutions until the pH was 7.4 at 37 °C. The solutions were transferred to a volumetric flask into which purified water was added to obtain the correct volume. The solution volumes were temperature-adjusted at room temperature.

2.3. Experimental setup

The experiments were conducted in a cascade setup consisting of three reactors connected in series with a continuous flow of the buffered solutions through the reactors. A detailed description of the setup can be found elsewhere [30,33,37]. The three reactors were assumed to represent different locations of dissolving particles in a bed. The glass particles in the first reactor were assumed to represent those with the first contact with the solution. Correspondingly, the particles in the second reactor would correlate to the bulk phase particles. Finally, the third reactor particles were assumed to have experienced a similar environment as the innermost particles in a single bed. 205 ± 5 mg S53P4 glass particles were added to each reactor.

A peristaltic pump fed the buffer solution through the cascade reactor system with a 0.2 ml/min flow rate. Thin thermoplastic Tygon® tubes connected the solution to the inflows and outflows from the reactors. The solution and reactors were kept in a 37 °C water bath to mimic the temperature inside the human body. After one, two, and all three reactors, the outflow solution was collected into test vials at various time points for 20 min to provide a total solution of 4 ml for further analyses. The solutions were collected every 20 min for the first hour and then at 2, 4, 6, 8, 16, and 24 h. After 24 h, the solution was collected every 24 h for 5 days. Additionally, 1 ml of the bulk solution outflow between each measurement point was collected for further ion analysis. Three parallel runs were conducted for experiments up to 5 days. Several samples of the buffer solution were used to obtain its average pH and initial inorganic ion concentrations. The cross-sections of partially reacted glass particles were analysed at 4, 24, and 72 h.

2.4. Temperature and pH

The temperature and pH (Mettler Toledo SevenEasy S20) were measured directly after collecting the solution from the outflow. As the solution temperature rapidly decreased to room temperature, the values were calculated to give the pH at 37 °C using equation (1) [38]. The equation was verified by measuring the pH of the reference solution at

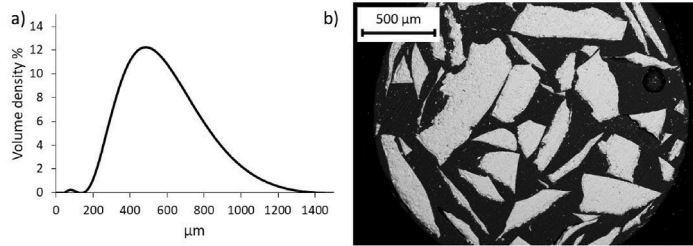


Fig. 1. Particle size distribution (a) and SEM image of unreacted S53P4 particles (b).

Table 1
Concentrations (g/l) of chemicals in SBF and Tris buffer solutions.

	NaCl	NaHCO ₃	KCl	K ₂ HPO ₄ ·3H ₂ O	MgCl ₂ ·6H ₂ O	1 M HCl (aq)	CaCl ₂ ·2H ₂ O	Na ₂ SO ₄	Tris
SBF	7.996	0.35	0.224	0.228	0.305	35 ml	0.368	0.071	6.057
Tris	–	–	–	–	–	–	–	–	6.057
Manufacturer	VWR Chemicals	J.T. Baker	Sigma Aldrich	Sigma Aldrich	Sigma Aldrich	Sigma Aldrich	VWR Chemicals	Sigma Aldrich	Sigma Aldrich

different temperatures in a water bath. Calibration of the pH meter was done with standardized buffer solutions with pH 4.01, 7.00, and 9.21.

$$pH_{37} = pH_{\text{measured}} - 0.02664 \cdot (37 - T_{\text{measured}})$$

Eq 1

2.5. Ion analysis

The concentrations of Si, Ca, Na, and P species in the collected solutions were analysed with inductively coupled plasma optical emission spectroscopy (ICP-OES, Optima 5300 DV; PerkinElmer, Waltham, MA). Three parallel samples were performed at each time point. The limits of quantification of the analysed ions were 0.004 mg/l for Si, 0.03 mg/l for Ca, 0.2 mg/l for Na, and 0.03 mg/l for P. The wavelengths for the conducted analyses were 251.622 nm for Si, 317.933 for Ca, 589.592 nm

for Na, and 213.617 for P. The collected solutions were diluted in the volume ratio of 1:10 before the ICP-OES analysis. The ICP-OES was calibrated with ultrapure water and a commercial multi-element standard (Spectrascan) with 1, 5 and 20 ppm Si, Ca, Na, and P. The calibration was verified by measuring the ion concentrations of the multi-element standard after every 60 samples. The background level was recorded before each sample run. All reported ion concentrations are background corrected.

2.6. Reaction layers on particle surfaces

The reaction layers on the particle surfaces were analysed with a scanning electron microscope with energy dispersive x-ray analysis (SEM-EDX, Leo Gemini; Carl Zeiss, Oberkochen, Germany). For this, the partly dissolved particles were removed from the reactors, washed with

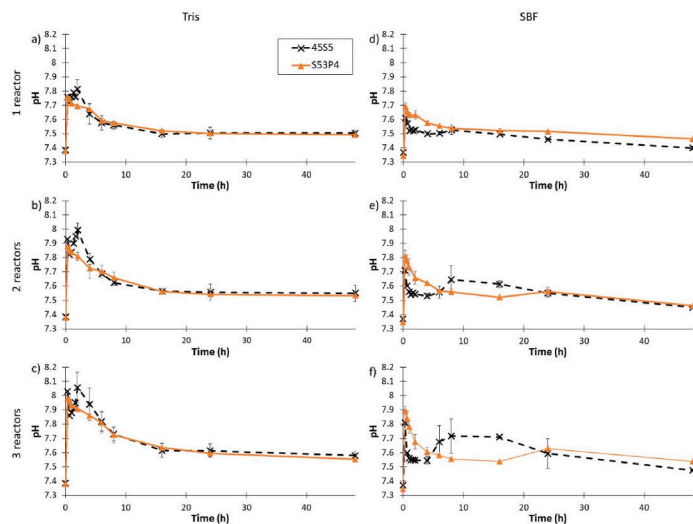


Fig. 2. The pH changes as functions of time for experiments conducted in Tris (left) and SBF (right) for the consecutive reactors with S53P4 and 45S5 [33].

ethanol to stop the reactions, dried at 40 °C in an oven overnight, and then embedded into epoxy resin. The cross-sectional areas of the particles were obtained by grinding and polishing the epoxy-embedded particles.

3. Results

3.1. Influence of glass dissolution on pH

Fig. 2 shows the pH changes during the first 48 h of dissolution of S53P4 particles in Tris (left) and SBF (right) after each reactor in the cascade reactor system, with an increasing number of reactors arranged vertically. The figure also displays the corresponding data for 45S5 [33]. For all reactors, pH first increased to 7.6–8, followed by a decrease in both solutions. In SBF, the pH first decreased more rapidly than in Tris. Between 2 and 8 h, the pH decreased similarly in Tris and SBF. Interestingly, a second increase and decrease of pH in SBF can be observed after multiple reactors at around 24 h for S53P4. After 24 h, the pH of Tris stabilized in all reactors and the first reactor in SBF. The stabilization of the pH took longer for the second and third reactors.

In Tris and SBF, the initial pH increases were consistently highest after all three reactors and lowest after the first reactor. Also, the pH increased with the number of reactors at all times. However, the total pH increases between the solution inflows and outflows were lowest for the second and third reactors, and highest for the first reactor. In Tris, the

highest pH increase compared to the inflow pH was at 20 min (0.33 h) with the total increases as follows: 0.38 pH units (1st reactor); 0.12 (2nd reactor); 0.10 (3rd reactor). The corresponding pH differences in SBF were: 0.34; 0.12; 0.09.

3.2. Ion release

Fig. 3 shows the ion concentrations in the solutions after each reactor as functions of time. The highest Ca, Na, and P concentrations in Tris were measured at 20 min (the first measuring point). On the other hand, the highest Si concentration was measured at shorter dissolution times for increasing number of reactors according to 2 h, 40 min, and 20 min. In SBF, the highest Si concentration was measured at 1 h after one and two reactors and at 20 min after all three reactors. The highest Ca concentration in SBF was measured at 20 min for all reactors. The high initial Na concentration in SBF prevented accurate simultaneous analyses with the other ions. Thus, the reported Na concentrations released from the glass into SBF are only indicative. The highest Na concentrations were measured at 120 h in the first and second reactors. For three reactors, the highest Na concentration was measured already at 20 min. Correspondingly, the highest P concentrations in SBF were measured at 20–60 min after the two first reactors and at 2 h after all three reactors. Noticeably, the highest P concentrations in SBF were measured after one reactor, followed by all three reactors. The relatively low initial P content of the unreacted S53P4 was assumed to provide only minor changes

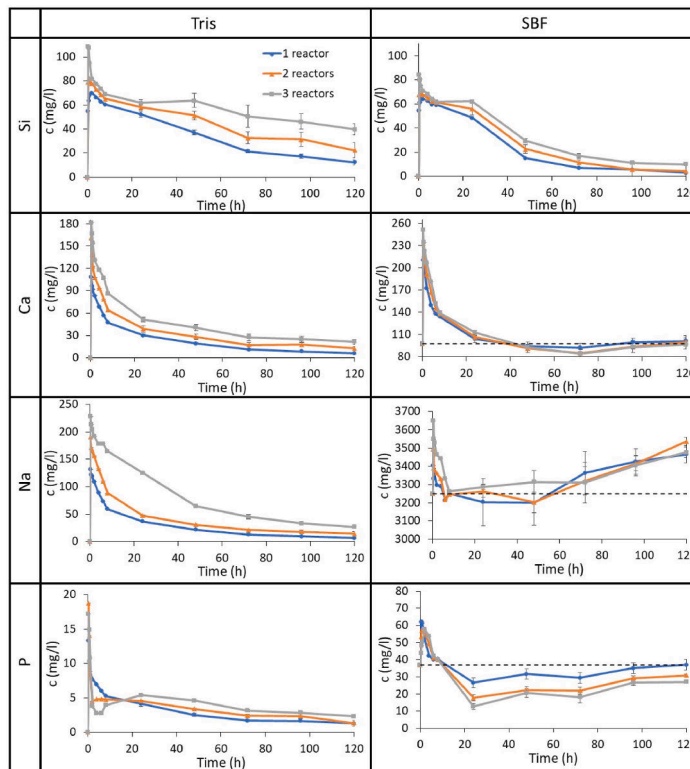


Fig. 3. Average concentrations of Si, Ca, Na and P species released into Tris and SBF in the three consecutive reactors as functions of dissolution time. The standard deviations are shown for the analyses from 24 h onward. The dashed lines give the initial concentrations in SBF.

in the ion concentration of the solution, thus influencing the accuracy of the measurements.

The changes in Si concentration in Tris and SBF after each reactor are presented in Fig. 4. The figure also includes results of 45S5 under similar conditions [33]. The values for S53P4 were calculated from the Si concentrations (mg/l) given in Fig. 3. In general, the Si trends were similar for both Tris and SBF. The highest Si concentrations were observed in the first reactor in both solutions and for both glasses. For S53P4, it should be noted that the Si concentration decreased more rapidly in SBF than in Tris. On the other hand, the decrease of Si concentration was more rapid in Tris than SBF for 45S5. However, the Si concentration in Tris for 45S5 was stable at around 25 mg/l after the decrease. A similar stabilization level for S53P4 was also seen in Tris, but the decrease was less rapid than for 45S5. For the second and third reactors, the first 48 h show apparent differences between S53P4 and 45S5. In both Tris and SBF, the biggest change of Si concentration can be seen for the first measuring point for S53P4, while for 45S5, the high and broad peak of the change of Si concentration can be seen between 8 and 48 h in SBF.

3.3. Reaction layers

SEM images of S53P4 after dissolutions in Tris and SBF for 4, 24, and 72 h are shown in Figs. 5 and 6. Already at 4 h in Tris, thin silica-rich (Si-rich) layers (light grey) are visible for particles from the first and second reactors. At 4 h, no surface layer can be seen on the particles in the third reactor in Tris or any of the reactors in SBF. At 24 h, distinct Si-rich layers and indications of calcium phosphate (Ca/P) layers are seen on some particles in all reactors in Tris and SBF. However, the SEM images and line imply that surface layers formed in Tris were indistinct.

The line analyses (EDX) close to the external surface of separate particles is shown in Fig. 5 for S53P4 particles after dissolution in Tris for 4, 24, and 72 h. Particles from the first and second reactors have a silica-rich layer at 4 h, while no layers can be seen on glass particles taken from the third reactor. The line analysis along the particle surface cross-section shows the silica-rich layer as increased Si and decreased

Ca, Na, and P contents. The Na content is almost constant in the unreacted particle parts below the surface layer. With increasing dissolution times, the thickness of the Si-rich layer increased. Also, the Ca and P concentrations at the outermost surface increased. At 72 h, Ca and P increased within the Si-rich layer. This mixed Si-rich + Ca/P layer was more pronounced in the second and third reactors than in the first. These analyses suggest that no pure Ca/P outer surface layer had formed on the particles in Tris in any of the investigated cases.

The EDX-line analyses of S53P4 particles after dissolution in SBF for 4, 24, and 72 h is shown in Fig. 6. No layers can be seen in particles from any reactor at 4 h, implying that the reaction layers formed later. The line analyses also show an almost constant concentration of the elements throughout the particle cross-section in all reactors. However, after 24 h in SBF, distinct Si-rich layers can be seen on particles from all reactors. Additionally, a mixed layer consisting of Ca/P and Si, followed by a Ca/P outer surface layer can be noticed in the first and second reactor particles. The line analyses also confirm the Ca/P layer in this case; the Si content decreases towards zero, while only Ca and P are present on the outer surface. On the other hand, only a mixed layer of Ca/P and Si was analysed on the third reactor particles.

Between 24 and 72 h, the reaction layer thickness increased in SBF. The first reactor particles display a distinct Si-rich layer, indications of a mixed layer, and an extensive outer, almost pure Ca/P-layer. The analysed particle in the second reactor showed similar but notably thinner layers. Finally, the analysed particle in the third reactor showed an uneven Si-rich layer, a mixed layer, and a thin pure Ca/P-layer.

The EDX line analyses along the particle surfaces in Figs. 5 and 6, show increases in the Ca and P contents after 24 and 72 h in Tris and SBF. In Tris, Ca and P increases are accompanied by Si. In contrast, the outer layer consisted of almost pure Ca/P, with Si and Na close to zero after SBF dissolution. At 24 h and onward, only the third reactor particles showed a mixed layer of Si, Ca, and P in SBF. These results suggest that the phosphate content released in Tris was not high enough to form a pure Ca/P layer on the S53P4 particles. Instead, a mixed layer formed in Tris. In contrast, the particles had visibly fused by the outermost Ca/P layer after 120 h in SBF.

4. Discussion

Highly reactive materials, such as bioactive glasses, release ions when in contact with physiological solutions. However, the role of the released ions on the dissolution of bioactive glasses has been poorly studied. Only a few studies discuss the impact of the dissolution products. The main emphasis has been on the cellular responses to the dissolution products from the dissolved bioactive glass [39–41]. For example, dissolution products from bioactive glass 45S5 have been shown to shorten the human osteoblast growth cycle [40].

In an earlier study, we showed that a cascade reactor could be utilized in the continuous dissolution flow-through to investigate the release of ions between each section of a larger implanted particle bed [33]. The ability of bioactive glasses to exchange ions with the surrounding solution is one of the most distinctive properties of the material and is correlated to the pH increase. In this study, an increasing number of reactors increased the pH of the solution flowing through the bioactive glass particles (Fig. 2), indicating that fewer hydrogen ions were available for ion exchange with the particles. Consequently, this led to delayed reactions between material and solution in subsequent reactors. The impact of the reaction products on the dissolution of bioactive glasses was especially noticeable in SBF. Interestingly, with added reactors in SBF, a second increase in the pH was seen for S53P4 and 45S5. This indicates that the reaction products delayed the solution-material reactions as the increase of pH is one of the earliest steps of the reaction behaviour. However, the second increase was measured later for S53P4 than 45S5 (at 24 h compared to 8 h). For S53P4, there is a dramatic decrease of P in SBF between 8 and 24 h (Fig. 3). The lowest levels of P concentrations were measured in SBF at

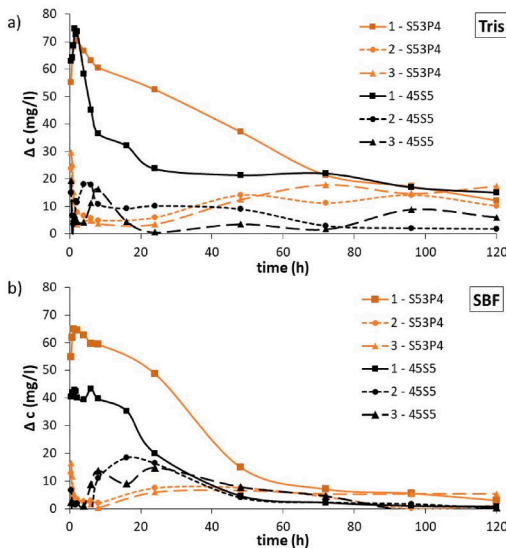


Fig. 4. Si concentration change in Tris (above) and SBF (below) after each reactor for S53P4 and 45S5 [33].

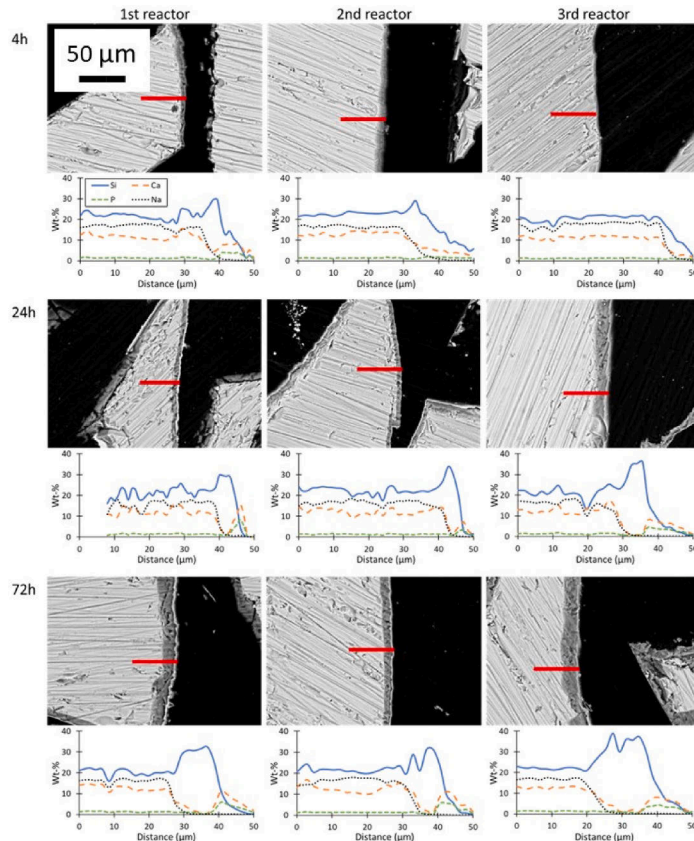


Fig. 5. SEM images and EDX-analyses of S53P4 particle cross-sections after different dissolution times in a continuous flow of Tris.

24 h as 27 mg/l after one reactor, 18 mg/l after two reactors, and 13 mg/l after all three reactors. Only after the first reactor did the P concentration at 120 h increase to the measured P levels in the reference SBF. Whereas for 45S5, a similar P decrease was seen earlier, between 6 and 8 h of continuous dissolution. A decrease in the P species concentration of SBF is usually seen in static experiments when the phosphate in the solution precipitates on the material surfaces [42]. However, precipitation of Ca/P starts at established nucleation sites (Si-rich layer). The decrease of P in the inflow to the second and third reactors indicate that P in the SBF precipitates in the first reactor as soon as a suitable nucleation site is present. As particles in the later reactors lack the Si-rich layer during the first hours, Ca/P cannot precipitate from the solution rich in P. Reaction layers, especially the outer Ca/P layer, are crucial for bonding to the bone *in vivo* [43]. In SBF (Fig. 6), a pure outer Ca/P layer can be seen from the line analyses in the two first reactors at 72 h, whereas the outer Ca/P layer in the third reactor suggests decreasing Si concentrations along the line. In Tris (Fig. 5), similar mixed Si and Ca/P layer could be seen at 72 h in all reactors. Similar reaction patterns were identified for 45S5 in the cascade reactor [33].

Fig. 7 shows the cumulative dissolution of Si from S53P4 and earlier studied 45S5 [33]. The cumulative dissolution is calculated from data in Fig. 3, the volume of the solution fed through the system, and the amount of Si in the unreacted bioactive glass sample placed in the

reactors. Overall Si-release from S53P4 and 45S5 into the two solutions correlated with the total SiO₂ content in the glasses. A high Si release from the first reactor particles decreased the concentration gradients around the particles in the consecutive reactors, thus leading to lower cumulative Si dissolution. Although S53P4 has a higher concentration of Si-species available for dissolution, the glass also has higher chemical durability. Accordingly, Si-rich and Ca/P layers formed slower on S53P4 than on 45S5 particles. Thicker Si-rich and Ca/P layers more effectively decreased the Si-release from the 45S5 particles to both solutions [33]. The large differences in the cumulative Si-release from S53P4 between the first and the two consecutive reactors were assumed to depend on a combined effect of chemical durability, higher concentration gradients around the second and third reactor particles, and also, to some degree, the Ca/P layers retarding the Si-species diffusion from the bulk glass. Thus, larger differences were measured between the S53P4 particles in the three reactors than reported for 45S5. However, the trends measured for S53P4 were similar to 45S5, verifying the impact of local ion concentrations on bioactive glass dissolution. The release of all ions from S53P4 increased with an increased number of reactors (Fig. 3). However, when comparing Si concentrations after each reactor, the decrease in the release was not proportional to the sample amount in the reactor (Fig. 4). The Si concentrations in the outflows from the second and third reactors were almost identical when correlated to the Si concentration in

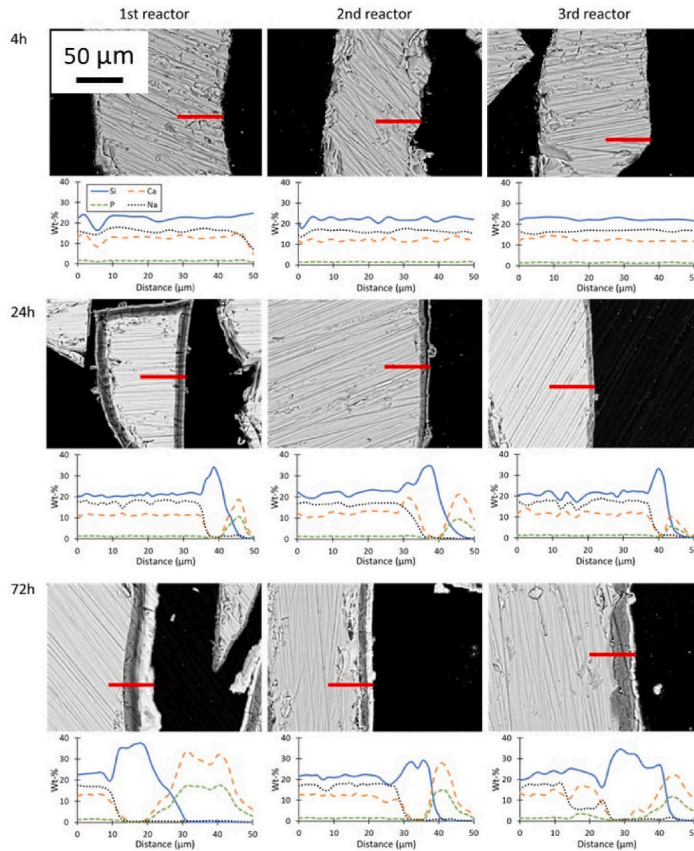


Fig. 6. SEM images and EDX-analyses of S53P4 particle cross-sections after different dissolution times in a continuous flow of SBF.

the inflow. At 72 h, 39.8 mg of the total 50.8 mg Si in the first reactor was dissolved. Corresponding amounts were 11 mg from the second reactor and 7.4 mg from the third reactor. In SBF, the release of Si decreased from 29.1 to 5.2 and 1.9 mg from the three consecutive reactors. The dissolved Si from the first reactor is thus suggested to slow down the further dissolution of Si in the second and third reactors. This effect is likely due to soluble Si species in the solutions being close to saturation levels in the second and third reactors.

S53P4 contains 8 wt-% more SiO_2 than 45S5, indicating that more Si can be released from S53P4 (in this study 50.8 mg Si in S53P4 and 44.9 mg in 45S5 in each reactor). S53P4 has been shown to initially dissolve slower than 45S5 in static conditions [11,44]. However, S53P4 has been reported to show a more consistent dissolution over a two-week immersion test than 45S5. Further, S53P4 dissolved more in Tris than in SBF [11]. In the present work, the Si release was higher from S53P4 than 45S5 in prolonged continuous flow experiments in Tris. Similar trends were measured in SBF for only one reactor. However, more Si was released from 45S5 than S53P4 in multiple reactors (Fig. 7).

The role of pH on bioactive glass dissolution has also been studied. Precipitation of Ca and P species has been demonstrated to occur more rapidly on 45S5 upon immersion at increasing pH in static conditions [45]. The precipitated Ca and P on the glass surface simultaneously decreased the ion release from the bulk glass. Hence, the release of Ca

and P is expected to increase at decreased pH, as reported in acidic solutions [46]. Si release also increases with pH due to the ion exchange between the solution and the glass [18,47]. In this work, the solution pH after each reactor was still within the buffering range of the solutions, thus partly explaining that the Si release rate slowed down with dissolution time. However, all Si was dissolved from the S53P4 in the first reactor into Tris at 120 h (Fig. 7). This can be explained by the thin Ca/P layer and the Si species concentration being below the saturation level.

Even though it has been proposed that released ions hinder the dissolution of bioactive glasses, the dissolution products only initially slowed down the dissolution in this work. However, as soon as the bioactive glass particles in the first reactor had developed a Ca/P reaction layer, the dissolution of Si increased in the next reactors. After the Ca/P layer had formed on the first reactor particles, it retarded their further dissolution. Thus, Si concentration gradients around the particles in the following reactors increased, leading to increased Si dissolution.

The results suggest that the released ions strongly affect the dissolution rate of bioactive glasses. Small changes in local ion concentrations had a dramatic effect on the dissolution of S53P4 and 45S5 in SBF. This implies that a larger implanted particle bed may be expected to react non-uniformly *in vivo* under similar flow conditions as reported in this work. However, Fig. 6 shows that an outer pure Ca/P layer had formed

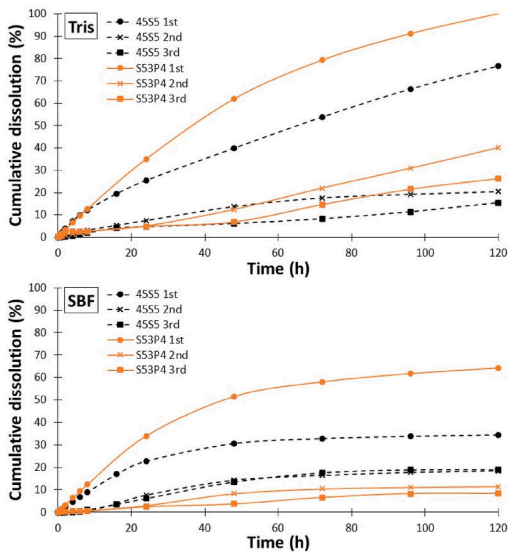


Fig. 7. Cumulative dissolution of silicon (%) from the bioactive glass particles 45S5 and S53P4 in each reactor with experiments conducted with Tris (above) and SBF (below). (For interpretation of the references to colour in this figure legend, the reader is referred to the Web version of this article.)

even in the third reactor particles at 72 h. Thus, these areas representing the conditions inside the particle bed, or the interior part of a porous implant, are gradually covered by Ca/P. This layer can then develop into hydroxyapatite and further convert into bone tissue.

5. Conclusion

This study investigated the effect of released ionic species on the dissolution and reaction layer formation on bioactive glass S53P4 particles in a three-reactor cascade in continuous flow conditions. The released ions from the glass particles in the first reactor influenced the dissolution of the particles in the consecutive reactors. The ion release occurred more rapidly in the first reactor representing the exterior surfaces of an implanted particle bed. In contrast, the increased ion concentrations in solution inflows to the second and third reactors, representing the interior surfaces of the particle bed, led to markedly slower dissolution. Si-rich and Ca/P surface layers developed more rapidly in the first reactor particles than particles in the following two reactors. After a Ca/P layer had formed, the dissolution slowed down. The results imply that the increased local ion concentrations delay reactions in the interior parts of implanted particle beds. Finally, the cascade reactor system provided additional confidence to the established static and dynamic dissolution tests.

Summary of novel conclusions Turku, 17.8.2022

This work enhances the understanding of the *in vitro* reactions of bioactive glass S53P4 particles in different locations of a particle bed in continuous fluid flow. This approach simulates the actual conditions, e.g., grafting bone cavities with bioactive glass particles. When a fresh fluid, such as the co-called simulated body fluid, is fed through the particles, the ions released from the particles with the first contact affect the reactions of the other particles. As the particles were separated into three different reactors in series, the reactions could be studied

individually for each reactor. The results showed that the dissolution of bioactive glass in later reactors were affected by the ions released from the first reactor. The results provide new knowledge on the gradual degradation patterns of implanted bioactive glass particles or porous bodies.

Declaration of competing interest

The authors declare that they have no known competing financial interests or personal relationships that could have appeared to influence the work reported in this paper.

Acknowledgements

This work is part of the Business Finland project Smart materials at biomaterial industry (882/31/2019). BonAlive Biomaterials Ltd is acknowledged for material and collaboration. Financial support by Svenska Kulturfonden Project 157767 (Minna Siekkinen) and The Academy of Finland Project 321598 (Oskar Karlström) are acknowledged. Luis Bezerra and Linus Silvander are acknowledged for their technical assistance with ICP-OES and SEM.

References

- [1] G.-I. Im, Biomaterials in orthopaedics: the past and future with immune modulation, *Biomater. Res.* 24 (2020) 7, <https://doi.org/10.1186/s40824-020-0185-7>.
- [2] L. Hench, The story of Bioglass, *J. Mater. Sci. Mater. Med.* 17 (2006) 967–978, <https://doi.org/10.1007/s10856-006-0432-z>.
- [3] L.L. Hench, G.P. LaTorre, Ö.H. Andersson, The kinetics of bioactive ceramics Part III: surface reactions for bioactive glasses compared with an inactive glass, *Bioceramics*, Elsevier Ltd (1991) 155–162, <https://doi.org/10.1016/B978-0-7506-0269-3.50025-6>.
- [4] A.L.B. Maçon, T.B. Kim, E.M. Valliant, K. Goetschius, R.K. Brow, D.E. Day, et al., A unified *in vitro* evaluation for apatite-forming ability of bioactive glasses and their variants, *J. Mater. Sci. Mater. Med.* 26 (2015) 115, <https://doi.org/10.1007/s10856-015-5403-9>.
- [5] A. Anand, V. Lalzawliana, V. Kumar, P. Das, K.B. Devi, A.K. Maji, et al., Preparation and *in vivo* biocompatibility studies of different mesoporous bioactive glasses, *J. Mech. Behav. Biomed. Mater.* 89 (2019) 89–98, <https://doi.org/10.1016/j.jmbmm.2018.09.024>.
- [6] P.K. Vallittu, J.P. Posti, J.M. Piitulainen, W. Serlo, J.A. Määttä, T.J. Heino, et al., Biomaterial and implant induced ossification: *in vitro* and *in vivo* findings, *J. Tissue Eng Regen Med* 14 (2020) 1157–1168, <https://doi.org/10.1002/term.3056>.
- [7] Ö.H. Andersson, I. Kangasniemi, Calcium phosphate formation at the surface of bioactive glass *in vitro*, *J. Biomed. Mater. Res.* 25 (1991) 1019–1030, <https://doi.org/10.1002/jbm.b.820250808>.
- [8] L.L. Hench, Chronology of bioactive glass development and clinical applications, *New J. Glass Ceram.* 3 (2013) 67–73, <https://doi.org/10.4236/njgc.2013.32011>.
- [9] Ö.H. Andersson, G. Liu, K.H. Karlsson, L. Niemi, J. Miettinen, J. Juhanoja, *In vivo* behaviour of glasses in the SiO₂-Na₂O-CaO-P₂O₅-Al₂O₃-B₂O₃ system, *J. Mater. Sci. Mater. Med.* 1 (1990) 219–227, <https://doi.org/10.1007/BF00701080>.
- [10] S. Fagerlund, L. Hupa, M. Hupa, Dissolution patterns of biocompatible glasses in 2-amino-2-hydroxymethyl-propane-1,3-diol (Tris) buffer, *Acta Biomater.* 9 (2013) 5400–5410, <https://doi.org/10.1016/j.actbio.2012.08.051>.
- [11] L. Varila, S. Fagerlund, T. Lehtonen, J. Tuominen, L. Hupa, Surface reactions of bioactive glasses in buffered solutions, *J. Eur. Ceram. Soc.* 32 (2012) 2757–2763, <https://doi.org/10.1016/j.jeurceramsoc.2012.01.025>.
- [12] O. Leppäranta, M. Vaahtio, T. Peltola, D. Zhang, L. Hupa, M. Hupa, et al., Antibacterial effect of bioactive glasses on clinically important anaerobic bacteria *in vitro*, *J. Mater. Sci. Mater. Med.* 19 (2007), <https://doi.org/10.1007/s10856-007-3018-5>.
- [13] E. Munukka, O. Leppäranta, M. Korkeamäki, M. Vaahtio, T. Peltola, D. Zhang, et al., Bactericidal effects of bioactive glasses on clinically important aerobic bacteria, *J. Mater. Sci. Mater. Med.* 19 (2008) 27–32, <https://doi.org/10.1007/s10856-007-3143-1>.
- [14] L. Drago, D. Romano, E. De Vecchi, C. Vassena, N. Logoluso, R. Mattina, et al., Bioactive glass BAG-S53P4 for the adjunctive treatment of chronic osteomyelitis of the long bones: an *in vitro* and prospective clinical study, *BMC Infect. Dis.* 13 (2013) 584, <https://doi.org/10.1186/1471-2334-13-584>.
- [15] M.T. Cunha, M.A. Murça, S. Nigro, G.B. Klautau, M.J.C. Salles, *In vitro* antibacterial activity of bioactive glass S53P4 on multiresistant pathogens causing osteomyelitis and prosthetic joint infection, *BMC Infect. Dis.* 18 (2018), <https://doi.org/10.1186/s12879-018-3069-x>.
- [16] N.C. Lindfors, P. Hyvönen, M. Nyyssönen, M. Kirjavainen, J. Kankare, E. Gullichsen, et al., Bioactive glass S53P4 as bone graft substitute in treatment of osteomyelitis, *Bone* 47 (2010) 212–218, <https://doi.org/10.1016/j.bone.2010.05.030>.

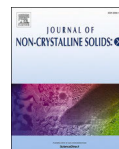
- [17] N.C. Lindfors, I. Koski, J.T. Heikkilä, K. Mattila, A.J. Aho, A prospective randomized 14-year follow-up study of bioactive glass and autogenous bone as bone graft substitutes in benign bone tumors, *J. Biomed. Mater. Res. B Appl. Biomater.* 94B (2010) 157–164, <https://doi.org/10.1002/jbm.b.31636>.
- [18] J.R. Jones, Review of bioactive glass: from Hench to hybrids, *Acta Biomater.* 9 (2013) 4457–4486, <https://doi.org/10.1016/j.actbio.2012.08.023>.
- [19] T. Kokubo, H. Kushitani, C. Ohtsuki, S. Sakka, T. Yamamuro, Chemical reaction of bioactive glass and glass-ceramics with simulated body fluid, *J. Mater. Sci. Mater. Med.* 3 (1992) 79–83, <https://doi.org/10.1007/BF00705272>.
- [20] J. Massera, L. Hupa, M. Hupa, Influence of the partial substitution of CaO with MgO on the thermal properties and in vitro reactivity of the bioactive glass S53P4, *J. Non-Cryst. Solids* 358 (2012) 2701–2707, <https://doi.org/10.1016/j.jnoncrysol.2012.06.032>.
- [21] A.H. De Aza, P. Velásquez, M.I. Alemany, P. Pena, P.N. De Aza, In situ bone-like apatite formation from a Bioeutectic® ceramic in SBF dynamic flow, *J. Am. Ceram. Soc.* 90 (2007) 1200–1207, <https://doi.org/10.1111/j.1551-2916.2007.01534.x>.
- [22] Y.R. Duan, Z.R. Zhang, C.Y. Wang, J.Y. Chen, X.D. Zhang, Dynamic study of calcium phosphate formation on porous HA/TCP ceramics, *J. Mater. Sci. Mater. Med.* 15 (2004) 1205–1211, <https://doi.org/10.1007/s10856-004-5673-0>.
- [23] S. Taipale, P. Ek, M. Hupa, L. Hupa, Continuous measurement of the dissolution rate of ions from glasses, *Adv. Mater. Res.* 39–40 (2008) 341–346, <https://doi.org/10.4028/www.scientific.net/AMR.39-40.341>.
- [24] D. Rohanová, D. Horkavcová, A. Helebrant, A.R. Boccaccini, Assessment of in vitro testing approaches for bioactive inorganic materials, *J. Non-Cryst. Solids* 432 (2016) 59, <https://doi.org/10.1016/j.jnoncrysol.2015.03.016>.
- [25] G. Theodorou, O.M. Goudouri, E. Kontonasaki, X. Chatzistavrou, L. Papadopoulou, N. Kanitranis, et al., Comparative bioactivity study of 45S5 and 58S bioglasses in organic and inorganic environment, *Bioceram. Dev. Appl.* 1 (2011) 1–4, <https://doi.org/10.4303/bda/D110154>.
- [26] Y. Zhang, M. Mizuno, M. Yanagisawa, H. Takadama, Bioactive behaviors of porous apatite- and wollastonite-containing glass-ceramic in two kinds of simulated body fluid, *J. Mater. Res.* 18 (2003) 433–441, <https://doi.org/10.1557/JMR.2003.0055>.
- [27] S. Yue, P.D. Lee, G. Poologusandarampillai, J.R. Jones, Evaluation of 3-D bioactive glass scaffolds dissolution in a perfusion flow system with X-ray microtomography, *Acta Biomater.* 7 (2011) 2637–2643, <https://doi.org/10.1016/j.actbio.2011.02.009>.
- [28] D. Zhang, M. Hupa, L. Hupa, In situ pH within particle beds of bioactive glasses, *Acta Biomater.* 4 (2008) 1498–1505, <https://doi.org/10.1016/j.actbio.2008.04.007>.
- [29] D. Zhang, M. Hupa, H.T. Aro, L. Hupa, Influence of fluid circulation on in vitro reactivity of bioactive glass particles, *Mater. Chem. Phys.* 111 (2008) 497–502, <https://doi.org/10.1016/j.matchemphys.2008.04.055>.
- [30] S. Fagerlund, P. Ek, L. Hupa, M. Hupa, Dissolution kinetics of a bioactive glass by continuous measurement, *J. Am. Ceram. Soc.* 95 (2012) 3130–3137, <https://doi.org/10.1111/j.1551-2916.2012.05374.x>.
- [31] M.G. Cerruti, D. Greenspan, K. Powers, An analytical model for the dissolution of different particle size samples of Bioglass® in TRIS-buffered solution, *Biomaterials* 26 (2005) 4903–4911, <https://doi.org/10.1016/j.biomaterials.2005.01.013>.
- [32] P. Sepulveda, J.R. Jones, L.L. Hench, In vitro dissolution of melt-derived 45S5 and sol-gel derived 58S bioactive glasses, *J. Biomed. Mater. Res.* 6 (2002) 301–311, <https://doi.org/10.1002/jbm.10207>.
- [33] M. Siekkinen, O. Karlström, L. Hupa, Effect of local ion concentrations on the in vitro reactions of bioactive glass 45S5 particles, *Int. J. Appl. Glass Sci.* 13 (2022) 695–707, <https://doi.org/10.1111/ijag.16579>.
- [34] T. Kokubo, H. Takadama, How useful is SBF in predicting in vivo bone bioactivity? *Biomaterials* 27 (2006) 2907–2915, <https://doi.org/10.1016/j.biomaterials.2006.01.017>.
- [35] M. Bohner, J. Lemaître, Can bioactivity be tested in vitro with SBF solution? *Biomaterials* 30 (2009) 2175–2179, <https://doi.org/10.1016/j.biomaterials.2009.01.008>.
- [36] ISO - ISO 23317, Implants for surgery — in vitro evaluation for apatite-forming ability of implant materials, n.d., <https://www.iso.org/standard/65054.html>, 2014. (Accessed 6 June 2022).
- [37] H.S. Sidhu, M.I. Nelson, E. Balakrishnan, An analysis of a standard reactor cascade and a step-feed reactor cascade for biological processes described by monod kinetics, *Chem. Prod. Process Model.* 10 (2015) 27–37, <https://doi.org/10.1515/cppm-2014-0022>.
- [38] New England Biolabs Inc, pH vs temperature for tris buffer, n.d., <https://international.neb.com/tools-and-resources/usage-guidelines/ph-vs-temperature-for-tris-buffer>, 2020. (Accessed 7 February 2022).
- [39] I.D. Xynos, A.J. Edgar, L.D.K. Buttery, L.L. Hench, J.M. Polak, Ionic products of bioactive glass dissolution increase proliferation of human osteoblasts and induce insulin-like growth factor II mRNA expression and protein synthesis, *Biochem. Biophys. Res. Commun.* 276 (2000) 461–465, <https://doi.org/10.1006/bbrc.2000.3503>.
- [40] J.-Y. Sun, Y.-S. Yang, J. Zhong, D.C. Greenspan, The effect of the ionic products of Bioglass® dissolution on human osteoblasts growth cycle in vitro, *J. Tissue Eng Regen Med* 1 (2007) 281–286, <https://doi.org/10.1002/term.34>.
- [41] A. Hoppe, N.S. Guldal, A.R. Boccaccini, A review of the biological response to ionic dissolution products from bioactive glasses and glass-ceramics, *Biomaterials* 32 (2011) 2757–2774, <https://doi.org/10.1016/j.biomaterials.2011.01.004>.
- [42] S. Fagerlund, J. Massera, N. Moritz, L. Hupa, M. Hupa, Phase composition and in vitro bioactivity of porous implants made of bioactive glass S53P4, *Acta Biomater.* 8 (2012) 2331–2339, <https://doi.org/10.1016/j.actbio.2012.03.011>.
- [43] A.C.M. Renno, P.S. Bossini, M.C. Crovace, A.C.M. Rodrigues, E.D. Zanotto, N. A. Parizotto, Characterization and in vivo biological performance of biosilicate, *BioMed Res. Int.* (2013) 1–7, <https://doi.org/10.1155/2013/141427>, 2013.
- [44] S. Fagerlund, L. Hupa, M. Hupa, Comparison of reactions of bioactive glasses in different aqueous solutions, *Adv. Bioceram. Biotechnol.* 218 (2010) 101–113, <https://doi.org/10.1002/9780470909898.ch11>. USA: John Wiley & Sons, Ltd.
- [45] M. Cerruti, D. Greenspan, K. Powers, Effect of pH and ionic strength on the reactivity of Bioglass® 45S5, *Biomaterials* 26 (2005) 1665–1674, <https://doi.org/10.1016/j.biomaterials.2004.07.009>.
- [46] L. Björkvik, X. Wang, L. Hupa, Dissolution of bioactive glasses in acidic solutions with the focus on lactic acid, *Int. J. Appl. Glass Sci.* 7 (2016) 154–163, <https://doi.org/10.1111/ijag.12198>.
- [47] R.K. Iler, *The Solubility of Silica*. Chem. Silica, John Wiley & Sons, 1979, pp. 30–49.

Siekinen M., Engblom M., Hupa L. ***"Impact of solution pH (5-9) and dissolution products on in vitro behaviour of the bioactive glass S53P4"*** Journal of Non-Crystalline Solids: X, Vol 20 (2023) DOI: 10.1016/j.nocx.2023.100199



Contents lists available at ScienceDirect

Journal of Non-Crystalline Solids: X

journal homepage: www.sciencedirect.com/journal/journal-of-non-crystalline-solids-x

Impact of solution pH (5–9) and dissolution products on *in vitro* behaviour of the bioactive glass S53P4

Minna Siekkinen, Markus Engblom, Leena Hupa*

Johan Gadolin Process Chemistry Centre, Åbo Akademi University, Henrikinkatu 2, Turku 20500, Finland

ARTICLE INFO

Keywords:

Bioactive glass

In vitro

Dissolution kinetics

Buffer solutions

ABSTRACT

The impact of dissolution products on the reaction behaviour of bioactive glasses was explored. Bioactive glass S53P4 particles were immersed in solutions with initial pH of 5–9. After 24 and 72 h, the solution extracts were used for testing unreacted particles. The pH, ion concentrations, and glass surfaces were analysed as functions of immersion time. More Ca, Na, and P dissolved at lower pH (5) than at higher pH (7.4 or 9). The dissolution changed from an incongruent to an apparent congruent with increasing pH. Dissolution products in extracts changed the reaction layer structure on glass particles and led to lower ion release at pH 7.4 and 9. Dissolution increased almost linearly with time in acidic solutions. Silica-rich layer and calcium phosphate were identified on the particles after immersion in all solutions except at pH 9. Local ion concentration variations affected dissolution, leading to nonuniform ion release rates.

1. Introduction

Bioactive glasses are commonly characterised by their ability to form a chemical bond with living tissues, mainly bone, through the hydroxyapatite layer that develops at the glass surface *in vivo* [1]. Controlled degradation and release of ions are unique properties of bioactive glasses [2]. Since their discovery in the late 1960s [3], bioactive glasses have evolved from bone grafting materials to implants and scaffolds for various tissue engineering applications [4–6]. Professor Hench, the inventor of bioactive glasses, observed the strong bond between bone and silicate-based glasses of a narrow composition range. The first bioactive glass reported by Hench is known as Bioglass® 45S5 [7]. The oxide composition of this glass is (in wt%) 45 SiO₂, 24.5 CaO, 24.5 Na₂O, and 6 P₂O₅ [8].

Today, a wide range of glass compositions has been studied for their potential bioactivity. For example, bioactive glass S53P4 with higher silica and lower contents of the other oxides compared to 45S5 showed desired properties for bone tissue applications in several *in vitro*, *in vivo* and clinical studies [9]. Today, 45S5 and S53P4 are widely used in commercial implant products in the human body [9–13]. Besides stimulating bone growth, S53P4 showed antibacterial effects *in vitro* against 29 aerobic and 17 anaerobic bacteria [14,15]. Clinical studies verified its suitability for treating osteomyelitis in long bones [16,17]. The antibacterial properties are suggested due to the dissolution behaviour

of bioactive glasses [18], *i.e.*, the increased pH and the increased ion concentrations in the surrounding solution. Additionally, the release of ions from the glass was verified to stimulate cellular processes in bone regeneration and, accordingly, to produce new bones in an injured site [19].

Similar reactions between the bioactive glass and surrounding solution occur *in vivo* and *in vitro*. The reactions are rapid and are proposed to take place in the following five steps [20]: [i] ion exchange of the alkali and alkaline ions in the bioactive glass surface with the hydrogen ions in the solution, [ii] increase of the solution pH, followed by the release of soluble silicon groups (Si(OH)₄) from the glass, [iii] condensation and repolymerisation of silicon on the glass surface to a silica-rich layer, [iv] migration of Ca²⁺ and PO₄³⁻ groups from the glass and precipitation from the solution to amorphous calcium phosphate (Ca/P) layer, [v] crystallisation of the Ca/P-layer to a hydroxyapatite layer as a result of carbonates and hydroxyls incorporating from the surrounding solution. *In vivo* mechanisms then conclude the bonding to the bone.

The dissolution rate of bioactive glasses depends, among other things, on the solution pH, glass surface area to solution volume ratio, and solution composition [21]. An early study showed that the extraction of alkali ions from a binary alkali silicate glass (K₂O-SiO₂) decreased rapidly above pH 9 [22]. Also, calcium dissolved more rapidly from bioactive glass 45S5 in an acidic solution (pH 5) compared to neutral (pH 7.4) and alkaline (pH 9) solutions [23]. On the other hand, at

* Corresponding author.

E-mail address: lhupa@abo.fi (L. Hupa).<https://doi.org/10.1016/j.nocx.2023.100199>

Received 15 February 2023; Received in revised form 30 May 2023; Accepted 31 August 2023

Available online 1 September 2023

2590-1591/© 2023 Published by Elsevier B.V. This is an open access article under the CC BY-NC-ND license (<http://creativecommons.org/licenses/by-nc-nd/4.0/>).

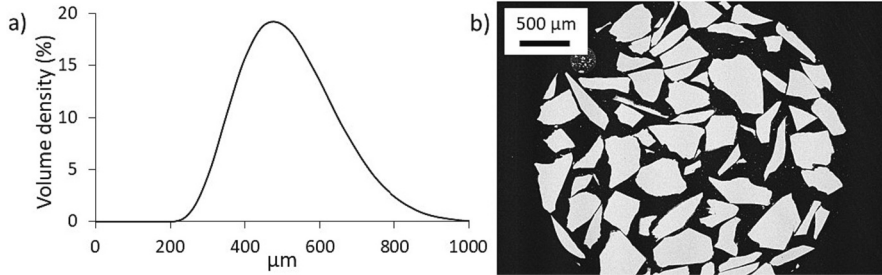


Fig. 1. Particle size distribution (a) and cross-sectional SEM image (b) of unreacted S53P4 particles.

increased pH levels, Si is expected to dissolve more rapidly than alkalis. The critical pH level of increased Si dissolution from the glass structure is pH 9 [24]. As smaller particles have a larger surface area, they dissolve faster than larger particles [25]. In addition, particles in a cascade reactor, *i.e.*, in separate reactors connected in series, were reported to react differently in a continuous solution flow due to increasing concentration of dissolution products [26]. This implies that particles inside an implanted bioactive glass particle bed will be in contact with a solution already containing dissolution products from the outer bed particles. Consequently, these interior particles likely experience a higher pH than the outer particles. However, the dynamic body system strives to maintain the pH of the extracellular fluid constant, *i.e.*, around 7.4 [27]. At the same time, the pH can be within 5.5–6.7 at bone infection sites [28]. Even lower local pH levels can occur if the bioactive glass is used as a component in a composite with a biodegradable polymer, *e.g.*, polylactic acid, giving an acidic environment due to degradation reactions [29]. Also, the oral cavity can experience an environment with decreased pH due to the intake of drinks or food with a lower pH [30]. On the other hand, locally increased pH at the implant site can appear at the glass/solution interface and affect the dissolution behaviour of the glass [31].

Immersion bioactive glass in a static solution is a standard procedure when investigating *in vitro* behaviour [32]. Experiments conducted with solutions containing dissolution products from bioactive glasses are limited and mainly focused on the biological response. For example, the human osteoblast growth cycle was shortened when ions dissolved from bioactive glass 45S5 were present [33]. Furthermore, ions dissolving from bioactive glasses induced osteogenesis *in vitro* [34]. Dissolved ions from an experimental bioactive glass promoted strong mineralization of human adipose stem cells in hydrogels [35]. Similarly, ions common in bioactive glasses have been identified to induce HA precipitation (aqueous Si) [36], increase osteoblast proliferation and differentiation, increase mineralization of the extracellular matrix (Ca ions) [37], and stimulate the main protein (matrix Gla protein) for bone formation (phosphate) [38]. In a dynamic environment, the increase of ion concentrations and, consequently, the decrease of available hydrogen ions for ion exchange have been proposed to delay the reactions of bioactive glasses [26,39]. However, the impact of dissolution products in the solution on the reaction behaviour of bioactive glasses at different pH levels is not fully understood.

This study aimed to investigate bioactive glass S53P4 particles in different environments that could occur in the human body, including changes in the surrounding solution pH due to infection or material/solution reactions. Also, the solution composition might change as it flows in voids of particle beds or porous bodies, thus affecting the reactions in various parts of the implanted material. In this work, the reactions of bioactive glass S53P4 particles were studied in solutions at three pH levels (5–9) in static conditions for up to 120 h. In addition, the extracts after 24 and 72 h of dissolution were reused to study the impact

Table 1

Reagents for 0.5 l buffer solutions, solution pH, and calculated base and acid molarities of the solutions at 37 °C.

	Tris (g)	HAc (ml)	HCl (ml)	NaOH (ml)	pH	base (mM)	acid (mM)
Tris (9)	3.03	–	1.5	–	9	50	3
Tris (7.4)	3.03	–	17.9	–	7.4	50	36
Tris (5)	3.03	24.7	–	–	5	50	50
HAc (5)	–	3	–	34.1	5	68	100

of increased ion concentrations on the dissolution of unreacted particles. The results give indications of the dissolution mechanisms of bioactive glasses in various *in vitro* and *in vivo* conditions.

2. Materials and methods

2.1. Bioactive glass samples

Bioactive glass S53P4 (in wt%) 53 SiO₂, 20 CaO, 23 Na₂O, and 4 P₂O₅ was produced by mixing quartz sand with analytical grade reagents Na₂CO₃, CaHPO₄·2H₂O, and CaO₃. The batch was added into a platinum crucible and melted in an electric furnace at 1360 °C for 3 h. The melt was cast in a graphite mould to give a glass bar, annealed at 520 °C for 1 h and cooled down to room temperature in the oven. The bar was crushed and remelted to obtain a homogeneous glass. Finally, bioactive glass particles were produced with a ring and puck mill. Particles that passed through a 500 μm sieve but stayed on a 300 μm sieve were used for the immersion studies. Before immersion, the particles were cleaned in acetone in an ultrasound bath to remove fine powder adhered to the particle surfaces. Fine, rapidly dissolving powder might affect the accuracy of dissolution studies [40]. Fig. 1 shows a) the particle size distribution (Malvern Panalytical Mastersized 3000) and b) an SEM image of the S53P4 particle cross-sections. The median diameter of the analysed particles was 445 μm, and 69% were in the size range of 310–516 μm. 28% of the particles were > 516 μm, and 3% were < 310 μm. The irregular-sized particles increased the possibility of elongated particles passing through the sieve, contributing to the increased particle size distribution.

2.2. Immersion solutions

Tris(hydroxymethyl)aminomethane (Tris), with the pH indicated in parenthesis after the solution symbol, was prepared using the reagents given in Table 1. The pH of Tris (5) was adjusted using acetic acid instead of the usual hydrochloric acid (HCl) to minimize the risk of Cl ions interfering with the apatite formation on the glass particle surfaces

Table 2

pH as functions of the immersion time for the solutions used to dissolve S53P4 particles: as-prepared (0), extracted after 24 h (24) and 72 h (72). Bold values indicate the pH measured above the glass particles at 24 and 72 h, while the underlined values give the extracted and mixed solution pH before adding new particles.

h	Tris 9			Tris 7.4			Tris 5			HAc 5		
	(0)	(24)	(72)	(0)	(24)	(72)	(0)	(24)	(72)	(0)	(24)	(72)
0	8.97	<u>9.12</u>	<u>9.10</u>	7.35	<u>7.46</u>	<u>7.58</u>	4.96	<u>5.09</u>	<u>5.15</u>	4.93	<u>5.05</u>	<u>5.08</u>
2	9.10	<u>9.15</u>	9.11	7.44	<u>7.57</u>	7.59	5.06	<u>5.11</u>	5.19	5.01	<u>5.05</u>	5.11
4	9.11	9.15	9.12	7.46	7.53	7.61	5.07	5.12	5.22	5.05	5.07	5.14
6	9.12	9.15	9.14	7.47	7.52	7.62	5.08	5.13	5.24	5.03	5.09	5.16
8	9.13	9.17	9.15	7.49	7.53	7.59	5.10	5.15	5.26	5.04	5.08	5.17
24	9.15	9.20	9.17	7.52	7.57	7.69	5.15	5.23	5.32	5.11	5.14	5.17
48	9.23	9.25	9.28	7.59	7.60	7.69	5.26	5.26	5.48	5.16	5.15	5.24
72	9.31	9.29	9.33	7.62	7.64	7.71	5.26	5.36	5.55	5.16	5.20	5.29
96	9.31	9.34	9.37	7.62	7.65	7.73	5.27	5.35	5.60	5.23	5.25	5.35
120	9.38	9.37	9.41	7.66	7.68	7.75	5.38	5.42	5.68	5.27	5.30	5.40

[41]. The buffer capacity of Tris is between 7 and 9 [42]. Therefore, an additional HAC-NaOH (HAc) buffer solution was used for immersion studies within the buffering range of 3.6–5.6. The reagents (in bold, Table 1) were added to purified water and wholly dissolved before the temperature of the solutions was increased in a water bath to 37 °C. Finally, the pH of the solutions was adjusted by slowly adding 1 M HCl, 1 M HAc, or 1 M NaOH under continuous stirring. The theoretical mass/volume and molarity of the acids and bases are also presented in Table 1. The acid and base concentrations for the desired buffer pH values were calculated using the Henderson-Hasselbalch equation [43], with the pKa (37 °C) of Tris as 7.8 and of HAc as 4.67.

2.3. Immersion tests

A shaking incubator (Stuart Orbital Incubator SI500) with a rotation speed of 100 rpm at 37 °C was used for the immersions. 210 ± 5 mg of bioactive glass particles were added in 30 ± 0.1 ml solution in a covered polypropylene centrifuge tube (50 ml). Assuming spherical particles with an average diameter of 400 μm gave an approximate surface area to volume ratio of 0.4 cm^{-1} . The immersion tests were carried out for 24, 72, and 120 h. The 120 h experiments had three parallel runs. The pH of the solutions was measured every other hour for up to 8 h, and from 1 day forward, every 24 h. At hours 8, 24, and 72, an aliquot of 1 ml was extracted for ion analysis. Further, the ion concentrations were measured at 120 h. The reacted particles were washed with ethanol and dried at 40 °C before being stored in a desiccator until further analyses.

Additional glass samples were immersed for 24 and 72 h to achieve extracts for investigating the effect of the released ions on the dissolution of new, unreacted S53P4 particles. For a surface area to volume ratio similar to the initial immersion tests (0.4 cm^{-1}), 202 ± 3 mg of bioactive glass particles were immersed in 28.5 ml of the extracted solutions. The solutions and glass particles were collected for further analyses at the same measurement points as experiments with as-prepared solutions.

2.4. Change of solution pH

The pH is temperature dependent and was therefore measured by placing the vials with the immersed particles in a 37 °C water bath to keep the temperature constant during the pH measurement. The measurements were conducted close to the particle bed without the pH electrode touching the particles. The pH has been shown to increase the closer the pH electrode is to the particle bed in a container [44]. However, the agitation during the immersion likely contributed to equalising pH throughout the solution. Also, the pH of the reference solutions, kept in the same incubator as the bioactive glass immersion solutions, was measured at 0 and 120 h. The pH-meter (VWR pHenomenal pH 1100 L) was calibrated with the pH standards 4.01 and 7.00 (25 °C).

2.5. Ion analysis

The collected solutions were analysed with inductively coupled plasma-optical emission spectrometry (ICP-OES, Optima 5300 DV; Perkin Elmer, Waltham, MA). The extracted 1 ml solution was diluted with 9 ml of purified water. The ICP was calibrated with 1, 5, and 20 ppm commercial (Spectrascan) multi-element standards of Si, Ca, Na, and P. Before and after the measurements, the background level was recorded by analysing the 1 ppm standard of each element. The reported ion concentrations were background corrected accordingly. The elements were analysed with the limit of quantification (LOQ) $\text{Si} = 0.04 \text{ mg/l}$, $\text{Ca} = 0.003 \text{ mg/l}$, $\text{Na} = 0.2 \text{ mg/l}$, and $\text{P} = 0.03 \text{ mg/l}$. Ion analysis was conducted for three parallel samples, and each sample was analysed 3–5 times. Aliquots were extracted at 8, 24, and 72 h, so the surface area to volume ratio changed accordingly. Therefore, the measured values were calculated according to Eq. (1) [45].

$$C_{ij}^* = C_{ij} + \frac{V^a}{V_s} \sum_j^N C_{ij-j-1} \quad (1)$$

where C_{ij}^* is the normalised concentration of element i at time j , C_{ij} the measured concentration of element i at time j , V^a the volume of the extracted aliquot, V^s the volume of the immersion solution before extraction of the aliquot, and C_{ij-j-1} the measured concentration of element i at time point $j-1$. The normalised mass loss of each element was then calculated according to Eq. (2) [46].

$$NL_i = \frac{C_i^* - C_0}{\left(\frac{SA}{V}\right)_i} \quad (2)$$

where NL_i is the normalised loss of each element (g/m^2), C_i^* is the normalised ion concentrations of element i calculated with Eq. (1) (mg/l), C_0 is the ion concentration of element i measured with ICP-OES in the reference solution (mg/l), SA is the total surface area of the unreacted immersed glass particles (m^2), V is the volume of immersion solution (l), and f_i is the mass fraction of element i in the unreacted glass sample.

2.6. Glass surface analysis

After 120 h, the glass particles from the dissolution experiments in the four as-prepared immersion solutions and their 24 and 72 h extracts were embedded in epoxy resin. The embedded particles were ground and polished with abrasive sandpaper to reveal the cross-sections. A scanning electron microscope (SEM, Leo Gemini; Carl Zeiss, Oberkochen, Germany) was used to take images of the cross-sections and the surfaces of particles immersed for 120 h. For particles with visible layer formations, energy dispersive X-ray line analysis (EDX, Leo Gemini; Carl Zeiss, Oberkochen, Germany, coupled with SEM) of the cross-sections was also taken.

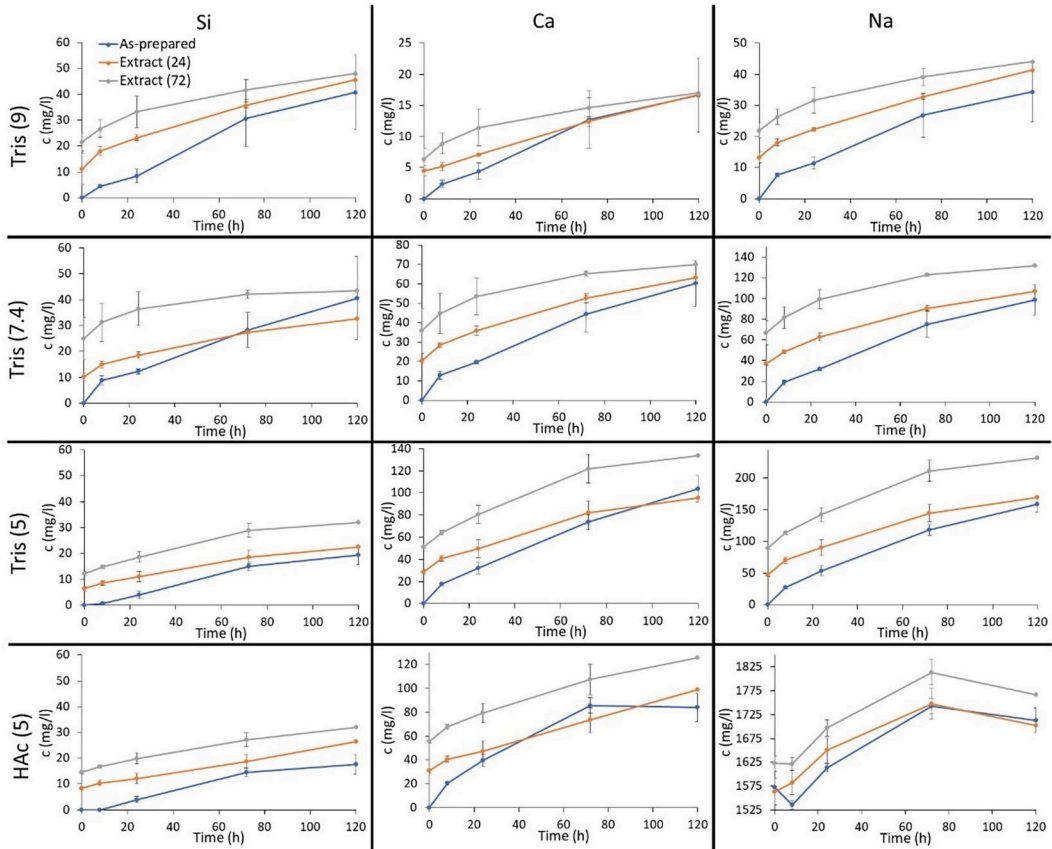


Fig. 2. Normalised ion concentrations of Si, Ca, and Na in the solutions during 120 h dissolution of S53P4 particles.

3. Results

3.1. pH of immersion solutions

Table 2 shows the average pH of the four immersion solutions as functions of the immersion time, where 0 indicates the as-prepared solutions, and 24 and 72 are for the extracts. Due to the minor pH differences between the parallel samples, the table does not include the variations. The three measured parallel samples for the immersion using the as-prepared solutions gave a variation of ± 0.04 (Tris 9), ± 0.02 (Tris 7.4), ± 0.02 (Tris 5), and ± 0.02 (HAc 5) pH units. Similarly, the variations in immersions using the extracts were also minor, *i.e.*, $\pm 0.01 - \pm 0.08$ pH units. The pH values of the supernatants measured above the glass particles at 24 and 72 h are marked in bold, and the pH of the extracted and mixed solutions before adding new particles are underlined in Table 2. The difference between the two pH values for the supernatant and extract varied between 0.03 and 0.21 pH units depending on the solution. These differences were likely due to the time lag for pH equalisation throughout the solution. However, as the pH of all samples containing glass particles was measured similarly, the pH trends for each solution were assumed to correlate with the progress of the glass reactions. In addition, the total volume of the solutions decreased by up to

3 ml due to the sampling of the aliquots for elemental analysis. Thus, the pH from 24 to 96 h cannot directly be compared with pH values measured at earlier points or 120 h. The pH of all solutions increased with increasing immersion times and was highest for the immersions done using the 72 h extracted solutions.

3.2. Ion analysis

Fig. 2 shows the normalised Si, Ca, and Na concentrations (mg/l) in the static solutions as functions of time. As the pH of HAC (5) was adjusted with NaOH, the high Na levels in the solutions (1570 mg/l in the as-prepared solution) questioned the accuracy of Na in HAC solutions. However, the Na concentration trends in HAC (5) and its extracts were assumed to correlate with the Na release. In general, the ions released from S53P4 particles into the solutions increased with immersion time but in lower concentrations when using the extracts.

Similar Si concentration levels were measured in the as-prepared Tris (9) and Tris (7.4) throughout the immersions. In contrast, the Si concentration was lower in the as-prepared Tris (5) and HAC (5). Interestingly, the Si concentrations increased roughly linearly with time in the as-prepared solutions and extracts of Tris (5) and HAC (5), independent of the concentration before the immersion. However, the changes

Table 3

Concentration of P (mg/l) after the dissolution of S53P4 particles in the as-prepared solutions (0) and extracts (24 and 72). n/a = values below the LOQ.

Time (h)	Tris (9)			Tris (7.4)			Tris (5)			HAc (5)		
	(0)	(24)	(72)	(0)	(24)	(72)	(0)	(24)	(72)	(0)	(24)	(72)
0	n/a	n/a	n/a	n/a	n/a	0.2	n/a	n/a	n/a	n/a	0.3	0.8
8	n/a	n/a	n/a	0.3	n/a	0.7	n/a	0.5	0.5	n/a	0.9	1.4
24	n/a	n/a	n/a	0.5	n/a	0.7	0.1	0.5	0.8	0.7	0.9	1.5
72	n/a	n/a	n/a	0.4	n/a	0.6	0.5	0.7	1.5 ± 1	1.8 ± 1	1.3	1.8
120	n/a	n/a	n/a	0.8 ± 1	n/a	0.5	1.9 ± 1	0.7	1.3	1 ± 1	1.9	2.8

**Fig. 3.** SEM images of S53P4 particles immersed in the four as-prepared solutions and their 24 and 72 h extracts for 120 h.

in Si concentration during 120 h dissolution in the as-prepared Tris (9) at its 72 h extract were 41 mg/l and 26 mg/l. Corresponding values for the as-prepared Tris (7.4) and its 72 h extract were 41 mg/l and 18 mg/l, respectively.

The lowest Ca and Na concentrations were measured in Tris (9). Ca and Na releases were the least in the 72 h extract of Tris (9). Correspondingly, the highest Ca and Na concentrations were measured in Tris (5) and HAc (5). For most solutions, the concentration of P species was close to or below the limit of quantification (LOQ), as shown in Table 3.

3.3. Glass particle surface changes

Fig. 3 shows SEM images with two magnifications of S53P4 particle cross-sections immersed for 120 h in the four as-prepared solutions and their two extracts. It should be noted that not all particles in the sample had formed similar surface reaction layers, as shown in the figure. The magnified images present typical single particles with distinct changes

in the surface composition. Notably, no distinct layers were seen after the dissolution in Tris (9). After the dissolution in all other solutions and extracts, typical silica-rich and calcium phosphate layers were identified on the particle surfaces. The thickness of the silica-rich layer seen with the dark-grey colour increased with the decrease of the solution pH.

Fig. 4 shows SEM images of particle surfaces before and after 120 h in the four as-prepared solutions in two magnifications. Even though the cross-sectional images of Tris (9) immersed particles (Fig. 3) did not show any reaction layers typical for bioactive glasses *in vitro*, the surface images suggest glass corrosion. After the immersion in Tris (7.4), large cracks typical for SEM images of the silica-rich layer are seen in the particle surfaces. The accumulations after the immersions consisted of calcium phosphate (Fig. 5). Similarly, the cracks in particles immersed in Tris (5) and HAc (5) suggest a silica-rich layer. Some calcium phosphate precipitates had also formed in these solutions.

The element composition of the surface layers on the particles after 120 h in all solutions except the Tris (9) is given by the EDX line analyses

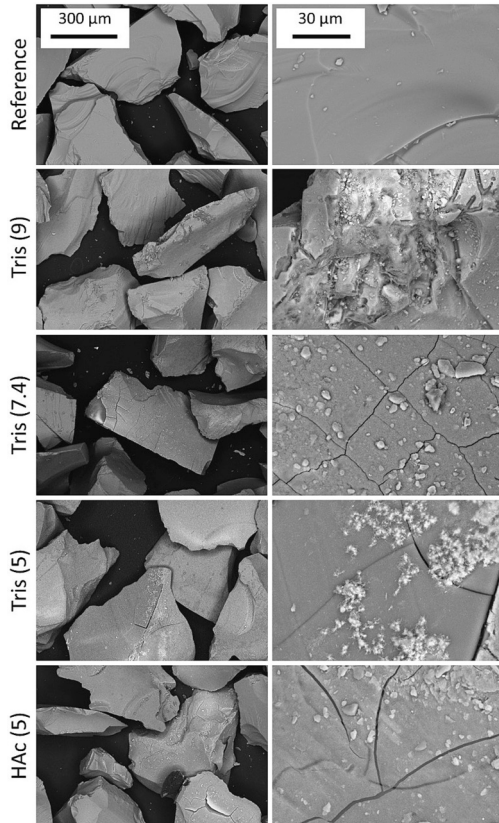


Fig. 4. SEM images of S53P4 particles before (Reference, 0 h) and after immersion (120h) in the as-prepared solutions in two magnifications.

in Fig. 5. After the immersion in Tris (7.4), the line analyses indicate a silica-rich layer next to the bulk glass (start of the arrow). The silica-rich layer appears thicker and almost free of Ca, Na, and P for the as-prepared solution. Then, the outermost layer suggests peaks of Ca and P in molar ratios typical for hydroxyapatite. After the immersion in the 24 and 72 h extracts, Ca and P are also present in the silica-rich layer. However, after immersion in Tris (5), the silica-rich layer appears thicker and is almost free of Ca and P.

4. Discussion

Immersion of bioactive glasses in Tris buffer enables a significantly easier comparison of dissolution reactions than studies in the complex simulated body fluid (SBF) [47,48]. In this work, Tris buffer solutions and their extracts after 24 and 72 h immersion of bioactive glass S53P4 were used to gain an increased understanding of the impact of dissolution products in the solution on surface reactions leading to tissue bonding of bioactive glasses. Earlier studies *in vitro* have been conducted with, for example, 75 mg of small particles (<50 μm in diameter, some even 2 μm) immersed in 50 ml of buffered solutions [23,41,49,50]. Such small particles have a large surface area, leading to much faster glass dissolution and, consequently, a notable increase in the pH of the surrounding solution. For example, inside a bed of S53P4 particles of a

diameter of <45 μm, the pH of SBF had increased to 11 after 24 h, while for particles in the size range of 315–500 μm, the pH had increased to 8.6 [51]. Therefore, using larger particles, 300–500 μm, was assumed to retard the rapid initial reactions.

Fig. 6 shows the normalised mass loss rate from the original samples of S53P4 particles in the as-prepared solutions and their extracts for 120 h and the dissolution of elements (mol%) at 120 h. The ion concentrations dissolved in the extracts at 120 h were calculated as the difference between the values at the beginning of the experiment (0 h) and after 120 h (Fig. 2).

In Tris (9) and its extracts, the release of Si, Ca, and Na was around 1 to 3 mol%, suggesting congruent dissolution within the experimental error. The normalised mass loss rate also shows similar dissolution throughout the immersion time. However, the dissolution of alkalis was much less in Tris (9) than in the other solutions, thus explaining that no reaction layers could be verified at the surface (Figs. 3 and 4). This decrease in the dissolution rate aligns with the observations from the dissolution studies of borosilicate glasses, for which the dissolution rate markedly decreased around pH 9 [52]. The phosphorous levels below LOQ (Table 3) also implied a minor dissolution. After 120 h, the pH was slightly higher for the extracts than as-prepared Tris (9). Further, it was assumed that the local solution pH next to the dissolving particles was higher than the measured supernatant pH above the particles [44]. Consequently, network dissolution of the glass above pH 9 led to a slow congruent dissolution of Si, Ca, and Na. On the other hand, the dissolved amount of the glass decreased with increasing content of dissolved ions in the extracts, thus suggesting that the impact of dissolution products retarded the reactions. In a study immersing the International Simple Glass in a Si-saturated solution with a starting pH of 9 at 90 °C, an amorphous alteration layer formed on the glass surface hindered the Si network dissolution [52]. Similarly, Si in the immersion solution hindered the dissolution. In the present work, the maximum initial Si in Tris (9) was 22 mg/l compared to 260 mg/l in the saturated Si study [52]. Interestingly, this small increase in the Si concentration in the solution also slowed the dissolution. However, it should be emphasised that the four-oxide bioactive glass S53P4 contains only one network former compared to two or three in the more complicated aluminoborosilicate glasses studied for an enhanced understanding of the dissolution mechanisms in alkaline solutions [52]. The lack of an alteration layer on the bioactive glass S53P4 implies that the experimental time was too short for a detectable surface layer to form. The low network connectivity might have also supported congruent dissolution at pH 9.

The higher dissolved amounts of Na and Ca than Si in Tris (7.4) suggest incongruent dissolution typical for bioactive glasses (Fig. 6). The higher the concentrations of dissolved ions in the extracts, the less the concentrations increased during the 120 h immersions in Tris (7.4). Interestingly, the accumulation of calcium and phosphate on the glass surface and in the silica-rich layer during the immersion in the extracts suggests that calcium and phosphate ions in the solution affected the diffusion of the released ions through the silica-rich layer (Figs. 4 and 5). The pH of the as-prepared Tris (7.4) and its extracts slightly increased but was well within the buffering range throughout the immersions (Table 2). Na, Ca and P concentration profile changes were sharp at the interface of the unreacted glass and silica-rich layer after the dissolution in the as-prepared Tris (7.4) (Fig. 5). However, the Ca and P profiles were less steep for the particles immersed in the extracts. Thus, the diffusion of the ions through the alteration layer on the glass particles was retarded by the increased ion concentrations in the solution or by early precipitated calcium phosphates on the surface. A further implication is that increasing concentrations of released ions might locally retard the reactions of implants based on bioactive glass S53P4.

Finally, the dissolution of S53P4 particles was highly incongruent in the acidic solutions, Tris (5) and HAC (5) (Fig. 6). The thick silica-rich layers also verify the rapid release of Ca and Na ions (Figs. 3 and 5). Interestingly, the silicon release was almost constant in the as-prepared solutions and their extracts. This implies that the dissolution of the silica

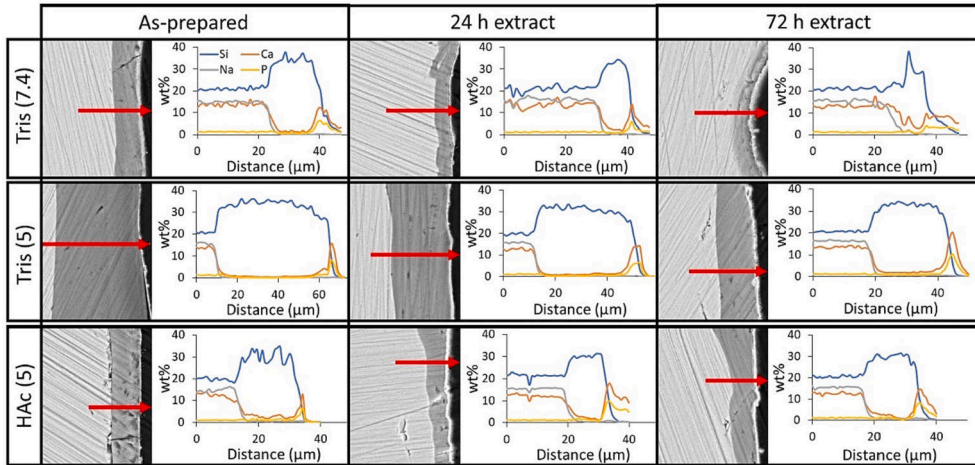


Fig. 5. EDX line analyses of S53P4 particles after 120 h in as-prepared solutions of Tris (7.4), Tris (5) and HAC (5) and their extracts.

network was not affected by the dissolution products in the solution but depended on the immersion time. The pH of the solution increased to 5.2–5.7, thus favouring the precipitation of calcium phosphate species [29]. However, the release trends of Ca and Na ions imply a slight decrease caused by the dissolution products in the solution. No apparent differences were observed in the dissolution of the glass particles in Tris (5) and HAC (5), most likely due to the relatively small differences in the pH of the solutions at different time points. Thus, the reaction mechanisms were similar, and the high content of hydrogen ions in the solutions favoured rapid ion exchange with Ca and Na ions, *i.e.*, incongruent dissolution. The Si release increased with time and likely correlated with the low network connectivity and silica content in S53P4.

Interestingly, the dissolved Si concentrations were almost similar in Tris (9) and Tris (7.4). Tris (7.4) solution was well within the buffering range, while the pH of Tris (9) did not markedly increase beyond the range. This implies that classical hydration and ion exchange reactions can be used to describe the *in vitro* behaviour of silicate-based bioactive glasses. These reactions led to the formation of thick silica-rich layers on the particles in Tris (7.4). Whether this took place through the classical multistep mechanism, including the ion exchange of mobile cations to protons in solution, followed by protonation, condensation and re-polymerisation to form a silica-rich layer or through an interfacial-dissolution-re-precipitation mechanism is unclear [53]. In contrast, the dissolution was congruent but markedly slower already at pH 9, with no detectable silica-rich layer. The higher dissolution of Ca and Na ions in Tris (7.4) and its extracts can be explained by the higher concentration of hydrogen ions available for ion exchange between the glass particles and solution. This results in slower ion release at a higher pH [23].

Partly reacted bioactive glasses have been reported to continue dissolving in replenished solutions [54]. This work investigated the reversed situation when extracts with dissolved ions were added to unreacted S53P4 bioactive glass particles. The dissolution reactions were not hindered but retarded by dissolution products in the extracted solutions. The observations imply that the dissolution of, *e.g.*, the outer section of a porous implant exposed to an extracellular solution with the nominal composition will affect the dissolution of the inner sections of a porous implant or particle beds. Ca ions in the solution have been suggested to promote apatite precipitation on bioactive glasses [55]. Dynamic *in vitro* studies of bioactive glasses 45S5 and S53P4 using

solutions buffered at pH 7.4 indicated that the formation of reaction layers was delayed when the concentration of dissolution products in the solution increased [26,39]. The static tests in this work showed that the dissolved ions from the bioactive glass affected the dissolution of unreacted particles most in the pH range typical for the extracellular fluid, *i.e.*, around 7.4. In contrast, the dissolution products had a minor impact on the glass dissolution in alkaline and acidic environments.

5. Conclusions

This work explored the impact of dissolution products in the immersion solution on the ion release from bioactive glass S53P4 in static alkaline (pH 9), physiological (pH 7.4) and acidic (pH 5) solutions. The as-prepared solutions initially contained no dissolved ions from the glass, while the solutions extracted after 24 and 72 h of immersion served as solutions with released ions in typical ratios dissolving from the glass. Glass particles immersed in the alkaline solution dissolved slowly and almost congruently, without forming typical reaction layers on the particle surfaces. The extracts slightly decreased ion release, but the reaction mechanisms were unchanged. Incongruent dissolution followed by the formation of typical silica-rich and calcium phosphate layers at the particle surfaces took place in the solution buffered at pH 7.4. The presence of dissolution products retarded the dissolution. Also, increasing calcium and phosphorus concentrations were identified in the silica-rich layer formed during immersion in the extracts. Finally, the dissolution was highly incongruent in the acidic solutions and increased almost linearly with immersion time. The dissolution products in the solution had a minor effect on the reactions. Despite the ion release, the pH of the buffered solutions increased only to a limited degree. Thus, changes in glass dissolution were mainly attributed to the dissolved ions in the solution. The results imply that implanted bioactive glass particles experiencing different local solution compositions react nonuniformly at a physiological pH and more uniformly in lower and higher pH environments.

Declaration of Competing Interest

The authors declare that they have no known competing financial interests or personal relationships that could have appeared to influence the work reported in this paper.

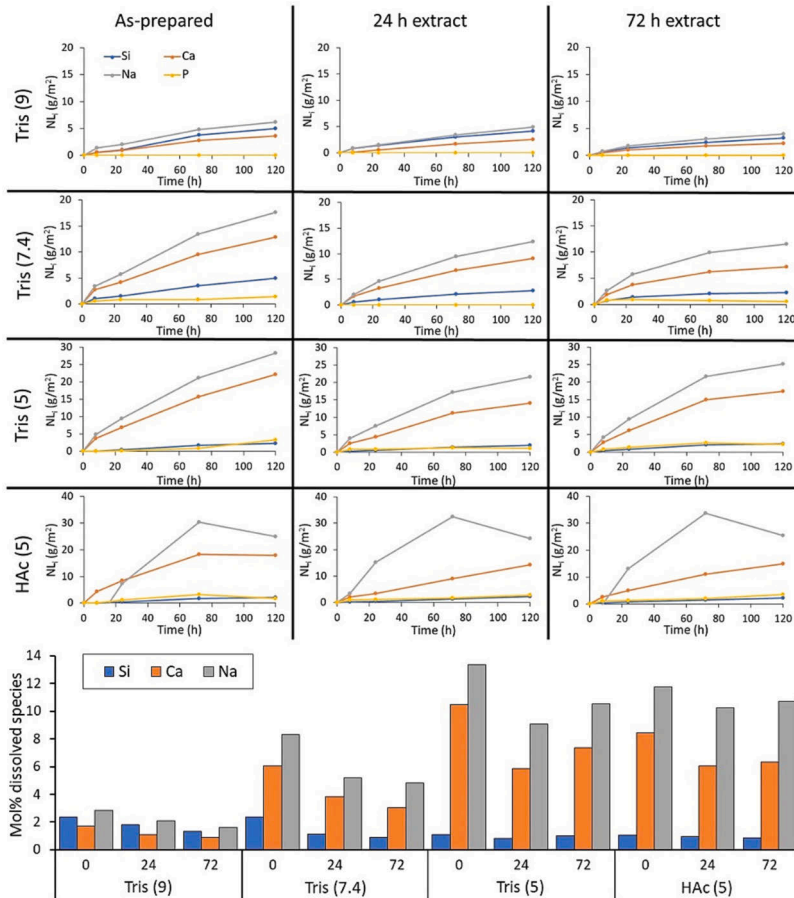


Fig. 6. Normalised mass loss rate from the unreacted S53P4 particles for 120 h of immersion and the dissolution of Si, Ca, and Na (mol%) at 120 h in the as-prepared solutions (0) and extracts (24 and 72).

Data availability

Data will be made available on request.

Acknowledgements

Ms. Siekkinen would like to acknowledge financial support from Victoriastiftelsen Project 20220174. Luis Bezerra and Linus Silvander are acknowledged for their assistance with ICP-OES and SEM-EDX.

References

- D.J. Hulsen, N.A. van Gestel, J.A.P. Geurts, J.J. Arts, S53P4 bioactive glass, in: *Management of Periprosthetic Joint Infections (PJIs)*, Elsevier, 2017, pp. 69–80, <https://doi.org/10.1016/B978-0-08-100205-6.00004-5>.
- M.N. Rahaman, D.E. Day, B.S. Bal, Q. Fu, S.B. Jung, L.F. Bonewald, et al., Bioactive glass in tissue engineering, *Acta Biomater.* 7 (2011) 2355–2373, <https://doi.org/10.1016/j.actbio.2011.03.016>.
- L.L. Hench, R.J. Splinter, W.C. Allen, T.K. Greenlee, Bonding mechanisms at the interface of ceramic prosthetic materials, *J. Biomed. Mater. Res.* 5 (1971) 117–141, <https://doi.org/10.1002/jbm.820050611>.
- Ö.H. Andersson, K. Vähätalo, A. Yli-Urpo, R.-P. Happonen, K.H. Karlsson, Short-Term Reaction Kinetics of Bioactive Glass in Simulated Body Fluid and in Subcutaneous Tissue, *Bio Ceramics*, Elsevier Ltd, 1994, pp. 67–72, <https://doi.org/10.1016/B978-0-08-042144-5.50014-5>.
- Ö.H. Andersson, I. Kangasniemi, Calcium phosphate formation at the surface of bioactive glass in vitro, *J. Biomed. Mater. Res.* 25 (1991) 1019–1030, <https://doi.org/10.1002/jbm.b.820250808>.
- E.J.G. Schepers, P. Ducheyne, L. Barbier, S. Schepers, Bioactive glass particles of narrow size range: a new material for the repair of bone defects, *Implant. Dent.* 2 (1993) 151–157, <https://doi.org/10.1097/00008505-199309000-00002>.
- L. Hench, The story of bioglass, *J. Mater. Sci. Mater. Med.* 17 (2006) 967–978, <https://doi.org/10.1007/s10856-006-0432-z>.
- L.L. Hench, Chronology of bioactive glass development and Clinical applications, *NJGC* 3 (2013) 67–73, <https://doi.org/10.4236/njgc.2013.32011>.
- L. Hupa, N.C. Lindfors, Bioactive Glass S53P4 – From a Statistically Suggested Composition to Clinical Success, *Bioactive Glasses and Glass-Ceramics*, John Wiley & Sons, Ltd, 2022, pp. 33–59, <https://doi.org/10.1002/9781119724193.ch3>.
- J.R. Jones, D.S. Brauer, L. Hupa, D.C. Greenspan, Bioglass and bioactive glasses and their impact on healthcare, *Int. J. Appl. Glas. Sci.* 7 (2016) 423–434, <https://doi.org/10.1111/ijag.12252>.
- N. Al Tamami, N. Bawazeer, M. Fieux, S. Zouache, S. Tringali, Tolerance and safety of 45S5 bioactive glass used in otolabration procedures during middle ear surgery: preliminary results, *Am. J. Otolaryngol.* 41 (2020), 102542, <https://doi.org/10.1016/j.amjoto.2020.102542>.

Siekinen M., Engblom M., Karlström O., Hupa L. ***"Dissolution of bioactive glass S53P4 in continuous flows of Tris and lactic acid"***
Biomedical Materials & Devices, (2023), DOI: 10.1007/s44174-023-00140-6



Dissolution of Bioactive Glass S53P4 in Continuous Flows of Tris Buffer and Lactic Acid

Minna Siekkinen¹ · Markus Engblom¹ · Oskar Karlström² · Leena Hupa¹

Received: 30 August 2023 / Accepted: 10 October 2023
© The Author(s) 2023

Abstract

In vitro dynamic dissolution of bioactive glass S53P4 particles was studied in a cascade of three reactors. Tris buffer (pH 7.40) and lactic acid (pH 2.00) with flow rates of 0.2 and 0.04 ml/min were fed through the reactors for 24 h. The increased ion concentrations in Tris inflows to the second and third reactors decreased the dissolution of the particles. However, the normalised surface-specific mass loss rate decreased from the first to the third reactor and with decreasing flow rate. No distinct differences were observed in the reaction layers on the particles in the three consecutive reactors. This implied that the ions released in the previous reactors contributed to the reaction layers formed in the following reactors. Highly incongruent dissolution with similar dissolution rates of sodium, calcium, and phosphorus occurred with the two flow rates in lactic acid. Although a thick silica-rich layer formed on the particles, the low pH prevented calcium phosphate layer precipitation. The results imply that S53P4 particles in an implant react at different rates depending on their location but form similar reaction layer morphologies independent of their location in physiological solutions (pH 7.4). On the other hand, S53P4 particles exposed to acidic solutions with a pH < 5 likely dissolve incongruently, leaving a slowly dissolving Si-rich layer. In such an environment, the dissolution rates of Na, Ca, and P are independent of the location of the S53P4 particle in the implant. Thus, the pH and fluid flow are critical factors for the dissolution of S53P4 bioactive glass particles.

Keywords Bioactive glass · In vitro · Biomaterial · Dissolution behaviour · Dynamic · Cascade reactor · Tris-buffer · Lactic acid

Introduction

Bioactive glasses dissolve and react to form surface layers when in contact with aqueous solutions [1]. Since their discovery in the 1960s, bioactive glasses have been studied in many sample forms and various aqueous environments [2]. Today, two bioactive glasses, 45S5 (in wt% 45SiO₂–24.5CaO–24.5Na₂O–6P₂O₅) [3] and S53P4 (in wt% 53SiO₂–20CaO–23Na₂O–4P₂O₅) [4] are clinically used chiefly as filler materials for bone cavities [5]. Bioactive glasses' low silica content indicates lower chemical durability than conventional soda–lime–silica glasses [6]. For

example, the low durability provides antibacterial properties in vivo due to a rapid exchange of alkali and alkaline earth ions in the glass surface with hydrogen ions in the surrounding solution [7].

The reactions between the bioactive glass and surrounding solution begin with the rapid ion exchange reaction. In this reaction, hydrogen ions (H⁺) in the solution form silanol groups (Si–OH) on the glass surface. Phosphate ions (PO₄^{3–}) are also released into the surrounding solution in the initial steps. The decreased H⁺ concentration, and thus, the increased pH and hydroxyl ion (OH[–]) concentration, lead to the breaking of silicon–oxygen bonds in the glass network. Accordingly, the concentration of dissolved Si species [Si(OH)₄] in the solution increases. Then, the insoluble Si–OH at the surface condensates and repolymerises to a silica-rich layer. Ca²⁺ and PO₄^{3–} ions migrate from the bulk glass to the surface and, together with ions from the solutions, precipitate into an amorphous CaO–P₂O₅ layer. After reacting with carbonate, this layer crystallises into

✉ Minna Siekkinen
minna.siekkinen@abo.fi

¹ High-Temperature Processes and Materials, Åbo Akademi University, Henrikinkatu 2, 20500 Turku, Finland

² Industrial Engineering and Management, Department of Mechanical and Materials Engineering, University of Turku, Turku, Finland

carbonated hydroxyapatite and provides bonding to the bone apatite. [3, 8]

The reaction steps above are often studied *in vitro* with simplified solutions mimicking the extracellular body fluid [9, 10]. Conventional *in vitro* experiments are usually conducted by immersing the bioactive glass sample in static solutions and studying its reactions as functions of time [11]. Circulating the immersion solution has been suggested to mimic the dynamic human body [12]. The environment has been created by replenishing static solutions [13, 14], circulating the solution above a particle bed [15], or introducing a single-pass flow-through setup where an as-prepared solution is continuously fed through the sample [16]. The dynamic *in vitro* environment is assumed to provide a homogeneous environment, typically seen as more uniform reaction layers on the particle surfaces than in static solutions. Most experiments utilising fluid circulation have been conducted with a fixed flow rate.

The flow rate in bones depends on the diameter and length of the vessels, as well as the differences in the pressure and viscosity of blood [17]. Also, location in the body and the patient's age and health affect the blood flow in the bones [18]. Measuring the exact flow rates inside the bones is challenging, and non-invasive methods for precise measurements are needed. Thus, only estimations based on measuring the flow rate in vessels surrounding the bones are available [19]. One study suggests an intraosseous blood flow rate of 5–20 ml/min per 100 g of bone [20]. *In vitro* studies in a dynamic environment showed that the reaction behaviour of bioactive glasses markedly varied with the flow rate. During the first 20 min of dynamic dissolution, slower flow rates released ions from the bioactive glass 1–98 (in wt% $53\text{SiO}_2\text{--}22\text{CaO--}6\text{Na}_2\text{O--}2\text{P}_2\text{O}_5\text{--}11\text{K}_2\text{O--}5\text{MgO--}1\text{B}_2\text{O}_3$) in a more considerable extent than a faster flow [16]. For bioactive glass S53P4, the pH in the dynamic solution outflow was consistently higher for slower flow rates compared to faster flow rates [21].

The pH highly affects the reactions of bioactive glasses [22]. Most *in vitro* studies are conducted at a physiological pH of 7.40. However, the local pH around bone infections can be lower, around 5.5–6.7 [23]. Such an environment might build up when bioactive glasses are used to treat, e.g. osteomyelitis in long bones [24–26]. Even though the pH of solutions in contact with bioactive glasses seldom decreases below 5, a reduced local acidic environment may occasionally occur [27]. Additionally, bioactive glasses are used in the oral cavity as dental implants [28], where acidic drinks, e.g. lemon juice and soft drinks, might give a local environment with a pH below 3 [29]. Also, bioactive glass and polylactic acid (PLA) composites have been studied *in vitro* and *in vivo* for possible bone replacement [30]. The PLA degrades in body solutions to lactic acid (LA) through hydrolysis [31]. The impact of PLA degradation products

on the bioactive glass dissolution in composites is not fully understood. However, initial studies on bioactive glass dissolution in LA suggested that immersed bioactive glass plates gradually turn into silica-rich samples [32]. At the same time, alkali and alkaline ion concentrations increased in static and dynamic solutions [32, 33]. Thus, further studies in LA environments are vital for understanding the glass/solution behaviour in challenging environments and the role of the silica-rich layer as a nucleation site for Ca and P [34].

The dissolution of the bioactive glasses 45S5 and S53P4 in a dynamic environment [35, 36] suggested that the combination of an increased pH, concentrations of released ions, and reaction layers at the glass surface affected but did not wholly hinder further dissolution. Additional *in vitro* test parameters would increase the utilisation of results in, for example, modelling. Most studies discussing ions dissolving from bioactive glasses focus on the biological and cellular effects. Dissolution products from bioactive glass 45S5 increased osteoblast proliferation, leading to increased bone regeneration [37]. *In vitro* cell culture studies suggested mineralised human adipose stem cells due to dissolution products from an experimental bioactive glass [38]. The dissolution products from bioactive glass S53P4 promoted fast calcium phosphate (Ca/P) mineralisation in an osteogenic medium [39]. However, estimating the interactions of bioactive glasses with cellular processes in the dynamic environment calls for an enhanced understanding of the impact of fluid flow on ion release.

This study compares the impact of the local fluid environment on the dissolution reactions of bioactive glass S53P4 particles at the physiological pH of 7.40 (Tris buffer) and an acidic solution at pH 2.00 (lactic acid). The solutions were fed through the glass particles in three reactors coupled in a series using two flow rates, 0.04 and 0.2 ml/min. The results provide novel information on the impact of differences in interfacial conditions on the reaction behaviour of bioactive glass particles.

Materials and Methods

Bioactive Glass Particles

Bioactive glass S53P4 was melted in-house from quartz sand (SiO_2) and analytical grade reagents [CaCO_3 , Na_2CO_3 , and $\text{CaHPO}_4\cdot 2(\text{H}_2\text{O})$] at 1360 °C in an electric furnace for 3 h. The melt was cast to a bar in a graphite mould, annealed for 1 h at 520 °C and then cooled to room temperature overnight. The bar was crushed, remelted, and annealed for homogeneity. Then, the glass was crushed with a ring and puck mill. The glass particles were sieved to a size range of 300–500 µm. The particles were cleaned with acetone in an ultrasound bath to remove the powder attached to the

surfaces. Fine powder dissolving rapidly or transported by the fluid flow through the reactor filter would challenge the accuracy and interpretation of the dissolution mechanisms.

The crushed and cleaned particles were stored in a plastic bag in a desiccator until further use. The particle size distribution (Malvern Panalytical Mastersized 3000) and an SEM image (scanning electron microscope; Leo Gemini, Carl Zeiss) of the crushed and cleaned particles are shown in Fig. 1. The elongated particles passed through the 500 μm sieve and increased the size distribution beyond the range, as seen by the curve and SEM image. The measured surface area moment mean ($D[2,3]$) was 493 μm , and the volume moment mean ($D[3,4]$) was 526 μm . The size fraction's specific surface area (SSA) was 4.686 m^2/kg .

In Vitro Solutions

This work studied the ion release from S53P4 into Tris buffer (Tris) and lactic acid (LA). Tris buffer was used as a reference for dissolution into a simplified medium. For 1 l of Tris buffer, 6.057 g of tris(hydroxymethyl)aminomethane (Fisher Chemical) was dissolved in 900 ml of purified water (ELGA Veolia). The temperature of the solution mixture was increased to 37 $^{\circ}\text{C}$ in a water bath before adjusting the pH with 1 M HCl to 7.40. LA enabled estimating the impact of an acidic dynamic environment on bioactive glass dissolution. 0.4 M lactic acid was prepared by adding 35 ml of 85% DL-lactic acid (Sigma) to 965 ml of purified water to give a solution pH of 2.00.

Dissolution Study

Dissolution Setup

The setups for the continuous flow-through reactors have been described elsewhere [16, 35]. One, two, or three polypropylene reactors were coupled in a series to a cascade reactor to allow the analysis of the outflows from each reactor combination and particles in each reactor. 210 ± 5 mg of S53P4 particles were placed in each reactor, and the solution

was fed through them with 0.04 or 0.2 ml/min using a peristaltic pump (Ismatec IPC High Precision Multichannel Pump). The lower flow rate was chosen to fit into the suggested flow rate of 5–20 ml/min per 100 g of bone [20], whilst the faster flow rate has been used in our previous studies. The pump was connected to the solutions and reactors with thin thermoplastic tubes (Tygon®). The solutions and reactors were kept in a 37 $^{\circ}\text{C}$ water bath during the dissolution. For the flow rate of 0.04 ml/min, the solution outflow was collected for 1 h (2.4 ml) every hour for up to 8 h and then at hour 24. For the solution flow rate of 0.2 ml/min, the solution outflow was collected for 20 min (4 ml), every 20 min for the first hour, then every other hour for up to 8 h, and finally, at hour 24. The measured values are given for the endpoint of each solution collection. Parallel static experiments were also conducted as a control using 210 ± 5 mg of S53P4 particles immersed in 30 ml Tris and LA in a 100 rpm shaking incubator (Stuart Orbital Incubator SI500) at 37 $^{\circ}\text{C}$. At 24 h, the reactions were stopped by washing with ethanol, followed by drying the particles overnight at 40 $^{\circ}\text{C}$. Each experiment was done in triplicates.

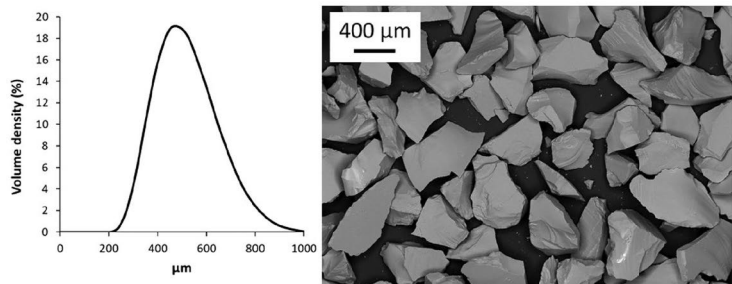
Solution pH

The pH meter (VWR, pHenomenal pH 1100 L) was calibrated with standardised buffer solutions (4.01 and 7.00, VWR). The pH measurements were conducted directly in a water bath directly after the solution collection. Each reported value is an average of three parallel measurements. The pH of the static solutions was measured from the supernatants as close to the particles as possible without the electrode touching the particle beds at 2, 4, 6, 8, and 24 h. The pH of the reference solutions was measured before and after each experiment.

Ion Release

The ion concentrations were measured with inductively coupled plasma-optical emission spectrometry (ICP-OES, Optima 5300 DV; Perkin Elmer). Three parallel

Fig. 1 Size distribution of S53P4 particles crushed and sieved to 300–500 μm size range (left) and SEM image of crushed and cleaned particles (right)



samples from each time point were analysed 3–5 times. The ICP-OES was calibrated with 1, 5, and 20 ppm of Si, Ca, Na, and P (Spectrascan) between every 60 samples. The reported results are background corrected accordingly. The limit of quantification and wavelengths were Si = 0.04 ppm; 251.622 nm, Ca = 0.003 ppm; 317.933 nm, Na = 0.2 ppm; 589.592 nm, and P = 0.03 ppm; 213.617 nm.

Normalised Surface-Specific Mass Loss

The measured ion concentrations were converted into normalised surface-specific mass loss rate according to Eq. (1) [16]:

$$NR_i = \frac{C_i}{f_i \left(\frac{SA}{F} \right)}, \quad (1)$$

where C_i is the concentration of element i (mg/l), f_i is the mass fraction of element i in the glass, SA is the initial total surface area of the glass particles (m^2), and F is the flow rate of the solution (m^3/s). Equation (1) gives the normalised surface-specific mass loss rate (NR_i) for element i at a desired time point ($g m^{-2} s^{-1}$). The initial total surface area was calculated from the analysed specific surface area ($4.686 m^2/kg$) and the initial mass of bioactive glass particles. NR_i was calculated for each element for the bioactive glass dissolution to the two solutions at the two flow rates.

Reaction Layers

After the dissolution, the glass particles were cast in epoxy resin for analysis with a scanning electron microscope coupled to an energy-dispersive X-ray (EDX; Thermo Scientific UltraDry, Thermo Scientific). The embed particles were ground and polished with ethanol and abrasive paper to reveal the cross-sections.

Results

Solution pH

Figure 2 shows the pH of Tris and LA in the dynamic and static experiments as functions of time. The results for the experiments using 0.2 ml/min Tris and static Tris have been reported earlier [36, 40]. The pH graphs do not include deviations of the parallel measurements as most were below ± 0.05 pH units, with a maximum deviation of ± 0.12 . The pH increased during the first hour and then gradually decreased towards the values before dissolution.

For both solutions, the highest pH was measured after three reactors at 1 h for the flow rate of 0.04 ml/min. The pH was consistently higher in the slower flow than in the faster one. In each experiment, the pH of Tris was within the solution's buffering capacity range. In contrast, the pH of the static solutions increased slowly during the immersion. At 24 h in Tris, the pH of the static solution was the same as after one reactor in the cascade reactors for both

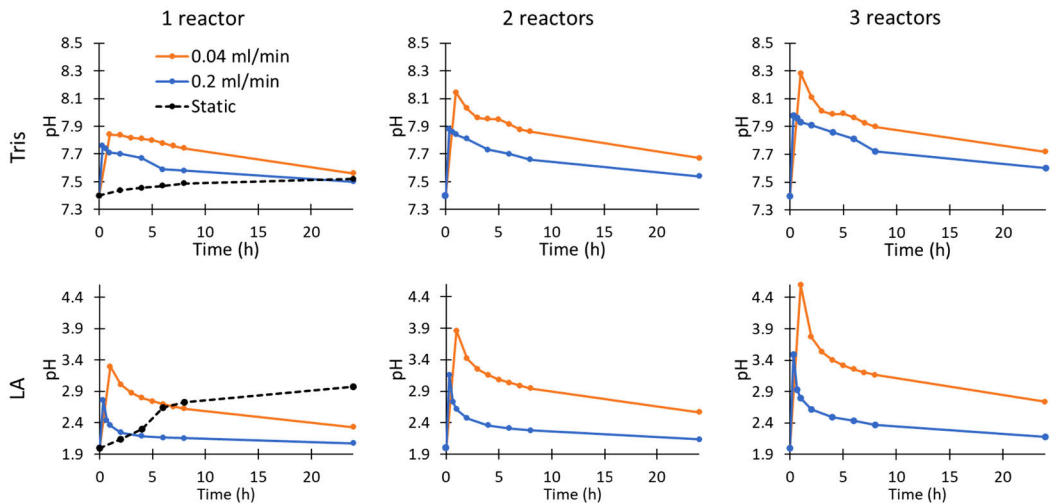


Fig. 2 Change of pH in the outflow of dynamic and static 0.05 M Tris (pH 7.4) and 0.4 M lactic acid (pH 2.00) with an increasing number of reactors horizontally. Static and 0.2 ml/min Tris are from results reported elsewhere [36, 40]

flow rates. In contrast, the pH of the static LA corresponded to the value after three reactors for the 0.04 ml/min flow rate at 24 h.

Ion Release

Tables 1 (Tris) and 2 (LA) show the average ion concentrations (mg/l) in the outflows measured with ICP-OES. Also, results in Tris using the flow rate of 0.2 ml/min are included [36]. The ion concentrations at 24 h static experiments in Tris [40] and LA are marked in the table using the symbol 24S. The highest deviations (± 13 mg/l Na in Tris, and ± 200 mg/l Ca in LA) were measured for the slowest flow rate and at the first measurement points. The deviations are omitted from the table for clarity. The significant difference in the solution volume fed through the reactors using the two flow rates explains the concentration differences between the two flow rates at each time point. The total solution volumes consumed during the 24 h were 57.6 and 288 ml for the flow rates of 0.04 and 0.2 ml/min, respectively. Although the concentrations of released ions into Tris increased with the number of reactors, the relative increases in the second and third reactors were markedly less than in the first reactor. In contrast, the dissolved ion concentrations in LA increased after each reactor equally.

Reaction Layers

SEM–EDXA of particles reacted for 24 h in 0.2 and 0.04 ml/min Tris are shown in Fig. 3. Si concentration increased in all reactors from the bulk glass towards the glass surface. Increased Ca and P concentrations at the outermost surfaces suggested calcium phosphate (Ca/P) precipitation. However, no pure Ca/P was analysed on particles from any reactor, as silicon was also present in the outer layer. The reaction layers developed similarly on the particles in both flow rates. However, the precipitated Ca/P layer was slightly thicker at the 0.2 ml/min flow rate. Also, the silica-rich layer was thicker on the third reactor particles in the faster flow.

Figure 4 shows SEM micrographs and line analyses of cross-sections of particles after 24 h of continuous LA flow. Contrary to Tris, an almost pure silica-rich layer had formed on the particle surfaces. No distinct difference was observed between the thickness of the layers when comparing the reactor number or flow rate.

Figure 5 shows SEM images of particles from experiments in static and dynamic 0.04 ml/min LA for 24 h. A more even silica-rich layer had formed on particles in the dynamic than in the static system. The formed layer was also thicker on the particles in the dynamic fluid flow.

Table 1 Measured ion concentrations (mg/l) in 0.05 M Tris outflows after 1, 2, or 3 reactors for 0.2 ml/min [36] and 0.04 ml/min, n/a = <LOQ

h	Si						Ca					
	0.2 ml/min			0.04 ml/min			0.2 ml/min			0.04 ml/min		
	1	2	3	1	2	3	1	2	3	1	2	3
1	68	80	95	83	106	126	92	123	155	162	204	223
2	70	78	82	82	91	95	83	108	131	128	178	189
4	67	73	78	78	81	83	68	93	118	114	144	151
6	63	69	74	75	77	80	57	79	107	106	130	144
8	61	66	69	70	74	76	47	64	86	89	116	128
24	53	59	62	55	65	70	30	39	51	43	71	84
24S	12						19					
h	Na						P					
	0.2 ml/min			0.04 ml/min			0.2 ml/min			0.04 ml/min		
	1	2	3	1	2	3	1	2	3	1	2	3
1	119	165	205	212	305	365	8.8	8.4	11	10	4.8	2.8
2	109	156	192	176	246	277	7.7	4.5	3.8	4.7	5.5	5.2
4	89	133	178	167	211	232	6.9	4.8	2.8	1.2	n/a	0.4
6	73	110	164	154	203	219	6.0	4.9	2.8	1.6	0.6	0.6
8	59	88	125	130	177	195	5.3	4.8	3.9	2.1	0.9	0.8
24	37	48	65	55	100	123	4.1	4.6	5.4	3.6	3.1	2.0
24S	31						0.5					

24S gives the concentration after 24 h of static dissolution in Tris [40]

Table 2 Measured ion concentrations (mg/l) in the outflow of 0.4 M lactic acid after 1, 2, or 3 reactors for 0.2 ml/min and 0.04 ml/min

h	Si						Ca					
	0.2 ml/min			0.04 ml/min			0.2 ml/min			0.04 ml/min		
	1	2	3	1	2	3	1	2	3	1	2	3
1	2.2	4.4	6.4	15.8	31.7	48.6	211	409	582	1489	2640	3627
2	2.1	4.3	5.8	10.4	19.9	30.6	138	283	399	863	1659	2475
4	2.2	4.3	6.2	9.9	18.4	26.8	103	206	296	585	1131	1673
6	2.5	4.6	6.5	10.2	18.7	26.5	86	169	248	469	909	1314
8	2.8	4.8	6.9	10.8	19.9	26.7	71	143	209	402	809	1142
24	3.8	6.8	9.8	16.0	25.4	34.1	32	64	91	171	330	512
24S	3.2						154					

h	Na						P					
	0.2 ml/min			0.04 ml/min			0.2 ml/min			0.04 ml/min		
	1	2	3	1	2	3	1	2	3	1	2	3
1	233	456	654	1625	2869	3963	25	49	71	187	319	449
2	152	316	446	932	1760	2614	16	35	48	109	226	338
4	112	231	334	630	1201	1771	12	25	37	74	142	210
6	94	190	278	504	981	1439	10	21	31	59	114	168
8	79	162	234	434	857	1226	9	18	26	51	102	144
24	35	70	104	202	363	552	4	8	12	22	42	65
24S	269						11					

24S gives the concentrations after 24 h of static dissolution in LA

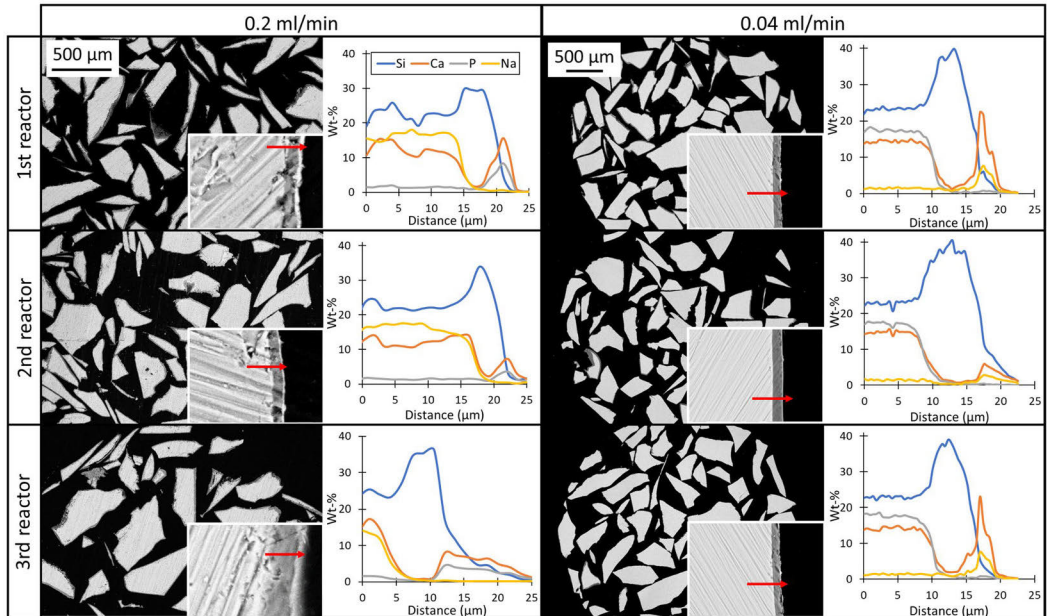


Fig. 3 SEM-EDXA of S53P4 particles in the three reactors in experiments conducted with 0.2 and 0.04 ml/min Tris for 24 h. Each arrow in the magnified figure corresponds to 25 μm

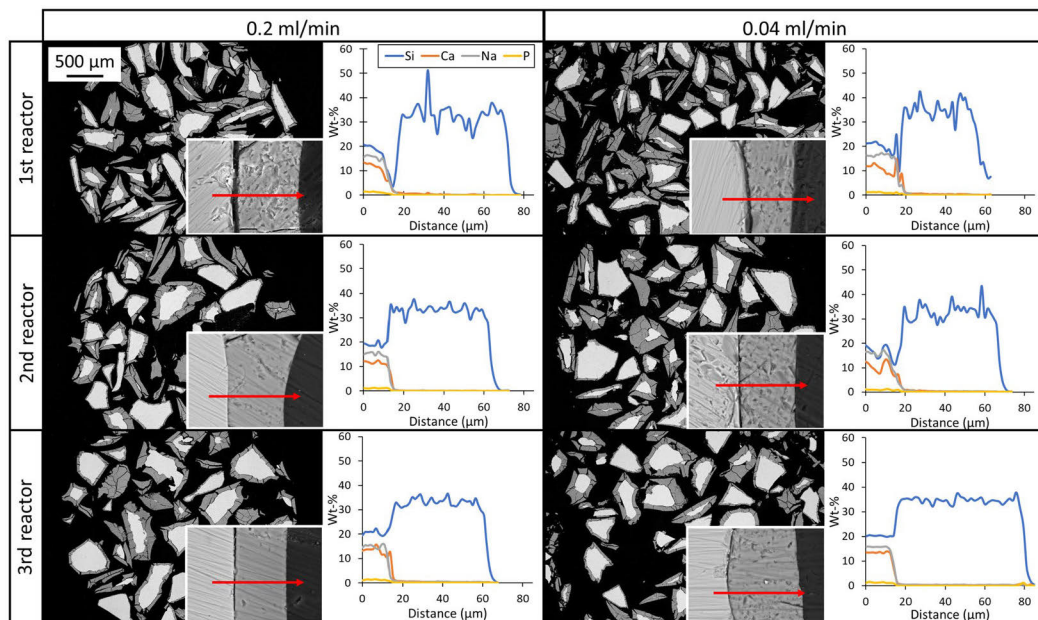


Fig. 4 SEM–EDXA of S53P4 particles in the three reactors after dynamic lactic acid exposure for 24 h. Each arrow in the magnified figure corresponds to 80 μm

Discussion

This work studied the impact of ions released from bioactive glass S53P4 on the dissolution trends of neighbouring glass particles in dynamic solutions of Tris (pH 7.40) and lactic acid (pH 2.00) using two flow rates of 0.04 and 0.2 ml/min. Static immersions served as references. The dynamic dissolution studies were performed in a cascade system of three reactors to analyse changes in the solution composition (ICP-OES) and particle surface composition (SEM–EDXA) with progressive dissolution during 24 h. In contrast to conventional static immersion studies where pH and ion concentrations increase gradually [41, 42], these values first increased rapidly, decreasing then towards the values in the reference solutions (Fig. 2; Table 1).

The ion dissolution into Tris gradually decreased with time after the initial dissolution peaks of all ions around one hour. Despite the significant differences in the solution volume fed through the samples using the two flow rates, the concentration of silicon species released into Tris at 24 h was on the same level, around 55 mg/l in the first reactor (Table 1). Similarly, the Si release was much less, 10 mg/l or lower, from the second reactor for the two flow rates, whilst still less dissolved from the third reactor particles. The lower Tris flow rate led to clearly higher calcium ion

release throughout the 24 h dissolution. Sodium ion concentration after the first reactor was higher for the lower flow rate. Calcium and sodium ion concentrations released from the second and third reactor particles were significantly lower than from the first reactor. The phosphate concentrations suggested that all phosphate released from the particles in the first reactor had formed calcium phosphate in the two following reactors. Especially the sodium concentration was relatively high after the third reactor. This implies that toxic effects due to locally high ion concentrations must be considered for bioactive glasses containing elements critical for tissue healing and regeneration at elevated concentrations.

SEM–EDX results suggested some calcium phosphate on the particles' outer surface (Fig. 3). The thicknesses of the reaction layers were almost similar for both flow rates of Tris. However, the precipitated Ca/P layer was slightly thicker in the faster flow. This suggests that Ca/P precipitated faster due to the increased Ca and P concentrations in the faster Tris flow. Silica-rich and Ca/P layers were identified on the particles, although the ion dissolution decreased after the first reactor (Table 1). Likely, the ions dissolved from the first reactor particles in Tris contributed to the layer growth in the consecutive reactors. Thus, the increasing ion concentrations retarded the glass dissolution but did not significantly affect the reaction layer morphology of the glass

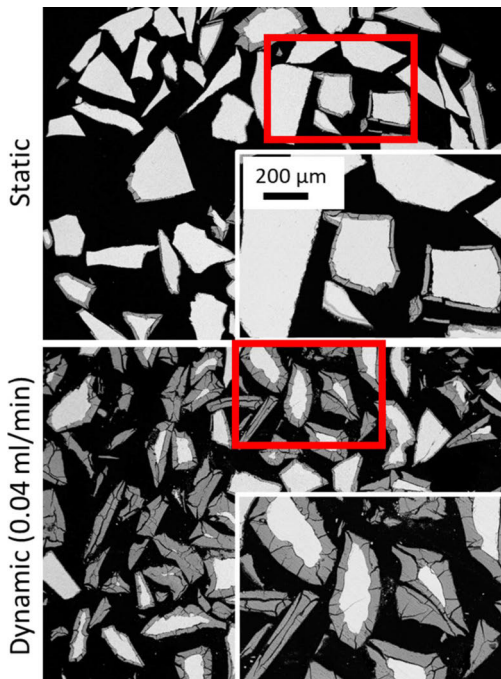


Fig. 5 S53P4 particles after 24 h in static LA (above) and 0.04 ml/min LA in the 1st reactor (below)

particles in Tris. The particle surface composition implies that the primary silica-rich layer on the first reactor particles, i.e. particles representing exterior particles in a bed, was due to ion exchange. At the same time, dissolved species recondensed in the subsequent reactors representing interior particle behaviour as soon as suitable nucleation sites had formed on them. Compared to static conditions, the ion release concentrations suggested similar trends, i.e. high release of sodium ions, some silicon species released, and precipitation of Ca/P. The incongruent and particle unspecific dissolution in LA led to similar silica-rich layers on all glass particles in the three reactors (Fig. 4).

Interestingly, the ion release into LA showed different trends. First, the release of silicon species was much less than in Tris. The relative ion release from each reactor stayed on similar levels, independent of the concentration in the inflow. The dissolution of Si was around 9–16 mg/l for the slower flow rate, 0.04 ml/min, at 24 h. Less silicon dissolved into each reactor using the faster flow rate, around 3–4 mg/l. In contrast, calcium, sodium, and phosphorus were readily released from the glass particles. Similar results due to accelerated ion exchange and alkali hydrolysis have been reported for alkali aluminoborosilicate glasses in static HCl

(pH 2.00) [43]. The SEM images showed thick silica-rich surface layers without signs of calcium phosphate precipitation (Fig. 4). Fast dissolution kinetics in an acidic static environment has been reported to lead to faster polymerisation of the silica-rich layer [44]. In this work, the pH after the reactors did not significantly increase due to the continuous feed of as-prepared LA. Further, no calcium phosphate precipitated (Figs. 4, 5) because calcium compounds dissolve in acidic solutions [45]. The solution pH did not in any experiment increase above 5, i.e. levels at which amorphous calcium phosphate precipitates [46]. Calcium and phosphate ions released were likely effectively chelated by LA [47]. Whether this means that lactic acid produced in the degradation of polylactide-based biopolymers prevents hydroxyapatite precipitation in a PLA-bioactive glass composite needs further study.

The pH of Tris stayed within the stability range of Ca/P precipitation and the silica-rich layer provided suitable nucleation sites during the dynamic and static experiments (Figs. 2, 3). On the other hand, increased dissolution of amorphous silica occurs in solutions with a pH above 8 [48] and Si dissolution from a two-component glass was promoted in alkaline solutions with a pH well above 9 [49], consequently leading to a decreased silica-rich layer for Ca/P-precipitation. In this work, the pH of Tris outflows was below 8.28. However, the pH inside the particle beds might have been higher locally than the measured pH of the outflow solutions [15]. Thus, the changes in Si species concentrations after the first reactor (Table 1) indicate that the local pH stayed below the level leading to increased Si dissolution (Tris). Thus, the continuous solution feeds prevented high local pH and promoted dissolution. Similarly, a large reactor study *in vitro* with 3 $\mu\text{m/s}$ SBF flow over a bioactive glass 13–93 implant concluded that the dynamic environment allowed the pH to stay below levels that would impact the reaction behaviour [50].

Apart from our previous reports implementing a cascade reactor system [35, 36], studies on the impact of bioactive glass ion dissolution products on the reactions of nearby glass particles are sparse. Further, to the authors' knowledge, studies of the effects of dissolution products on the reactions of neighbouring bioactive glass particles in LA are limited [32, 33]. Alkali and alkaline ion release in these studies was higher than in physiological pH. Furthermore, bioactive glass 45S5 neutralised replenished LA (pH 4.00) when incorporated in a resin composite [51].

Figure 6 shows the share (wt%) of the dissolved elements (silicon, calcium, sodium, and phosphorus) in dynamic Tris and LA. The dissolution was calculated from the ion concentration differences between outflows and inflows (Tables 1, 2), the volume of solution flowing through the setup, and the total mass of the elements in the unreacted glass. In 0.04 ml/min Tris, the dissolution decreased in the consecutive

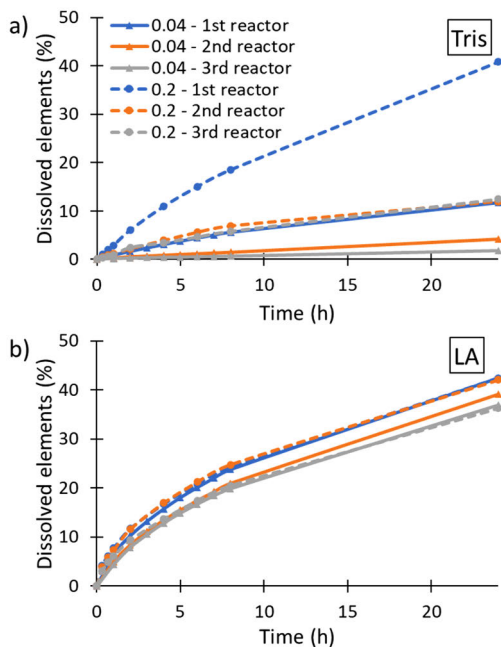


Fig. 6 Cumulative dissolution of Si, Ca, Na, and P to dynamic Tris (a) and LA (b) for 24 h of continuous flow-through with 0.04 and 0.2 ml/min solution flow

reactors from 12% in the first reactor, to 4 and 1.8% in the second and third reactors. In contrast, the total dissolution decreased from 41% (first reactor) to 12% (second and third reactors) for the faster flow rate. The decreasing dissolution suggests that the dissolved ions in the solution flowing into the second and third reactors decreased the dissolution. At the same time, the reaction layer morphologies were almost similar (Fig. 3). Likely, the dissolved ions from the first and second reactor particles contributed to the layer formation by recondensation and precipitation in the consecutive reactors. On the other hand, no similar decrease was measured in the dissolution in the consecutive reactors in LA at 24 h. The dissolution consisting mainly of Ca, Na, and P varied between 36 and 42% in both flow rates. In the static conditions, the dissolution was 1.5% in Tris and 10% in LA at 24 h. The differences in the dissolution degrees and reaction layer morphologies were assumed to depend on lower concentration gradients in the interfacial solution inside the particle bed in dynamic conditions compared to the static systems. The location of the S53P4 particles in the particle beds, the solution pH, and the flow rate thus affected the dissolution rate. Accordingly, a thorough understanding of the fluid flow rate around and within an implant is crucial for tailoring a bioactive glass-based implantable device.

Figure 7 shows the calculated normalised surface-specific mass loss rate (NR_s) for the glass particles in each reactor as a function of time for experiments conducted in Tris for the two flow rates. Although the ion concentrations measured were higher for the slower flow rate, a higher share of glass

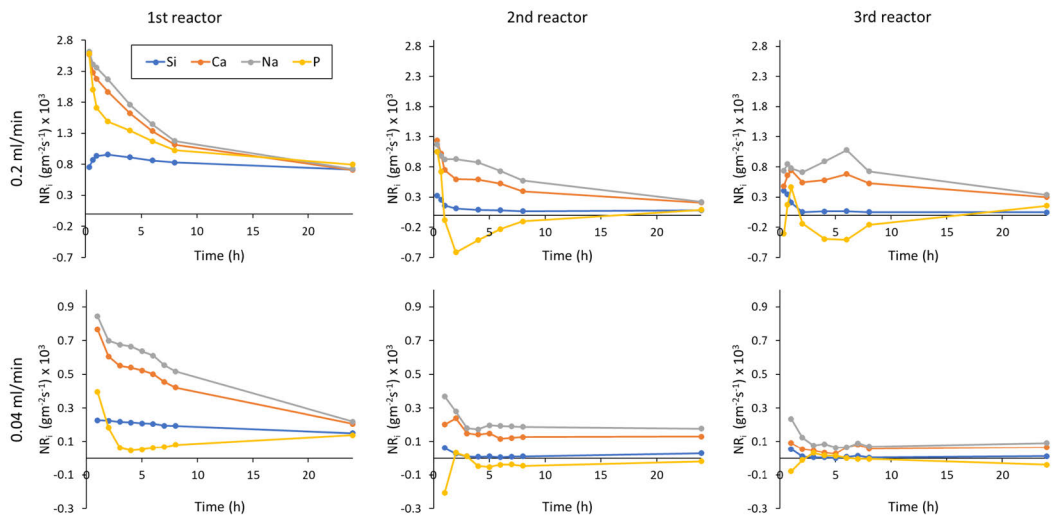


Fig. 7 Normalised surface-specific mass loss rate for S53P4 particles in experiments with 0.2 and 0.04 ml/min Tris for the three consecutive reactors

was dissolved in the Tris buffer fed with a higher flow rate after 24 h, explained by the larger total solution volume fed through the reactors. Accordingly, the normalised surface-specific mass loss rate was higher for the higher flow rate. The normalised dissolution trends also imply decreased rates with the increasing number of reactors. The higher flow rate gave a higher NR_i for all elements. The elements initially leached at different rates (incongruent dissolution) with higher rates for Ca, Na, and P than Si. The dissolution in the first reactor with a flow rate of 0.2 ml/min was congruent at 24 h. In the two other reactors, the initially incongruent dissolution also approached congruent dissolution at longer times. The differences between Ca and Na rates were assumed to depend on the precipitation of Ca/P based on the P dissolution trends. The ion release trends to the lower Tris flow rate showed similar trends but slower normalised dissolution as the higher flow rate. However, the lower dissolution is seen as a much lower normalised dissolution. Ca/P precipitation was assumed based on the line analyses of the reaction layers (Fig. 3). Negative P-values in the second and third reactors in Fig. 7 also indicate Ca/P precipitation. The dissolution rate of P was markedly less in the consecutive reactors and the lower flow rate. In vivo, Ca/P precipitation is likely more rapid due to the higher ion concentrations in the physiological solution.

Calculated NR_{Si} in LA are presented in Fig. 8. In contrast to Tris, the surface-specific mass loss rates of Ca, Na, and P were similar throughout the experiments. Thus, the particles

dissolved similarly in all three reactors at both flow rates. Correspondingly, the surface-specific Si mass loss rate was much lower. NR_{Si} was slightly higher in the first reactor for both flow rates. As the silica-rich layer thickness was almost equal on particles in each reactor, the slightly higher release rate in the first reactor might indicate a recondensation of silicon species in the second and third reactor particles.

Studies in a dynamic environment are limited, and most have used a flow rate of 0.2 ml/min [35, 36, 52–54]. A slower fluid flow rate has been suggested to increase the ion exchange [21, 55]. This study showed higher ion concentrations in slower flows of Tris and LA (Tables 1, 2). The lower flow rate (0.04 ml/min per 0.210 g glass) was still on the higher end of the estimated blood flow in bones [20]. Thus, lower rates are recommended for future studies to understand the impact of ion release from bioactive glasses. NR_i of Ca, Na, and P were considerably higher in LA than in Tris. Interestingly, the NR_i values were similar regardless of the reactor and flow rate. This aligns with the increased ion release of Ca and P from bioactive glass 45S5 in a 0.56 ml/min dynamic acetic acid sodium acetate buffer (pH 4) compared to the Tris-buffered simulated body fluid [56].

The three-step cascade reactor in this study can be compared with a bed of implanted bioactive glass particles. The first reactor in the cascade is proposed to mimic the outer part of the implanted particles in first contact with the solution. The solution with the dissolved ions then flows further in the implanted particle bed, mimicked in vitro by

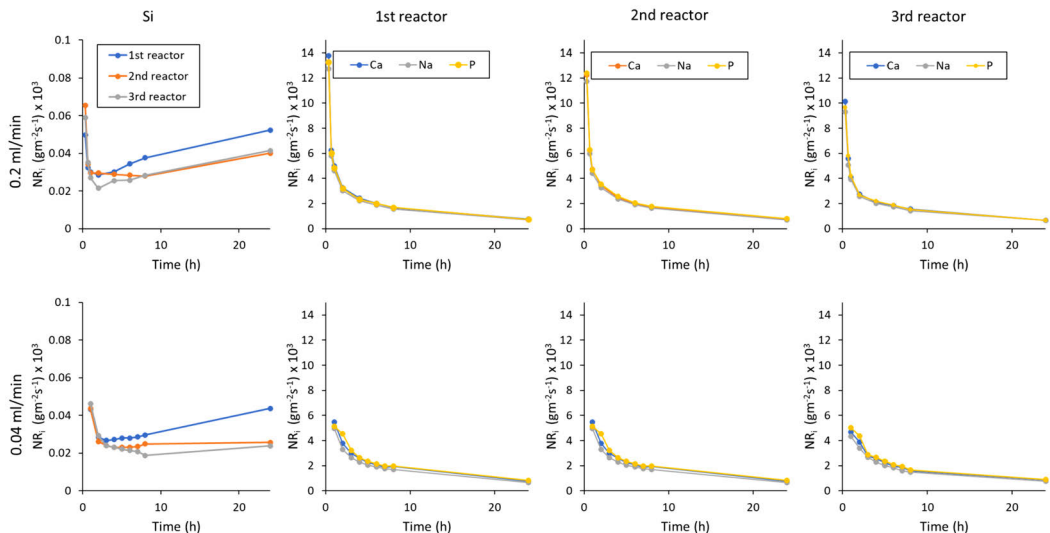


Fig. 8 Normalised surface-specific mass loss rate for S53P4 particles in experiments with 0.2 and 0.04 ml/min LA for the three consecutive reactors

the second and third reactors in the cascade. The results in this study, combined with previously reported results [35, 36], suggested that dissolved ions decreased the surface-specific mass loss rate after the first reactor at pH 7.4. In contrast, a similar decrease was not noticed at the acidic pH. This implies that the implanted particles would dissolve incongruently and similarly in an acidic solution. Thus, the dissolved ions would not affect the ion release from the neighbouring particles or condense on these if the pH stays well below levels where Ca/P precipitation takes place. For a PLA composite implant, gradual polymer degradation would lead to an incongruent dissolution of bioactive glass particles if the local pH was less than around pH 5, independent of the fluid flow rate or the glass particle location in the implant. In contrast, implanted bioactive glass particles would dissolve at different rates depending on their location in physiological solutions (around pH 7.4).

The dissolution rate of a bioactive glass depends not only on its composition but also, to a great extent, on the local pH environment. Temperature also affects the dissolution kinetics and mechanism [16] but has a minor impact in the narrow body temperature range. Further, the porosity of the implant and the fluid flow rate around and through the implant affect the dissolution rate and mechanism. Interestingly, the reaction layers in different locations of a porous S53P4 scaffold implanted in the rabbit femur were similar [57].

The results of this study provided some insights into the impact of the pH environment on the reactions in different implant parts for designing devices based on bioactive glass to various fluid flow conditions. Longer runs in the continuous flow conditions are needed to better understand the long-term fate of the glass and how the findings correlate with the in vivo behaviour.

Conclusion

Dissolution behaviour and reaction layers were studied for bioactive glass S53P4 particles in a dynamic cascade reactor system in physiological (Tris buffer solution, pH 7.4) and acidic (lactic acid, pH 2.00) conditions. In Tris, the ion concentration increased in the solution inflow to the second and third reactors, leading to decreased ion release from the particles in these reactors. In contrast, the dissolution was less affected by the changes in the ion concentrations in the acidic solution. The cascade reactor enabled following the impact of ions dissolved from the glass particles on the reaction behaviour of nearby particles. Despite the decreasing ion release in Tris, the reaction layer thicknesses were equal on the particles in the three reactors at 24 h. Thus, the dissolved ions readily recondense on particles, decreasing the dissolution at physiological pH. However, the dissolved ions only slightly affected Si release or reaction layer thicknesses

in lactic acid. The glass particles dissolved incongruently and at almost the same rate, independent of their location in the lactic acid flow. The slower flow of the Tris (0.04 ml/min) gave higher ion concentrations in the outflow than the faster rate (0.2 ml/min). The normalised surface-specific mass loss rate decreased with the flow rate. Correlating the results with an implanted bioactive glass particle bed suggested that particles inside the bed react slower than exterior particles in the physiological pH range. In contrast, inside a system where pH might decrease to around 2, e.g. due to a degrading biopolymer composite, the bioactive glass particles would dissolve incongruently and similarly throughout the implant. How an acidic degradation of polylactic acid in a bioactive glass composite would locally affect the bioactive glass reactions in the physiological pH range is unclear and needs further study.

Acknowledgements Financial support by Victoriastiftelsen (Project 20230362) is acknowledged (Siekkinen). Luis Bezerra and Linus Silvander are acknowledged for their technical help with ICP-OES measurements and SEM–EDX analysis.

Funding Open access funding provided by Åbo Akademi University.

Data Availability Data will be made available on reasonable request.

Declarations

Conflict of interest There are no conflicts of interest.

Open Access This article is licensed under a Creative Commons Attribution 4.0 International License, which permits use, sharing, adaptation, distribution and reproduction in any medium or format, as long as you give appropriate credit to the original author(s) and the source, provide a link to the Creative Commons licence, and indicate if changes were made. The images or other third party material in this article are included in the article's Creative Commons licence, unless indicated otherwise in a credit line to the material. If material is not included in the article's Creative Commons licence and your intended use is not permitted by statutory regulation or exceeds the permitted use, you will need to obtain permission directly from the copyright holder. To view a copy of this licence, visit <http://creativecommons.org/licenses/by/4.0/>.

References

1. L.L. Hench, Bioceramics: from concept to clinic. *J. Am. Ceram. Soc.* **74**, 1487–1510 (1991). <https://doi.org/10.1111/j.1151-2916.1991.tb07132.x>
2. L.L. Hench, The story of Bioglass®. *J. Mater. Sci. Mater. Med.* **17**, 967–978 (2006). <https://doi.org/10.1007/s10856-006-0432-z>
3. L.L. Hench, Bioceramics. *J. Am. Ceram. Soc.* **81**, 1705–1728 (1998)
4. Ö.H. Andersson, I. Kangasniemi, Calcium phosphate formation at the surface of bioactive glass in vitro. *J. Biomed. Mater. Res.* **25**, 1019–1030 (1991). <https://doi.org/10.1002/jbm.820250808>
5. E. Fiume, J. Barberi, E. Verné, F. Baino, Bioactive glasses: from parent 45S5 composition to scaffold-assisted tissue-healing therapies. *J. Funct. Biomater.* **9**, 24 (2018). <https://doi.org/10.3390/jfb9010024>

6. L.L. Hench, D.E. Clark, Physical chemistry of glass surfaces. *J. Non-Cryst. Solids* **28**, 83–105 (1978). [https://doi.org/10.1016/0022-3093\(78\)90077-7](https://doi.org/10.1016/0022-3093(78)90077-7)
7. E. Munukka, O. Leppäranta, M. Korkeamäki, M. Vaahito, T. Pelto, D. Zhang, L. Hupa, H. Ylänen, J. Salonen, M. Viljanen, E. Eerola, Bactericidal effects of bioactive glasses on clinically important aerobic bacteria. *J. Mater. Sci. Mater. Med.* **19**, 27–32 (2008). <https://doi.org/10.1007/s10856-007-3143-1>
8. J.R. Jones, Review of bioactive glass: from Hench to hybrids. *Acta Biomater.* **9**, 4457–4486 (2013). <https://doi.org/10.1016/j.actbio.2012.08.023>
9. T. Kokubo, H. Takadama, How useful is SBF in predicting in vivo bone bioactivity? *Biomaterials* **27**, 2907–2915 (2006). <https://doi.org/10.1016/j.biomaterials.2006.01.017>
10. International Organization for Standardization, *ISO—ISO 23317:2014—Implants for Surgery—In Vitro Evaluation for Apatite-Forming Ability of Implant Materials* (ISO). <https://www.iso.org/standard/65054.html>
11. A. Maçon, T. Kim, E. Valliant, K. Goetschius, R. Brow, D. Day, A. Hoppe, A. Boccaccini, I. Kim, C. Ohtsuki, T. Kokubo, A. Osaka, M. Vallet-Regí, D. Arcos, L. Fraile, A. Salinas, A. Teixeira, Y. Vueva, R. Almeida, M. Miola, C. Vitale-Brovarone, E. Verné, W. Höland, J. Jones, A unified in vitro evaluation for apatite-forming ability of bioactive glasses and their variants. *J. Mater. Sci. Mater. Med.* **26**, 1–10 (2015). <https://doi.org/10.1007/s10856-015-5403-9>
12. S. Yue, P.D. Lee, G. Poologasundarampillai, J.R. Jones, Evaluation of 3-D bioactive glass scaffolds dissolution in a perfusion flow system with X-ray microtomography. *Acta Biomater.* **7**, 2637–2643 (2011). <https://doi.org/10.1016/j.actbio.2011.02.009>
13. G. Theodorou, O.M. Goudouri, E. Kontonasaki, X. Chatzistavrou, L. Papadopoulou, N. Kantiranis, K.M. Paraskevopoulos, Comparative bioactivity study of 45S5 and 58S bioglasses in organic and inorganic environment. *Bioceram. Dev. Appl.* **1**, 1–4 (2011). <https://doi.org/10.4303/bda/D110154>
14. D. Rohanová, A.R. Boccaccini, D.M. Yunos, D. Horkavcová, I. Březovská, A. Helebrant, TRIS buffer in simulated body fluid distorts the assessment of glass–ceramic scaffold bioactivity. *Acta Biomater.* **7**, 2623–2630 (2011). <https://doi.org/10.1016/j.actbio.2011.02.028>
15. D. Zhang, M. Hupa, H.T. Aro, L. Hupa, Influence of fluid circulation on in vitro reactivity of bioactive glass particles. *Mater. Chem. Phys.* **111**, 497–502 (2008). <https://doi.org/10.1016/j.matchemphys.2008.04.055>
16. S. Fagerlund, P. Ek, L. Hupa, M. Hupa, Dissolution kinetics of a bioactive glass by continuous measurement. *J. Am. Ceram. Soc.* **95**, 3130–3137 (2012). <https://doi.org/10.1111/j.1551-2916.2012.05374.x>
17. R.E. Tomlinson, M.J. Silva, Skeletal blood flow in bone repair and maintenance. *Bone Res.* **1**, 311–322 (2013). <https://doi.org/10.4248/BR201304002>
18. M. Marenzana, T.R. Arnett, The key role of the blood supply to bone. *Bone Res.* **1**, 203–215 (2013). <https://doi.org/10.4248/BR201303001>
19. S. Salles, J. Shepherd, H.J. Vos, G. Renaud, Revealing intraosseous blood flow in the human tibia with ultrasound. *JBMR Plus* (2021). <https://doi.org/10.1002/jbmb.4.10543>
20. M. Laroche, Intraosseous circulation from physiology to disease. *Jt Bone Spine* **69**, 262–269 (2002). [https://doi.org/10.1016/S1297-319X\(02\)00391-3](https://doi.org/10.1016/S1297-319X(02)00391-3)
21. A. Stiller, M. Engblom, O. Karlström, M. Lindén, L. Hupa, Impact of fluid flow rate on the dissolution behavior of bioactive glass S53P4. *J. Non-Cryst. Solids* **607**, 122219 (2023). <https://doi.org/10.1016/j.jnoncrysol.2023.122219>
22. L. Bingel, D. Groh, N. Karpukhina, D.S. Brauer, Influence of dissolution medium pH on ion release and apatite formation of Bioglass 45S5. *Mater. Lett.* **143**, 279–282 (2015)
23. M. Cicuéndez, J.C. Doadrio, A. Hernández, M.T. Portolés, I. Izquierdo-Barba, M. Vallet-Regí, Multifunctional pH sensitive 3D scaffolds for treatment and prevention of bone infection. *Acta Biomater.* **65**, 450–461 (2018). <https://doi.org/10.1016/j.actbio.2017.11.009>
24. L. Drago, D. Romanò, E. De Vecchi, C. Vassena, N. Logoluso, R. Mattina, C.L. Romanò, Bioactive glass BAG-S53P4 for the adjunctive treatment of chronic osteomyelitis of the long bones: an in vitro and prospective clinical study. *BMC Infect. Dis.* **13**, 584 (2013). <https://doi.org/10.1186/1471-2334-13-584>
25. N.C. Lindfors, P. Hyvönen, M. Nyssönen, M. Kirjavainen, J. Kankare, E. Gullichsen, J. Salo, Bioactive glass S53P4 as bone graft substitute in treatment of osteomyelitis. *Bone* **47**, 212–218 (2010). <https://doi.org/10.1016/j.bone.2010.05.030>
26. E. Steinhäuser, R. Lefering, M. Glombitza, N. Brinkmann, C. Vogel, B. Mester, M. Dudda, Bioactive glass S53P4 vs. autologous bone graft for filling defects in patients with chronic osteomyelitis and infected non-unions—a single center experience. *JBJS* **6**, 73–83 (2021). <https://doi.org/10.5194/jbji-6-73-2021>
27. C.M. Agrawal, K.A. Athanasiou, Technique to control pH in vicinity of biodegrading PLA-PGA implants. *J. Biomed. Mater. Res.* **38**, 105–114 (1997). [https://doi.org/10.1002/\(SICI\)1097-4636\(199722\)38:2%3c105::AID-JBM4%3e3.0.CO;2-U](https://doi.org/10.1002/(SICI)1097-4636(199722)38:2%3c105::AID-JBM4%3e3.0.CO;2-U)
28. H.E. Skallevoid, D. Rokaya, Z. Khurshid, M.S. Zafar, Bioactive glass applications in dentistry. *Int. J. Mol. Sci.* **20**, 5960 (2019). <https://doi.org/10.3390/ijms20235960>
29. C. Loke, J. Lee, S. Sander, L. Mei, M. Farella, Factors affecting intra-oral pH—a review. *J. Oral Rehabil.* **43**, 778–785 (2016). <https://doi.org/10.1111/joor.12429>
30. G. Vergnol, N. Ginsac, P. Rivory, S. Meille, J.-M. Chenal, S. Balvay, J. Chevalier, D.J. Hartmann, In vitro and in vivo evaluation of a polylactic acid-bioactive glass composite for bone fixation devices. *J. Biomed. Mater. Res. B* **104**, 180–191 (2016). <https://doi.org/10.1002/jbm.b.33364>
31. M.A. Elsayy, K.-H. Kim, J.-W. Park, A. Deep, Hydrolytic degradation of polylactic acid (PLA) and its composites. *Renew. Sustain. Energy Rev.* **79**, 1346–1352 (2017). <https://doi.org/10.1016/j.rser.2017.05.143>
32. L. Björkvik, X. Wang, L. Hupa, Dissolution of bioactive glasses in acidic solutions with the focus on lactic acid. *Int. J. Appl. Glass Sci.* **7**, 154–163 (2016). <https://doi.org/10.1111/ijag.12198>
33. M. Arango-Ospina, L. Hupa, A.R. Boccaccini, Bioactivity and dissolution behavior of boron-containing bioactive glasses under static and dynamic conditions in different media. *Biomed. Glass* **5**, 124–139 (2019). <https://doi.org/10.1515/bglass-2019-0011>
34. M.M. Pereira, L.L. Hench, Mechanisms of hydroxyapatite formation on porous gel-silica substrates. *J. Sol-Gel Sci. Technol.* **7**, 59–68 (1996). <https://doi.org/10.1007/BF00401884>
35. M. Siekkinen, O. Karlström, L. Hupa, Effect of local ion concentrations on the in vitro reactions of bioactive glass 45S5 particles. *Int. J. Appl. Glass Sci.* **13**, 695–707 (2022). <https://doi.org/10.1111/ijag.16579>
36. M. Siekkinen, O. Karlström, L. Hupa, Dissolution of bioactive glass S53P4 in a three-reactor cascade in continuous flow conditions. *Open Ceram.* **13**, 100327 (2023). <https://doi.org/10.1016/j.oceram.2022.100327>
37. I.D. Xynos, A.J. Edgar, L.D.K. Buttery, L.L. Hench, J.M. Polak, Ionic products of bioactive glass dissolution increase proliferation of human osteoblasts and induce insulin-like growth factor II mRNA expression and protein synthesis. *Biochem. Biophys. Res. Commun.* **276**, 461–465 (2000). <https://doi.org/10.1006/bbrc.2000.3503>
38. K. Vuornos, M. Ojansivu, J.T. Koivisto, H. Häkkinen, B. Belay, T. Montonen, H. Huhtala, M. Kääräinen, L. Hupa, M. Kellomäki, J. Hyttinen, J.A. Ihalainen, S. Miettinen, Bioactive glass ions induce efficient osteogenic differentiation of human adipose stem cells

- encapsulated in gellan gum and collagen type I hydrogels. *Mater. Sci. Eng. C* **99**, 905–918 (2019). <https://doi.org/10.1016/j.msec.2019.02.035>
39. M. Ojansivu, S. Vanhatupa, L. Björkvik, H. Häkkinen, M. Kellomäki, R. Autio, J.A. Ihalainen, L. Hupa, S. Miettinen, Bioactive glass ions as strong enhancers of osteogenic differentiation in human adipose stem cells. *Acta Biomater.* **21**, 190–203 (2015). <https://doi.org/10.1016/j.actbio.2015.04.017>
40. M. Siekkinen, M. Engblom, L. Hupa, Impact of solution pH (5–9) and dissolution products on in vitro behaviour of the bioactive glass S53P4. *J. Non-Cryst. Solids X* **20**, 100199 (2023). <https://doi.org/10.1016/j.nocx.2023.100199>
41. V. Aina, L. Bertinetti, G. Cerrato, M. Cerruti, G. Lusvardi, G. Malavasi, C. Morterra, L. Tacconi, L. Menabue, On the dissolution/reaction of small-grain Bioglass® 45S5 and F-modified bioactive glasses in artificial saliva (AS). *Appl. Surf. Sci.* **257**, 4185–4195 (2011). <https://doi.org/10.1016/j.apsusc.2010.12.019>
42. M. Cerruti, D. Greenspan, K. Powers, Effect of pH and ionic strength on the reactivity of Bioglass® 45S5. *Biomaterials* **26**, 1665–1674 (2005). <https://doi.org/10.1016/j.biomaterials.2004.07.009>
43. N. Stone-Weiss, R.E. Youngman, R. Thorpe, N.J. Smith, E.M. Pierce, A. Goel, An insight into the corrosion of alkali aluminoborosilicate glasses in acidic environments. *Phys. Chem. Chem. Phys.* **22**, 1881–1896 (2020). <https://doi.org/10.1039/C9CP06064B>
44. Q. Qin, N. Stone-Weiss, T. Zhao, P. Mukherjee, J. Ren, J.C. Mauro, A. Goel, Insights into the mechanism and kinetics of dissolution of aluminoborosilicate glasses in acidic media: impact of high ionic field strength cations. *Acta Mater.* **242**, 118468 (2023). <https://doi.org/10.1016/j.actamat.2022.118468>
45. E. Fernández, F.J. Gil, M.P. Ginebra, F.C.M. Driessens, J.A. Planell, S.M. Best, Calcium phosphate bone cements for clinical applications. Part I: solution chemistry. *J. Mater. Sci. Mater. Med.* **10**, 169–176 (1999). <https://doi.org/10.1023/A:1008937507714>
46. S.V. Dorozhkin, Calcium orthophosphates (CaPO₄): occurrence and properties. *Prog. Biomater.* **5**, 9–70 (2016). <https://doi.org/10.1007/s40204-015-0045-z>
47. J.G. Neves, D. Navarro da Rocha, C.C. Lopes, M.H. Prado da Silva, M.A.C. Sinhoretto, L. Correr-Sobrinho, M.A.A. Fraga, A.B. Correr, Effect of pH level and calcination on the production of calcium phosphates by acidic route of wet precipitation. *Cerâmica* **67**, 236–243 (2021). <https://doi.org/10.1590/0366-69132021673822965>
48. R.K. Iler, The solubility of silica. In: *The Chemistry of Silica* (Wiley, Hoboken, 1979), pp. 30–49
49. R.W. Douglas, T.M.M. El-Shamy, Reactions of glasses with aqueous solutions. *J. Am. Ceram. Soc.* **50**, 1–8 (1967). <https://doi.org/10.1111/j.1151-2916.1967.tb14960.x>
50. M. Höner, F. Böke, M. Weber, H. Fischer, Mimicking physiological flow conditions to study alterations of bioactive glass surfaces in vitro: MIMICKING PHYSIOLOGICAL FLOW CONDITIONS. *J. Biomed. Mater. Res.* **106**, 228–236 (2018). <https://doi.org/10.1002/jbm.b.33847>
51. M. Par, A. Gubler, T. Attin, Z. Tarle, A. Tarle, T.T. Tauböck, Ion release and hydroxyapatite precipitation of resin composites functionalized with two types of bioactive glass. *J. Dent.* **118**, 103950 (2022). <https://doi.org/10.1016/j.jdent.2022.103950>
52. P. Sinitsyna, O. Karlström, L. Hupa, In vitro dissolution of bioactive glass S53P4 microspheres. *J. Am. Ceram. Soc.* **105**, 1658–1670 (2022). <https://doi.org/10.1111/jace.18014>
53. P. Sinitsyna, O. Karlström, C. Sevoniuss, L. Hupa, In vitro dissolution and characterisation of flame-sprayed bioactive glass microspheres S53P4 and 13–93. *J. Non-Cryst. Solids* **591**, 121736 (2022). <https://doi.org/10.1016/j.jnoncrysol.2022.121736>
54. L. Aalto-Setälä, M. Siekkinen, N. Lindfors, L. Hupa, Dissolution of glass–ceramic scaffolds of bioactive glasses 45S5 and S53P4. *Biomed. Mater. Devices* (2023). <https://doi.org/10.1007/s44174-022-00059-4>
55. I. Izquierdo-Barba, A.J. Salinas, M. Vallet-Regí, Effect of the continuous solution exchange on the in vitro reactivity of a CaO–SiO₂ sol–gel glass. *J. Biomed. Mater. Res.* **51**, 191–199 (2000). [https://doi.org/10.1002/\(SICI\)1097-4636\(200008\)51:2%3c191::AID-JBM7%3e3.0.CO;2-T](https://doi.org/10.1002/(SICI)1097-4636(200008)51:2%3c191::AID-JBM7%3e3.0.CO;2-T)
56. D. Galusková, H. Kaňková, A. Švančárková, D. Galusek, Early-stage dissolution kinetics of silicate-based bioactive glass under dynamic conditions: critical evaluation. *Materials* **14**, 3384 (2021). <https://doi.org/10.3390/ma14123384>
57. E. Eriksson, R. Björkenheim, G. Strömberg, M. Ainola, P. Uppstu, L. Aalto-Setälä, V.-M. Leino, L. Hupa, J. Pajarinen, N.C. Lindfors, S53P4 bioactive glass scaffolds induce BMP expression and integrative bone formation in a critical-sized diaphysis defect treated with a single-staged induced membrane technique. *Acta Biomater.* **126**, 463–476 (2021). <https://doi.org/10.1016/j.actbio.2021.03.035>

Aalto-Setälä L., Siekkinen M., Lindfors N., Hupa L. "***Dissolution of Glass-Ceramic Scaffolds of Bioactive Glasses 45S5 and S53P4***" Biomedical Materials & Devices, (2023), DOI: 10.1007/s44174-022-00059-4



Dissolution of Glass–Ceramic Scaffolds of Bioactive Glasses 45S5 and S53P4

Laura Aalto-Setälä¹ · Minna Siekkinen¹ · Nina Lindfors² · Leena Hupa¹

Received: 22 October 2022 / Accepted: 19 December 2022
© The Author(s) 2023

Abstract

Although the initial *in vitro* dissolution of bioactive glasses (BAG) is well characterized, the long-term behaviour of crystallized BAG scaffolds in a continuous fluid flow is incompletely understood. A detailed understanding of the long-term dissolution of scaffolds is vital for predicting their behaviour in clinical applications. Here, we explored the dissolution and reaction mechanisms of partly crystalline and glass–ceramic scaffolds based on the bioactive glasses S53P4 and 45S5 using a continuous flow-through method in Tris-buffer (Tris) and simulated body fluid (SBF) for up to 21 days. Granules of the parent glasses were used as references. The main crystalline phase in both scaffolds was sodium-calcium-silicate. The scaffolds' dissolution suggested that the sodium-calcium-silicate crystals dissolved incongruently to yield hydrous silica. The silica phase then provided abundant nucleation sites for hydroxyapatite precipitation, resulting in fine-grained crystalline structures. When exposed to Tris, the scaffolds almost completely dissolved within the test period, leaving only highly porous remnant phases. For the 45S5 scaffolds, the calcium phosphate reaction layers that formed on their surfaces effectively slowed the dissolution in SBF. In contrast, this effect was less apparent for the S53P4 specimens.

Keywords Bioactive glass · Crystallization · Scaffolds · Biomedical materials · Biodegradable materials · Dissolution behaviour · Continuous · Dynamic · Tissue engineering

Introduction

The dissolution of bioactive glasses (BAGs) determines their ability to produce therapeutic effects, stimulate tissue growth, and interact with cellular processes in bone tissue regeneration [1–3]. Improved understanding of the dissolution process is necessary to develop tissue-engineering scaffolds based on BAGs. Despite extensive research on the *in vitro* dissolution of BAGs in static [4–7], half-dynamic

[8], and closed circulation systems [9], knowledge on the reaction kinetics using continuous flow-through test methods is limited. Furthermore, previous studies have mainly focussed on glass powders or particles [10–15].

Ideally, a BAG dissolves at a rate comparable to tissue regeneration, thus providing space for neogenesis [16]. The biological reactions at the BAG lead to a dual-surface layer that chemically binds the BAG to tissue, especially to bone [3, 17]. The release of soluble silicate species and calcium ions from the BAG during dissolution induces osteostimulation [18–20]. Moreover, the gradual formation of a dual surface, consisting of an inner silica-rich and an outer crystalline hydroxyapatite (HA) layer, likely changes the dissolution kinetics of the glass, which also affects the biological response of the BAG [21].

When designing BAG-based implants for new medical applications, one major challenge is understanding the short- and long-term behaviour of the implant *in vivo*. Release of ions from the BAG to the surrounding solution should be sufficiently high to stimulate the cellular processes needed to support tissue regeneration or bacteriostasis [1, 22]. If HA deposition retards overall dissolution, ions released from

✉ Leena Hupa
leena.hupa@abo.fi
Laura Aalto-Setälä
laura.aalto-setala@lasifaasi.fi
Minna Siekkinen
minna.siekkinen@abo.fi
Nina Lindfors
nina.c.lindfors@hus.fi

¹ Johan Gadolin Process Chemistry Centre, Åbo Akademi University, Henrikinkatu 2, 20500 Turku, Finland

² Department of Hand Surgery, Helsinki University Hospital, University of Helsinki, PL 3, 00014 Helsinki, Finland

the BAG may decrease below the critical biological levels needed to support cellular processes. Conversely, a BAG that does not develop a suitably thick HA layer may dissolve too rapidly, making it an ineffective scaffold [21, 23].

BAGs are currently used primarily as granules in various bone-filling clinical applications [3]. Increased research is devoted to developing porous BAG-based scaffolds [24–35]. The strong crystallization tendency of two well-known commercial BAGs (45S5 and S53P4) limits their hot-working into amorphous scaffolds. Consequently, amorphous porous scaffolds from other glass compositions with relatively high silica content have been developed, allowing hot-working without crystallization [36, 37]. Interestingly, amorphous S53P4 scaffolds have recently been successfully sintered under carefully controlled conditions [38, 39].

Several variables affect the *in vivo* degradation behaviour of BAGs [40]. The dissolution of 45S5 and S53P4 depends on the location of the implant [41]. Unreacted 45S5 has been found several months after implantation in rabbit femurs [42]. Similar findings were reported for clinical studies of S53P4. In addition to anatomical location, bone remodelling also depends on the amount and particle size of the implanted BAG [41, 43]. Crystallization reduces the dissolution rate compared with the parent BAG [44, 45]. Understanding the detailed dissolution kinetics of partially crystallized S53P4 and glass–ceramic 45S5 scaffolds may aid in developing mechanically strong implants for load-bearing applications.

This work reports on the dissolution behaviour of crystalline and partially crystalline scaffolds of 45S5 and S53P4 BAGs using a continuous flow-through test method in simulated body fluid (SBF) and Tris for up to 21 days. The objective of this study was to assess the impact of crystallization on scaffold dissolution. The results provide insight into the reaction kinetics of these crystalline phases, which may lead to improved tissue-engineering scaffold designs with controlled degradation.

Materials and Methods

Scaffold Preparation

BAGs S53P4 and 45S5 were prepared by mixing appropriate amounts of Na_2CO_3 , $\text{CaHPO}_4 \cdot 2(\text{H}_2\text{O})$, CaCO_3 , and glass-quality Belgian quartz sand (Sigma-Aldrich, Steinheim, Germany). The batches were melted at 1360 °C in separate platinum crucibles for 3 h before casting the glass into a block-form graphite mould. For homogeneity, the glasses were melted twice and crushed between melts. After casting, the glass blocks were annealed at 520 °C for 1 h before the annealer was allowed to cool. The nominal oxide compositions of 45S5 and S53P4 are shown in Table 1. The annealed

Table 1 Nominal oxide compositions of BAGs 45S5 and S53P4 in wt% (mol%)

Glass	SiO_2	Na_2O	CaO	P_2O_5
45S5	45.0 (46.1)	24.5 (24.3)	24.5 (26.9)	6.0 (2.6)
S53P4	53.0 (53.9)	23.0 (22.7)	20.0 (21.8)	4.0 (1.7)

blocks were crushed and sieved to yield granules between 300 and 500 μm . These granules were filled into separate cylindrical graphite moulds ($\text{Ø}5 \times 10 \text{ mm}$) and sintered at 720 °C (S53P4) and 1030 °C (45S5) in nitrogen for 90 min to form porous scaffolds. Based on prior studies [46, 47], the sintering temperature of the S53P4 BAG was chosen to yield a partially crystallized scaffold that was strong enough for handling. The sintering temperature for the 45S5 BAG was higher because it does not form an adequate glass–ceramic scaffold below 1000 °C [47, 48].

In Vitro Dissolution Setup

The *in vitro* dissolution of the glass granules, crushed scaffolds, and sintered scaffolds was studied in continuous flow-through reactors. Simulated body fluid (SBF) and Tris-buffer (Tris) were continuously fed through the samples at an average flow rate of 0.2 mL/min. Fagerlund et al. described the reactor cell configuration in detail [12]. The flow rate was assumed to mimic the typical laminar flow of extracellular fluid in the human body [13]. SBF was prepared according to the protocol developed by Kokubo et al. [49]. Tris (50 mM, Trizma base, Sigma-Aldrich) was adjusted with 1 M HCl (J.T. Baker) to a pH of 7.40 at 37 °C.

The mass of the S53P4 granules and scaffolds varied from 270 to 300 mg. Dissolution tests with the more rapidly dissolving 45S5 granules and scaffolds were performed using smaller samples, ranging from 195 to 230 mg. The smaller 45S5 specimens ensured ion release in concentrations sufficiently low to prevent blockage. HA deposition within the reactor tubes was noted in preliminary tests when larger 45S5 masses were used.

The dissolution characteristics of granules and crushed scaffolds were analysed for 14 days. Sintered scaffolds were evaluated for 21 days. Solution temperatures were maintained at 37 °C.

The solution volume fed through the samples was measured at each time point. For each experiment, three discrete samples were sequentially collected at 15-min intervals every 1 to 3 days for up to 21 days. These samples were subsequently analysed for the amount of released inorganic ions. Then, once the total solution volume and the measured ions at each timepoint were known, an estimation of the amount of dissolved elements at each timepoint t was determined as a mean of the three consecutive measurements,

$$n_i(t) = \frac{1}{3} \sum_{j=1}^3 c_{ij} V_j(t) \quad (1)$$

where c_i is the measured concentration (mg/L) of element i , and $V(t)$ is the volume of the sample. The pH was also measured at each time point. When estimating the cumulative overall dissolution of each element, ion release between two consecutively measured time point was assumed as a mean of the two values. The dissolved fraction of element i cumulated until each time point t can then be written as

$$D_{ik}(t) = D_{ik}(t-1) + \frac{n_i(t-1) + n_i(t)}{2} \frac{V(\Delta t)}{x_i m_k} 100\% \quad (2)$$

where $D_i(t-1)$ is the dissolved fraction of element i determined at the previous measurement point, $V(\Delta t)$ is the measured volume of solution between the current time point and the previous measurement, x_i is the weight fraction of the element i in the glass, and m_k is the total original mass of the sample k .

Released ion concentrations were analysed using an inductively coupled plasma optical emission spectrometer (ICP-OES, Optima 5300 DV; Perkin Elmer, Waltham, MA). Before analysis, the solutions were diluted 1:10 using ultrapure water. The analysed elements included silicon ($\lambda = 251.611$ nm), calcium ($\lambda = 317.933$ nm), and sodium ($\lambda = 589.592$ nm). Phosphorus concentrations were too low to provide reliable data after the first few test days. Thus, phosphorus was omitted from the analyses. Calibration of the spectrometer was conducted using ultrapure water and multielement standards (Perkin Elmer Multi-Element Standard 25; silicon standard from Ultra Scientific) with 1 ppm Si, Ca, and Na. The calibration was reverified after every 20 samples. All values were background corrected. Due to the breakage of several 45S5 scaffolds when they were initially

inserted into the reactor cells ($\text{Ø}5 \times 11$ mm), larger diameter reactor cells ($\text{Ø}5.7 \sim 5.8$ mm) were used for subsequent specimens.

Scaffold and Granule Analyses After Immersion

After the *in vitro* experiments, the remaining scaffold pieces and granules were rinsed with ethanol to terminate the reactions, dried, weighed, and cast into epoxy resin. The resin-embedded samples were polished to reveal cross-sections of the reaction layers. The thickness and composition of the reaction layers were examined with a scanning electron microscope (SEM, Leo Gemini 1530, Carl Zeiss, Oberkochen, Germany) equipped with an energy dispersive X-ray analyser (EDX, UltraDry X-ray detector, Thermo Fisher Scientific, MA, USA).

The crystallized surface layer to the amorphous core ratio was identified from seven cross-sectional scaffold SEM panorama images for each S53P4 sample using image-analysis software (Photoshop CS6, Adobe Systems, Inc, San Jose, CA, USA). The percentage of the crystallized layer was then calculated from manipulated images by comparing the number of pixels in crystalline and amorphous areas. The amount of the crystalline and glassy phases in the thin crystallized layer was also calculated from 10 cross-sectional SEM images (5 k magnification), as described above.

Results

Ion Release

The concentrations of silicon released in both solutions and sodium and calcium released in Tris from S53P4-based samples are shown in Fig. 1. The phosphorus concentration

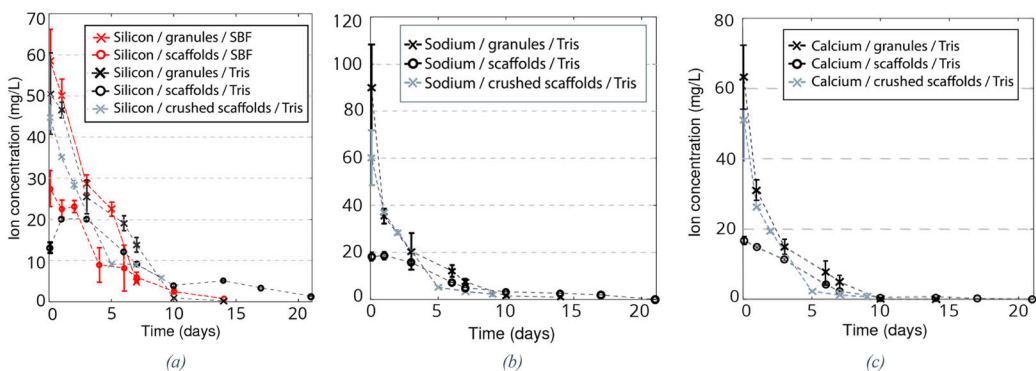


Fig. 1 Concentrations of ions released from S53P4 granules, scaffolds, and crushed scaffolds into the continuous flow of Tris and SBF: **a** Si in Tris and in SBF, **b** Na in Tris, and **c** Ca in Tris. Dashed lines provide visual guidance only

was close to the limit of quantification (LOQ). The corresponding ion concentrations released from 45S5-based samples are shown in Fig. 2. Although the initial ion concentrations released from the scaffolds were generally lower than those released from the glass granules, the differences diminished over time. After 21 days in continuous Tris flow, only a 1–3 mg remained of the amorphous S53P4 and 45S5 granules.

Sodium, calcium, and silicon species were released from the S53P4 scaffolds into Tris at measurable concentrations for 17 days. After longer periods, only the values for silicon were greater than the LOQ. The concentrations were lower for the scaffolds than granules for all elements, especially during the first days. There were no notable differences between the crushed scaffolds and the granules.

Despite its lower mass, the initial ion release was higher from the 45S5 samples than S53P4 samples. However, the

ion concentrations dissolving from 45S5 granules rapidly decreased after the initial peak. The released silicon concentration was higher from 45S5 scaffolds than from granules only for 1 day and 3 days for Na and Ca. The ion concentrations released from crushed 45S5 scaffolds were similar to the concentrations measured for granules. After 6 days in SBF, the ion concentrations dissolving from all 45S5 sample types also decreased below LOQ. In Tris, the concentrations for the crushed 45S5 scaffolds were below LOQ after 9 days. In contrast, the ion dissolution from 45S5 scaffolds was within the measurable range for 17 days.

The calculated cumulative dissolved fractions (calculated from Eqs. 1 and 2) of silicon for S53P4 and 45S5 samples are shown in Fig. 3. The last concentrations above the LOQ were measured at after 17 days after which the concentrations were below the LOQ for all measured elements. The values over 100% are considered due to having only a few

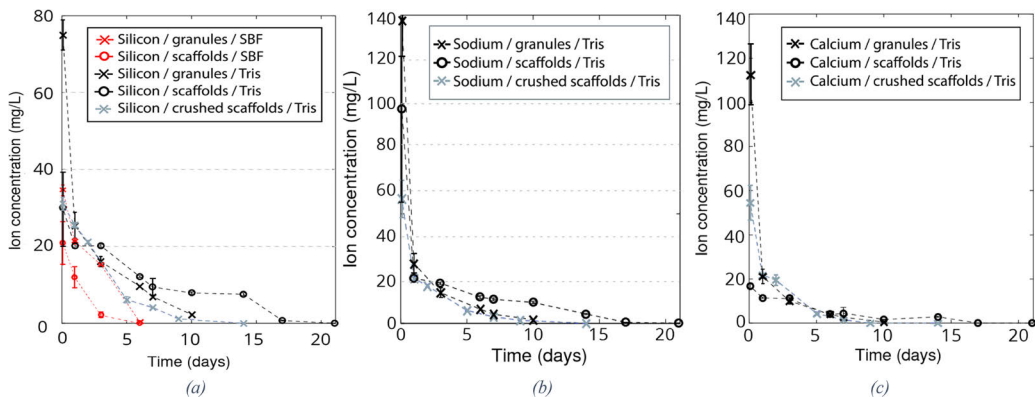
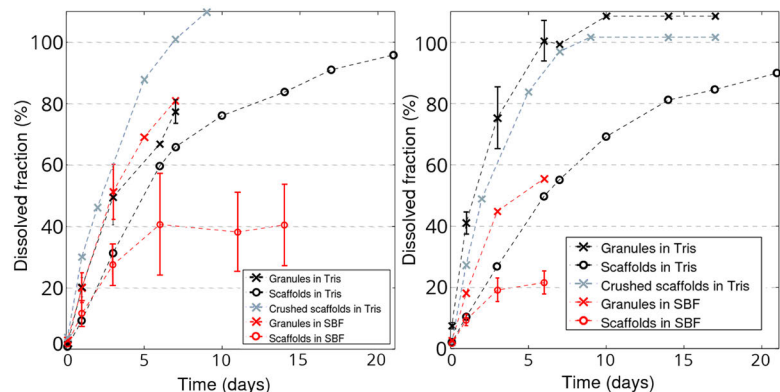


Fig. 2 Concentrations of ions released from 45S5 granules, scaffolds, and crushed scaffolds into continuous flow of Tris and SBF: **a** Si in Tris and in SBF, **b** Ca in Tris, and **c** Na in Tris. Lines provide visual guidance only

Fig. 3 Cumulative silicon dissolution of samples based on **a** S53P4 and **b** 45S5. Lines provide visual guidance only



measurement points during the initial diffusion-dominated phase of dissolution. The approximation here assumes the concentration between two consecutively measured time points as a mean of the two values.

The evolution of pH was examined throughout the dissolution (data not shown). The highest pH values, 7.81 for 45S5 granules and 7.72 for S53P4 granules, were measured at 60 min (the first measurement point). After 24 h, the pH decreased to 7.44 for S53P4 scaffolds and 7.58 for 45S5 scaffolds.

Scaffold Morphology Before Dissolution

According to SEM images and EDX analyses of S53P4 scaffolds, the crystallized surface layer appeared to contain a high share of amorphous phase, with more Si and less Na and Ca than the crystals. The calculated percentage of the phases in the manipulated (black and white colours) SEM image in Fig. 4b suggested $67 \pm 3\%$ (95% confidence level) crystals in the layer, with the remaining 33% being an amorphous phase. The thickness of the crystallized layer varied from 40 to 80 μm , depending on the measuring point in the scaffold. The smaller particles in the SEM image (Fig. 5) that suggest total crystallization were assumed to show the top or bottom cross-sections of the sintered granules in the scaffold and were thus disregarded in the thickness calculation. Figures 4b and 5 show that the crystallized surface layer covered $65 \pm 9\%$ (95% confidence level). Combining the thickness of the layer and its share of crystals yields an average of $44 \pm 6\%$ (95% confidence level) of crystals in the

Fig. 4 **a** SEM image and EDX line analysis along the arrow showing minor compositional differences between amorphous S53P4, crystals, and residual amorphous phase around the crystals. **b** SEM image of S53P4 scaffold showing crystals embedded in the amorphous phase (lower image) and a manipulated SEM image showing the residual amorphous (black) and crystalline (white) phases (upper image). The calculated amount of crystals in the SEM image is 62.5%

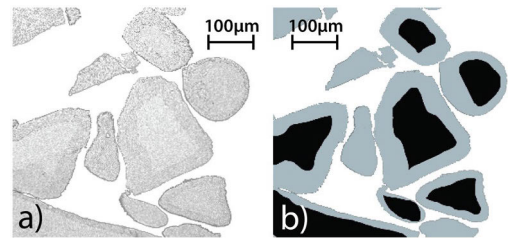
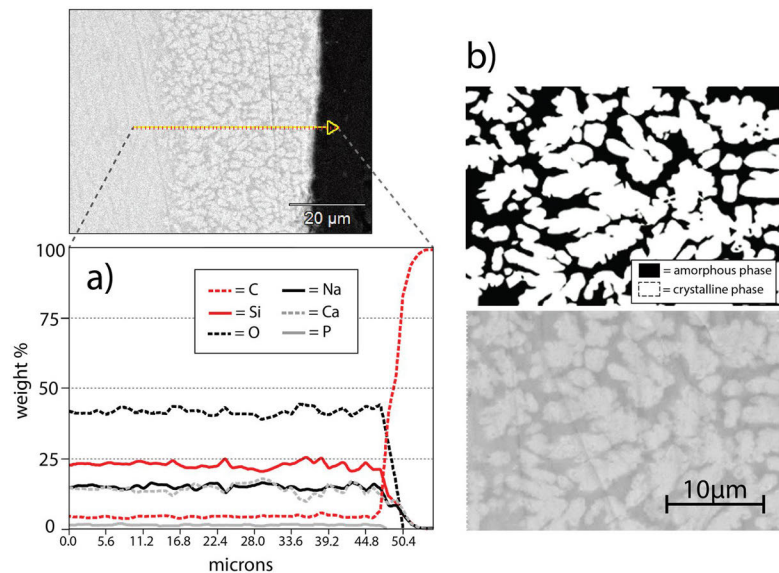


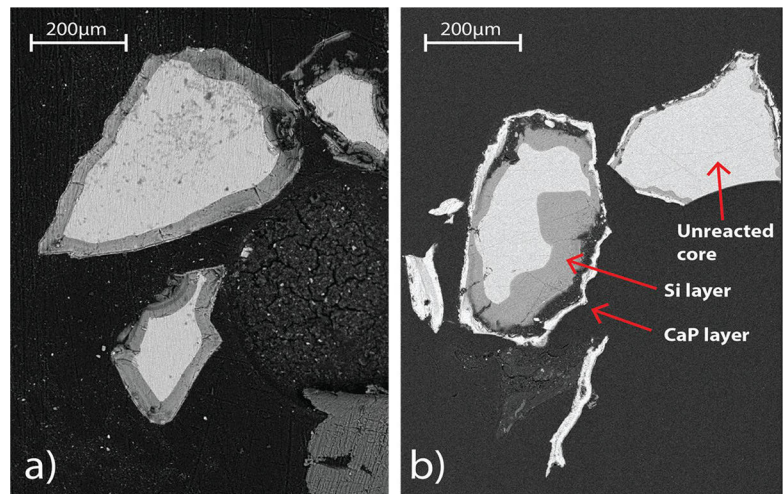
Fig. 5 **a** SEM image of S53P4 cross-section showing crystallized surface layer and amorphous cores **b** Manipulated SEM image showing the crystalline layer (grey) and amorphous cores (black)

cross-sectional area of sintered S53P4 scaffolds. Assuming spherical particles and their isotropic distribution, 58 vol-% of glass had crystallized. In contrast, the glass-ceramic 45S5 consisted of fine-grained crystals and a minor residual amorphous phase throughout the structure. Thus, similar estimations of the shares of the phases in 45S5 scaffolds could not be performed.

Reaction Layer Formation at Sample Surfaces

Figure 6 shows SEM analyses of S53P4 granule cross-sections after 14 days in continuous flow of Tris and 6 days in SBF. A silica-rich layer had formed on the granules in both solutions, but a calcium phosphate (CaP) layer could be identified only on granules exposed to SBF. The granules had dissolved to different extents in the two solutions. Some

Fig. 6 SEM images of cross-sections of amorphous S53P4 granules after **a** 14 days in continuous flow (0.2 mL/min) of Tris and **b** 7 days in continuous flow (0.2 mL/min) of SBF



granules had dissolved almost entirely in Tris, whilst others still seemed intact after 14 days in Tris (Fig. 6a, b). All three S53P4-based specimens showed similar differences in degradation after the dissolution tests. After SBF dissolution, the shred-like CaP formations (Fig. 6b) were assumed to be CaP

reaction layers either left after the granules had dissolved or detached from the granule surfaces.

There was no observable CaP layer on S53P4 scaffolds after 21 days of continuous Tris flow (Fig. 7). The scaffolds had lost their structure due to degradation of the

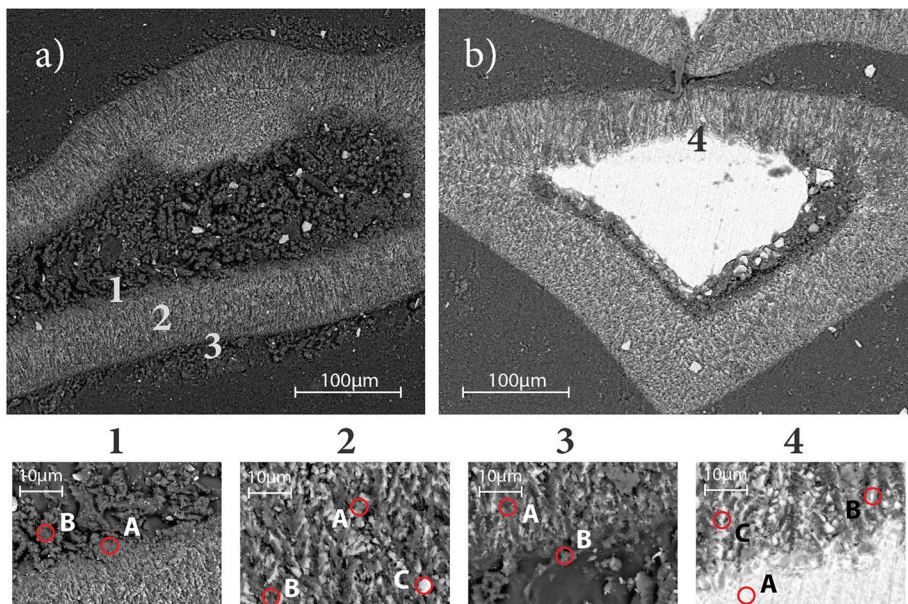


Fig. 7 SEM images of S53P4 scaffold remnant cross-sections after 21 days of dynamic Tris flow. **a** Granule-level detail of partly dissolved crystallized layer and almost completely dissolved core. **b**

Granule-level detail of partly dissolved amorphous core. EDX analyses of the points 1A-B, 2A-C, 3A-B, and 4A-C are shown in Table 2

Table 2 EDX analyses of points shown in Fig. 7

	SiO ₂	Na ₂ O	CaO	P ₂ O ₅
1A	93.4	1.0	1.8	0
1B	73.6	13.5	12.9	0
2A	91.1	0.3	6.8	1.0
2B	92.4	0	5.8	0.7
2C	99.0	0	1.0	0
3A	94.2	0	4.8	0
3B	45.2	28.1	26.7	0
4A	56.1	20.4	19.2	4.2
4B	87.9	2.6	7.8	1.0
4C	87.2	2.5	8.1	1.7

All values in wt%

necks between the granules. The most degraded scaffold granules also comprised of shells of the partly leached

crystallized surface layers (Fig. 7a). According to EDX analyses, these shells mainly consisted of silicon and oxygen, with minimal amounts of sodium and calcium in locations next to the granule core (Table 2).

After the dissolution of S53P4 scaffolds in SBF, a CaP-rich layer was identified on the outer surfaces and within the partly leached crystallized surface layer (Fig. 8a, b). The molar ratio Ca/P in the layer was close to 1.67 (i.e. the hydroxyapatite ratio). The amorphous cores of the scaffold granules started to dissolve during the experiments, as indicated by the gap between the core and outer CaP-rich surface layer (Fig. 8b).

There were thin CaP-rich surface films on the 45S5 scaffolds after 21 days in Tris (Figs. 9a, b). In contrast, the CaP layer formation was so extensive in SBF on glass 45S5 samples that the CaP layer connected granules after 7 days (Fig. 10b).

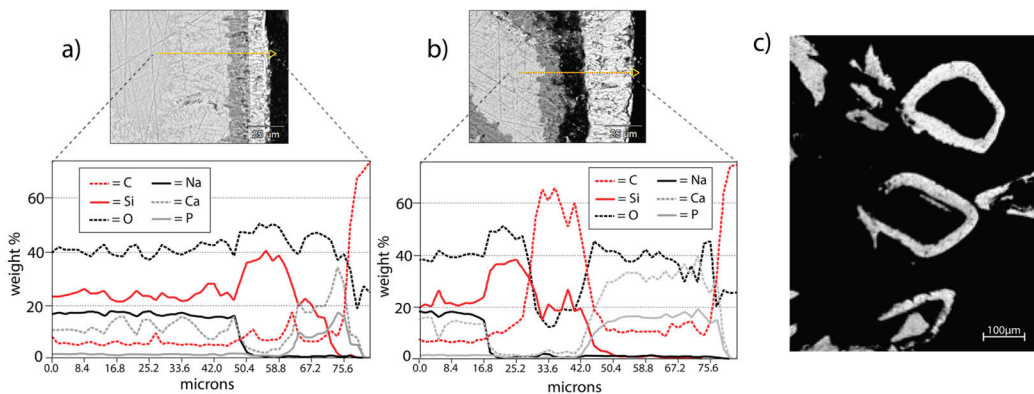


Fig. 8 SEM-EDXA of S53P4 scaffold after 14 days of continuous flow in SBF: **a** Reaction layer formation at the granule surface, **b** crystallized layer has formed CaP and the amorphous core has started to react, **c** granules with CaP surface layers left

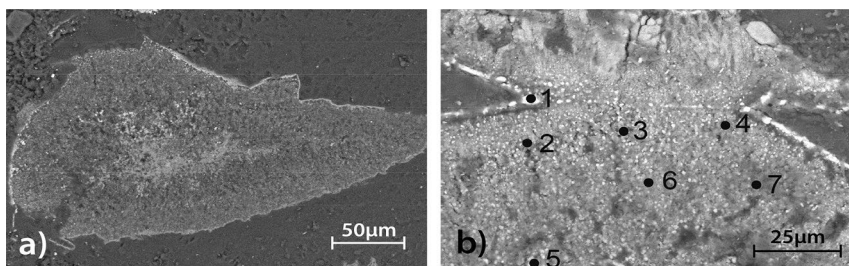
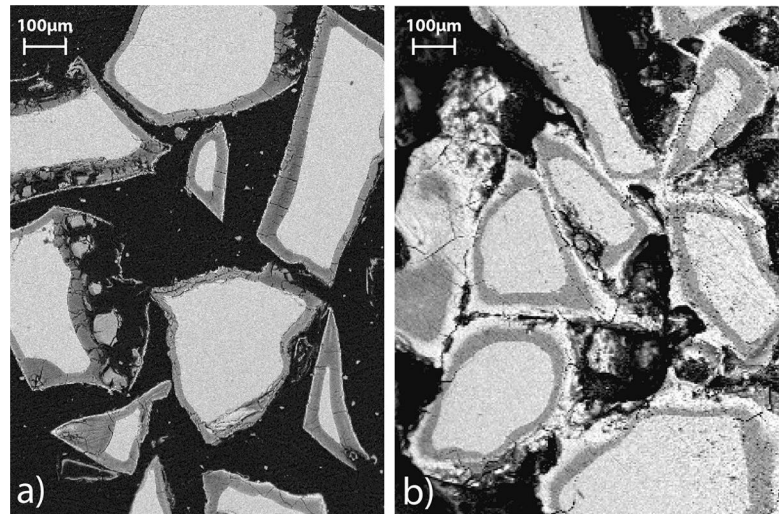


Fig. 9 SEM images of 45S5 scaffolds after 21 days in continuous flow of Tris: **a** Fine-grained structure showing various degrees of dissolution and reaction. **b** Higher magnification of the structure. EDX

analysis of the brighter coloured points 1, 2, 4, and 5 suggested Ca, P, and O, whereas the darker points 3, 6, and 7 consisted of Si, Na, Ca, O, and P

Fig. 10 Glass 45S5 granules after **a** 3 days in continuous flow (0.2 mL/min) of Tris and **b** 7 days in continuous flow (0.2 mL/min) of SBF. In the latter, the CaP formation (seen in white) has joined granules together. In the former, there is no considerable CaP layer but only a silica-rich layer (seen in dark grey)



Discussion

The degradation of porous S53P4 scaffolds with a crystallized surface layer and porous 45S5 glass–ceramic scaffolds was studied in continuous flow-through of Tris-buffer and SBF solutions for up to 21 days. The two BAGs exhibit different crystallization behaviours during sintering [46–48, 50]. Glass 45S5 exhibits bulk crystallization, with the primary crystalline phase $\text{Na}_2\text{CaSi}_2\text{O}_6$ precipitating at approximately 610 °C and the secondary phase $\text{Na}_2\text{Ca}_4(\text{PO}_4)_2\text{SiO}_4$ precipitating above 800 °C [48, 50]. 45S5 scaffolds sintered at 1030 °C consist of a fine-grained crystallized structure with a small residual glass share [51]. Glass S53P4 has a somewhat lower crystallization tendency than 45S5 and exhibits surface crystallization [46]. S53P4 can be sintered into amorphous or partially crystalline scaffolds under controlled conditions [38, 39, 47].

The *in vitro* degradation of the bioactive glass-based samples was studied in continuous fluid flow conditions to better mimic *in vivo* conditions than static *in vitro* tests. Further, feeding a fresh solution through the sample does not lead to saturation of the solutions [9, 12, 52, 53]. In static conditions, the solution saturation and high pH lead to extensive hydroxyapatite precipitation on the BAG, thus retarding the glass dissolution [54]. The overall validity of *in vitro* studies in SBF has been questioned during the past decade [53, 55], as highly reactive materials can exhaust the SBF solution in hours under static conditions. However, in a flow-through reactor setup the pH stays within the buffering range of the solution.

Silicate-based glasses have been studied under dynamic conditions for 30 min to four days [10–15]. The results are

consistent with those in this study: after an initial rapid burst, the dissolution changes into a more steady ion release. The initial ion release observed for all BAG-based samples is well established [7, 12, 13, 15, 56]. The initial rapid increase in pH might have contributed to the release of silicon species (Figs. 1 and 2). However, the highest solution pH values (7.7–7.8) did not exceed the buffering capacity of the solutions. Thus, the low network connectivity (NC), rather than hydrolysis of the Si–O–Si bonds in the glass structure contributed to the gradual degradation of the samples [57]. The calculated NC is higher for S53P4 than for 45S5 ($\text{NC}_{\text{S53P4}} = 2.54$; $\text{NC}_{\text{45S5}} = 2.12$), explaining the higher dissolution of Si from 45S5.

Overall, the amorphous granules dissolved more rapidly than crystallized scaffolds, which was observed in both solutions. Interestingly, ion dissolution from the amorphous granules and crushed scaffold particles of S53P4 and 45S5 exhibited no notable differences in Tris solution (Figs. 1 and 2). This indicates that the slower dissolution of scaffolds in Tris was mainly due to lower surface area and the different fluid flow paths through granules beds and porous structures.

In Tris, the crystallized structure of the scaffold particles did not prevent the dissolution, as almost all material dissolved. After 21 days of Tris solution immersion, only a small (1–3 mg) amount of material was left after the experiments. All material from amorphous granules was exhausted. Interestingly, very fragile, shell-like Si–O structures were left from the crystallized scaffolds of both glasses. This implies that the crystalline phases in 45S5 and S53P4 dissolved incongruently, releasing Na and Ca ions after the residual amorphous phase had leached out. This was observed by EDX analyses, showing only Si and O in

the most degraded sites of the structures. No XRD analyses could be performed to identify the phase compositions of the remnants, due to the small amount of material.

In SBF, the crystalline structures did not slow the formation of the HA layer. The SEM images showed CaP precipitation inside the crystallized surface layer for both glasses (Fig. 8), as also reported by Fagerlund et al. for glass S53P4 [46]. The HA layer was more extensive on the crystallized scaffold particles than on amorphous granules. This suggested that the leached crystallized layer provided a large number of nucleation sites for CaP precipitation. This led to a dense mixed layer that slowed (for glass S53P4) and stopped (for glass 45S5) the dissolution of the amorphous core. The differences between the two glasses were assumed to be due to their different phase compositions and crystal microstructures.

For S53P4, it is unclear, whether the ion-exchange reaction occurred primarily between Na^+ in the scaffold and H^+ in the solution or also with Ca^{2+} . The larger size of the calcium ions compared to sodium ions may retard their diffusion from the fine-grained 45S5 glass–ceramic structure. The observations of the 45S5 scaffold in SBF agree with the reported transformation of sodium–calcium–silicate crystals to amorphous calcium phosphate in vitro through a series of interactions between the crystals and solution [24, 31].

Our results show that despite the crystalline glass–ceramic structure, the dissolution continues until almost all material has been exhausted even though some remnant, highly porous phases were left. This implies that the remnant phases do not prevent the dissolution but provide nucleation sites for HA precipitation. These findings are important for future modelling of the crystallized BAG dissolution.

Conclusion

The long-term dissolution behaviours of sintered scaffolds of BAGs 45S5 and S53P4 were studied in continuous flow of Tris and SBF for up to 21 days. Amorphous granules of both glasses were used as references. S53P4 scaffolds consisted of granules with amorphous core and crystallized surface layers, whereas 45S5 scaffolds were throughout crystallized.

The crystallized layers dissolved incongruently. In Tris, the dissolution continued of crystallized S53P4 and 45S5 scaffolds until almost all material had been exhausted even though some remnant, highly porous phases were left. In SBF, the HA formation was more extensive on the leached crystalline surfaces than on the amorphous granules. The HA layer precipitated extensively inside the crystalline structure, whereas for the amorphous granule surfaces, the HA layer only precipitated on the granule surface. The remnant phases did not prevent the dissolution but provided more nucleation sites for HA precipitation.

The results suggested that the glass–ceramic specimens would fully dissolve with prolonged immersion time also in SBF, even though the solution pH values after the reactor did not markedly increase from the inflow values.

Acknowledgements The Graduate School of Materials Research at Åbo Akademi University is acknowledged for financial support of this work (Laura Aalto-Setälä). Financial support by Svenska Kulturfonden Project 157767 (Minna Siekkinen) is also acknowledged. Luis Bezerra and Linus Silvander are acknowledged for their technical assistance with ICP-OES and SEM.

Funding Open access funding provided by Abo Akademi University (ABO).

Declarations

Conflict of interest There are no conflict to declare.

Open Access This article is licensed under a Creative Commons Attribution 4.0 International License, which permits use, sharing, adaptation, distribution and reproduction in any medium or format, as long as you give appropriate credit to the original author(s) and the source, provide a link to the Creative Commons licence, and indicate if changes were made. The images or other third party material in this article are included in the article's Creative Commons licence, unless indicated otherwise in a credit line to the material. If material is not included in the article's Creative Commons licence and your intended use is not permitted by statutory regulation or exceeds the permitted use, you will need to obtain permission directly from the copyright holder. To view a copy of this licence, visit <http://creativecommons.org/licenses/by/4.0/>.

References

1. A. Hoppe, N.S. Gldal, A.R. Boccaccini, A review of the biological response to ionic dissolution products from bioactive glasses and glass-ceramics. *Biomaterials* **32**(11), 2757–2774 (2011). <https://doi.org/10.1016/j.biomaterials.2011.01.004>
2. A. Hoppe, V. Mouro, A.R. Boccaccini, Therapeutic inorganic ions in bioactive glasses to enhance bone formation and beyond. *Biomater. Sci.* **1**(3), 254–256 (2013). <https://doi.org/10.1039/C2BM00116K>
3. J. Jones, D. Brauer, L. Hupa, D. Greenspan, Bioglass and bioactive glasses and their impact on healthcare. *Int. J. Appl. Glass Sci.* **7**, 423–434 (2016). <https://doi.org/10.1111/ijag.12252>
4. A.L. Maon et al., A unified in vitro evaluation for apatite-forming ability of bioactive glasses and their variants. *J. Mater. Sci. Mater. Med.* **26**, 5403 (2015). <https://doi.org/10.1007/s10856-015-5403-9>
5. L. Varila, T. Lehtonen, J. Tuominen, M. Hupa, L. Hupa, In vitro behaviour of three biocompatible glasses in composite implants. *J. Mater. Sci. Mater. Med.* **23**(10), 2425–2435 (2012). <https://doi.org/10.1007/s10856-012-4693-4>
6. T.J. Lehtonen, J.U. Tuominen, E. Hiekkänen, Resorbable composites with bioresorbable glass fibers for load-bearing applications. In vitro degradation and degradation mechanism. *Acta Biomater.* **9**(1), 4868–4877 (2013). <https://doi.org/10.1016/j.actbio.2012.08.052>
7. M.G. Cerruti, D. Greenspan, K. Powers, An analytical model for the dissolution of different particle size samples of Bioglass® in TRIS-buffered solution. *Biomaterials* **26**(24), 4903–4911 (2005). <https://doi.org/10.1016/j.biomaterials.2005.01.013>

8. S. Radin, P. Ducheyne, S. Falaize, A. Hammond, In vitro transformation of bioactive glass granules into Ca-P shells. *J. Biomed. Mater. Res.* **49**(2), 264–272 (2000). [https://doi.org/10.1002/\(SICI\)1097-4636\(200002\)49:2%3c264::AID-JBM16%3e3.0.CO;2-2](https://doi.org/10.1002/(SICI)1097-4636(200002)49:2%3c264::AID-JBM16%3e3.0.CO;2-2)
9. P. Siriphannon, Y. Kameshima, A. Yasumori, K. Okada, S. Hayashi, Comparative study of the formation of hydroxyapatite in simulated body fluid under static and flowing systems. *J. Biomed. Mater. Res.* **60**(1), 175–185 (2002). <https://doi.org/10.1002/jbm.10056>
10. K. Schuhladen, X. Wang, L. Hupa, A.R. Boccaccini, Dissolution of borate and borosilicate bioactive glasses and the influence of ion (Zn, Cu) doping in different solutions. *J. Non-Cryst. Solids* **502**, 22–34 (2018). <https://doi.org/10.1016/j.jnoncrysol.2018.08.037>
11. L. Hupa, S. Fagerlund, J. Massera, L. Björkvik, Dissolution behavior of the bioactive glass S53P4 when sodium is replaced by potassium, and calcium with magnesium or strontium. *J. Non-Cryst. Solids* **432**, 41–46 (2016). <https://doi.org/10.1016/j.jnoncrysol.2015.03.026>
12. S. Fagerlund, P. Ek, L. Hupa, M. Hupa, Dissolution kinetics of a bioactive glass by continuous measurement. *J. Am. Ceram. Soc.* **95**(10), 3130–3137 (2012). <https://doi.org/10.1111/j.1551-2916.2012.05374.x>
13. S. Fagerlund, L. Hupa, M. Hupa, Dissolution patterns of biocompatible glasses in 2-amino-2-hydroxymethyl-propane-1,3-diol (Tris) buffer. *Acta Biomater.* **9**(2), 5400–5410 (2013). <https://doi.org/10.1016/j.actbio.2012.08.051>
14. M. Arango-Ospina, L. Hupa, A.R. Boccaccini, Bioactivity and dissolution behavior of boron-containing bioactive glasses under static and dynamic conditions in different media. *Biomed. Glas.* **5**(1), 124–139 (2019). <https://doi.org/10.1515/bglass-2019-0011>
15. D. Galuskova, H. Kaňková, A. Švančárková, D. Galusek, Early-stage dissolution kinetics of silicate-based bioactive glass under dynamic conditions: critical evaluation. *Materials* **14**, 3384 (2021). <https://doi.org/10.3390/ma14123384>
16. M.N. Rahaman et al., Bioactive glass in tissue engineering. *Acta Biomater.* **7**(6), 2355–2373 (2011). <https://doi.org/10.1016/j.actbio.2011.03.016>
17. L.L. Hench, R.J. Splinter, W.C. Allen, T.K. Greenlee, Bonding mechanisms at the interface of ceramic prosthetic materials. *J. Biomed. Mater. Res.* **5**(6), 117–141 (1971). <https://doi.org/10.1002/jbm.820050611>
18. L.L. Hench, Genetic design of bioactive glass. *J. Eur. Ceram. Soc.* **29**(7), 1257–1265 (2009). <https://doi.org/10.1016/j.jeurceramsoc.2008.08.002>
19. J. Jones, P. Sepulveda, L. Hench, Dose-dependent behavior of bioactive glass dissolution. *J. Biomed. Mater. Res.* **58**, 720–726 (2001). <https://doi.org/10.1002/jbm.10053>
20. I.D. Xynos, M.V.J. Hukkanen, J.J. Batten, L.D. Buttery, L.L. Hench, J.M. Polak, Bioglass (R) 45S5 stimulates osteoblast turnover and enhances bone formation in vitro: implications and applications for bone tissue engineering. *Calcif. Tissue Int.* **67**, 321–329 (2000)
21. W. Liang, C. Rüssel, D.E. Day, G. Völksch, Bioactive comparison of a borate, phosphate and silicate glass. *J. Mater. Res.* **21**(1), 125–131 (2006). <https://doi.org/10.1557/jmr.2006.0025>
22. V. Miguez-Pacheco, L.L. Hench, A.R. Boccaccini, Bioactive glasses beyond bone and teeth: emerging applications in contact with soft tissues. *Acta Biomater.* **13**, 1–15 (2015). <https://doi.org/10.1016/j.actbio.2014.11.004>
23. J. Massera, C. Claireaux, T. Lehtonen, J. Tuominen, L. Hupa, M. Hupa, Control of the thermal properties of slow bioresorbable glasses by boron addition. *J. Non-Cryst. Solids* **357**(21), 3623–3630 (2011). <https://doi.org/10.1016/j.jnoncrysol.2011.06.037>
24. F. Westhauser et al., Gelatin coating increases in vivo bone formation capacity of three-dimensional 45S5 bioactive glass-based crystalline scaffolds. *J. Tissue Eng. Regen. Med.* **13**(2), 179–190 (2019). <https://doi.org/10.1002/term.2780>
25. E. Boccardi et al., Bioactivity and mechanical stability of 45S5 bioactive glass scaffolds based on natural marine sponges. *Ann. Biomed. Eng.* **44**(6), 1881–1893 (2016). <https://doi.org/10.1007/s10439-016-1595-5>
26. E. Fiume, J. Barberi, E. Verné, F. Baino, Bioactive glasses: from parent 45S5 composition to scaffold-assisted tissue-healing therapies. *J. Funct. Biomater.* (2018). <https://doi.org/10.3390/jfb9010024>
27. F. Baino, E. Verné, C. Vitale-Brovarone, 3-D high-strength glass–ceramic scaffolds containing fluoroapatite for load-bearing bone portions replacement. *Mater. Sci. Eng. C* **29**(6), 2055–2062 (2009). <https://doi.org/10.1016/j.msec.2009.04.002>
28. F. Baino, E. Fiume, Elastic mechanical properties of 45S5-based bioactive glass–ceramic scaffolds. *Materials* **12**, 3244 (2019). <https://doi.org/10.3390/ma12193244>
29. F. Baino, E. Fiume, Mechanical characterization of 45S5 bioactive glass-derived scaffolds. *Mater. Lett.* **245**, 14–17 (2019). <https://doi.org/10.1016/j.matlet.2019.02.086>
30. A. Boccaccini, Q. Chen, L. Lefebvre, L. Gremillard, J. Chevalier, Sintering, crystallisation and biodegradation behaviour of bioglass-derived glass-ceramics. *Faraday Discuss.* **136**, 27–44 (2007). <https://doi.org/10.1039/B616539G>
31. D. Bellucci, V. Cannillo, A. Sola, An overview of the effects of thermal processing on bioactive glasses. *Sci. Sinter.* (2010). <https://doi.org/10.2298/SOS1003307B>
32. B. Thavornnyutikarn, P.F.A. Wright, B. Feltis, W. Kosorn, T.W. Turney, Bisphosphonate activation of crystallized bioglass scaffolds for enhanced bone formation. *Mater. Sci. Eng. C* **104**, 109937 (2019). <https://doi.org/10.1016/j.msec.2019.109937>
33. Q. Nawaz et al., Bioactive glass based scaffolds incorporating gelatin/manganese doped mesoporous bioactive glass nanoparticle coating. *Ceram. Int.* **45**(12), 14608–14613 (2019). <https://doi.org/10.1016/j.ceramint.2019.04.179>
34. S. Fagerlund, L. Hupa, Crystallization of 45S5 during isothermal heat treatment. *Ceram Mater.* **62**, 349–354 (2009)
35. Q. Fu, E. Saiz, N. Rahaman, A. Tomsia, Bioactive glass scaffolds for bone tissue engineering: state of the art and future perspectives. *Mater. Sci. Eng. C Mater. Biol. Appl.* **31**, 1245–1256 (2011). <https://doi.org/10.1016/j.msec.2011.04.022>
36. M. Brink, T. Turunen, R. Happonen, A. Yli-Urpo, Compositional dependence of bioactivity of glasses in the system Na₂O–K₂O–MgO–CaO–B₂O₃–P₂O₅–SiO₂. *J. Biomed. Mater. Res.* **37**, 114–121 (1997). [https://doi.org/10.1002/\(SICI\)1097-4636\(199710\)37:1%3c114::AID-JBM14%3e3.0.CO;2-G](https://doi.org/10.1002/(SICI)1097-4636(199710)37:1%3c114::AID-JBM14%3e3.0.CO;2-G)
37. F. Westhauser et al., Bioactive Glass (BG) ICIE16 shows promising osteogenic properties compared to crystallized 45S5-BG. *Int. J. Mol. Sci.* (2020). <https://doi.org/10.3390/jms21051639>
38. L. Aalto-Setälä, P. Uppstu, P. Sinitsyna, N.C. Lindfors, L. Hupa, Dissolution of amorphous S53P4 glass scaffolds in dynamic in vitro conditions. *Materials* (2021). <https://doi.org/10.3390/ma14174834>
39. J.R. Jones, Review of bioactive glass: from Hench to hybrids. *Acta Biomater.* **9**(1), 4457–4486 (2013). <https://doi.org/10.1016/j.actbio.2012.08.023>
40. M.J. Peltola, K.M.J. Aitasalo, J. Suonpää, A. Yli-Urpo, In Vivo model for frontal sinus and calvarial bone defect obliteration with bioactive glass S53P4 and hydroxyapatite. *J. Biomed. Mater. Res.* **58**, 261–269 (2001). [https://doi.org/10.1002/1097-4636\(2001\)58:33.3.CO;2-0](https://doi.org/10.1002/1097-4636(2001)58:33.3.CO;2-0)
41. H. Oonishi et al., Quantitative comparison of bone growth behavior in granules of bioglass, A-W glass-ceramic, and hydroxyapatite. *J. Biomed. Mater. Res.* **51**, 37–46 (2000). [https://doi.org/10.1002/\(SICI\)1097-4636\(200007\)51:1%3c37::AID-JBM6%3e3.0.CO;2-T](https://doi.org/10.1002/(SICI)1097-4636(200007)51:1%3c37::AID-JBM6%3e3.0.CO;2-T)

42. N. Lindfors, I. Koski, J.T. Heikkilä, K. Mattila, A.J. Aho, A prospective randomized 14-year follow-up study of bioactive glass and autogenous bone as bone graft substitutes in benign bone tumors. *J. Biomed. Mater. Res. B Appl. Biomater.* **94B**(1), 157–164 (2010). <https://doi.org/10.1002/jbm.b.31636>
43. O.P. Filho, G.P. La Torre, L.L. Hench, Effect of crystallization on apatite-layer formation of bioactive glass 45S5. *J. Biomed. Mater. Res.* **30**(4), 509–514 (1996). [https://doi.org/10.1002/\(SICI\)1097-4636\(199604\)30:4%3c509::AID-JBM9%3e3.0.CO;2-T](https://doi.org/10.1002/(SICI)1097-4636(199604)30:4%3c509::AID-JBM9%3e3.0.CO;2-T)
44. O. Peitl, E. Zanotto, L. Hench, Highly bioactive P2o5-Na2o-Cao-Sio2 glass-ceramics. *J. Non-Cryst. Solids* **292**, 115–126 (2001). [https://doi.org/10.1016/S0022-3093\(01\)00822-5](https://doi.org/10.1016/S0022-3093(01)00822-5)
45. J. Massera, S. Fagerlund, L. Hupa, M. Hupa, L. Pinckney, Crystallization mechanism of the bioactive glasses, 45S5 and S53P4. *J. Am. Ceram. Soc.* **95**, 607–613 (2012). <https://doi.org/10.1111/j.1551-2916.2011.05012.x>
46. S. Fagerlund, J. Massera, N. Moritz, L. Hupa, M. Hupa, Phase composition and in vitro bioactivity of porous implants made of bioactive glass S53P4. *Acta Biomater.* **8**(6), 2331–2339 (2012). <https://doi.org/10.1016/j.actbio.2012.03.011>
47. L. Lefebvre, L. Gremillard, J. Chevalier, R. Zenati, D. Bernache-Assolant, Sintering behaviour of 45S5 bioactive glass. *Acta Biomater.* **4**(6), 1894–1903 (2008). <https://doi.org/10.1016/j.actbio.2008.05.019>
48. T. Kokubo, H. Kushitani, S. Sakka, T. Kitsugi, T. Yamamuro, Solutions able to reproduce in vivo surface-structure changes in bioactive glass-ceramic A-W3. *J. Biomed. Mater. Res.* **24**(6), 721–734 (1990). <https://doi.org/10.1002/jbm.820240607>
49. D. Zhang, M. Hupa, H.T. Aro, L. Hupa, Influence of fluid circulation on in vitro reactivity of bioactive glass particles. *Mater. Chem. Phys.* **111**(2), 497–502 (2008). <https://doi.org/10.1016/j.matchemphys.2008.04.055>
50. O. Bretcanu, X. Chatzistavrou, K. Paraskevopoulos, R. Conrad, I. Thompson, A. Boccaccini, Sintering and crystallisation of 45S5 bioglass (R) powder. *J. Eur. Ceram. Soc.* **29**, 3299–3306 (2009). <https://doi.org/10.1016/j.jeurceramsoc.2009.06.035>
51. H. Arstila, L. Hupa, K. Karlsson, M. Hupa, In vitro bioactivity of partially crystallised glasses. *Glass Technol. Eur. J. Glass Sci. Technol. A* **48**, 196–199 (2007)
52. D. Rohanová, D. Horkavcová, A. Helebrant, A.R. Boccaccini, Assessment of in vitro testing approaches for bioactive inorganic materials. *J. Non-Cryst. Solids* **432**, 53–59 (2016). <https://doi.org/10.1016/j.jnoncrsol.2015.03.016>
53. M. Bohner, J. Lemaître, Can bioactivity be tested in vitro with SBF solution? *Biomaterials* **30**(12), 2175–2179 (2009). <https://doi.org/10.1016/j.biomaterials.2009.01.008>
54. L.L. Hench, D.E. Clark, Physical chemistry of glass surfaces. *J. Non-Cryst. Solids* **28**(1), 83–105 (1978). [https://doi.org/10.1016/0022-3093\(78\)90077-7](https://doi.org/10.1016/0022-3093(78)90077-7)
55. M. Cerruti, D. Greenspan, K. Powers, Effect of pH and ionic strength on the reactivity of Bioglass® 45S5. *Biomaterials* **26**(14), 1665–1674 (2005). <https://doi.org/10.1016/j.biomaterials.2004.07.009>
56. J.R. Jones, L.L. Hench, Biomedical materials for new millennium: perspective on the future. *Mater. Sci. Technol.* **17**(8), 891–900 (2001). <https://doi.org/10.1179/026708301101510762>
57. V. Mouriño, J.P. Cattalini, A.R. Boccaccini, Metallic ions as therapeutic agents in tissue engineering scaffolds: an overview of their biological applications and strategies for new developments. *J. R. Soc. Interface* **9**(68), 401–419 (2012). <https://doi.org/10.1098/rsif.2011.0611>

ISBN 978-952-12-4342-4